

A. Dykha,
J. Padgurskas,
J. Musial,
S. Matiukh

**WEAR MODELS AND DIAGNOSTICS
OF CYLINDRICAL SLIDING TRIBOSYSTEM**

A. Dykha,
J. Padgurskas,
J. Musial,
S. Matiukh

**WEAR MODELS AND DIAGNOSTICS
OF CYLINDRICAL SLIDING TRIBOSYSTEM**

Bydgoszcz, 2020

A. Dykha, J. Padgurskas, J. Musial, S. Matiukh. Wear models and diagnostics of cylindrical sliding tribosystem. Bydgoszcz: Foundation of Mechatronics Development, 2020

Reviewers:

Mykhaylo Pashechko

Prof. dr hab. eng, Department of Fundamental of Technology, Lublin University of Technology, Poland

Andrei Ya. Grigoriev

Dr. Sci. Eng., V.A. Belyi Metal-Polymer Research Institute, National Academy of Sciences of Belarus, Gomel, Belarus

Audrius Zunda

Assoc. Prof. Dr., Institute of Power and Transport Machinery Engineering, Vytautas Magnus University, Kaunas, Lithuania

ISBN 978-83-938655-5-0

© Copyright by Foundation of Mechatronics Development, 2020
85-343 Bydgoszcz, ul. Jeżynowa 19, Poland

TABLE OF CONTENTS

Introduction	6
Chapter 1. Wear-contact Problems and Wear Models for Cylindrical Sliding Tribosystems	
1.1. Modern studies of tribological bearing systems	9
1.2. The wear models of cylindrical sliding tribosystems	21
1.2.1. Solution of the wear-contact problem for a cylindrical sliding bearing	21
1.2.2. Identification of wear resistance parameters for the method of wear test by the "cone - three balls" scheme	25
1.2.3. Experimental setup and the test procedure.....	29
1.2.4. The results of sliding bearings wear tests and calculations	32
1.2.5. Results obtained in computational and experimental modeling of cylindrical plain bearings wear	34
1.3. Direct wear-contact task for radial sliding bearing	36
1.4. Variational approach for determining tribocontact parameters of sliding bearings	43
1.4.1. Fundamentals of the variational approach in contact mechanics.....	43
1.4.2. Calculation-experimental method of estimation of wear of a bearing of sliding	45
1.4.3. Contact shaft and bearing, taking into account frictional forces.....	49
1.5. Modeling of wear processes in a cylindrical plain bearing	52
1.6. Wear and reliability of cylindrical vehicle joints	60
1.6.1. Calculation of wear and contact pressures in ball bearings of a vehicle suspension.....	61
1.6.2. Reliability calculations of ball bearings.....	64
1.6.3. Determination of wear parameters of ball joint.....	66
References for chapter 1	68

Chapter 2. Research of Tribological Properties of Lubricants. Theory and Experiment

2.1. Testing of lubricants according to the four-ball scheme. Test method theory	73
2.2. Determination of wear resistance characteristics based on the results of laboratory wear tests	86
2.3. Study of the viscosity properties of lubricants by the pendulum method	94
2.3.1. Damped vibration method in the study of friction processes	94
2.3.2. Theoretical model of pendulum in the sliding supports with a lubricant for examining the viscous friction	96
2.3.3. Results of determining the characteristics of viscous	101
2.4. Research of the contact and deformation properties of lubricated surfaces	108
2.5. The biological aspect of contact of lubricated surfaces	115
References for chapter 2	119

Chapter 3. Diagnostic Approaches to Assessing the State of Sliding Friction Tribosystems

3.1. Tribo-acoustic analysis of the processes of dynamic friction	123
3.2. Quantum-acoustic analysis of tribosystem behavior	129
3.2.1. The pseudo-equilibrium and collapse models of contact disturbance generation in tribosystems	131
3.2.2. Generating disturbances under the modes of fretting, sliding and rolling friction	136
3.2.3. Contact-induced flutter and buffeting under the cutting modes of materials ..	143
3.2.4. Corpuscular-vortex-wave mechanism of selective transfer and hydrogen wear	145
3.2.5. Results of studying the quantum-mechanical processes in the contact interaction of tribosystems	145
3.3. Diagnostics-experimental analysis of friction pairs at stick-slip sliding	148
References for chapter 3	156

Chapter 4. Technological Support of Wear Resistance of Cylindrical Tribosystems

4.1. Hardening of cylindrical friction surfaces with a roller tool.....	160
4.1.1. Materials and methods used in the tribological study of the effect of reeling parts on the contact strength.....	163
4.1.2. Results of tribological tests and process parameters of reeling steel parts with rollers.....	164
4.1.3. Results of tribological studies and process conditions of reeling steel parts with rolls.....	177
4.2. Discrete electromechanical hardening of steel shafts	181
4.2.1. Fundamentals of the method of discrete hardening of cylindrical parts....	183
4.2.2. The calculation model of the contact tool-detail	185
4.2.3. Stress-deformed state and geometrical parameters with the electromechanical strengthening	187
4.2.4. Calculation-experimental investigation of wear resistance at discrete hardening.....	189
References for chapter 4	193

INTRODUCTION

The current stage of development of tribology is characterized by the creation of methods for calculating friction pairs for wear. It has long been considered that the creation of such methods is impossible due to the extreme complexity of wear processes. If there are no calculation methods, respectively, there will be no methods for predicting wear resistance and durability of tribosystems. Development of analytical methods of calculation of wear resistance of tribosystems is complicated by nonlinearity of models of wear owing to difficult interrelations of mechanical, thermophysical and frictional properties. To obtain correct results, analytical methods for calculating tribosystems require proof by numerical methods using powerful computing systems. Cylindrical tribosystems of sliding in many power, technological and transport machines are one of the main elements that determines the durability and reliability of the machine as a whole. Therefore, the creation of a system of computational and experimental methods and numerical models for predicting the durability of cylindrical sliding tribosystems, taking into account the variety of operating conditions is an important scientific problem.

The monograph consists of four chapters. The first chapter deals with the issues of modeling the laws of wear and solving wear-contact problems for cylindrical tribosystems. A literature review of the current state of the problem of calculating the wear of cylindrical tribosystems is carried out. A model of wear of a sliding bearing in conditions of boundary friction was proposed. The wear model was presented in a form of dimensionless complexes taking into account geometric, kinematic, friction and lubrication characteristics of sliding bearings. The wear-contact problem for cylindrical sliding bearings was solved. A calculation-experimental procedure for identifying parameters of wear resistance based on the two-factor model of wear. An approximate method is proposed for solving a direct wear-contact problem for a sliding bearing. Trigonometric functions in the solution process were replaced by approximate power series expansions. The variational-experimental method for determining the distribution of contact pressure in

a cylindrical slider bearing is proposed. The functional problem is obtained as a deviation of the experimental function from the integral equilibrium condition. For the calculation the kinetics of wear and contact parameters, a step-by-step procedure is proposed.

In the second chapter, computational and experimental approaches to the analysis of the processes of friction and wear of tribosystems taking into account the properties of lubricants are proposed. The theory of the test method for wear with lubrication according to the four-ball scheme with the determination of the parameters of steady-state wear models is proposed. The approximate solution of the problem is based on the assumption of a uniform distribution of contact pressures at any moment of testing. The calculation procedure for determining the parameters of wear models has been determined. A methodical example of the method implementation is given. A two-factor model of wear (contact pressure, sliding speed) in a dimensionless form, taking into account the properties of structural and lubricants of a friction pair, is proposed. The proposed methodology for identifying wear laws based on laboratory tests is recommended for predicting wear and optimizing the design and performance characteristics of lubricated tribosystems. The methods of determining the basic characteristics of viscous friction are proposed based on the model of pendulum oscillations: coefficient of energy absorption and dynamic viscosity. The obtained method for calculating the indicator of dynamic viscosity of a lubricant according to the decrement of pendulum oscillation damping is recommended for the practical application. The questions of the influence of the lubricant on the conditions of deformation in the contact of solids are considered. The microstructures of the structure of the surface layer are studied under various conditions of deformation. The diagrams of the relative deformation of the surface layers are constructed. The mechanism of the formation and distribution of internal stresses for dry and greased contact is described. Experimental studies of the introduction of a moving steel indenter into a lubricated surface have been carried out. The analogy between wear resistance of technical surfaces with a discrete relief and the similar problems in the wildlife is lead. As a result of carried out scanning research it is established, that parameters geometrical structures of a skin of finitenesses in the majority coincide with optimum parameters of a microrelief of technical surfaces.

The third chapter of the book offers modern ideas on diagnostics of tribological systems based on quantum theory and acoustic experimental methods. The experimental results of the tribo-acoustic control in real time the integrity of nominally stationary friction joints under conditions of fretting are presented. The physical mechanisms have been investigated that form and transform the corpuscular-vortex-wave thermal complexes of disturbances in contact tribosystems based on the quantum-mechanical

exchange interaction. This investigation gives specific technical examples of the generation of thermal complexes at fretting, during the friction of sliding and rolling, and at cutting. It has been established that the destructive nature of the process of fretting at low values of reverse sliding speeds is caused by the generation and collapse of the corpuscular-vortex-wave thermal complexes. It is shown that the properties of a servovite film under the mode of selective transfer are provided by the collapse processes in the system of disturbances. On the basis of the laboratory diagnostic complex studies of the characteristics of friction during movement with a low speed of the loaded plate on the working surface in the presence of lubrication were carried out. As a result of processing the experimental data, statistical characteristics of the friction parameters were obtained, which characterize the effect on them of the load and lubrication mode. The quantitative characteristics of the plate motion, which characterize the deformation properties of the contact layer, are established.

The fourth chapter of the monograph describes some modern approaches to technological reliability assurance based on the wear criterion of cylindrical tribosystems. The study of the efficiency of hardening the parts working in spalling conditions through reeling with rollers were performed with the help of physical simulation and showed the high effect of hardening cast steels. A procedure for determining conditions of reeling with a wedge roller was developed. A method, technology, and a device for reeling the rope blocks with a wedge roller were developed to provide low roughness and high degree of work hardening of the surface. Optimal reeling conditions were found due to experiment planning using the steep convergence method. A new method of increasing the wear resistance of steel parts by discrete electromechanical processing has been developed by forming linear reinforcement areas with controlled geometry. A computer simulation of the conditions of the contact between the tool roller and the machined shaft has been carried out. The contact areas, contact stresses, depths of deformation and temperature distribution in depth are calculated.

The book can be useful for scientists and young researchers in the field of creating computational and experimental methods for predicting the durability of friction pairs of modern machines by the criterion of wear resistance.

CHAPTER 1

Wear-contact Problems and Wear Models for Cylindrical Sliding Tribosystems

1.1. Modern studies of tribological bearing systems

Bearings are technical devices that are part of the supports of rotating axles and shafts. They take radial and axial loads applied to the shaft or axis and transfer them to the frame, housing or other parts of the structure. At the same time, they should also keep the shaft in space, provide rotation, swing or linear movement with minimal energy loss. The quality of bearings, efficiency and durability of the machine largely depend on the quality of bearings. This review presents the results of studies of bearings, published in the world specialized scientific journals over the past 3 years.

The article [1] employs an adaptive wear modeling method to study the wear progress in radial sliding bearings contacting with a rotary shaft. Mixed Lagrangian–Eulerian formulation has been used to simulate the contact condition between the bearing and the shaft, and the local wear evolution is modeled using the Archard equation. In the developed wear processor algorithm, not only remeshing is performed on the contact elements, but also is executed for their proximity elements. In this way the wear simulation becomes independent of the size of the contact elements. Validation was done for a laminated polymeric composite bearing. The composite has been modeled as a linear orthotropic material. The wear coefficients were obtained from flat-on-flat experiments and were applied as pressure and velocity dependent parameters in the wear processor. Finally, the effect of the clearance on the wear of the radial bearings has been studied numerically. The simulations also demonstrate how the contact pressure evolves during the wear process, and how the clearance influences this evolution.

The study [2] aims to predict the wear in journal bearings during steady-state operation in the mixed-lubrication regime starting with a critical assessment of commonly used wear laws. A novel numerical method is introduced that calculates journal bearing wear on macroscopic and asperity

contact scale. For validation of the numerical method, the friction and wear behavior was studied on a special test-rig for journal bearings. Both experimental and numerical results show an initial period of high friction and wear. After the first minutes of operation reduced friction can be observed. The simulations clarify, that this is caused by bearing wear on asperity roughness scale. By considering the reduced asperity interaction due to wearing-in in the calculation of contact conditions a higher accuracy of wear prediction is achieved.

Leaded tin bronze alloys are widely used in heavy machinery bearings operating in boundary and mixed lubrication regions due to the excellent dry lubrication properties of lead. However, restrictions on the use of lead have created an increasing demand for lead-free or low-lead bearing materials. In the study [3], suitability of a novel bismuth bronze bimetal material for possible substitution of leaded tin bronze was studied with a special thrust bearing test device, which simulates the contact conditions in the main thrust bearing of mineral crushers. The oil-lubricated test bearings have a flat-on-flat type contact with oil grooves and a constant eccentric motion against a case hardened steel counter plate under a periodically increased axial pressure. The test was continued until a sudden rise in friction, which indicates bearing failure and risk of an imminent seizure. The bismuth bronze showed a load capacity of the same level with the reference material, continuously cast CuSn10Pb10. Characterization by electron microscopy showed that the dry-lubricating bismuth precipitations had a fine grain size and an even distribution, which explains the good load carrying capacity. It was concluded that the bismuth bronze has potential for substituting the leaded tin bronzes in the studied operating conditions.

The paper [4] investigates the performance of a ferrofluid based hydrodynamic journal bearing system considering different combination of shaft and bearing materials. An investigation was first carried out for the material combination of ferrous and non-ferrous for shaft and bearing respectively, in the presence of a ferrofluid. Thereafter, analysis was conducted for the ferrous with ferrous material combination. Film pressure and temperature rise were measured for varying speeds and loads. It was noticed that the film pressure generation failed owing to the attraction in the case of ferrous and ferrous material combination for the bearing and magnetic shaft. Further, the temperature rise was found to be nearly double in the case of ferrous with ferrous, in comparison with ferrous with non-ferrous material combination under certain operating conditions. Besides, for moderate loads and speeds, the film pressure in case of ferrofluid lubrication for ferrous and non-ferrous combination increased considerably as compared to that of the conventional lubricant based journal bearing systems. Moreover, the temperature rise was much smaller for ferrofluid lubricants as compared to conventional lubricants, thus, making the system cooler while running.

Finally, wear analysis was carried out on the ferrofluid based journal bearing system by microscopic observation of the bearing surfaces, weight loss and DLS of fluid. This study indicated that the ferrous and non-ferrous material combination could probably turn out to be a suitable option for the ferrofluid based journal bearing system.

Hydrodynamic sliding bearings are designed to operate under fully flooded conditions to enable adequate film formation. In actual operating conditions, journal bearings could operate in a mixed or even boundary lubrication regime, for example, during the start-up/shut-down period. To prevent bearing destruction, a specific surface texture can be created on the sliding zones. One of the roles of surface irregularities is to maintain a certain amount of oil in the case of its shortage.

The aim of the study [5] was to identify the characteristic parameters, such as the sliding velocity, Hersey number, and friction torque or friction coefficient, when the transition of lubrication regimes occurs for different journal bearing types. The study demonstrates the results achieved in experimental investigations conducted on journal bearings, with the oil pockets on the journal surface mating with the smooth bearing and with the texture on the bearing surface co-acting with a standard smooth journal. The obtained results were also compared with the tested effects of the classical, smoothly finished journal bearing. It was found that, during shut-down, the textured journal bearings remained in hydrodynamic lubrication for longer and moved to mixed lubrication at lower speeds compared to the smooth journal bearing.

Oil contamination resulting from externally ingested particles is one of the major causes of journal bearing failure in industrial machinery. The present study has been carried out to assess the case of externally ingested particle contaminants in a journal bearing lubrication using acoustic emission (AE) and vibration monitoring techniques. Besides quantitative evaluation, the features of AE and vibration spectra have been classified and key parameters for condition monitoring deduced. Furthermore, cases involving different particles sizes and concentrations have been exhaustively examined and illustrated; and the capability of these two methods described in terms of detectability.

This paper [7] investigates the impact of heat transfer between leading and trailing pad free surfaces and the space between pad regions of high-speed tilting-pad journal bearings. General influence on pad metal temperature distributions as well as magnitudes of resulting heat convection coefficients are theoretically analyzed and validated with test data for sliding speeds up to 94 m/s and specific loads up to 3.0 MPa. Results indicate significant impact of trailing pad free surface heat transfer on maximum pad metal temperatures as well as potential for optimization based on the general flow pattern. Moreover, limitations, extensions, and improvements of the presented study are comprehensively discussed.

In [8] a transient Mixed Lubrication-Wear coupling model (MLW coupling model) is developed to investigate the mixed lubrication and wear performances of journal bearings, and a wear experiment for journal bearing is performed to support the validity of the developed numerical model. In the coupling numerical model, the transient interaction between the behaviour of mixed lubrication and wear is considered by incorporating the wear depth distribution, which is determined by the developed friction fatigue wear model, into the film gap equation. The evolutions of the worn surface profile, wear rate, fluid pressure and asperity contact pressure over operating time are calculated by the developed numerical model. The simulated results demonstrate that the transient wear process affects the distribution trend of lubrication performances significantly, and a worn surface profile may exist that provides an optimal tribology performance of journal bearings. The simulated results also demonstrate that there are two wear stages, identified by initial and steady wear stage, of journal bearings under mixed lubrication condition. Furthermore, the effects of the input parameters, including the radius clearance (C), surface roughness (σ), asperity curvature radius (β) and boundary friction coefficient (μ_c), on the predicted mixed lubrication and wear performance are evaluated.

Currently used turbulent lubrication model [9] that considers the effects of surface roughness can only handle the isotropic rough surfaces and cannot handle the rough surfaces with directional properties. In this paper, based on the stochastic method and the Ng-Pan turbulent model, the stochastic turbulent lubrication models of one-dimensional longitudinal rough surface, one-dimensional transverse rough surface and isotropic rough surface are derived. The turbulent lubrication performance of a journal bearing with isotropic rough surface is calculated by the stochastic turbulent lubrication model. The results are in good agreement with the corresponding experimental data. Moreover, the proposed stochastic turbulent lubrication models are also suitable for parts of friction pairs such as journal bearing and thrust bearing.

The dynamic contact behavior of hydrodynamic journal bearings during start-up is investigated [10]. The hydrodynamic oil force and asperity contact force are obtained by solving the mixed lubrication model. The motion of the journal center, the contact time, and the lift-off speed of the bearing are determined. The effects of the relative clearance and acceleration time are discussed. The result shows that the hydrodynamic oil force increases sharply during the early stage of the start-up process, leading to a sharp decrease in the contact force. An increase in the relative clearance of the bearing generates a decrease in both the contact force and the contact time. Also, a high start-up acceleration leads to a sharp decrease in the contact force.

This paper discusses the further development of an analytical model to calculate the minimum film thickness and the transition speed in journal

bearings with consideration of bearing deformations. The focus of the development was on generalising an existing model to include any relative eccentricities and width/diameter ratios. Furthermore, the influence of different bearing types and the layer structure of plain bearings on the deformation are taken into account. Using two white metal journal bearings as examples, the results of the new approach are discussed and compared with previous analytical models and full numerical calculations.

Hydrostatic assistance is a commonly used method to improve limited load carrying ability of tiltingpad thrust bearings during transient states of operation of vertical shaft hydro-generators [12]. Despite of special hydraulic equipment (as pumps, valves, etc.), it also requires manufacturing of special recesses/pockets at pad sliding surfaces, into which oil is injected under high pressure. It allows to lift the rotor before start-up of the machine and form a hydrostatic film between pads and collar. There is a quite wide variety of geometry of recesses (shape, depth, and size) met in practical large bearing applications. The presence of a hydrostatic pocket (usually located in the sliding surface above the pivot area, where thin film, high oil pressure and temperature are observed) affects bearing performance under hydrodynamic operation.

In theoretical researches, there is an almost common practice not to include hydrostatic recess in thermohydrodynamic (THD) or thermoelasto-hydrodynamic (TEHD) analysis. This is probably due to the problems with obtaining solution for oil film geometry with pocket, the order of magnitude of the pocket depths being larger than gap thickness. In this paper, an attempt was taken to study the effect of lifting pocket on THD performance of a large tilting-pad thrust bearing of Itaipu power plant. Bearing performance was evaluated including recess shape for several cases of its depth. The results show that hydrostatic recess changes calculated bearing properties quite significantly, especially in vicinity of the pocket.

It has been shown [13] before that liquids can slip at a solid boundary, which prompted the idea that parallel-surfaces bearings can be achieved just by alternating slip and non-slip regions in the direction of fluid flow. The amount of slip at the wall depends on the surface tension at the liquid–solid interface, which in turn depends on the chemical state of the surface and its roughness. In the present study a heterogeneous surface was obtained by coating half of a circular glass disc with a coating repellent to glycerol. A rotating glass disc was placed at a known/calibrated distance and the gap was filled with glycerol. With the mobile surface moving from the direction of slip to non-slip region it can be theoretically shown that a pressure build up can be achieved. The pressure gradient in the two regions is constant, similar to that in a Rayleigh step bearing, with the maximum pressure at the separation line. The heterogeneous disc was placed on a holder supported by a load cell thus the force generated by this pressure increase can be

measured accurately. Tests were carried out at different sliding speeds and gaps and the load carried was measured and subsequently compared with theoretical calculations. This allowed the slip coefficient to be evaluated.

In the study [15], based on the classical Archard adhesion wear theory, a three-dimensional finite element model was established, with the aim of simulating the failure process of self-lubricating spherical plain bearings in the swinging wear condition. The results show that the self-lubricating spherical plain bearings go through two different stages during the wear process, namely, initial wear stage and stable wear stage. Because the large contact points wear out during the initial wear stage, the maximum contact pressure decreases as the test period increases. The relatively larger wear depth region shows elliptical distribution, and the maximum distribution appears in the central contact area. The wear depth reaches 0.974 mm after swinging 25,000 times. PTFE fibers, which possess a good friction performance but poor abrasion resistance, abundantly exist on the friction surfaces of the fabric liner. Consequently, the friction torque during the initial wear stage is slightly smaller than the friction torque during the stable wear stage; however, the wear rate during the initial wear stage is high. The reliability and effectiveness of the finite element model are verified by experiment. The developed finite element model can be used for the analysis of the wear mechanisms of bearings and the prediction of the service life of bearings.

I paper [15] developed a technique to assess the workability of sealed-for-life greased rolling bearings after a long-term storage. In this framework, we devised a model of equivalent transition between the conditions of natural ageing under daily and seasonally fluctuating temperature, and the conditions of accelerated thermal ageing at a constant high temperature. The tested bearings were thermally aged, and then their steady state friction and outer ring temperature were examined in a custom high-speed spindle. These results were compared to the performance of a reference new bearing tested under the same loading conditions. Our findings suggest that long-term storage can significantly degrade the performance of sealed-for-life greased rolling bearings. However, a proper running-in can substantially deter the ageing-driven degradation of the bearings.

The paper [16] presents a numerical study for nonlinear rotordynamic response with bifurcations of tilting pad journal bearings when pad-pivot friction forces are taken into account. A Stribeck friction model is employed to determine the friction coefficient for the contacts between the pads and the spherical-type pivots. The boundary/mixed/hydrodynamic friction mode is determined for each pad surface based on the instantaneous angular motion of the pads. A Jeffcott type rotor supported on 5-pad tilting pad journal bearings is used for the structural model, and finite element fluid film models are utilized to calculate the reaction forces and moments on the

pads. The simulation results show that pad–pivot friction plays an important role in determining the stability of the rotor system. For the autonomous condition, the friction induces a Hopf bifurcation and generates limit cycles at high rotor spin speed (>14 krpm), which were originally stable equilibrium states with a no friction condition. For the nonautonomous condition, the $1\times$ synchronous response becomes subsynchronous/quasiperiodic responses in the high-speed range (>14 krpm) with the appearances of Neimark-Sacker bifurcations. It is shown that the outbreak points and corresponding response types are highly dependent on the state of disk imbalance. A comparison of the linear and nonlinear models clearly illustrates the importance of retaining nonlinear forces to determine potential deleterious vibration.

In [17] it becomes impossible to use conventional fluid film journal bearings in the hot working environments ($500\text{--}800$ °C) due to rapid thermal degradation of lubricating oils. Under this situation, powder lubricants prove beneficial in spite of high friction values associated with them in comparison to lubricating oils. Thus, reduction of friction in powder-lubricated journal bearings is an essential task for making the operation energy efficient. Hence, the objective of this paper is to explore the reduction of coefficient of friction in a powder-lubricated journal bearing employing different pocket shapes (elliptical, parabolic, rectangular, and trapezoidal) placed on bore surface. Based on the investigations reported herein, it is found that the journal bearing having rectangular pocket yields least coefficient of friction among all the cases.

Surface texturing is a technique for improving frictional and hydrodynamic performances of journal bearings because microtextures can serve as reservoirs for oil or traps for debris and may also generate hydrodynamic pressure. Over the past two decades, many researchers have experimentally demonstrated that texturing of various tribological elements can reduce friction force and wear, contributing to improvement of lubrication performance. Some numerical studies have examined the hydrodynamic lubrication conditions and reported that surface texturing affects the static characteristics of journal bearings, such as their load carrying capacity and friction torque. However, the validity of these numerical models has not been confirmed because of a lack of experimental studies. This study [18] proposes a numerical model that includes both inertial effects and energy loss at the edges of dimples on the surface of a journal bearing in order to investigate the bearing's static characteristics. Experimental verification of journal bearings is also conducted with a uniform square-dimple pattern on their full-bearing surface. The results obtained by the model agree well with those of experiment, confirming the model's validity. These results show that under the same operating conditions, textured bearings yield a higher eccentricity ratio and lower attitude angle than the conventional ones with a smooth surface. This

tendency becomes more marked for high Reynolds number operating conditions and for textured bearings with a large number of dimples.

By enhancing surface properties and by reducing weight and size of machine elements, future trends in resource efficiency for machines can be fulfilled. Rolling element bearings are widely used machine elements. By improving their boundary zone properties, there is a potential to extend maintenance-free operating periods, postpone replacements or increase the lifespan of the complete system. The aim is to set favorable boundary zone properties by enhancing the residual stress state within the manufacturing process. For this, the processes hard turning and deep rolling were investigated in [19]. The influence of the initial residual stress state on fatigue life was calculated using a model based on the approach of Ioannides and Harris. The resulting residual stresses after the manufacturing process and their changes during operation in a bearing test rig are discussed and compared to those of standard bearings. The tests prove that pre-induced residual stresses increase is able to significantly delay rolling contact fatigue-related bearing failures.

The friction properties of a range of viscosity modifier-containing oils in an engine bearing have been studied in the hydrodynamic regime using a combined experimental and modelling approach [20]. The viscometric properties of these oils were previously measured and single equations derived to describe how their viscosities vary with temperature and shear rate (Marx et al. Tribol Lett 66:92, 2018). A journal bearing machine has been used to measure the friction properties of the test oils at various oil supply temperatures, while simultaneously measuring bearing temperature using an embedded thermocouple. This shows the importance of taking account of thermal response in journal bearings since the operating oil film temperature is often considerably higher than the oil supply temperature. For Newtonian oils, friction coefficient measurements made over a wide range of speeds, loads and oil supply temperatures collapse onto a single Stribeck curve when the viscosity used in determining the Stribeck number is based on an effective oil film temperature. Journal bearing machine measurements on VM-containing oils show that these give lower friction than a Newtonian reference oil. A thermo-hydrodynamic model incorporating shear thinning has been used to explore further the frictional properties of the VM-containing oils. These confirm the findings of the journal bearing experiments and show that two key factors determine the friction of the engine bearing; (i) the low shear rate viscosity of the oil at the effective bearing temperature and (ii) the extent to which the blend shear thins at the high shear rate present in the bearing.

Ultra-high molecular weight polyethylene (UHMWPE)/graphene nanoplatelets (GNPs) nanocomposite coatings were developed [21] to

reduce friction and wear in the absence of liquid lubrication. UHMWPE nanocomposite powders with different loadings (0.25, 1, and 2 wt.%) of GNPs were prepared and electrostatic spraying technique was then used to deposit the nanocomposite powders on aluminum alloy to form a thin coating. Friction and wear tests were conducted on the coatings against a flat-end pin, made of hardened tool steel to determine the best loading of GNPs. That was further tested to investigate the effect of sliding speed and contact pressure on its tribological properties and to establish coating operating limits. Results showed that UHMWPE nanocomposite coating reinforced with 1 wt. % GNPs showed the best tribological performance. It reduced wear rate by about 51 % as compared to the pristine UHMWPE coating. The coating sustained a maximum sliding speed of 1 m/s at a contact pressure of 4 MPa equivalent to a pressure and velocity (PV) value of 4 MPa.m/s.

Wind turbine drive train system failures have been the major source of down time and costly repairs. One of the main failure modes associated with gearbox failures is the formation of white etching cracks (WECs) in bearings. In this paper, low-speed intermediate shaft (LSIS) and high-speed intermediate shaft (HSIS) bearings are collected from failed gearboxes to examine microstructural alterations and evaluate damage [22]. Butterfly wing formations are detected in LSIS bearings around nonmetallic inclusions at depths of up to about 260 μm from the contact surface and the measured span length ranging from 5 to 70 μm . Circumferential cracks oriented parallel to the contact surface are detected at depths greater than 300 μm . Irregular white etched cracks are revealed in HSIS bearings with random crack orientations. The crack depth is measured to be 7000 μm in the cross section perpendicular to the bearing axis. The bearing characterization revealed that microstructural alterations can occur with and without the formation of cracks. Evidence found supports the existing hypotheses that (1) white etch areas precedes crack formations and (2) cracks are prerequisites for white etch formation. The microstructural alterations detected in LSIS and HSIS bearings are observed to have different crack morphology and could be initiated by different mechanisms. The results presented in this paper can be used to develop materials-based prognostic life prediction models. This can be achieved by linking WECs and butterfly wings qualitative observations to turbine real operating conditions, bearing design, and manufacturing process.

A general, CFD-based frequency response method for obtaining the dynamic coefficients of hydrodynamic bearings is presented [23]. The method is grounded in experimental parameter identification methods and is verified for an extremely long, slider bearing geometry as well as short and long journal bearing geometries. The influence of temporal inertia on the dynamic response of the bearings is discussed and quantified through the inclusion of added mass coefficients within the mechanical models of the hydrodynamic bearing

films. Methods to separate the dynamic stiffness into static stiffness and added mass contributions are presented and their results compared. Harmonic perturbations are applied to the bearings at varying frequencies to determine the frequency dependence of the dynamic coefficients and to facilitate the decomposition of the dynamic stiffness into its constituents. Added mass effects are shown to be significant for the extremely long slider bearing geometry and negligible for the short and long journal bearing geometries under operating conditions motivated by those typical of marine bearings.

The paper [24] focuses on the operating behavior of journal bearings for industrial machinery application during run-ups. For this purpose, a numerical simulation code that is based on a two-dimensional extended and generalized Reynolds equation and a full three-dimensional energy equation, was advanced by a theoretical model considering the effects of mixed friction and warming of journal components during start-up. The mixed friction routine contained the elastic half-spaces model proposed by Boussinesq, which considers the influence of rough surfaces by implementing flow factors and calculates additional stiffness and dissipation in areas with solid interactions. Furthermore, a transient term was added in the energy equation to consider the thermal inertia of journal, and bearing to ensure a realistic heating during run-ups. Results of the prediction were compared to experimental data taken from a special test rig built up for validation procedures. Besides the conventional sensors for temperature, oil flow, and relative motion between shaft and stator, a contact voltage measurement was installed to determine the intensity of mixed friction. The evaluation of experimental data by Stribeck curves, based on a shaft torsion measurement, indicated a significant influence of run-up time on frictional moment. The friction coefficient of the rotor bearing system was strongly influenced by the run-up time. A short run-up time reduced the frictional coefficient in the mixed lubrication regime while the opposite behavior was observed in the hydrodynamic lubrication regime. The numerical code predicted these tendencies in good agreement with experimental data, however, only if the transient energy model was applied.

A comparative study between a conventional- and leading edge grooved (LEG) tilting pad journal bearing (TPJB) segment is performed in [25]. The developed model uses the Shear Stress Transport (SST) turbulence model, coupled with the energy equation and a partial differential equation for the fluid domain mesh displacement to predict the thermal flow characteristics. Instead of using an effective boundary condition to determine the inlet temperature of the LEG pad and excluding the additional LEG portion, as is common practice, the whole geometry of the LEG is modeled. Several sizes of the LEG portion is investigated and it is shown to have quite a small influence on pressure, temperature, film thickness and turbulence intensity. Moreover, the results also show that the conventional

pad gives rise to higher levels of turbulence in the mid plane compared to its LEG counterpart, while the latter has a marginally higher value of turbulence when the volume average value is computed. The maximum value of turbulence is however present in the conventional model.

New stress-based life models are introduced to define “dynamic stress capacity” in rolling bearings for the first time. The generalized stress capacity equations are formulated, for both point and line contacts, in terms of distinct geometrical and materials parameters while the empirical constants are now material independent [26]. Life equations are first developed for individual rolling element to race contacts and then statistically combined to estimate lives of both races, rolling elements, and, finally, the whole bearings for both ball and roller bearings. An estimate of the empirical constant for the ball bearing equation is derived by regression analysis of available experimental data. The applicable constant for roller bearings is then derived by relating the ball and roller bearing constants to the fundamental subsurface fatigue hypothesis applicable to both point and line contacts. For AISI 52100 bearing steel at room temperature, life predictions with the new stress-based equations are in complete agreement with those currently provided by widely used load-based formulations, where the empirical constant contains the elastic properties of AISI 52100 bearing steel. In addition to these life equations based on the magnitude and depth of maximum orthogonal subsurface shear stress and the volume of material stressed, a new model that eliminates life dependence on the depth of maximum orthogonal shear stress and relates life to only the subsurface maximum shear stress and the stressed volume is presented. Though the predicted life estimates with the currently used and newly introduced life models are comparable in the contact stress range of 2 to 3 GPa, the new model provides significantly higher lives at low contact stresses.

In the article [27], a method for identification of equivalent stiffness was proposed based on a genetic algorithm by studying the stiffness characteristics of autoeliminating clearance auxiliary bearing devices (ACABDs) in static condition. Subsequently, the equivalent stiffness damping model and the Hertz contact theory were combined to establish the theoretical equations of the ACABD. Moreover, the linear equivalent model of the ACABD was established to eliminate the influence of contact of the revolute pair on mode shape and mode frequency of the rotor. In addition, simulations and experiments were carried out to verify the effectiveness of the genetic algorithm-based stiffness identification method. The results indicated that the relative errors between the equivalent stiffness in the X and Y directions identified by the linear equivalent model and the theoretical values were 6.22 and 7.19 % respectively, demonstrating the feasibility of this identification method.

A method for forming an exact self-similar solution to the problem of hydrodynamic calculation of a radial plain bearing that operates in a steady-

state friction mode in the presence of a lubricant has been constructed [28]. Based on the equation of motion for a viscous incompressible electrically conducting liquid in the case of a “thin layer,” the continuity equation, and expressions for the dissipation rate of mechanical energy, an analytical relationship for the molten surface profile of fusible coating on a bearing bush taking into account the viscosity and electrical conductivity of a liquid lubricant depending on pressure is obtained. The effect of the parameters characterizing the dependence of viscosity and electrical conductivity on pressure and the effect of a parameter caused by melting the fusible coating surface of the bearing bush exerted on the bearing capacity and friction force are demonstrated.

The second version of the original Bearing Builder Finite Element Method (BBFEM) software and its application for analyzing the hydrodynamics of cylindrical sliding bearings has been briefly described [29]. The two-dimensional problem of the lubricating fluid flow in a bearing clearance taking into consideration the different types of deviations in the contact surface from a cylindrical shape has been solved by the finite element method. The bearing design that leads to the formation of several hydrodynamic friction zones (fluid wedges) has been considered. The role of the contact compliance of a shaft and a bush and the operation factors that cause the deviation from the initial cylindrical shape of a bearing, including the deformations and the misalignment of the shaft and bush is shown by citing specific examples of antifriction composites of different compositions.

Effective conditions of friction in units that ensure performance and maximum longevity have been created by flood lubrication under the conditions of elastohydrodynamic (EHD) lubrication. In connection with this, prolonging the service life of friction units by ensuring local requirements to the amount of oil in the contact area and establishing the optimum choice of lubricating material in terms of its viscosity ratings is a topical problem for rolling bearings. Thus, it is suggested to determine the parameter of the lubricating layer (λ) values for the conditions of flood lubrication (λ_o) and progressing ($\lambda_{o,s}$) and catastrophic ($\lambda_{c,s}$) oil starvation for a wide spectrum of lubricating materials of different viscosity, since, in oil starvation mode, the efficiency of EHD conditions is violated, the lubrication mode is disturbed, and the bearing capacity of the EHD lubricating layer is lost.

The issues of creating efficient structural bearing assemblies, including through the use of new hybrid materials and structures, are considered. Much attention is paid to the problem of bearing wear and reducing the coefficient of friction. Separately considered issues of computer modeling of working conditions and design of structures. Considered modern approaches to the calculated evaluation of bearings, the solution of contact problems. This review allows scientists and engineers to do the right task setting when planning further research on bearing tribosystems.

1.2. The wear models of cylindrical sliding tribosystems

The current stage in development of tribology is characterized by creation of methods for calculating the wear of friction units. It was believed for a long time that creation of such methods is impossible because of an extreme complexity of wear processes. At the same time, if there are no methods of calculation at the stage of designing and machine creation, then respectively there will be no methods for predicting wear resistance and durability of the friction units. Development of analytical methods for calculating wear resistance of tribosystems is complicated by nonlinearity of wear models because of complex interrelationships of mechanical, thermo-physical and frictional properties. To obtain correct results, analytical methods for calculating tribosystems require a number of parameters that characterize real operating conditions. Cylindrical sliding bearings in many manufacturing, transport and power machines are among the main components determining durability and reliability of the machine as a whole. Thus, creation of calculation and experimental methods and models of wear resistance for predicting wear-related durability of cylindrical sliding bearings taking into account the variety of operating conditions is a focal scientific problem.

Creation of methods for calculation and wear test of cylindrical sliding bearings is currently being given considerable attention.

1.2.1. Solution of the wear-contact problem for a cylindrical sliding bearing

The wear-contact problem is the problem of determining maximum linear wear in the bearing depending on the friction path (1.working life). In this case, the bearing parameters of design, loading and kinematics as well as regularity of wear depending on wear-resistance parameters were taken as the starting data.

By their design scheme, cylindrical sliding bearings represent an internal contact of two cylinders of close radii with a radial clearance Δ (Fig. 1.1). The shaft with radius R_1 is loaded with force Q and rotates at a sliding velocity V in the bearing bush 2 having radius R . In the process of force interaction of the shaft and the bearing bush, the contact pressure σ distributed over the arc of contact $2\varphi_0$ arises at the place of contact of two cylinders.

Assuming wear resistance of the shaft much greater than the wear resistance of the bushing (1.direct friction pair), an arc zone of wear with a maximum wear u_w value at the contact center is worn out during operation in the inner surface of the bushing.

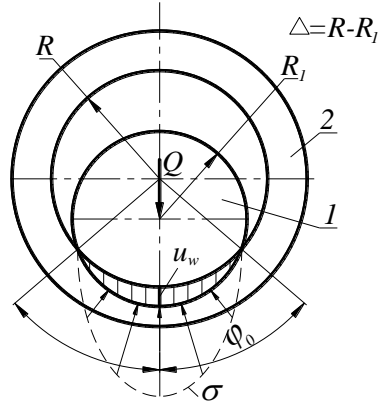


Fig. 1.1. Calculation scheme of a cylindrical sliding bearing

For analytical solution of the problem of the sliding bearing wear calculation, in addition to the indicated geometrical, force and kinematic parameters, a mathematical form of wear regularity is also taken as the initial value. Representation of such regularities in a form of dependence of the wear rate on the determining parameters of the process (1.contact pressure, sliding velocity, temperature, etc.) was of the greatest use. Here, we propose regularity (1.model) of wear in a form of a dimensionless set of determining factors:

$$\frac{du_w}{dS} = C_w \left(\frac{f\sigma}{HB} \right)^n \left(\frac{VR}{v} \right)^p, \quad (1.1)$$

where u_w is bearing wear; S is friction path; f is coefficient of friction in the shaft-bushing pair; σ is normal contact pressure; HB is hardness of the bushing material; V is sliding velocity; R is bearing (1.bushing) radius; v is kinematic oil viscosity; C_w , n , p are parameters of wear resistance.

In the basic dependence (1.1), value of the contact pressure will be determined from the mean values (1.equation of equilibrium):

$$\sigma = \frac{Q}{2bR\phi_0}, \quad (1.2)$$

where Q is load acting on the bearing; b is width of the contact between the shaft and the bushing; ϕ_0 is half-angle of the contact between the shaft and the bushing.

The relationship of the maximum wear u_w and the contact angle is determined from geometry of the internal contact of two cylinders with an initial radial clearance Δ from the dependence:

$$u_w(\varphi_0) = \Delta(\sec \varphi_0 - 1). \quad (1.3)$$

For further use, it is convenient to represent function $\sec \varphi_0 - 1$ in a form of a power approximation. For the range of changes in the contact angle $0 \dots \pi/2$ (Table 1.1), use the Excel program to construct graphical dependence of function $\sec \varphi_0 - 1$ on the contact angle φ_0 (Fig. 1.2) and obtain a power approximation of this function.

Table 1.1

Numerical dependences for the function of contact angle in the bearing

φ_0 , rad	0.2	0.4	0.6	0.8	1.0	1.2	1.4
$\sec \varphi_0 - 1$	0.02	0.086	0.212	0.435	0.851	1.76	4.88

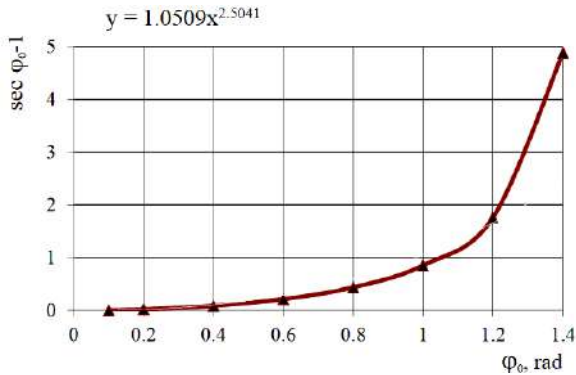


Fig. 1.2. Power approximation of function $\sec \varphi_0 - 1$ on the contact angle φ_0

With a sufficient accuracy, it can be assumed that

$$\sec \varphi_0 - 1 \approx \varphi_0^{2.5}. \quad (1.4)$$

Thus, expression (1.3) can be represented in the following form:

$$u_w = \Delta \varphi_0(s)^{\frac{1}{2}}. \quad (1.5)$$

Differentiate the dependence (1.5) in the friction path s :

$$\frac{du_w}{ds} = 2 \frac{1}{2} \Delta \varphi_0(s)^{\frac{1}{2}} \frac{d\varphi_0}{ds}. \quad (1.6)$$

Equate (1.1) and (1.6) and substitute into the left-hand side the expression for the contact pressure (1.2) to obtain:

$$c_W \left(\frac{VR}{v} \right)^p \left(\frac{f}{HB} \right)^n \left(\frac{Q}{2bR\varphi_0} \right)^n = 2 \frac{1}{2} \Delta \varphi_0(s)^{\frac{1}{2}} \frac{d\varphi_0}{ds}. \quad (1.7)$$

Transform (1.7) to the form:

$$\frac{c_W}{2,5\Delta} \left(\frac{VR}{v} \right)^p \left(\frac{fQ}{HB 2bR} \right)^n = \varphi_0^{n+1,5} \frac{d\varphi_0}{ds}. \quad (1.8)$$

or

$$\frac{2c_W}{5\Delta} \left(\frac{VR}{v} \right)^p \left(\frac{fQ}{HB2bR} \right)^n ds = \varphi_0^{n+1,5} d\varphi_0. \quad (1.9)$$

This is an ordinary differential equation with separating variables. Integrate equation (1.9) to obtain:

$$\frac{\varphi_0^{n+2,5}}{n+2,5} = \frac{2c_W}{5\Delta} \left(\frac{VR}{v} \right)^p \left(\frac{fQ}{HB2bR} \right)^n s + C. \quad (1.10)$$

Assuming that the contact angle $\varphi_0 = 0$ at the initial moment of the wear process ($s = 0$), the integration constant $C = 0$.

Thus, the dependence of the contact angle on the friction path takes the form:

$$\varphi_0 = \left[\frac{(n+2,5) 2^{1-n} c_W}{5\Delta} \left(\frac{VR}{v} \right)^p \left(\frac{fQ}{HB bR} \right)^n s \right]^{\frac{1}{n+2,5}}. \quad (1.11)$$

Or finally, taking into account dependence (1.5), the calculation formula for dependence of the maximum wear u_W in the sliding bearing on the magnitude of the friction path s will be:

$$u_W = \Delta \left[\frac{(n+2,5) 2^{1-n} c_W}{5\Delta} \left(\frac{VR}{v} \right)^p \left(\frac{fQ}{HB bR} \right)^n s \right]^{\frac{2,5}{n+2,5}}. \quad (1.12)$$

In the obtained formula (1.12), the wear resistance parameters C_W , n , p show the degree of influence of the determining factors of the bearing wear process. As a rule, their numerical values are determined experimentally by laboratory tests. On the one hand, these tests will not be cumbersome with the use of geometrically simple specimens and on the other hand, the test

conditions tend to be as close as possible to the actual unit operating conditions in order to obtain a more adequate wear model. Further, the procedure for calculating wear resistance parameters from the results of laboratory wear tests is considered for a complete identification of formula (1.12).

1.2.2. Identification of wear resistance parameters for the method of wear test by the "cone – three balls" scheme

Balls, cylinders, rollers, rectangular prisms, etc. were used in laboratory tests as specimens. Here, it was proposed to use the "cone – three balls" scheme of test to determine wear characteristics. Standard 12.7 mm diameter steel balls made of steel SH15/1.3505 were used as control specimens. A conical specimen of a corresponding bearing material was used as a test specimen. Conical specimens are easily prepared and are characterized by the wear spot dimensions changing during the test. The change of the wear spot leads to a change of contact pressures which makes it possible to obtain a set of test results by the load characteristics without changing the external load on the conical specimen. Below, a calculation and experimental procedure for identifying wear resistance parameters C_w , n , p in the model of wear (1.1) for testing by the "cone – three balls" scheme is considered.

The calculation "cone – three balls" test scheme is shown in Fig. 1.3. Three balls 1, 2, 3 of the same radius R are situated on the plane so that their centers form an equilateral triangle $O_1O_2O_3$. The cone 4 with vertex angle γ is contacting the lower placed balls at points $A_1A_2A_3$. Force Q applied to the cone is transmitted to the lower balls along perpendiculars to the cone generatrix with equal forces $Q_1 = Q_2 = Q_3$.

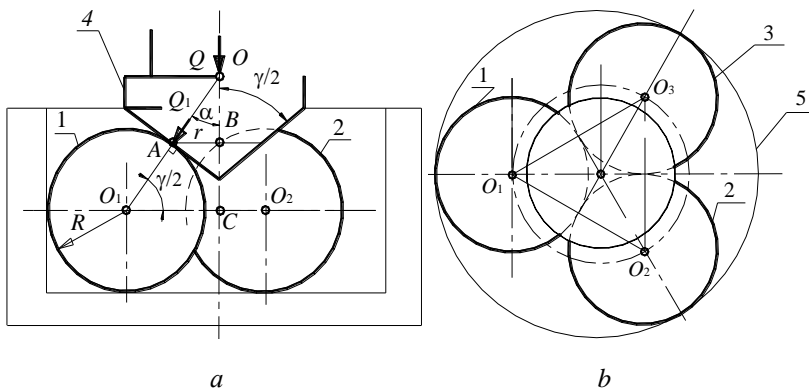


**Fig. 1.3. The calculation "cone – three balls" test scheme:
front view (a); top view (b)**

The cage 5 ensures immobility of the balls under action of loading from the vertical force and a moment around the vertical axis.

The forces acting on the balls are expressed through a common force by the relation:

$$Q_1 = Q_2 = Q_3 = \frac{Q}{3 \cos(\gamma / 2)}. \quad (1.13)$$

To determine linear sliding velocity of the cone on the balls, it is necessary to know the distance r from the cone rotation axis to the points of contact with the balls.

From similarity of the triangles OO_1C and OAB , the following is obtained:

$$r = O_1C \left(1 - \frac{R}{OO_1} \right). \quad (1.14)$$

The value of O_1C is defined as the radius of the circle circumscribed around the regular triangle $O_1O_2O_3$:

$$r = O_1C \left(1 - \frac{R}{OO_1} \right).$$

Then from a right-angled triangle (Fig. 1.3):

$$OO_1 = \frac{O_1C}{\cos \gamma / 2} = \frac{2\sqrt{3}R}{3 \cos \gamma / 2}.$$

After intermediate substitutions, the following is obtained:

$$r = R \left(\frac{2\sqrt{3}}{3} - \cos(\gamma / 2) \right). \quad (1.15)$$

Take the shape of the worn-out cone surface as a circular groove with a profile radius a . Assume also that the contact pressure under the rigid wear-free ball is evenly distributed over the worn-out cone surface. Then the following relation holds:

$$\sigma = \frac{Q_1}{\pi a^2}. \quad (1.16)$$

The relation of the maximum wear u_w with dimensions of the wear spot a is determined from the geometry of contact of the conjugated cone of radius R with a cylinder of radius r . With a sufficient accuracy, the sought dependence is represented as:

$$u_W(S) = \frac{a(S)^2}{2R^*}, \quad (1.17)$$

where R^* is the equivalent radius in the cone - ball contact:

$$R^* = \frac{Rr}{R + r}.$$

In determining wear resistance parameters, use equivalent radius of the ball - cone contact in the model of wear resistance (1.1) instead of the bearing radius.

Represent the experimental dependence of the radius of a circular groove worn out in the cone as a power approximation:

$$a(S) = cS^\beta, \quad (1.18)$$

where c and β are the approximation parameters determined from the results of the wear tests.

Integrate the regularity of wear (1.1) to obtain an integral form of the model of cone wear:

$$u_W(S) = C_W \int_0^S \left(\frac{f\sigma(S)}{HB} \right)^n \left(\frac{VR^*}{v} \right)^p dS. \quad (1.19)$$

Substitute the expression for wear (1.17) in the left side of the obtained dependence and the expression for the contact pressure (1.16) in the right-hand side to obtain:

$$\frac{a^2(S)}{2R^*} = C_W \int_0^S \left[\left(\frac{fQ_1}{\pi \bar{a}^2(S)} \right) \frac{1}{HB} \right]^n \left(\frac{VR^*}{v} \right)^p dS, \quad (1.20)$$

or taking into account (1.18) and integrating along the friction path, the following is obtained:

$$\frac{c^2 S^{2\beta}}{2R^*} = C_W \left(\frac{fQ_1}{c^2 \pi HB} \right)^n \left(\frac{VR^*}{v} \right)^p \frac{S^{1-2\beta n}}{1-2\beta n}. \quad (1.21)$$

From the condition of satisfiability of equation (1.21) for all values of S , it follows that:

$$2\beta = 1 - 2\beta n, \quad (1.22)$$

whence:

$$n = \frac{1 - 2\beta}{2\beta}. \quad (1.23)$$

To determine parameter p , tests should be carried out at two values of the sliding velocity V_1 and V_2 from which two groups of experimental data with approximating functions are obtained:

$$a_1 = c_1 S^\beta; a_2 = c_2 S^\beta. \quad (1.24)$$

Consider the problem of determining parameters of wear according to the results of testing specimens with the contact spot a ($1.S$) changing in the process of wear. The change of the wear spot causes the change in the values of the contact pressures σ ($1.a$). The exponent n in expression (1.1) characterizes the rate of change of contact pressures during wear. It is directly related to the exponent β of the experimental dependence (1.18) which, accordingly, characterizes the rate of change of the contacting spot during wear. The relationship between n and β in the accepted wear regularity (1.1) is uniquely described by relation (1.23). Since the sliding velocity V in the considered ratios does not depend on the friction path S , it does not affect parameters n and β during the tests. In this case, the change in the slip velocity V affects just the scale factor C_w in expression (1.1). The above reasoning is confirmed by the test results.

Substitute expressions (1.24) into (1.21) and obtain a system of equations:

$$\left. \begin{aligned} \frac{c_1^2 \beta}{R^*} &= C_w \left(\frac{fQ_1}{c_1^2 \pi HB} \right)^n \left(\frac{V_1 R^*}{v} \right)^p; \\ \frac{c_2^2 \beta}{R^*} &= C_w \left(\frac{fQ_1}{c_2^2 \pi HB} \right)^n \left(\frac{V_2 R^*}{v} \right)^p. \end{aligned} \right\} \quad (1.25)$$

Divide the first equation by the second and obtain the following after transformations:

$$(c_1 / c_2)^{2n+2} = (V_1 / V_2)^p. \quad (1.26)$$

whence:

$$p = (2n + 2) \frac{\lg(c_1 / c_2)}{\lg(V_1 / V_2)}. \quad (1.27)$$

To determine coefficient K_w , use one of the equations (1.25):

$$C_w = \frac{\beta c_1^{2n+2}}{R^*} \left(\frac{3\pi HB \cos \alpha}{fQ} \right)^n \left(\frac{v}{V_1 R^*} \right)^p. \quad (1.28)$$

Thus, the calculation-experimental procedure for identifying wear resistance parameters for the "cone – three balls" scheme of wear test based on the two-factor wear model of the sliding bearing (contact pressure, sliding velocity) was proposed.

1.2.3. Experimental setup and the test procedure

The experimental setup for the "cone – three balls" scheme of testing is shown in Fig. 1.4.

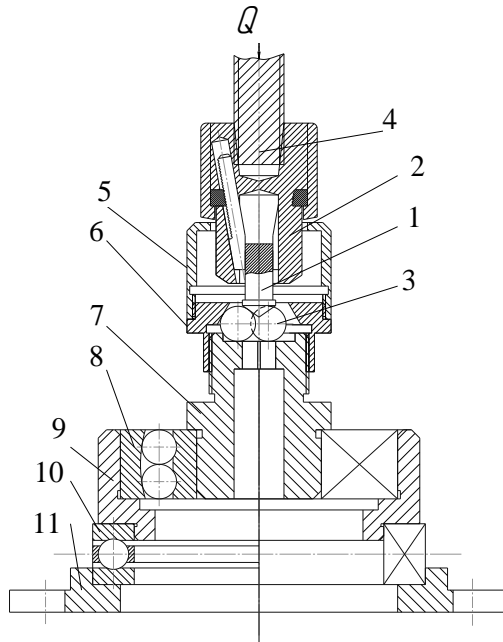


Fig. 1.4. The experimental setup

The test specimen 1 with a hardened conical surface is fixed in a universal self-centering drilling chuck 2. The specimen 1 is pressed with a vertical load Q onto the lower placed balls made of a ball bearing steel and is given a rotational motion from the spindle 4 of the experimental setup. The control ball specimens 3 are placed on the flat hardened surface of the

support 7 and are centered by a special nut 6 with a conical working surface. Before testing, the cup 5 is filled with lubricant. A two-row self-centering bearing 10 located in the bottom housing 11 of the setup is used for self-adjustment of the specimens.

The tests were carried out under the following conditions.

The vertical load acting on the conical specimen was taken equal to $Q = 100$ N. The forces transmitted to the lower balls along the normal were determined from formula (1.2):

$$Q_1 = \frac{Q}{3 \sin 55^\circ} = 40,6 \text{ N.}$$

The cone angle of the conical sample was $\gamma = 110^\circ$. Diameter of the lower control ball specimens was $D = 12.7$ mm. The radius of the circular slipping path of the conical sample over the balls was calculated by formula (1.4):

$$r = R \left(\frac{2\sqrt{3}}{3} - \cos(\gamma/2) \right) = 3,68 \text{ mm.}$$

The equivalent radius of the ball – cone contact will be $R^* = 2.35$ mm.

The tests were carried out at two rotation velocities of the setup spindle: $n_1 = 500 \text{ min}^{-1}$ and $n_2 = 1000 \text{ min}^{-1}$. These rotation velocities corresponded to linear sliding velocities for the conical sample:

$$V_1 = \frac{\pi r n_1}{30} = \frac{3,14 \cdot 3,68 \cdot 500}{30} = 192 \text{ mm/s;}$$

$$V_2 = \frac{\pi r n_2}{30} = 384 \text{ mm/s.}$$

The conical samples were made of tin-phosphorous bronze CuSn10P having hardness $HB = 90$ MPa. The balls were made of ball-bearing steel SH15/1.3505. The samples were lubricated with engine oil Magnum 15W - 40 (TNK, Ukraine) having kinematic viscosity $\nu = 40 \text{ mm}^2/\text{s}$ at the operating temperature. Friction coefficient of bronze rubbing against lubricated steel was taken $f = 0.08$.

The cone wear in the form of an annular groove on its generatrix was measured by the width of the worn-out groove using an МБС-10 microscope with an accuracy of 0.05 mm. A special device (Fig. 1.5) for locating the conical sample in the measurement plane was used in measurements. The cone generatrix of the sample 1 was arranged parallel to the table of microscope 4 by turning the bracket 2 relative to the body 3 of the device.

The depth of the worn-out groove was taken as the maximum normal wear of the bushing. The degree of wear can be calculated from the width of the worn-out groove according to geometric relationships if the shape of the groove profile is admitted to be circular.

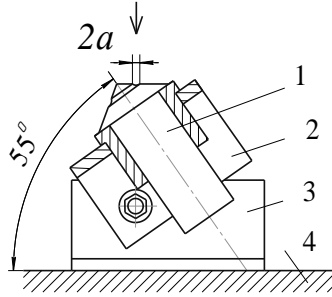


Fig. 1.5. The scheme of cone specimen holder for measuring width of the worn-out groove

To determine shape of the worn surface and the amount of linear wear u_w , a projector with a $\times 77$ magnification on the screen was used (Fig. 1.6).

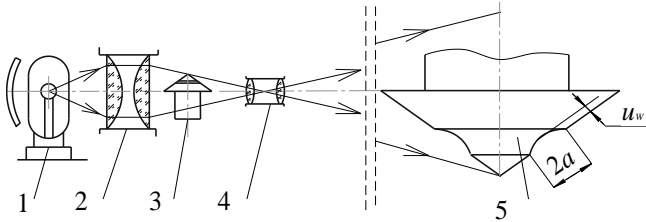


Fig. 1.6. Scheme of measuring the shape and depth of the worn surface: lighting lamp (1); lens (2); specimen (3); condenser (4); projection of the specimen on the screen (5)

Analysis of the worn out groove profile at a $\times 77$ magnification by the projector confirms its maximum closeness to a circular shape with a diameter equal to the ball diameter $D = 12.7$ mm. Thus, the amount of wear during testing depending on the width of the wear groove can be calculated from the above formula (1.6).

For example, a bronze specimen was tested under load $Q = 100$ N at sliding velocity $V = 0.19$ m/s and friction path $S = 342$ m. During the measurements, the depth of the worn-out groove on the projector screen was 12 mm, or $12/77 = 0.15$ mm taking in account the $\times 77$ magnification. The groove width was $2a = 205/77 = 2.66$ mm, respectively. The amount of wear

calculated from formula (1.6) depending on the half-width of the groove, was $u_w = 0.14$ mm. That is, discrepancy between the measured and calculated values did not exceed 7 % which permits the use of the calculated dependence of the depth of the groove of a circular profile on the groove width.

During the tests conducted to determine the wear resistance parameters, the wear values were measured every 10 minutes at a sliding velocity of 0.19 m/s and every 5 min at a sliding velocity of 0.38 m/s.

1.2.4. The results of sliding bearings wear tests and calculations

To determine wear resistance parameters C_w , n , p of the model (1.1) of the plain bearing wear, conical specimens of bronze CuSn10P were tested. For statistical representativeness, each test cycle was carried out for 3 identical specimens. The averaged values obtained in measuring width of the worn-out groove are shown in Table 1.2. The value of the coefficient of variation characterizing scatter of the obtained measurement results was in the range $v = 0.15...0.2$ which indicates sufficient homogeneity of the experimental sample.

Table 1.2

Results of measuring width of the wear groove and calculating the wear depth

S , m	$V_1 = 0.19$ m/s		$V_2 = 0.38$ m/s	
	a , mm	u_w , mm	a , mm	u_w , mm
115	0.4	0.01	0.45	0.012
231	0.45	0.012	0.475	0.016
346	0.465	0.014	0.55	0.018
462	0.55	0.016	0.6	0.026
577	0.55	0.019	0.625	0.031
693	0.6	0.021	0.675	0.036

Graphical interpretation of the test results, that is, the dependence of the half-width of the wear spot and their power approximation are shown in Fig. 1.7. Fig. 1.7 also shows the power approximation with parameters and the magnitude of veracity of approximation R .

Thus, to determine the parameter of influence of the slip velocity on the wear resistance p , the following parameters of approximating functions of the form (1.24): were obtained: $c_1 = 0.0337$; $c_2 = 0.0376$; $\beta_1 \approx \beta_2 = \beta = 0.21$.

Further, calculate the wear resistance parameters C_w , n , p using formulas (1.23), (1.27), (1.28).

As a result of calculation when testing steel sliding on bronze, parameters of wear resistance were obtained: $n = 1.38$; $p = 0.68$; $C_w = 9.625 \cdot 10^{-9}$.

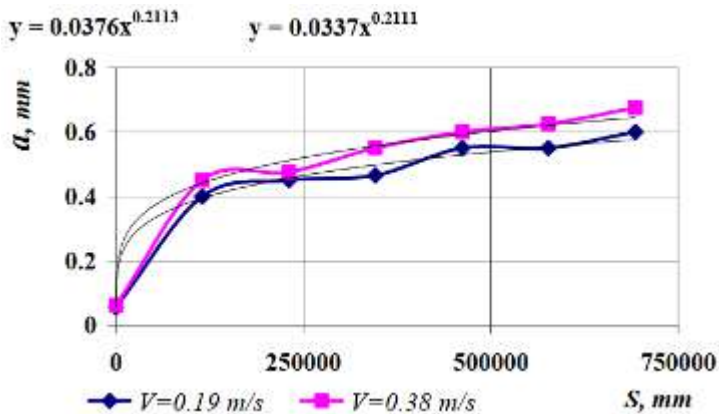


Fig. 1.7. Dependences of the half-width of the wear spot on the friction path and their power approximations

Using a similar procedure, wear resistance parameters for other bearing materials (brass, aluminum alloys) can be determined and used for a calculation assessment of the plain bearing wear. At the same time, using the averaged initial data characteristic for the working conditions of sliding bearings, these results can be used as normative parameters of wear resistance. To obtain values of the wear resistance parameters as close as possible to the real operating conditions, it is necessary to conduct laboratory tests according to the proposed scheme under specified conditions.

The following is an example of calculating wear of a sliding bearing with the found parameters of wear resistance.

Calculation will be carried out for materials of a friction pair "steel - bronze". Radial load on the bearing $Q = 500$ N; hardness of bronze CuSn10P $HB = 90$ MPa; width and radius of the bearing: $b = 20$ mm, $R = 20$ mm; radial clearance $\Delta = 0.1$ mm. Lubricant Magnum 15W-40 oil (TNK, Ukraine) was used with viscosity $\nu = 40$ mm²/s; coefficient of friction $f = 0.08$. Sliding velocity was assumed equal to 1 m/s which corresponds to the rotation frequency of the bearing shaft 475 min⁻¹. The initial data were substituted into the formula for calculating wear (1.12) and the results of calculating wear as a function of the friction path are presented in Table 1.3.

Table 1.3

Results of calculating wear u_w of the sliding bearing as a function of friction path S and working time t

S , km	10	10^2	10^3	10^4
t , hr	1.5	15	150	1500
u_w , mkm	4	17	76	338

Beside calculation of wear for the specified lifetime, dependence (1.12) allows one to analyze effect of design and operation parameters of bearings on their wear. This makes it possible to select optimal parameters of bearings at the stage of design preparation of the machine by the criterion of maximum wear resistance. Fig. 1.8 shows the graphs of influence of sliding velocity and load on the bearing wear obtained from the dependence (1.12).

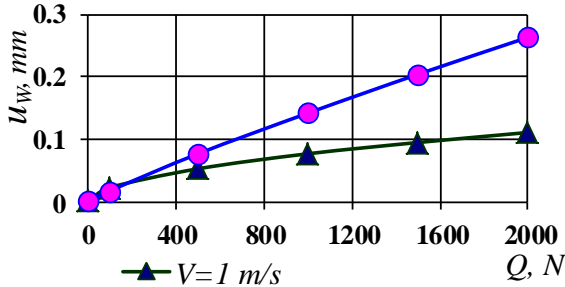


Fig. 1.8. Effect of sliding velocity and load on wear of the slide bearing

Analysis of the obtained results has shown that all obtained dependences for the bearing wear were nonlinear. This is because of the type of the obtained calculated dependence (1.12). Such a character of influence of determining factors is caused by the features of geometry of the sliding bearing when the contact spot (contact arc) changes during the wear process which leads to a change in the contact pressures and, correspondingly, the wear rate. Besides, the proposed wear model in a nonlinear form (1.1) with wear resistance indexes n and p can adequately take into account almost all wear mechanisms including abrasive wear at $n = 1$. The calculated values of wear are consistent with the operational data of the sliding bearing wear.

1.2.5. Results obtained in computational and experimental modeling of cylindrical plain bearings wear

The resulting calculation model (1.12) for estimating wear of sliding bearings assumes a simple algorithm for obtaining wear values from the friction path under given operation conditions. This was achieved through the use of certain assumptions in solution of the wear-contact problem. Firstly, a uniform distribution of contact pressures over the wear spot was taken for average values. Secondly, difficult for integral-differential transformations trigonometric dependence of wear on the contact angle (1.3) was approximated by plain power dependence (1.5). As a rule, known solutions require numerical algorithms to overcome mathematical difficulties. At the same time, in solving the problem, this approach has allowed us to use a nonlinear model of wear

from the determining factors (1.1) which adequately describes the actual wear processes. It is impossible to obtain numerical results using formula (1.12) without the values of the wear parameters C_w , n , p . That is, the wear model (1.12) can be applied in practice if an algorithm for determining parameters of this regularity is known. It is the parameters that enable quantitative estimation of the effect of determining factors (pressure and slip velocity). The wear parameters can only be established by the test results which makes the model approximated to the real tribosystem operation conditions.

The procedure for determining parameters of wear models was developed based on solution of an inverse wear-contact problem. In this case, dependences for calculating parameters (1.23), (1.27), (1.28) were obtained according to the adopted mathematical form of the wear law (1.1), the equilibrium condition (1.16), the geometric condition of continuity in the contact (1.17) and the wear test results. In this process, a proper choice of scheme of laboratory wear tests is very important. The scheme to be chosen for the tests should be one which mostly corresponds to the real tribounit as to its geometric and technological features. For example, the widely used four-ball test scheme is suitable for the tribounits in which a linear or dot contact takes place (toothed drives, cam mechanisms). For the conjunctions in which the contact spot is commensurable with the dimensions of the contacting bodies (slide bearings, ball bearings), it is preferable to use the proposed "cone – three balls" scheme more adequately corresponding to the actual contact.

Besides, it is advisable to use schemes when the contact pressure changes during the test due to a change in the wear spot which allows one to have results for the pressure range from the results of tests of one specimen. In particular, the proposed "cone – three balls" scheme applies to this test scheme.

As a result, based on the obtained model of bearing wear, one can:

- predict bearing wear under various conditions on contact pressures and sliding velocities at the stage of design calculation of the friction unit;
- optimize design and operation parameters of the friction unit by the wear criteria.

The proposed approach does not ensure absolute correspondence to the actual course of the wear process but is an indispensable step in development of computational engineering methods for predicting wear resistance of friction units. Further studies in this direction should be carried out by extending the proposed methodology to other friction units of machines and the corresponding schemes of laboratory wear tests.

Conclusions

1. A model of wear of a sliding bearing in conditions of boundary friction was proposed in a form of a nonlinear dependence of the wear rate

on the determining factors, i.e. contact pressure and sliding velocity. The wear model was presented in a form of dimensionless complexes taking into account geometric, kinematic, friction and lubrication characteristics of sliding bearings.

2. The wear-contact problem for cylindrical sliding bearings was solved. The dependence for average pressures in the bearing and the approximating function of linear wear on the contact arc were used as determining equations. The closed-form solution was obtained as a dependence of wear on the friction path.

3. A calculation-experimental procedure for identifying parameters of wear resistance for the wear tests by the "cone – three balls" scheme was developed based on the two-factor model of wear. Calculation dependences were obtained based on solution of an inverse wear-contact problem for a cylindrical sliding bearing with the results obtained in wear tests of conical bronze specimens with a variable wear spot and two sliding velocities taken as a base.

1.3. Direct wear-contact task for radial sliding bearing

In many energy and transport vehicles (internal combustion engines, turbines, cars, etc.), plain bearings are one of the main components that determine the durability and reliability of the machine as a whole. Analysis of the current state of methods for calculating and designing sliding bearings shows that they are lagging behind the general level and requirements. Therefore, for engineering applications, it is advisable to use approximate approaches. In this direction there is a small number of studies presented below.

In paper [31] using a generalized cumulative wear model, the tribo-contact problem has been solved for a sliding bearing, the shaft of which has small contour lobing with various forms. The effect of lobing on the bearing life has been investigated at the complete single-area and mixed-area contact. It has been found that the ovality and trilobing of the shaft promote a rise in the service life. Features of this effect are presented graphically.

The evolution of contact pressure is analyzed in paper [32] during the wear of a thrust sliding bearing following the law of nonlinear wear. The coating's deformation properties are described using the nonlinear Winkler model. It is demonstrated that steady wear can exist with a definite contact pressure distribution.

In article [33] the problem of simultaneous wear of an elastic cylinder and a cylindrical notch surface in an elastic space is discussed (in the planar formulation). The contact problem formulation omits the limitation of the contact area. The contact is solved in steps; the linear wear and contact parameters of the shaft and bush are solved at each step in time. The Multopp-Kalandia method is applied to the solution of the contact problem.

The constructed model is used to investigate the evolution of contact pressure and form changes of the shaft and bush in the process of wear.

The parameter of the wear law of bronze coupled with steel under dry friction is identified by comparing the results of mathematical modeling with experimental data [34]. The wear tests were carried out according to the steel-ball–flat-bronze sample scheme under relative reciprocal sliding of the tested samples. The modeling of the wear of the sample was based on asymptotic behavior of the solution of the corresponding wear-contact problem. The effectiveness of using this asymptotic behavior to identify the wear law based on the tribological test results has been demonstrated.

Based on pin-on-disk friction and wear testing, the parameters of the wear rate as a function of sliding velocity and pressure with account for their distribution over the contact spot are computed in paper [35]. The parameters are compared to those obtained assuming a uniform distribution of velocities and pressures. It is assumed in the work that the contact spot does not vary, the disk does not wear out, and the study is carried out under steady-state wear conditions.

The kinetics of sample wear on a four-ball friction-testing machine using various lubricants is analyzed in [36]. It is shown that the growth of the contact-patch area on the balls obeys the kinetic second-order equation, which, within the limits, corresponds to catastrophic wear. The linear wear rates and the strain level of the ball material in different lubricating media are estimated.

The article [37] employs an adaptive wear modeling method to study the wear progress in radial sliding bearings contacting with a rotary shaft. Mixed Lagrangian–Eulerian formulation has been used to simulate the contact condition between the bearing and the shaft, and the local wear evolution is modeled using the Archard equation. In the developed wear processor algorithm, not only remeshing is performed on the contact elements, but also is executed for their proximity elements. In this way the wear simulation becomes independent of the size of the contact elements. Validation was done for a laminated polymeric composite bearing. The composite has been modeled as a linear orthotropic material. The wear coefficients were obtained from flat-on-flat experiments and were applied as pressure and velocity dependent parameters in the wear processor. Finally, the effect of the clearance on the wear of the radial bearings has been studied numerically. The simulations also demonstrate how the contact pressure evolves during the wear process, and how the clearance influences this evolution.

In our works [38–40], we have proposed experimental design approaches for solving wear-contact problems for sliding bearings. On the basis of direct and inverse wear-contact tasks, algorithms are presented for calculating bearing wear and identifying the parameters of their wear laws. At the same time there are difficulties in the engineering implementation of the solutions obtained.

Therefore, for practical use, algorithms for calculating the service life of bearings using simple algebraic dependencies and formulas are necessary.

Under the wear contact task is the task of determining the magnitude of the maximum linear wear in a bearing, depending on the friction path. The structural data, load, kinematic parameters of the bearing, as well as the wear law with the parameters of wear resistance are taken as the initial data.

Cylindrical sliding bearings represent the internal contact of two cylinders of similar radii with a radial clearance Δ (Fig. 1.8). The shaft of radius R_1 of the bearing is loaded with force Q and performs rotational movement with sliding speed V along sleeve 2 with radius R . In the process of force interaction of the shaft and bearing sleeve, a contact pressure σ appears along the contact arc $2\phi_0$ in the place of contact of two cylinders.

It is assumed that the wear resistance of the shaft is much greater than the wear resistance of the sleeve (straight friction pair). During operation, an arc zone is formed on the inner surface of the sleeve, with a maximum value at the center of contact u_w .

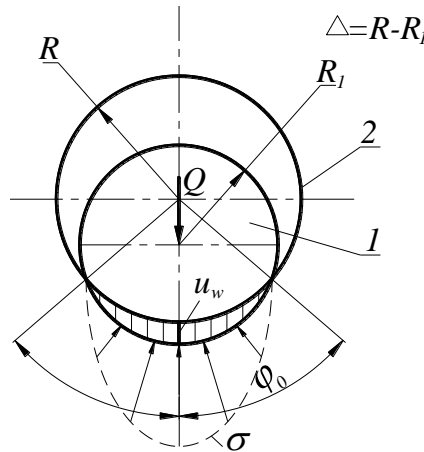


Fig. 1.8. The design scheme of the cylindrical sliding bearing

For an analytical solution of the problem of calculating the wear of a sliding bearing, the mathematical form of the law of wear is taken as the initial value. The representation of such laws as a dependence of the wear rate on the determining parameters of the process (contact pressure, sliding speed, temperature, etc.) is widely used. In our case, the law (model) of wear is adopted in the form of a dimensionless complex of determining factors: for an analytical solution of the problem of calculating wear of a sliding bearing, the mathematical form of the law of wear is taken as the initial

value. The representation of such laws as a dependence of the wear rate on the determining parameters of the process (contact pressure, sliding speed, temperature, etc.) is widely used. In our case, the law (model) of wear is adopted in the form of a dimensionless complex of determining factors:

$$\frac{du_w}{dS} = K_w f \left(\frac{\sigma(\varphi_0)}{E} \right)^m \left(\frac{V\Delta}{a} \right)^n, \quad (1.29)$$

where u_w is the bearing wear;
 S is the friction path;
 f is the coefficient of friction in a pair of shaft-sleeve;
 σ is the normal contact pressure;
 E is the modulus of elasticity of the sleeve material;
 V is the sliding speed;
 R is the radius of the bearing (sleeve);
 a is the coefficient of thermal diffusivity of the bearing material;
 K_w, m, n are the wear resistance parameters;
 φ_0 is the half angle of the contact shaft and sleeve

To calculate the maximum wear we use the values of the maximum contact pressure. With a known contact angle, the maximum contact pressures can be determined by the formula:

$$\sigma_0 = \frac{Q}{bR_1} \frac{1 - \cos \varphi_0}{\varphi_0 - \sin \varphi_0 \cos \varphi_0}. \quad (1.30)$$

We use the approximate decomposition of trigonometric functions in the series:

$$\sigma_0 = \frac{Q}{bR_1} \frac{1 - 1 + \frac{1}{2}\varphi_0^2}{\varphi_0 - \left(\varphi_0 - \frac{1}{6}\varphi_0^3 \right) \left(1 - \frac{1}{2}\varphi_0^2 \right)} \cong \frac{3Q}{4bR_1\varphi_0}, \quad (1.31)$$

where Q is the bearing load;
 b is the width of the contact shaft and sleeve.

The relationship between maximum wear u_w and the contact angle is determined from the geometry of the internal contact of two cylinders with a radial initial clearance Δ according to:

$$u_w = \Delta \left(\frac{1}{\cos \varphi_0} - 1 \right). \quad (1.32)$$

Where the contact angle is determined:

$$\varphi_0 = \arccos\left(\frac{\Delta}{u_w + \Delta}\right). \quad (1.33)$$

More convenient approximate algebraic formulas for determining the contact angle are possible. Formula (1.33) by decomposition of the cosine in a power series and discarding the members of the highest order of smallness is reduced to the form:

$$\varphi_0 = \left(\frac{2u_w}{u_w + \Delta}\right)^{\frac{1}{2}} 2 = \left(\frac{2}{1 + \Delta/u_w}\right)^{\frac{1}{2}} = \left(\frac{2(u_w/\Delta)}{u_w/\Delta + 1}\right)^{\frac{1}{2}}. \quad (1.34)$$

From (1.33) in the decomposition of the cosine:

$$\cos \varphi_0 = 1 - \frac{1}{2} \varphi_0^2 = \frac{\Delta}{u_w + \Delta};$$

$$\varphi_0 = \left(\frac{2u_w}{u_w + \Delta}\right)^{\frac{1}{2}}$$

Expression (1.33) can be inverted and presented as a secant:

$$\sec \varphi_0 = \frac{u_w + \Delta}{\Delta} = \frac{u_w}{\Delta} + 1$$

or

$$\sec \varphi_0 = 1 + \frac{1}{2} \varphi_0^2 = \frac{u_w}{\Delta} + 1,$$

$$\varphi_0 = \left(2 \frac{u_w}{\Delta}\right)^{\frac{1}{2}}. \quad (1.35)$$

From the fact that (1.34) goes into (1.35) with small displacements, it follows that expression (1.35) is more accurate. And the decomposition of the secant with the same number of members is less accurate than the decomposition of the cosine. This is confirmed by a numerical estimate of the accuracy of determining the contact angle using formulas (1.33), (1.34), and (1.35). Comparison results for different u_0/Δ are presented in Table 1.4.

Table 1.4

Comparison of the results of calculating the angle for different formulas

u_0 / Δ Formulas	0,1	0,5	1,0	1,5	2,0
(1.33)	24,62	48,19	60	66,42	70,53
(1.34)	24,43	46,78	57,3	62,76	66,16
(1.35)	25,62	57,3	81,03	99,24	114,6

From the numerical comparison it follows that the calculations by the formula (1.35) obtained by the decomposition of the secant are close to the calculations by the original formula (1.35) only at angles not exceeding 20° .

From formula (1.35), the dependence for wear on the contact angle in a bearing will look like:

$$u_w = \Delta \frac{\varphi_0^2}{2}. \quad (1.36)$$

The resulting expression (1.36) is differentiated along the path of friction and together with expression (1.31) we substitute into (1.29). As a result, we get:

$$\Delta \varphi_0(S) \frac{d\varphi_0}{dS} = K_w f \left(\frac{3Q}{4bR_1 \varphi_0(S) E} \right)^m \left(\frac{V\Delta}{a} \right)^n. \quad (1.37)$$

Or:

$$\Delta \varphi_0^{m+1} d\varphi_0 = K_w f \left(\frac{3Q}{4bR_1 E} \right)^m \left(\frac{V\Delta}{a} \right)^n dS. \quad (1.38)$$

This is an ordinary differential equation with separable variables. After integrating equation (1.38), we obtain:

$$\frac{\varphi_0^{m+2}}{m+2} = \frac{K_w f}{\Delta} \left(\frac{3Q}{4bR_1 E} \right)^m \left(\frac{V\Delta}{a} \right)^n S + C. \quad (1.39)$$

If we assume that in the initial period of time $S = 0$ the contact angle is zero $\varphi_0 = 0$, then the integration constant $C = 0$.

Thus, the dependence for the contact angle will take the form:

$$\varphi_0 = \left(\frac{(m+2)K_w f}{\Delta} \left(\frac{3Q}{4bR_1 E} \right)^m \left(\frac{V\Delta}{a} \right)^n S \right)^{\frac{1}{m+2}}. \quad (1.40)$$

Finally, taking into account expression (1.36), the calculation formula for maximum wear in a sliding bearing, depending on the friction path, will take the form:

$$u_w = \frac{\Delta^{\frac{2n-1}{m+2}}}{2} \left((m+2)K_w f \left(\frac{3Q}{4bR_1 E} \right)^m \left(\frac{V}{a} \right)^n S \right)^{\frac{2}{m+2}}. \quad (1.41)$$

The obtained dependence for the calculation of wear allows you to analyze the effect on wear of structural and operational parameters of bearings. This makes it possible to choose the optimal parameters of the bearings at the stage of design preparation of the machine according to the criterion of maximum wear resistance.

Example of calculating the wear of a sliding bearing.

We take the following initial data:

1. Clearance in bearing $\Delta = 0.05$ mm;
2. Wear resistance parameters: $K_w = 1.76 \cdot 10^{10}$; $m = 1.58$; $n = 1.14$;
3. Coefficient of friction $f = 0.05$;
4. Normal bearing load: $Q = 100 \dots 500$ N;
5. Bearing working width $b = 15$ mm, bearing radius $R_1 = 25$ mm;
6. The modulus of elasticity of bronze $E = 1.15 \cdot 10^5$ MPa;
7. Sliding speed in bearing $V_1 = 1$ m/s, $V_2 = 3$ m/s;
8. Coefficient of thermal diffusivity of bronze $a = 110$ m²/s;
9. Bearing life $T = 100$ h ($S = 10^8$ mm).

The results of the calculation of wear as a function of loading and sliding speed are shown in Fig. 1.10.

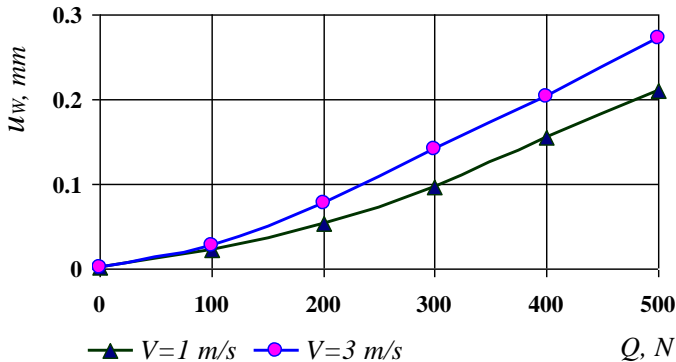


Fig. 1.10. The wear as a function of loading and sliding speed in sliding bearing

It is shown that the calculated estimate of wear of friction units is difficult due to the complexity of the interaction processes of the elements

of the tribosystem. Nonlinearity of wear processes leads to mathematical difficulties in the construction of wear models. The paper proposes an approximate method for solving a direct wear-contact problem for a sliding bearing. The calculation was carried out for maximum contact pressures at the center of the wear area. Trigonometric functions in the solution process were replaced by approximate power series expansions. An example is given of the numerical implementation of the obtained closed formula for calculating the wear of a sliding bearing.

1.4. Variational approach for determining tribocontact parameters of sliding bearings

1.4.1. Fundamentals of the variational approach in contact mechanics

Bearings of sliding are one of the most important structural elements of machines and devices and make up the main part of friction units. Technological failures are usually due to bounce of the bearings (along with the failures of other nodes) and thus limit the durability of the machine as a whole. Bearings of sliding, depending on the type of lubrication, operate in conditions of limiting and liquid friction. With limiting lubrication, the surfaces of the shaft and the bearing touch fully or in areas of great length. There is no layer of oil separating the surface. The lubricant is on metal surfaces in the form of an adsorbed film. In practice, the methods of calculating bearings are used when wearing only the bearing (direct friction pair), only the wear of the shaft (the reverse friction pair) and simultaneous wear of the shaft and bearing (mixed friction pair). When creating reliable friction units of machines, there is a need for calculations of contact pressures and stresses in the contact area. Calculations are numerical implementations of mathematical models, corresponding processes and states. Mathematical models of contact interaction consist of calculation schemes, state equations and boundary conditions. The basis of the estimated estimation of wear of bearings of sliding is the solving of wear of contact tasks [41–45]. In this paper, a variational-experimental approach was used to determine the contact pressure in the bearing.

The variational-experimental approach [41] is characterized by the introduction into the functional of the experimental dependence. Minimizing the functionality is looking for a solution according to this experiment. The contact problem of the theory of elasticity leads to a joint solution of a system of two equations: continuity and equilibrium:

$$\int_a^b \sigma(s)k(x-s)ds = f(x),$$

$$Q = \iint \sigma(x, y)dxdy.$$

The traditional way of solving the main part is to solve the integral equation of continuity, using the equilibrium condition as a limitation. This function is supposed to be known from the geometry of contacting bodies. The basis of the variational approach is that, as the basic equation for solving the contact problem, we take the integral equation of continuity rather than the equilibrium condition. In essence, this is also an integral equation, since an unknown function is under the integral sign. But this is an integral equation of a special type.

Next, the procedure consists in transforming the left side of the equation of equilibrium from a constant into a function. To do this, it is assumed that the experiment can find a function:

$$Q = cu_0^n,$$

where u_0 is the maximal normal movement in contact.

This function reflects the entire load process, not just one process point. After substitution:

$$cu_0^n = \iint \sigma(x, y) dx dy,$$

get the condition of equilibrium at any moment of loading.

The function of contact pressures can be obtained from the following expression, which reflects the mismatch of the experiment and the desired function:

$$\varepsilon = cu_0^n - \iint \sigma(x, y) dx dy,$$

The result is a quadratic functional of the contact problem:

$$F = \int_0^{u_0} \left[cu_0^n - \iint \sigma(x, y) dx dy \right]^2 du_0.$$

The traditional formulation of the contact problem contains two equations: continuity and equilibrium, and two unknown functions of the pressure $\sigma(x)$ and size of the contact area $a(Q)$. In the presence of an experimental dependence $a(Q)$, the dimensions of the contact area are known and the conditions of continuity are satisfied automatically.

The task minimization procedure is performed traditionally using the Ritz method. The desired function is represented in the form of a truncated series taken from a series that has the property of completeness.

For simplicity, consider the flat problem. Then the desired function can be represented as:

$$\sigma(x) = \sum c_i \varphi_i(x).$$

After substitution, we have the function of many variables c_i :

$$F(c_i) = \int_0^{u_0} \left[cu_0^n - \int_0^{u_0} \sum c_i \varphi_i(x) dx \right]^2 dx.$$

From the condition of the minimum of the function:

$$\frac{\partial F(c_i)}{\partial c_j} = 0.$$

1.4.2. Calculation-experimental method of estimation of wear of a bearing of sliding

Consider the application of the variational-experimental method [41] to calculate the contact parameters of a cylindrical bearing of sliding (Fig. 1.11).

The contact interaction of a solid cylinder of a radius R_1 (shaft) and a hollow cylinder (a bearing of a sliding bearing), a radius R_2 connected with a gap $\Delta = R_2 - R_1$ is considered.

Compression by force Q leads to plastic deformations in contact, while from the experiment the dependence of the contact angle $2\varphi_0$ on the load in the form of a power function is known:

$$Q = c\varphi_0^n, \quad (1.42)$$

where c, n are the dependency options:

$$Q = \frac{Q_n}{b},$$

where Q_n is the load on the shaft; b is the size of the shaft on the creature.

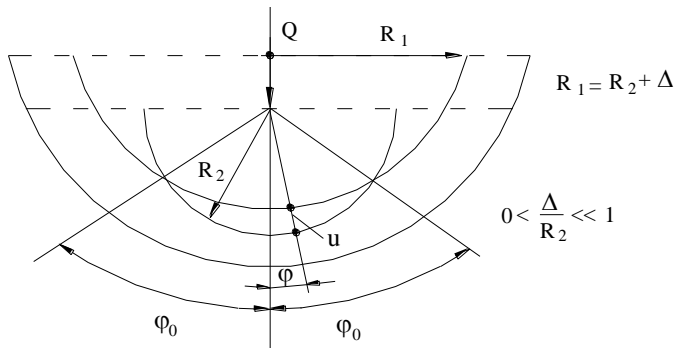


Fig. 1.11. Scheme of sliding bearing

The second main condition of the problem is the equilibrium condition of the external load and contact pressure $\sigma(\varphi)$ for the shaft:

$$Q = 2R \int_0^{\varphi_0} \sigma(\varphi) \cos \varphi d\varphi. \quad (1.43)$$

The condition of equilibrium must be fulfilled throughout the process of loading. This requirement leads to a quadratic functional:

$$F = \int_0^{\bar{\varphi}_0} \left[Q(\varphi_0) - 2R \int_0^{\varphi_0} \sigma(\varphi) \cos \varphi d\varphi \right]^2 d\varphi_0. \quad (1.44)$$

For the convenience of the solution, we take the function of the projection of pressure on the direction of the force as follows:

$$\sigma_1(\varphi) = \sigma(\varphi) \cos \varphi, \quad (1.45)$$

Then the functional takes the form:

$$F_1 = \int_0^{\bar{\varphi}_0} \left[Q(\varphi_0) - 2R \int_0^{\varphi_0} \sigma_1(\varphi) d\varphi \right]^2 d\varphi_0, \quad (1.46)$$

or taking into account (1.42):

$$F_1 = \int_0^{\bar{\varphi}_0} \left[c\varphi_0^n - 2R \int_0^{\varphi_0} \sigma_1(\varphi) d\varphi \right]^2 d\varphi_0. \quad (1.47)$$

The solution of the problem of determining the function of contact pressure we will look in the form of a power series of the form:

$$\sigma_1(\varphi) = \sum_k \xi_k (\varphi_0^k - \varphi^k), \quad (1.48)$$

where $k = 1, 2, 3, \dots$

After substitution (1.48), the functional (1.47) becomes a function of many variables:

$$F_1(\zeta_k) = \int_0^{\bar{\varphi}_0} \left[c\varphi_0^n - 2R \int_0^{\varphi_0} \sum_k \xi_k (\varphi_0^k - \varphi^k) d\varphi \right]^2 d\varphi_0. \quad (1.49)$$

After taking the internal integral (1.49) turns into a form:

$$F_1(\zeta_k) = \int_0^{\bar{\varphi}_0} \left[c\varphi_0^n - 2R \sum_k \xi_k \varphi_0^{k+1} \left(\frac{k}{k+1} \right) \right]^2 d\varphi_0. \quad (1.50)$$

Minimization of the function (1.50) of many variables is realized using the system of equations:

$$\frac{\partial F_1(\xi_k)}{\partial \xi_k} = 0. \quad (1.51)$$

After the rise (1.50) to the square, integrating and differentiating we arrive at the system of equations:

With a small number of members of a series, the system (1.52) regarding the coefficients ξ_k is solved analytically. With a large number of members in a series - numerically with the help of a computer.

After determining ξ_k the distribution function of pressure $\sigma_1(\varphi)$ is determined by (1.50).

$$\left. \begin{aligned} \sum_k \xi_k \bar{\sigma}_0^k \frac{k}{(k+1)(k+p+3)} &= \frac{1}{n+p+2}; \\ k, p &= 1, 2, 3; \\ \xi_k &= \bar{\xi}_k, \bar{\sigma}; \quad \bar{\sigma} = \frac{Q}{2R\varphi_0}. \end{aligned} \right\} \quad (1.52)$$

During wear, the contact angle φ_0 of the shaft and bearing increases. If you do not take into account the elastic deformation of the bearing, then the relationship between the angle φ_0 of contact and the linear wear u_w is as follows:

$$\varphi_0 = \arccos \left(\frac{\cos \varphi \cdot \Delta}{u_w + \Delta} \right). \quad (1.53)$$

The wear of a bearing will be determined by a algebraic form:

$$u_w = a\sigma^m(\varphi_0) \cdot t. \quad (1.54)$$

Thus, in order to obtain data describing the kinetics of bearing wear, it is necessary to use a step-by-step procedure. This procedure is as follows. The whole process of wear is divided into small segments of time. $\Delta t = t_0 = t_2 = t_3 \dots t_n$. Determine the contact pressure from the system (1.52) and the wear of the bearing according to expression (1.54) for the first period of time t_0 .

Then determine the new value of the angle of contact φ_0 (1.53) taking into account the increase in wear $u_w + \Delta u_w$. The new value φ_0 is determined by the contact pressure $\sigma(\varphi_0)$ (1.45). The procedure is repeated. Thus, based on the results of numerical calculations it is possible to obtain a change in the main parameters of the bearing in the process of wear: $\sigma(t)$, $\varphi_0(t)$, $u_w(t)$.

In the first stage, tests were performed on the press of the shaft into the bearing with the determination of the experimental pressure diagram [42].

According to the test results, the parameters c and n of the pressure diagram were determined in the form:

$$\frac{Q}{b\Delta} = c\varphi_0^n.$$

The results of determining the parameters of the pressure diagram (hard characteristics) are given in Table 1.6.

Table 1.6

Values of parameters of hard characteristics of a sliding bearing

Materials		Parameters of hard characteristics	
shaft	bearing	c , MPa	n
Steel 45 HRC 38 – 43	Steel 40H HRC 43 – 47	2,93.105	3,05
	Steel 20H HRC 60	3,02.105	3,50
	Cast iron Z120	3,36.105	4,35
	Bronze CuSn10P	2,36.105	3,95
	Bronze CuAl8Fe3	2,26.105	3,63
	Bronze CuSn5Zn5Pb5	2,15.105	3,74

Calculations of contact parameters were performed at the following initial data:

$R = 45$ mm, shaft length along a formative line $b = 15$ mm;

$\Delta = 0,1$ mm, shaft material – steel 45; material of bearing – Bronze CuSn10P;

$c = 2,36,105$ MPa; $n = 3,95$.

The results of calculations of the angle of contact and pressure on the proposed method are presented on Fig. 1.12 and on Fig. 1.13

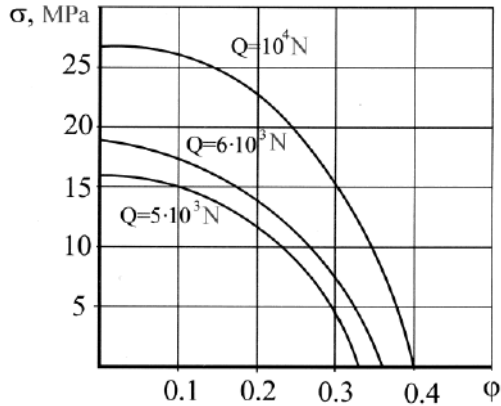


Fig. 1.12. Distribution of contact pressures at the angle of contact at different load values

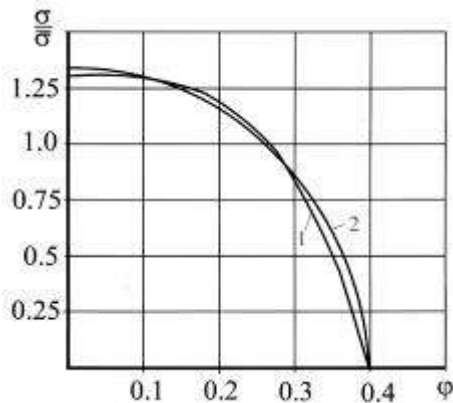


Fig. 1.13. Comparison of the distribution of contact pressure according to the proposed method [41] and by the method [43]

Comparison of the results of these calculations of contact pressure with calculations according to the known method [43] (Fig. 1.13), shows the sufficient accuracy of the proposed methodology.

1.4.3. Contact shaft and bearing, taking into account frictional forces

The contact of shaft and bearing on a large contact area in conditions without slipping at each point of contact is considered. The functional task based on minimizing the deviation of the work of external force on the way

of convergence from the work of normal and tangential stresses on contact movements was taken as:

$$F = \int_0^{\phi_0} \left[Q(\phi_0) d\phi_0 - 2\epsilon \int_0^{\phi_0} \int_0^u \sigma(u) du R d\phi - 2\epsilon \int_0^{\phi_0} \int_0^v \tau(v) dv R d\phi \right]^2 d\phi_0$$

From contact geometry for normal displacements follows:

$$u(\phi) = \Delta \left(\frac{\cos \phi}{\cos \phi_0} - 1 \right),$$

or approximation, expanding in a numerical series:

$$u(\phi) = \Delta \left[\left(\frac{\phi_0^2}{2} - \frac{\phi^2}{2} \right) + \left(\frac{\phi_0^4}{24} - \frac{\phi^4}{24} \right) \right] \left(1 + \frac{\phi_0^2}{2} \right).$$

For small first order: $du(\phi) = -\Delta \phi d\phi$.

For tangential displacements, respectively: $v = u(\phi) \operatorname{tg} \phi$,

$$v(\phi) = \Delta \left[\left(\frac{\phi_0^2}{2} - \frac{\phi^2}{2} \right) + \left(\frac{\phi_0^4}{24} - \frac{\phi^4}{24} \right) \right] \left(1 + \frac{\phi_0^2}{2} \right) \left(\phi + \frac{\phi^3}{3} \right),$$

$$dv(\phi) = \Delta \left(\frac{\phi_0^2}{2} - \frac{3}{2} \phi^2 \right) d\phi.$$

The solution of the problem will be sought in the form of numerical series: $\sigma(\phi) = \Sigma d_k (\phi_0^k - \phi^k)$, $\tau(\phi) = \Sigma \beta_e (\phi_0^e - \phi^e) \phi$, $k, l = 1, 2, 3$.

The dependence of external load on the angle of contact is taken in the form: $\bar{Q} = \phi_0^n$; $\bar{Q} = \frac{Q}{(\epsilon c \Delta)}$.

After the substitution of the resulting expressions, the functional is reduced to the following:

$$F = \int_0^{\phi_0} \left[\int_0^{\phi_0} \bar{Q}(\phi_0) d\phi_0 - \frac{2R}{c} \int_0^{\phi_0} \int_0^v \Sigma \alpha_k (\phi_0^k - \phi^k) (-\phi \Delta) d\phi - R d\phi - \frac{2R}{c} \int_0^{\phi_0} \int_0^{\phi} \Sigma \beta_e (\phi_0^e - \phi^e) \left(\frac{\phi_0^2}{2} - \frac{3}{2} \phi \right) \right]^2 d\phi_0.$$

Parameters α_k and β_e were determined from the condition of minimizing the functional of the task: $\partial F(\alpha_k, \beta_k) / \partial \alpha_k = 0$.

After the integration and differentiation the system of equations was obtained:

$$\begin{aligned} & \sum_k \bar{\alpha}_k \varphi_0^{k+1} \frac{k}{3(k+p+7)k+3} + \sum_l \bar{\beta}_l \varphi_0^{l+1} \frac{l}{4(l+3)} \times \\ & \times \left(\frac{\varphi_0 a_1}{l+p+9} - \frac{a_2}{l+p+8} \right) = \frac{1}{(n+p+5)(n+1)}, \\ & \sum_k \bar{\alpha}_k \varphi_0^{k+1} \frac{k}{(k+3)} \left(\frac{\varphi_0 \theta_1}{k+m+9} - \frac{\theta_2}{k+m+8} \right) + \\ & + \sum_l \bar{\beta}_l \varphi_0^{m+2l+11} \frac{l}{3(l+3)} \times \\ & \times \left(\frac{\varphi_0^2 a_1 \theta_1}{2m+2l+19} - \frac{\varphi_0 (a_1 \theta_2 + a_2 \theta_1)}{2(m+l+9)} + \frac{a_2 \theta_2}{2m+3l+17} \right) = \\ & = \frac{\varphi_0 \theta_1}{n+m+7} - \frac{\theta_2}{n+m+6}, \end{aligned}$$

where $k, p, l, m = 1, 2, 3, \dots$

$$\alpha_k = \bar{\alpha}_k \bar{\sigma}, \quad \beta_e = \bar{\beta}_e \bar{\sigma}, \quad \bar{\sigma} = \frac{Q}{(2eR\varphi_0)},$$

$$a_1 = \frac{l+5}{3(l+2)}, \quad a_2 = \frac{l+7}{2(l+4)}, \quad \theta_1 = \frac{m+5}{3(m+2)}, \quad \theta_2 = \frac{m+7}{2(m+4)}.$$

This solution requires a complicated computational procedure for the use of computer programs, in particular, MathCad.

The variational-experimental method for determining the distribution of contact pressure in a cylindrical slider bearing, taking into account frictional forces is proposed. In the solution, the experimental dependence of the dimensions of the contact arc in the bearing on the external load was used. In this work an example of determining the parameters of the indicated experimental dependence is implemented. The functional problem is obtained as a deviation of the experimental function from the integral equilibrium condition. For the calculation the kinetics of wear and contact parameters, a step-by-step procedure is proposed.

1.5. Modeling of wear processes in a cylindrical plain bearing

The problem of wear of radial plain bearings with misalignment of shaft and bush axes was considered elsewhere [46–50]. It should be noted that the authors of [46–48] paid insufficient attention to the wear mechanism of surface-profile formation at the initial moment of tribojoint operation. Furthermore, wear governing factors were considered to be determined values. In works [49, 50], the efficiency of plain bearings with thin one-layer [49] and multilayer [50] antifriction coatings with misaligned shaft and bush axes was considered stochastically; however, during the construction of the model, it was assumed that the elastic deformation of the coating is described by the Vinkler model, which reduces the applicability of the obtained results to thin coatings.

The aim of the work is to analyze the formation of wear-surface geometry in a radial plain bearing with misaligned shaft and bush axes. The method of triboelements with the ANSYS finite-element modeling package [51] was used to solve the problem. The joint application of the methods aims to extend the possibilities of the method of triboelements via using the findings of finite-element analysis of the stress-strain state of tribojoint elements as data for determining parameters of the triboelements model of wear. The joint application of these methods made it possible to eliminate some of the limitations in the calculation models.

A contact of a rigid shaft of R_1 radius with a cylindrical elastic antifriction layer of ε thickness in engagement with a rigid bush (Fig. 1.14) was considered. The shaft is positioned at angle α to the bush. The axis z is directed along the bearing axis. The bearing wear and contact pressures depend on the position of contact points. It is taken that only the antifriction layer is worn.

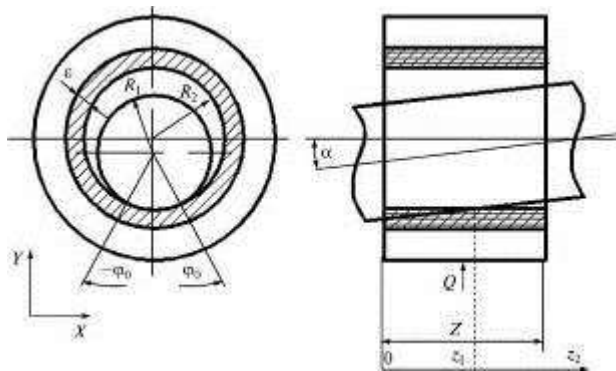


Fig. 1.14. Calculation model

General theses of the algorithm for the solution of wear contact problems using the method of triboelements with ANSYS package are discussed in [51]. In order to solve wear contact problems in a spatial setting, one should take into consideration that, in this case, a cubic spline of the worn surface is constructed. At each iteration of wear determination, a cubic spline of the worn surface is constructed, the geometry of which takes into account the wear of the previous step. The calculation scheme allowed us to build a parameterized calculation model in the preprocessor of the ANSYS package (Fig. 1.15).

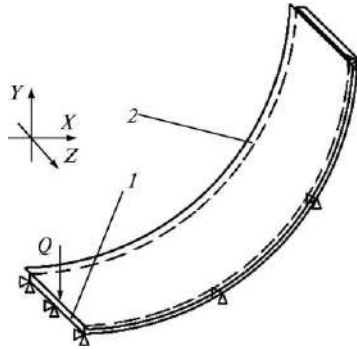


Fig. 1.15. Calculation model: 1. antifriction element, 2. rigid shaft

The contact interaction of elements of the tribojoint was simulated as a rigid–compliant contact. Shaft 2 (Fig. 1.15), which is rigid, was taken as a target surface. Antifriction layer 1 was taken as the contact surface. On the contact surface of the antifriction layer, the geometric position of the triboelements was determined. SOLID186 twenty-node spatial elements were used to generate a mesh of the finite-element model of the antifriction layer. Surface–surface contact elements were used to obtain a shaft–antifriction element friction pair. The target surface is described by TARGE170 elements and the contact surface is described by CONTA174.

Wear was considered to be a random Markov-type process with a discrete time and state. At the moment of time $t = 1$, the probabilities of finding TE in a given state were found as the product of the vector of initial states $[\pi_j]$ by the transition-probability matrix (TPM) $[W_{ij}]$:

$$[\pi_j(t=1)] = [\pi_j(t=0)] [W_{ij}], \quad i, j = 1, 2, \dots, K_C \quad (1.55)$$

where $[\pi_j(t=0)]$ is the vector of initial states; $[\pi_j(t=1)]$ is the vector of unconditional probabilities of finding TEs in i -th states

$i = 1, \dots, K_C$ at the moment of time $t = 1$; and $[\mathbf{W}_{ij}]$ is the transition-probability matrix.

The probabilities of TE states at a moment of time $t > 1$ were found as the product $[\pi_j(t-1)]$ of the vector of unconditional probabilities at the moment $t-1$ by TPM that specifies the behavior of TE at the moment t as follows:

$$[\pi_j(t)] = [\pi_j(t-1)] [\mathbf{W}_{ij}], \quad i, j = 1, 2, \dots, K_C \quad (1.56)$$

Components of the vector of initial states $[\pi_j(t=0)]$ were determined based on the assumption that, at the initial moment of time, the TE was in the first state as follows:

$$[\pi_j(t=0)] = [1, 0, 0, \dots, 0]. \quad (1.57)$$

The accumulation of tribodamage refers to cumulative damages; therefore, to describe the TE behavior, the TPM with singular upward jumps and absorbing state [52], which accounts for the mechanical essence of wear, namely, the subsequent damage of material layers, as follows:

$$[\mathbf{W}_{ij}] = \begin{bmatrix} w_{11}(t) & w_{12}(t) & 0 & 0 & \dots & 0 \\ 0 & w_{22}(t) & w_{23}(t) & 0 & \dots & 0 \\ \dots & \dots & \dots & \dots & \dots & \dots \\ 0 & 0 & 0 & 0 & \dots & 1 \end{bmatrix}. \quad (1.58)$$

The absorbing state is taken to mean the state of total wear of the antifriction layer.

According to [53], components $w_{ij}(t)$ were found as follows:

$$w_{ij}(t) \cong \lambda_I(t) \Delta t, \quad \text{for } i \neq j, \quad (1.59)$$

where the intensity of wear flow $\lambda_I(t) = V_I(t)/h$; Δt is the period of time that governs the loading cycle; h is the wear value that is found from the condition of ordinary nature of flow; $V_I(t)$ is the wear rate at the moment of time t .

The value of h is chosen from the condition that the probability of occurrence of a wear value more than h per a loading cycle is negligibly small. Wear values are found via the mathematical expectation \overline{m}_t of finding TE as follows:

$$z_t = (\overline{m}_t - 1) h, \quad (1.60)$$

where the mathematical expectation $\overline{m}_t = \sum_{i=1}^{K_C} i \pi_i(t)$, $i = 1, 2, \dots, K_C$;

$\pi_i(t)$ is unconditional probabilities of TE states; $h = \varepsilon / (K_C - 1)$.

It was assumed that, at the initial moment of time, all elements were in state 1. The following power dependence was used as a function of wear rate versus contact pressures and sliding velocities:

$$V_I = K_w V p(\phi, \phi_0(t))^\gamma, \quad (1.61)$$

where V_I is the wear rate, K_w is the coefficient of wear rate, V is the sliding velocity of shaft on antifriction layer, $p(\phi, \phi_0(t))$ is contact pressures, and γ is the exponent.

Numerical analysis was performed for the following parametric values: $Q = 300$ N; $\varepsilon = 2,6 \cdot 10^{-3}$ m; $\Delta = 2,0 \cdot 10^{-4}$ m; $R_1 = 1,12 \cdot 10^{-2}$ m; $V_{cp} = 0,95$ m/s; $K_C = 5$; $K_w = 1 \cdot 10^{-12}$ m²/N.

Calculation results were used to build contact pressure distributions on the surface (Fig. 1.16) for the initial moment of time, for the moment that corresponds to active geometry variation (0.75 ks) and the period of stationary wear of tribojoint elements (9 ks). An analysis of time variation of contact pressures (Fig. 1.17) and maximum wear (Fig. 1.18) has shown the basic processes of geometry formation of the wear surface to occur at the initial moment of time before 1.5–2.0 ks. At this time, the wear becomes stationary, which is evinced by almost all linear dependences of maximum pressure (Fig. 1.16) and maximum wear (Fig. 1.18).

An analysis of the shape of the contact pressure distribution on the surface at the initial moment of time in the absence of wear (Fig. 1.16, a) shows that maximum contact pressures that act along of axis of load application drop linearly from the maximum on the bush face to zero in the exit zone from the contact of the shaft with the bush.

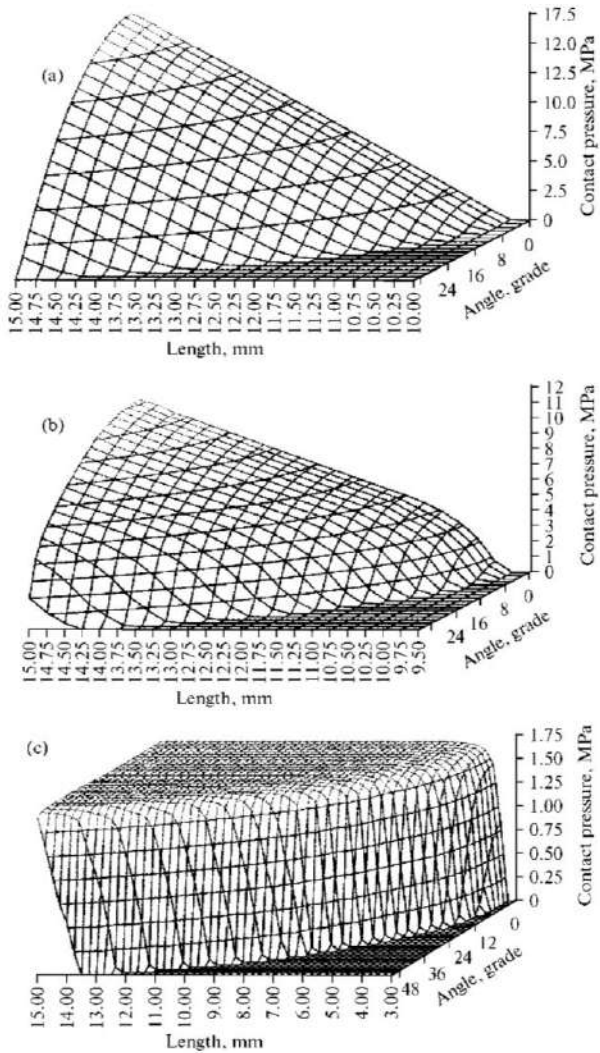


Fig. 1.16. Contact pressure distribution on the surface at an angle of misalignment of the shaft and bush axes of 0.5° at the following moments of time: (a) 0 ks; (b) 0.75 ks; (c) 9 ks

The beginning of wear results in variations in the surface geometry of the shaft–bush contact, and an increase in the area of contact interaction, and a substantial decrease in maximum contact pressures. Here, the contact

pressures rise near the contact surface boundaries (Fig. 1.16, b). Therefore, in the beginning of the wear, upon wear surface formation, contact pressures tend to be equalized both in axial and radial directions. This behavior of the contact pressures at the initial moment of wear is attributed to the fact that, retaining continuity of the shaft–bush contact and provision of the equality of the values of shaft point movements under the action of the applied forces and under wearing requires the uniform bush wear along the contact axis, which is provided by the equalized contact pressures (Fig. 1.16, c). In this case, the calculation model assumes a constancy of the axes misalignment angle during wear, which governs the above mechanism of the kinematic bush–shaft interaction. The additional degrees of freedom that govern the possibility of varying the angle of axis misalignment and taking into account nonuniform contact pressures and, consequently, wear (maximum at the bush face and zero in the contact exit zone) in the direction of the plane of load application would result in the increasing angle of mutual misalignment of the axes of the tribojoint elements.

The wear surface increases along the boundaries of the wear contact interaction owing to new contact elements of the unworn surface due to elastic deformation of the bush. As a result, a transitional wear zone arises on the boundaries of the interaction zone (Fig. 1.19, b), which is characterized by a nonlinear dependence of the wear values in the direction of the plane of load application. At the initial stage of contact surface geometry formation, contact pressures substantially drop. Here, the shape of pressure distribution on the surface tends to be uniform in both the axial and radial directions (Fig. 1.19, c). The linear mode of the time dependences of maximum contact pressures and wear (Figs. 1.17, 1.18) during this period makes it possible to conclude that the system starts operating under stationary wear conditions.

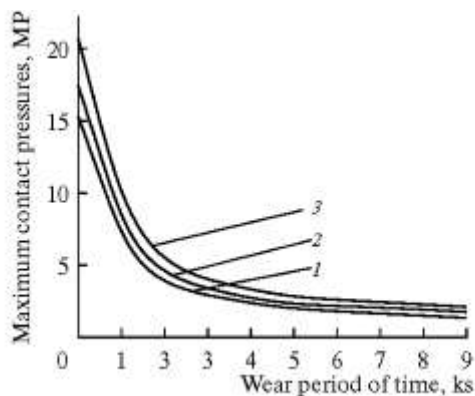


Fig. 1.17. Maximum contact pressures vs. wear time at misalignment of shaft and bush axes: (1) 0.35°; (2) 0.5°; (3) 0.75°

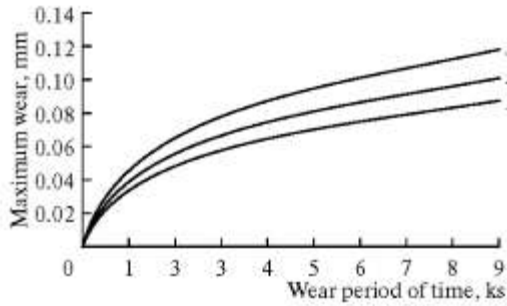


Fig. 1.18. Maximum wear vs. wear period at misalignment of shaft and bush axes: (1) 0.35°; (2) 0.5°; (3) 0.75°

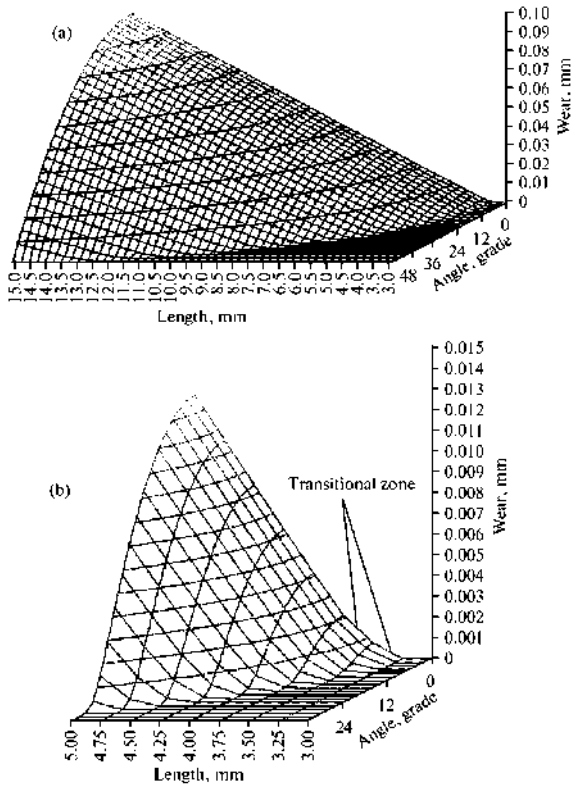


Fig. 1.19. (a) Wear surface and (b) transitional zone for axis misalignment angle 0.5° and wear time 9 ks

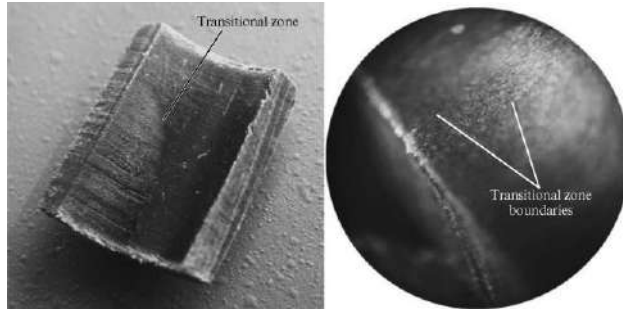


Fig. 1.20. Samples upon testing (axis misalignment is 0.5° , test time is 9 ks)

In order to validate the calculation results, we conducted experiments when a bush is worn by a rigid shaft with mutual axis misalignment at the geometrical and force friction parameters that correspond to the calculation analysis. A composite material based on Flubon 15 fluoroplastic was used as a material for the sample to be worn. The choice of the material is caused by its triboengineering characteristics to provide stable operation under unlubricated friction with a low coefficient of friction and absence of wear of the second element of the tribojoint. A cylinder made of 40X steel with hardness HRC 60 served as a counterbody. The test specimens were cylindrical bushes 15 mm long, 11.2 mm in nominal diameter, and 2.6 mm thick. The tests were carried out at a shaft rotation frequency of 800 rpm. A gap between the specimen and the counterbody should meet the condition that at misalignment, the shaft–bush contact occurs only along one bush face. The gap was 0.2 mm, correspondingly. The load to the specimens was 300 N.

A transitional wear zone between the worn and unworn surface can be seen on the pictures of the cut specimen (Fig. 1.20) upon testing.

The results of measurement of the transitional zone for different misalignment angles of shaft and bush axes are shown in the table. A comparison of the wear surfaces and dimensions of the transitional zones obtained via calculations and experiments demonstrates good quantitative and qualitative consistency (Table 1.7). The width of the transitional zone, as evidenced by the experimental findings and results of numerical analysis (the Table) depends on the mutual misalignment angle of shaft and bush axes. A decrease in the misalignment angle results in the increasing width of this zone. Experimental results show that a decrease in the angle from 0.75° to 0.35° caused an increase in the width of the transitional zone from 0.3 to 0.72 mm. A general analysis of the data obtained in experimental studies and numerical simulation has shown good consistence of quantitative and qualitative results.

Table 1.7

Width and length of wear area

Axes misalignment angle, grade		0,35	0,50	0,75
Wear surface length, mm	Experiment	14,52	11,68	9,15
	Calculation	14,50	11,75	9,25
Width of transitional zone in the direction of bush axis, mm	Experiment	0,72	0,55	0,30
	Calculation	0,75	0,50	0,25

Conclusions

It is discusses the findings of the study of wear surface geometry formation in plain bearings with misaligned shaft and bush axes. The calculation analysis made it possible to reveal and experimentally confirm the presence of a transitional wear zone, determine its quantitative parameters, and explain the mechanism of its origination. A comparative analysis of the numerical simulation and experimental data shows good consistency of qualitative and quantitative regularities. Data analysis shows that, for the given scheme of wear contact interactions, the initial wear period is the period of the active formation of the wear surface geometry. Large contact pressures that arise from the mutual misalignment of tribojoint element axes govern the high surface wear rate and the rapid increase in the surface of wear contact interaction.

This, in its turn, leads to a rapid decrease in actual contact pressures. In this case, the contact pressures are equalized in the axial and radial directions. In order to provide the continuity of shaft–bush contact, the wear-induced shaft displacement is compensated by elastic deformation on the surface boundaries that result in the augmentation of the contact pressures in the above mentioned places and afterwards to almost uniform pressure distribution on the wear surface. Newly appeared contact surface spots start to wear, a result of which a transitional wear zone is shaped. In the small period of time of surface geometry formation, the tribosystem is worn under stationary conditions.

1.6. Wear and reliability of cylindrical vehicle joints

The suspension is one of the most important parts of a car in terms of the comfort of transportation of goods and passengers and, most importantly, in terms of traffic safety. Wear of friction units is the main reason for the decrease in suspension reliability. The suspension structure of the front wheels of a car contains many important friction units. Among these supports, the most important are ball bearings. These bearings have different friction pairs: steel on steel, steel on polymers, steel on rubber, etc. The study of the

support structure is the first mandatory stage of calculations and tests for wear and reliability of friction units. It is also necessary to understand how the construction of the assembly works, as well as to understand the entire subsequent calculation methodology. Analysis of the design of ball joints of different cars allows us to trace the tendencies of their improvement. Suspension ball joints are applied between control arms and wheel carriers or knuckles of the suspension that allow relative articulation and rotation between the mating components. Depending on its application, the ball joint can transmit longitudinal and lateral forces with only a small proportion of forces as well as the complete vehicle weight in vertical direction. Much attention is currently paid to the study of the tribological aspects of extending the service life of the movable joints of a car [64]. At the same time, a comprehensive study of analytical and experimental methods for predicting the resource of vehicle friction units is an actual problem.

1.6.1. Calculation of wear and contact pressures in ball bearings of a vehicle suspension

To determine the effectiveness of construction and lubricants used in transport, a calculation method is proposed for determining the wear of vehicle parts. The technique takes into account the properties of materials and the operating conditions of the friction unit and makes it possible to determine the durability of the friction unit by the wear criterion. The basis is the solution of the wear contact problem for a given contact pattern of parts.

In this case, the design of the ball joint of the car suspension is considered. In the ball joint, there is a contact interaction of a rigid spherical liner and a rigid cage according to the scheme in Fig. 1.21 A ball bearing of radius R rotates around its axis along the body and wears out. It is necessary to obtain the dependence of the wear of the mating of the axes of the main factors. The angle of the liner ranges from $\varphi = \varphi_1$ to $\varphi = \varphi_2$.

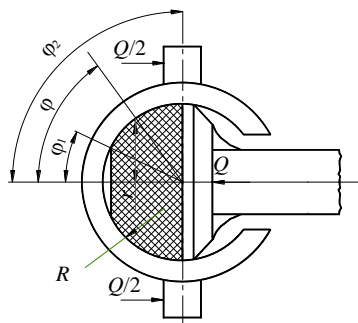


Fig. 1.21. Design scheme of the hinge

The mathematical formulation of the problem consists of an equilibrium condition, a geometric relationship, and a wear law.

The equilibrium condition for a spherical joint is:

$$Q = 2\pi R^2 \int_{\varphi_1}^{\varphi_2} \sigma(\varphi) \cos \varphi d\varphi, \quad (1.62)$$

where $\sigma(\varphi)$ is the required pressure function.

The geometric dependence of displacements u_0 on wear $u_w(\varphi)$ is as follows:

$$u_w(\varphi) = u_0 \cos \varphi. \quad (1.63)$$

The wear law with two parameters k_w and m is taken as:

$$\frac{du_w}{dt} = k_w \sigma^m 2\pi n r, \quad (1.64)$$

where n is the number of vibrations of the hinge per unit time t ; $r = R \cos \varphi$.

As a result of differentiating condition (1.62) and equating (1.64), we obtain:

$$k_w \sigma^m 2\pi n R^2 \cos \varphi = \frac{du_0}{dt} \cos \varphi, \quad (1.65)$$

from here we have:

$$\sigma = \left(\frac{du_w}{dt} \right)^{\frac{1}{m}} \left(\frac{1}{k_w 2\pi n R^2} \right)^{\frac{1}{m}}. \quad (1.66)$$

As a result of mutual substitutions, we obtain the resolving integral equation of the problem:

$$Q = 2R \left(\frac{du_w}{dt} \right)^{\frac{1}{m}} \left(\frac{1}{k_w 2\pi n R^2} \right)^{\frac{1}{m}} \int_{\varphi_1}^{\varphi_2} \cos \varphi \sin \varphi d\varphi. \quad (1.67)$$

After integration, we obtain the dependence for the maximum wear:

$$u_w(t) = \left(\frac{Q}{\pi R^2} \right)^m \frac{k_w 2\pi R n}{(\sin^2 \varphi_2 - \sin^2 \varphi_1)^m} t. \quad (1.68)$$

If we take the friction path for one cycle s_1 , then for the time t the total friction path is: $s = s_1 nt$ or $nt = \frac{s}{s_1}$. As a result, for the friction path we get:

$$u_w(s) = \left(\frac{Q}{\pi R^2} \right)^m \frac{k_w 2\pi R^2 s}{\sin^2 \varphi_2 - \sin^2 \varphi_1}. \quad (1.69)$$

The formula for determining the contact pressure is obtained by substituting (1.69) in (1.66):

$$\sigma = \left(\frac{Q}{\pi R^2} \right) \frac{(k_w 2\pi R^2 n)^{\frac{1}{m}}}{\sin^2 \varphi_2 - \sin^2 \varphi_1} \left(\frac{1}{k_w 2\pi n R^2} \right)^{\frac{1}{m}}. \quad (1.70)$$

After the transformations, we finally get:

$$\sigma = \frac{Q}{\pi R^2 (\sin^2 \varphi_2 - \sin^2 \varphi_1)}. \quad (1.71)$$

An example of calculating the wear of the lower support in the contact of a hardened steel shaft and a polyurethane polymer liner.

Initial data. Hinge load 2,000N. The total path of friction in the joint for 10,000 km of run. Ball pin radius 16 mm. The parameters of the wear model for polyurethane are: $m = 2.04$; $k_w = 0.5 \cdot 10^{-8}$ (MPa)^{-m}. Liner contact angles: $\varphi_1 = 35^\circ$; $\varphi_2 = 85^\circ$.

The calculation of the wear of the liner is performed according to dependence (1.68) with the selected initial data per 10,000 km of run:

$$u_w = \left(\frac{2000}{\pi 15^2} \right)^{2.04} \frac{0.5 \cdot 10^{-8} \cdot 2\pi \cdot 16^2 \cdot 3 \cdot 10^4}{\sin^2 85^\circ - \sin^2 35^\circ} = 0.233 \text{ mm.}$$

The obtained dependencies for calculations of wear are valid for all ball bearings of the front suspension. The difference lies in the different values of the contact angles φ_1 and φ_2 . The formula for calculating contact pressures is also common to all mates in ball joints. This calculates the wear due to the frictional path caused by the axial rotation of the ball pin during the rotation of the steering knuckle when turning from the steering. The friction path from lowering and raising the wheels while driving must be added to the total friction path in accordance with the suspension kinematics.

The maximum initial contact pressure in the hinge is determined by the dependence (1.71):

$$\sigma = \frac{Q}{\pi R^2 (\sin^2 \varphi_2 - \sin^2 \varphi_1)} = \frac{2,000}{\pi 15^2 (\sin^2 85^\circ - \sin^2 35^\circ)} = 3.95$$

It has been established that this value of contact pressure does not change with wear of the liner.

Contact pressure is the main, basic characteristic of the friction unit. To determine pressures, it is necessary to have a solution corresponding to the contact problem. The upper and lower supports each have two types of spherical couplings, which differ both in the sign of curvature and in the properties of the contacting bodies. However, all mates can be represented as one generalized mate: the convex spherical surface of the finger and the concave spherical surface of the support body (or vice versa). In all cases, contact starts at some angle $\varphi_1 > 0$ and ends at an angle $\varphi_2 \leq 90^\circ$.

1.6.2. Reliability calculations of ball bearings

Let us assume that the current wear of the suspension ball bearings is distributed according to the normal law. In this case, the quantile up of the reliability function is determined [53] by the dependence:

$$u_p = - \frac{n-1}{\left(n^2 V_{w^*}^2 + V_w^2\right)^{\frac{1}{2}}}(\varphi), \quad (1.72)$$

where V_{w^*}, V_w is variation coefficients of limit and current wear; n is safety factor for wear:

$$n = \frac{u_w^*}{u_w}. \quad (1.73)$$

The limit wear value can be taken constant $u_w^* = 0$, then the variation coefficient $V_{w^*} = 0$. In this case, from (12) we have:

$$u_p = - \frac{n-1}{V_w}. \quad (1.74)$$

By quantile, the reliability function is determined by the Laplace function: $\Phi(u_p)$:

$$P(u_w < u_w^*) = 0.5 + \Phi(u_p). \quad (1.75)$$

The determination of the general variation coefficient is performed through the partial coefficients of variation, taking into account the form of the main dependence (1.68).

The determination of the general variation coefficient is performed through the partial variation coefficients, taking into account the form of the main dependence (1.68).

In this case, the load, the wear rate factor and the friction path are random values. The variation coefficients for these quantities V_Q, V_{k_w}, V_s are assumed to be known.

In accordance with the general methodology [64] determining the coefficient of variation of a function by the variation coefficients of the arguments, we have:

$$V_w = \left(m^2 V_Q^2 + V_{k_w}^2 + V_s^2 \right)^{\frac{1}{2}}. \quad (1.76)$$

Let us determine the probability of failure-free operation of the ball joint of the car during 10,000 km of run. Let's use the initial data from the previous example. Let us take the coefficients of variation: $V_Q = 0.4$, $V_s = 0.4$, $V_{k_w} = 0.35$.

The general coefficient of variation of wear is determined by the dependence (1.76):

$$V_{u_w} = \left(m^2 V_Q^2 + V_{k_w}^2 + V_s^2 \right)^{\frac{1}{2}} = \left(2.04^2 0.4^2 + 0.35^2 + 0.4^2 \right)^{\frac{1}{2}} = 0.98;$$

Average wear is determined by the formula (1.69). According to the accepted data, the wear of the ball joint was obtained for 10,000 km. $u_w = 0.233$ mm.

According to [66], if, when checking the wear in the upper ball joint, the total indicators of the indicator exceed 0.8 mm, then the hinge must be repaired. Thus, dividing this value into two joints (lower and upper) we obtain the allowable wear value in the ball joint of the front suspension: $u_w^* = 0.3$ mm.

$$\text{Safety factor: } n = \frac{u_w^*}{u_w} = \frac{0.3}{0.233} = 1.85.$$

The quantile of the probability of no-failure operation is determined by the dependence (1.72):

$$u_p = -\frac{n-1}{V_w} = -\frac{1.85-1}{0.98} = -0.867.$$

According to the tables of the Laplace function: $\phi(-0.867) = 0.3078$
 Finally, reliability function according to (14):

$$P = 0,5 + \phi(u_p) = 0.5 + 0.3078 = 0.8078.$$

The given example is methodological in nature. For a more reliable assessment of reliability, it is necessary to perform an experimental determination of both the average values and their coefficients of variation.

1.6.3. Determination of wear parameters of ball joint

In the calculation formulas, the wear parameters m and k_w were taken as given. The problem of determining the parameters of the friction pair wear model is one of the stages of the computational and experimental evaluation of the wear of the ball joints. The problem of increasing the wear resistance of this unit can be solved in two directions: improving the wear-resistant properties of the liners and choosing new types of lubricants. Currently, great progress has been made in the development of lubricants with additives. The task is to assess the effectiveness of lubricants for use in ball joints. The wear characteristics of the materials were determined from the results of wear tests. The test scheme is shown in Fig. 1.22. An automobile ball joint polyurethane liner was used as a sample. The outer surface of the insert was tested with loading with a sphere diameter $R = 28$ mm (Fig. 1.22).

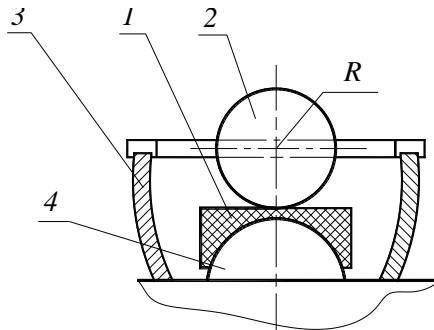


Fig. 1.22. Scheme of testing the polyurethane liner for wear:
 1 – polyurethane hinge liner; 2 – steel counter sample HRC 50;
 3 – container with grease; 4 – loading arm

The tests were carried out at a rotational speed $n = 830 \text{ rev}^{-1}$ and a load of 10N. For lubrication, we used: ShRB-4 grease, Mobil grease, Shell grease. Three samples of each variant were tested. The contact patch was measured in two directions. The average test results are presented in Table 1.8.

Table 1.8

Friction path s 10^6 , mm	a, mm			
	without lubrication	Shrb-4	Mobil	Shell
1	1,44	1,211	1,201	1,240
3	1,52	1,46	1,33	1,335
5	1,665	1,511	1,432	1,38
8	1,71	1,58	1,49	1,50
10	1,802	1,715	1,575	1,585

The test results were approximated by a power function of the dependence of wear on the friction path in the form: $a = cs^\beta$. The power-law approximation parameters were determined using the Excel program (Table 1.9).

Table 1.9

Results of determining wear parameters for various lubricants				
Parameters	Dry	ShRB-4	Mobil	Shell
β	0.105	0.14	0.118	0.14
c	0.33	0.25	0.269	0.295
m	3.65	3.15	3.52	3.34
k_w	$13.4 \cdot 10^{-6}$	$0.425 \cdot 10^{-6}$	$0.38 \cdot 10^{-6}$	$0.425 \cdot 10^{-6}$
$I(7\text{MPa}) \cdot 10^{-6}$	2.175	0.0827	0.064	0.0745
$I(2\text{MPa}) \cdot 10^{-6}$	0.0378	0.0029	0.00156	0.00175

The formulas for determining the wear parameters were determined by solving the inverse wear-contact problem [55]. Relationships (1 – 3) were used as the basic equations. As a result, we got the formulas:

$$m = \frac{1 - 2\beta}{2\beta}. \quad (1.77)$$

$$k_w = \frac{c^{2m+2}}{(2m+2)(Q/\pi)^m R}. \quad (1.78)$$

The results of calculating the wear parameters are shown in Table. 1.9. Comparison of the effectiveness of lubricants is carried out in terms of the wear rate at two pressures of 7 MPa and 2 MPa. The calculation of the intensity is carried out according to the main dependence:

$$I = \frac{du_w}{ds} = k_w \sigma^m. \quad (1.79)$$

The results of calculating the wear rate for various lubricants are shown in Table 1.9. From the results of comparison with the base grease ShRB-4 it follows: the use of Mobil grease reduces wear at 7 MPa by 1.2 times; at 2 MPa by 1.79 times; the use of Shell lubricant reduces wear at 7 MPa by 1.15 times; at 2 MPa, 1.70 times.

Conclusion

1. To estimate the wear of the ball joints of the car suspension, the wear-contact problem was solved. The solution is based on: the equilibrium equation of the tribosystem, the law of wear, the geometric equation of continuity in contact. As a result, closed formulas were obtained for determining the amount of wear and contact pressure.

2. A method is proposed for calculating the reliability of ball joints of a car half-suspension by the criterion of wear. A method of sequential calculation of the coefficient of variation of wear is considered by the coefficients of variation of random parameters that are included in the formula for calculating wear.

3. Based on the solution of the inverse wear-contact problem, formulas are proposed for calculating the parameters of the wear law. A comparative assessment of the tribological properties of lubricants for ball joints of the car suspension is carried out.

References for chapter 1

1. Ali Rezaeia, WimVan Paepegema, Patrick De Baets, Wouter Ost. Adaptive finite element simulation of wear evolution in radial sliding bearings. *Wear*. Volume 296, Issues 1–2, 660-671, (2012).

2. Florian König, Achraf Ouald Chaib, Georg Jacobs, Christopher Sous. A multiscale-approach for wear prediction in journal bearing systems – from wearing-in towards steady-state wear. *Wear*, Volumes 426–427, Part B, 2019, 1203–1211

3. V. T. Oksanen, A. J. Lehtovaara, M. H. Kallio. Load capacity of lubricated bismuth bronze bimetal bearing under elliptical sliding motion. *Wear*, Volumes 388–389, 2017, 72–80

4. Nimeshchandra S. Patel, D. P. Vakharia, G. M. Deheri, H. C. Patel. Experimental performance analysis of ferrofluid based hydrodynamic journal bearing with different combination of materials. *Wear*, Volumes 376–377, Part B, 2017, 1877–1884.

5. Lidia Galda, Jaroslaw Sep, Artur Olszewski, Tomasz Zochowski. Experimental investigation into surface texture effect on journal bearings performance. *Tribology International*, Volume 136, 2019, 372–384

6. Surojit Poddar, N. Tandon. Detection of particle contamination in journal bearing using acoustic emission and vibration monitoring techniques. *Tribology International*, Volume 134, 2019, 154–164.
7. Thomas Hagemann, Christopher Zeh, Hubert Schwarze. Heat convection coefficients of a tilting-pad journal bearing with directed lubrication. *Tribology International*, Volume 136, 2019, 114–126.
8. Guo Xiang, Yanfeng Han, Jiaxu Wang, Jiefu Wang, Xiaokang Ni. Coupling transient mixed lubrication and wear for journal bearing modeling. *Tribology International*, Volume 138, 2019, 1–15.
9. Shaoyu Zhu, Jun Sun, Biao Li, Xiaoyong Zhao, Guixiang Zhu. Stochastic models for turbulent lubrication of bearing with rough surfaces. *Tribology International*, Volume 136, 2019, 224–233.
10. Shuhui Cui, Le Gu, Liqin Wang, Bo Xu, Chuanwei Zhang. Numerical analysis on the dynamic contact behavior of hydrodynamic journal bearings during start-up. *Tribology International*, Volume 121, 2018, 260–268.
11. T. Illner, D. Bartel, L. Deters. Determination of the transition speed in journal bearings under consideration of bearing deformation. *Tribology International*, Volume 82, Part A, 2015, 58–67.
12. Fillon, M., Wodtke, M. & Wasilczuk, M. *Friction* (2015) 3: 266. <https://doi.org/10.1007/s40544-015-0092-4>
13. Thomas, E., Pascovici, M.D. & Glovnea, R.P. *Friction* (2015) 3: 287. <https://doi.org/10.1007/s40544-015-0098-y>.
14. Xue, Y., Chen, J., Guo, S. et al. *Friction* (2018) 6: 297. <https://doi.org/10.1007/s40544-018-0206-x>.
15. Varenberg, M., Kligerman, Y., Halperin, G. et al. *Friction* (2018). <https://doi.org/10.1007/s40544-018-0255-1>
16. Sitae Kim and Alan B. Palazzolo. Pad–Pivot Friction Effect on Nonlinear Response of a Rotor Supported by Tilting-Pad Journal Bearings. *J. Tribol* 141(9), 091701, 2019, doi: 10.1115/1.4043971
17. Faisal Rahmani, R. K. Pandey and J. K. Dutt. Performance Studies of Powder-Lubricated Journal Bearing Having Different Pocket Shapes at Cylindrical Bore Surface. *J. Tribol* 140(3), 031704, 2018, doi: 10.1115/1.4038678
18. Hiroyuki Yamada, Hiroo Taura and Satoru Kaneko. Static Characteristics of Journal Bearings With Square Dimples. *J. Tribol* 139(5), 051703, 2017, doi: 10.1115/1.403577
19. Pape, F., Neubauer, T., Maiß, O. et al. *Tribol Lett* (2017) 65: 70. <https://doi.org/10.1007/s11249-017-0855-3>
20. Vladescu, SC., Marx, N., Fernández, L. et al. *Tribol Lett* (2018) 66: 127. <https://doi.org/10.1007/s11249-018-1080-4>

21. Aliyu, I.K., Mohammed, A.S. & Al-Qutub, A. *Tribol Lett* (2018) 66: 144. <https://doi.org/10.1007/s11249-018-1096-9>
22. Singh, H., Pulikollu, R.V., Hawkins, W. et al. *Tribol Lett* (2017) 65: 81. <https://doi.org/10.1007/s11249-017-0861-5>
23. Troy Snyder and Minel Braun. A CFD-Based Frequency Response Method Applied in the Determination of Dynamic Coefficients of Hydrodynamic Bearings. Part 1: Theory. *Lubricants* 2019, 7(3), 23; <https://doi.org/10.3390/lubricants7030023>
24. Maximilian Prölb, Hubert Schwarze, Thomas Hagemann, Philipp Zemella and Philipp Winking Theoretical and Experimental Investigations on Transient Run-Up Procedures of Journal Bearings Including Mixed Friction Conditions. *Lubricants* 2018, 6(4), 105; <https://doi.org/10.3390/lubricants6040105>
25. Philip Croné , Andreas Almqvist and Roland Larsson. Thermal Turbulent Flow in Leading Edge Grooved and Conventional Tilting Pad Journal Bearing Segments–A Comparative Study. *Lubricants* 2018, 6(4), 97; <https://doi.org/10.3390/lubricants6040097>
26. Pradeep K. Gupta & Erwin V. Zaretsky. New Stress-Based Fatigue Life Models for Ball and Roller Bearings. *Tribology Transactions*, Volume 61, 2018 – Issue 2. pp. 304–324.
27. Chaowu Jin, Guochang Li, Yazhong Hu, Yuanping Xu & Longxiang Xu. Identification of Mechanism Stiffness of Autoeliminating Clearance for Auxiliary Bearing. *Tribology Transactions*, Volume 62, 2019 – Issue 2
28. Lagunova, E.O. & Mukutadze, M.A. *J. Frict. Wear* (2019) 40: 88. <https://doi.org/10.3103/S1068366619010112>
29. Zernin, M.V., Mishin, A.V., Rybkin, N.N. et al. *J. Frict. Wear* (2017) 38: 242. <https://doi.org/10.3103/S1068366617030163>
30. Dmitrichenko, N.F., Milanenko, A.A., Hluhonets, A.A. et al. *J. Frict. Wear* (2017) 38: 126. <https://doi.org/10.3103/S1068366617020076>.
31. Chernets, M. V. (2015). Prediction of the life of a sliding bearing based on a cumulative wear model taking into account the lobing of the shaft contour. *Journal of Friction and Wear*, 36(2), 163–169. doi: 10.3103/S1068366615020038
32. Soldatenkov, I. A. (2010). Evolution of contact pressure during wear of the coating in a thrust sliding bearing. *Journal of Friction and Wear*, 31(2), 102–106. doi:10.3103/S1068366610020029
33. Goryacheva, I.G. & Mezrin, A.M. Simulation of combined wearing of the shaft and bush in a heavily loaded sliding bearing *J. Frict. Wear* (2011) 32: 1. doi:10.3103/S1068366611010053
34. Soldatenkov I. A., Mezrin A. M., Sachek B. Ya. Implementation of asymptotics of the wear contact problem solution for identifying the wear law based on the results of tribological tests, *Journal of Friction and Wear*, 2017, 38(3), pp. 173–177.

35. Mezrin, A.M. (2009). Determining local wear equation based on friction and wear testing using a pin-on-disk scheme. *Journal of Friction and Wear*, 30(4), 242-245. doi:10.3103/S1068366609040035
36. Bulgarevich, S.B., Boiko, M.V., Lebedinskii, K.S., Marchenko D.Yu. (2014). Kinetics of sample wear on four-ball friction-testing machine using lubricants of different consistencies. *Journal of Friction and Wear*, 35(6), 531–537. doi:10.3103/S106836661406004X
37. Rezaei, A., Paepegem, W.V., Baets, P.D., Ost, W., Degrieck, J. (2012). Adaptive finite element simulation of wear evolution in radial sliding bearings. *Wear*, 296 (1–2), 660–671. <https://doi.org/10.1016/j.wear.2012.08.013>
38. Dykha, A.V., Kuzmenko, A.G. (2015). Solution to the problem of contact wear for four-ball wear-testing scheme. *Journal of Friction and Wear*, 36(2), 138–143. doi: 10.3103/S1068366615020051
39. Dykha, A., Sorokatyi, R., Makovkin, O., Babak, O. Calculation-experimental modeling of wear of cylindrical sliding bearings. *Eastern-European Journal of Enterprise Technologies*, 2017, 5/1 (89), 51–59. doi: 10.15587/1729-4061.2017.109638
40. Dykha A., Marchenko D. Prediction the wear of sliding bearings. *International Journal of Engineering & Technology*, 2018, 7 (2.23), pp. 4–8. doi: 10.14419/ijet.v7i2.23.11872
41. Kuzmenko A.G. Plastic contact Variational – experimental method. Monograph. Khmelnytsky: KhNU, 2009.
42. Kuzmenko, A.G., Kuzmenko, G.A., Sorokatyi, R.V., Dykha, A.V. (1992). Calculating and experimental method for solving contact problems. *Trenie i iznos*, 13(2), 257–264.
43. Dykha O.V. Approximate wear contact problem for cylindrical bearing with allowance for slip friction. *Problems of Tribology*. 2017. No. 4. Pp. 75–81.
44. Dykha, A.V., Kuzmenko, A.G. 2015. Solution to the problem of contact wear for four-ball wear-testing scheme. *Journal of Friction and Wear*, 36(2), 138–143. DOI: 10.3103/S1068366615020051
45. Dykha, A., Sorokatyi, R., Makovkin, O., and Babak, O. 2017. Calculation-experimental modeling of wear of cylindrical sliding bearings. *Eastern-European Journal of Enterprise Technologies*, 5 (1 (89), 51–59. doi: 10.15587/1729-4061.2017.109638. <http://journals.uran.ua/eejet/article/view/109638>
46. Galakhov, M.A. and Usov, P.P., *Differentsial'nye i integral'nye uravneniya matematicheskoi teorii treniya*, (Differential and Integral Equations of Mathematical Theory of Friction), Moscow: Nauka, 1990.
47. Kuzmenko A., Dykha A., Karazei V. The calculate–experimental approach to research of friction units with lubricant materials // *Proceedings*

of 7 International tribological Symposium "INSYCONT 2006", Energy And Environmental Aspects of Tribology, Cracow, Poland.– 2006.– P.233-240.

48. Kuzmenko, A.G., Lyubin, A.G., and Kuzmenko, V.A., Contact problem for RPS taking into account wear at misalignment of shaft and bushing axes, *Problemy Tribologii*, 1997, no. 4, pp. 76–80.

49. Sorokatyi, R.V., Analysis of efficiency of sliding bearings with misalignment of shaft and bushing axes, *J. Friction Wear*, 2006, vol. 27, pp. 21–29.

50. Sorokatyi, R.V., Analysis of efficiency of sliding bearings with thin multilayer antifriction coating and misaligned shaft and bushing axes, *J. Friction Wear*, 2006, vol. 27, pp. 29–37.

51. Sorokatyi, R.V., Solution of wear-contact problems by triboelement method in ANSYS finite element packet media, *Problemy Tribologii*, 2007, no. 3, pp. 9–17.

52. Bogdanoff, J.L. and Kozin, F., *Probabilistic Models of Cumulative Damage*, New York: Wiley, 1985; Moscow: Mir, 1989.

53. Sorokatyi, R.V., Simulation of tribosystem behavior by triboelement method, *Trenie Iznos*, 2002, vol. 23, pp. 16–22.

54. Chang-Fu Han, Hsiao-Yeh Chu, Ruei-Yang Luo & etc. 2018 Effects of groove factor and surface roughness of raceway in ball-bearing-like specimens on tribological behavior and the onsets of two instabilities of dry contacts. *Wear*. 406, 126. <https://www.sciencedirect.com/science/article/abs/pii/S004316481731551X>

55. Dykha A, Sorokatyi R, Makovkin O, Babak O 2017 Calculation-experimental modeling of wear of cylindrical sliding bearings. *Eastern-European Journal of Enterprise Technologies*. 5, 1, 51–59. doi: 10.15587/1729-4061.2017.109638

56. Sorokatyi R V, Dykha A V 2015 Analysis of Processes of Tribodamages under the Conditions of High-Speed Friction. *J. Friction and Wear*, 36, 422. doi: 10.3103/S106836661505013X

57. Sorokatyi R, Chernets M, Dykha A, Mikosyanchyk O 2019 Phenomenological Model of Accumulation of Fatigue Tribological Damage in the Surface Layer of Materials Mechanisms and Machine Science, 73, 3761. https://link.springer.com/chapter/10.1007%2F978-3-030-20131-9_371

CHAPTER 2

Research of Tribological Properties of Lubricants. Theory and Experiment

2.1. Testing of lubricants according to the four-ball scheme. Test method theory

The current stage of development of tribology is characterized by the creation and improvement of methods for calculating friction wear points [1–3]. The creation of such methods is constrained by the problems of mathematical description of the processes of wear. At the same time, the lack of calculation methods at the design stage and the creation of a machine makes it difficult to create methods for predicting the wear resistance and durability of friction units. The development of analytical methods for calculating the wear resistance of lubricated tribosystems requires consideration of the nonlinearity of the wear process due to the complex interrelationships of mechanical, thermal, and friction properties. To obtain correct results, analytical calculation methods require the use of their wear parameters, which can only be obtained from wear tests. Among the known methods of testing friction units with lubrication, the most perfect and common are four-ball testing [4–5]. The main disadvantage of testing according to this scheme is the lack of models for a quantitative description of the wear process, which in most cases results only in a qualitative assessment of test results. Also, tests on a four-ball pattern use standard samples from steel 52100, and the laboratory diagram of the contact of two balls does not always adequately simulate the wear of parts from other materials and structural forms [6–7]. Thus, the creation of computational-experimental wear models for predicting the wear resistance of tri-mats is relevant. For the theoretical basis of the approaches proposed in this study, the solutions of direct and inverse wear-contact problems for contact and wear of samples of various shapes were taken in [8–9]. Possible ways of applying the calculated estimates of the durability of lubricants for engines of transport vehicles are shown in scientific papers [10–12].

Lubrication is one of the most effective methods for enhancing the wear resistance of the friction units of machines. The success of research into the wear of lubricated surfaces is determined by the testing methods used. Among well known methods for testing lubricated friction units, the four ball wear testing scheme proposed by Berlage in 1933 is the most effective. This testing scheme may have different design solutions, the basic unit of it, however, a pyramid composed of three stationary balls and one movable ball is an integral part of every four ball friction testing machine. The testing methods using four ball friction machines have been standardized, e.g., GOST 9490–75 (USSR), ASTM D 2596 and ASTM D 2783 (United States), DIN 51350 (Germany), PN– 76/C_04147 (Poland), IP 300 (United Kingdom), and BDS 14150–77 (Bulgaria) and find many applications worldwide. In the authors' opinion, the main drawback of the tests according to this scheme is that the process of ball wear has not been mathematically described. As a result, the tests yield a qualitative, rather than quantitative, description of the process. Various approaches to the theoretical description and construction of mathematical wear models and the accompanying processes for the testing schemes are presented in.

Contact geometry and load. Three balls of the same radius R_1 and located on a plane so that they touch according to the scheme in Fig. 2.1, while the centers form an equilateral triangle $O_1O_2O_3$. The fourth top ball with the center O_4 of the radius R_2 is located on the bottom three so that it contacts each at points A_1, A_2, A_3 . A force is applied to the center of the fourth ball O_4 , which is transmitted to each of the three lower balls in the center-to-center directions Q_4O_1, Q_4O_2, Q_4O_3 , creating equal forces $Q_1 = Q_2 = Q_3$.

The presence of the cage provides a stable stationary position of the lower balls during vertical loading by force and rotation of the upper ball by a moment around its vertical axis. Such a simple stable system of four balls, the centers of which form a tetrahedron, is widely used as a tribological test scheme with liquid lubricant poured into the space between the balls.

To determine the forces acting between the balls, it is necessary to determine their direction and angle (Fig. 2.1):

$$\alpha = \arcsin \frac{r_1}{R_2}. \quad (2.1)$$

The value r_1 is determined from the similarity of triangles O_4AB and O_4O_1C :

$$r_1 = \frac{2R_1R_2}{\sqrt{3}(R_1 + R_2)}, \quad (2.2)$$

in particular, for $R_1 = R_2 = R$:

$$r_1 = \frac{R}{\sqrt{3}} = 0,5774R. \quad (2.3)$$

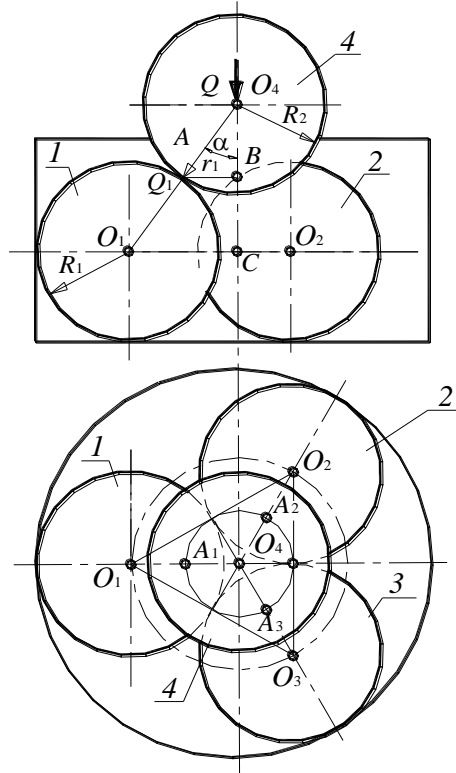


Fig. 2.1. Design scheme

The expression for determining the angle α is obtained after substituting (2.2) in (2.1):

$$\alpha = \arcsin \frac{2R_1}{\sqrt{3}(R_1 + R_2)} \quad (2.4)$$

at $R_1 = R_2 = R$:

$$\alpha = \arcsin \frac{1}{\sqrt{3}} = 35,26^\circ. \quad (2.5)$$

The forces Q_1 acting normal to each ball (Fig. 2.1) are expressed through the total force Q by the ratio:

$$Q_1 = \frac{Q}{3\cos\alpha}, \quad (2.6)$$

or taking into account (2.4):

$$Q_1 = \frac{Q}{3\cos\left(\arcsin\frac{2R_1}{\sqrt{3}(R_1+R_2)}\right)}. \quad (2.7)$$

If the radii of the balls are the same $R_1 = R_2 = R$, we have:

$$Q_1 = \frac{Q}{3\cos\left(\arcsin\frac{1}{\sqrt{3}}\right)} = 0,4082 \cdot Q. \quad (2.8)$$

The friction paths for the contact areas of the upper S_2 and lower balls S_1 are different.

When determining the friction paths, we will assume that the dimensions of the contact area on the lower balls are small in comparison with the size of the contact area of the upper ball ($a \ll r_1$), the calculation of the friction path will be carried out according to the average radius r_1 .

We will assume that the friction path for each point of the lower contact area is equal to:

$$S_1 = 2\pi r_1 n t, \quad (2.9)$$

where n is the number of revolutions of the upper ball per unit of time; t is the test duration.

The friction path S_2 for the contact points of the upper ball is different and depends on:

1) from the distance r_{1y} of the points of the axis of rotation of the ball (Fig. 2.2);

2) from the size of the contact $S_2' = S_{2,y}$ area at a distance r_{1y} ,

$$S_2' = 2a_y(a, y) = 2\sqrt{a^2 - y^2}.$$

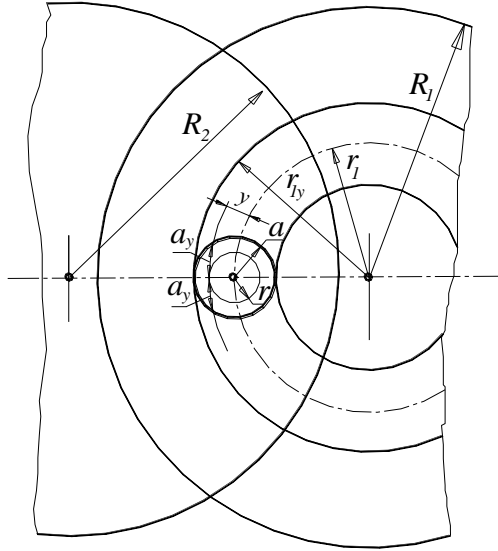


Fig. 2.2. Scheme for determining the paths of friction

On the other hand, S_2' the friction path in one pass of the contact points of the upper ball through the contact area of the upper ball: the shape of the lower contact area is a circle; the shape of the contact area of the upper ball is a ring.

Full friction path S_2 for the contact area of the upper ball:

$$S_2 = 3S_2'nt. \quad (2.10)$$

The ratio of the friction paths of the upper and lower platforms is an important characteristic of the system, sometimes called the overlap coefficient, taking into account (2.9) and (2.10):

$$K_{Fy} = \frac{S_2}{S_1} = \frac{3S_2'nt}{2\pi r_1 nt} = \frac{3}{\pi r_1} (a^2 - y^2)^{1/2}. \quad (2.11)$$

In the middle section (Fig. 2.2) at $r_{1y} = r_1$, $y = 0$

$$K_F = \frac{3a(S_1)}{\pi r_1}. \quad (2.12)$$

Thus, we have a relationship between the average friction paths:

$$S_2 = C_1 S_1 a(S_1), \quad (2.13)$$

where $C_1 = \frac{3}{\pi r_1}$.

When solving the problem, we make the following assumptions:

1) we assume that the balls are rigid, that is, contact displacements from deformations are negligible compared to displacements from wear;

2) contact pressures $\sigma(S_1)$ are evenly distributed over the contact area [2];

3) wear u_{w1}, u_{w2} of the lower and upper balls occurs in the steady state according to the models:

$$\frac{du_{w1}}{dS_1} = K_{w1} \sigma^{m_1}, \quad (2.14)$$

$$\frac{du_{w2}}{dS_2} = K_{w2} \sigma^{m_2}, \quad (2.15)$$

Where m_1, m_2, K_{w1}, K_{w2} is the parameters of the model, with this friction path S_1 and S_2 defined by the (2.9) and (2.13).

Contacting is carried out under the two conditions of continuity and equilibrium. The continuity condition in contact for one pair of balls has the form:

$$u_{w1}(S_1, r) + u_{w2}(S_2, r) = u(S_1, S_2, r), \quad (2.16)$$

where r is the radial coordinate of contact points (Fig. 2.2); $u_{w1}(S_1, r)$, $u_{w2}(S_2, r)$ is the linear wear of the lower and upper balls; $u(S_1, S_2, r)$ is the geometric function of coordination of contact movements.

Equilibrium condition in contact:

$$Q_1 = \int_F \sigma(r, S_1, S_2) dF, \quad (2.17)$$

where F is contact area on the lower ball; $\sigma(r, S_1, S_2)$ is the contact pressure distribution; Q_1 is the load on one contact area.

Relations (2.14–2.17) give a complete statement of the problem under consideration for balls with wear.

The geometric function of the coordination of contact displacements is determined from the geometry of the intersection of spherical surfaces R_1 and R_2 in the contact zone:

$$u(S_1, S_2, r) = \frac{1}{2R_{np}} \left[a(S_1, S_2)^2 - r^2 \right], \quad (2.18)$$

where $R^* = \frac{R_1 R_2}{R_1 + R_2}$.

The derivation of the differential equation of the problem is reduced to mutual substitutions of the basic relations and simple transformations. First, we represent the continuity condition in the contact in a differential form, differentiating the left and right sides along the friction path S_1 :

$$\frac{du_{w1}(S_1, r)}{dS_1} + \frac{du_{w2}(S_2, S_1, r)}{dS_2} \frac{dS_2}{dS_1} = \frac{du(S_1, S_2)}{dS_1}. \quad (2.19)$$

Taking into account (2.18), on the right-hand side we have:

$$\frac{du(S_1)}{dS_1} = a(S_1) \frac{da(S_1)}{dS_1}, \quad (2.20)$$

and on the left, taking into account (2.13):

$$\frac{dS_2}{dS_1} = \left(a(S_1) + \frac{da(S_1)}{dS_1} S_1 \right) C_1. \quad (2.21)$$

Substituting (2.14), (2.15), (2.20), (2.21) into (2.19) we obtain the following differential equation of the problem with respect to the function $a(S_1)$:

$$K_{w1} \sigma^{m_1} + K_{w2} \sigma^{m_2} C_1 \left(a + \frac{da}{dS_1} S_1 \right) = \frac{a}{R_{np}} \frac{da}{dS_1}. \quad (2.22)$$

This is the initial differential equation of the problem with respect to the function of the size of the contact $a(S_1)$ area depending on the friction path S_1 .

This equation must be solved when the equilibrium condition (2.17) is satisfied, which gives a complex relationship $a = a(S_1, \sigma, Q)$, complicating the solution of equation (2.22).

The situation is simplified if we assume the uniformity of the distribution of contact pressures over the site. This assumption is justified by the form of equation (2.22), which does not include the radial coordinate r .

With a uniform pressure distribution, the equilibrium condition (2.17) takes the form:

$$Q_1 = \pi a^2 (S_1) \sigma(S_1), \quad (2.23)$$

from here

$$\sigma(S_1) = \frac{Q_1}{\pi a^2 (S_1)}. \quad (2.24)$$

Substituting (2.24) into (2.22), we obtain a differential equation that explicitly connects the area $a(S_1)$ and friction path:

$$K_{w1} \left(\frac{Q_1}{\pi a^2} \right)^{m_1} + K_{w2} \left(\frac{Q_1}{\pi a^2} \right)^{m_2} C_1 \left(a + S_1 \frac{da}{dS_1} \right) = \frac{a}{R_{np}} \frac{da}{dS_1}. \quad (2.25)$$

We transform this nonlinear differential equation to a more convenient form:

$$\frac{b_1}{a^{2m_1}} + \frac{b_2 a}{a^{2m_2}} + \frac{b_2}{a^{2m_2}} \frac{da}{dS_1} S_1 = a \frac{da}{dS_1}, \quad (2.26)$$

where $b_1 = R_{np} K_{w1} (Q_1/\pi)^{m_1}$; $b_2 = R_{np} K_{w2} (Q_1/\pi)^{m_2} C_1$.

Further transformations give the following form:

$$\frac{da}{dS_1} \left(a^{2m_1+1} - b_2 S_1 a^{2(m_1-m_2)} \right) - b_2 a^{2(m_1-m_2)+1} - b_1 = 0. \quad (2.27)$$

At $m_1 = m_2 = 1$ equation (2.27) is reduced to the form:

$$\frac{da}{dS_1} \left(a^3 - b_2 S_1 \right) - b_2 a - b_1 = 0. \quad (2.28)$$

Solution to equation (2.27). If the top and bottom balls are made of the same material:

$$m_1 = m_2 = m; \quad K_{w1} = K_{w2} = K_w, \quad (2.29)$$

then equation (2.27) is reduced to a simpler form:

$$\frac{da}{dS_1} \left(a^{2m+1} - b_2 S_1 \right) - b_2 a - b_1 = 0. \quad (2.30)$$

We write this equation in the standard form:

$$M(a, S_1)dS_1 + N(a, S_1)da = 0;$$

$$M(a, S_1) = -b_2a - b_1; \quad N(a, S_1) = a^{2m+1} - b_2S_1.$$

We make sure that this is an ordinary differential equation in total differentials, since the condition is satisfied: $\frac{dM}{da} = \frac{dN}{dS_1}$.

The solution of equation (2.30) as a differential equation in total differentials is performed as follows:

$$u = \int MdS_1 + \phi(a) = -b_2aS_1 - b_1S_1 + \phi(a).$$

Further, using the property: $\frac{du}{da} = N$, we have: $\frac{d\phi(a)}{da} = a^{2m+1}$.

After integration: $\phi(a) = \frac{a^{2m+2}}{2m+2} + C$.

As a result, we get the equation:

$$-b_2aS_1 - b_1S_1 + \frac{1}{2m+2}a^{2m+2} = C. \quad (2.31)$$

If the condition is set $a(S_1 = 0) = 0$ we have $C = 0$. After substituting this value in (2.31), we have a nonlinear algebraic equation:

$$a^{2m+2} - (2m+2)b_2S_1a - (2m+2)b_1S_1 = 0, \quad (2.32)$$

where $b_2 = b_1C_1$; $b_1 = R_{np}K_w \left(\frac{Q_1}{\pi} \right)^m$

The solution to the problem of determining the size of the contact area is reduced to solving a nonlinear algebraic equation of the type:

$$a^n - \xi_1a - \xi_2 = 0, \quad (2.33)$$

where $\xi_1 = (2m+2)R_{np}K_w \left(\frac{Q_1}{\pi} \right)^m C_1S_1$;

$$\xi_2 = (2m+2)R_{np}K_w \left(\frac{Q_1}{\pi} \right)^m S_1; \quad n = 2m+2.$$

Obviously, only a numerical solution of the nonlinear algebraic equation (2.33) is possible.

Using the MathCad program, a numerical solution of the nonlinear equation (2.33) was carried out with the following initial data: $R = 3,175$ mm; $K_w = 1,7 \cdot 10^{-11}$ (MPa)^{-m}; $m = 1,5$; $Q_1 = 81,64$ N; $c_1 = 0,26$ mm⁻¹. The results of the numerical calculation are shown in Table 2.1.

Table 2.1.

Results of calculating dependence $a(S_1)$ at (2.33)

$S_1 \times 10^6$, mm	4	5	6	7	8	9	10
ξ_1	0,0086	0,011	0,013	0,015	0,017	0,019	0,022
ξ_2	0,033	0,041	0,05	0,058	0,066	0,075	0,083
a , mm	0,519	0,543	0,564	0,582	0,598	0,613	0,626

If the initial condition is given in the form $a(S_1 = 0) = a_0$, from (2.32) we have:

$$C = \frac{a_0^{2m+2}}{2m+2}. \quad (2.34)$$

Substituting (2.34) into (2.31) we have:

$$-b_2 a S_1 - b_1 S_1 + \frac{a^{2m+2}}{2m+2} - \frac{a_0^{2m+2}}{2m+2} = 0.$$

This leads to a non-linear algebraic equation:

$$a^{2m+2} - b_2 a S_1 (2m+2) - b_1 S_1 (2m+2) - a_0^{2m+2} = 0, \quad (2.35)$$

the exact analytical solution of which is also difficult.

Equations (2.32) and (2.35) are easily solvable with respect to the friction path. This can be used to solve the problem of determining the size of the wear area depending on the friction constraints.

So from (2.32) we have:

$$S_1 = \frac{a^{2m+2}}{(2m+2)(b_2 a - b_1)}. \quad (2.36)$$

Based on this dependence, a graph is built to determine the size of the site for a given friction path S_1 . With the above initial data, the graphical dependence $a(S_1)$, built using the MathCad program is shown in Fig. 2.3.

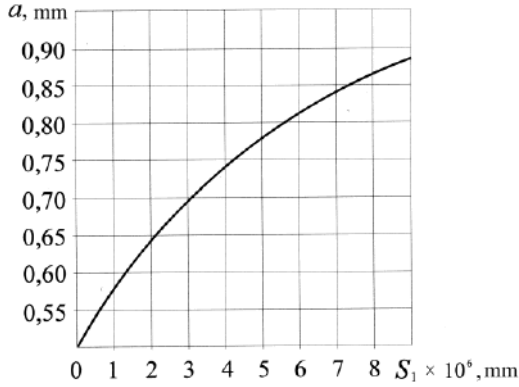


Fig. 2.3. Dependence $a(S_1)$

Inverse problem, determination of the parameters of the wear model. Now we set the following problem: determine the parameters K_w and m of the wear model of the ball material from the solution of the contact problem in the form (2.32).

Let the results of tests at two points (a_1, S_{11}) ; (a_2, S_{12}) be known from experiments: all other things being equal, including the load.

Let us write uranium (2.32) for the two indicated experiments:

$$\left. \begin{aligned} (a_1)^{2m+2} &= (2m+2)R_{np}K_w \left(\frac{Q_1}{\pi}\right)^m S_{11}(C_1a_1+1) \\ (a_2)^{2m+2} &= (2m+2)R_{np}K_w \left(\frac{Q_1}{\pi}\right)^m S_{12}(C_1a_2+1) \end{aligned} \right\}. \quad (2.37)$$

Having compiled the ratio of these equations to the left and right, we exclude the parameter K_w , namely:

$$\left(\frac{a_1}{a_2}\right)^{2m+2} = \frac{S_{11}(C_1a_1+1)}{S_{12}(C_1a_2+1)}. \quad (2.38)$$

From here we immediately obtain an expression for determining the exponent m :

$$m = \frac{\lg \frac{S_{11}(C_1a_1+1)}{S_{12}(C_1a_2+1)}}{2 \lg(a_1/a_2)} - 1. \quad (2.39)$$

Second parameter K_w we find from any of the equations (2.37):

$$K_w = \frac{(a_1)^{2m+2}}{(2m+2)R_{np} \left(\frac{Q_1}{\pi}\right)^m S_{11} (C_1 a_1 + 1)}. \quad (2.40)$$

In the case of initial contact a_0 over the site, the solution to the problem is obtained in the form (2.35), which, taking into account (2.32), can be reduced to the form:

$$a^{2m+2} - a_0^{2m+2} = (2m+2)K_w R_{np} \left(\frac{Q}{\pi}\right)^m S_1 (C_1 a + 1). \quad (2.41)$$

Let the results of tests at two points be known from experiments: $(a_1, S_{11}); (a_2, S_{12})$.

Using (2.41), we write the system of equations describing the state for the two indicated points:

$$\left. \begin{aligned} a_1^{2m+2} - a_0^{2m+2} &= (2m+2)K_w R_{np} \left(\frac{Q}{\pi}\right)^m S_{11} (C_1 a_1 + 1) \\ a_2^{2m+2} - a_0^{2m+2} &= (2m+2)K_w R_{np} \left(\frac{Q}{\pi}\right)^m S_{12} (C_1 a_2 + 1) \end{aligned} \right\}. \quad (2.42)$$

Having compiled the ratio of these equations, we get:

$$\frac{\bar{a}_1^{2m+2} - 1}{\bar{a}_2^{2m+2} - 1} = \frac{(C_1 a_1 + 1)S_{11}}{(C_1 a_2 + 1)S_{12}}, \quad (2.43)$$

where $\bar{a}_1 = a_1/a_0$; $\bar{a}_2 = a_2/a_0$.

The problem is to solve the nonlinear equation (2.43) with respect to the exponent m . A solution in a closed general form is not possible. Direct numerical solution of system (2.42) is practically possible.

It is more rational to first solve numerically the non-linear equation (2.43) with respect to the parameter m , and then defining the parameter K_w from any of equations (2.42). For example, from the first equation:

$$K_w = \frac{(a_1)^{2m+2} - a_0^{2m+2}}{(2m+2)R_{np} \left(\frac{Q}{\pi}\right)^m S_{11} (C_1 a_1 + 1)}.$$

The numerical solution of the nonlinear equation (2.43) and the determination of the parameters of the wear pattern were carried out using the MathCad program with the following initial data: $R_1 = R_2 = 6,35$ mm; $R = 3,175$ mm; $Q = 200$ N; $C_1 = 0,26$ mm⁻¹; $n = 300$ rev⁻¹ $t_1 = 60$ min; $t_2 = 300$ min.

Wear tests were carried out on a four-ball machine. As a result of the tests, the data presented in Table 2.2 were obtained.

Table 2.2

Test results

t , min	0	60	120	180	300
a , mm	0,15	0,42	0,5	0,6	0,65

Based on the actual experimental data, a graph is plotted $a = a(t)$ and $a = a(S_1)$ (Fig. 2.4).

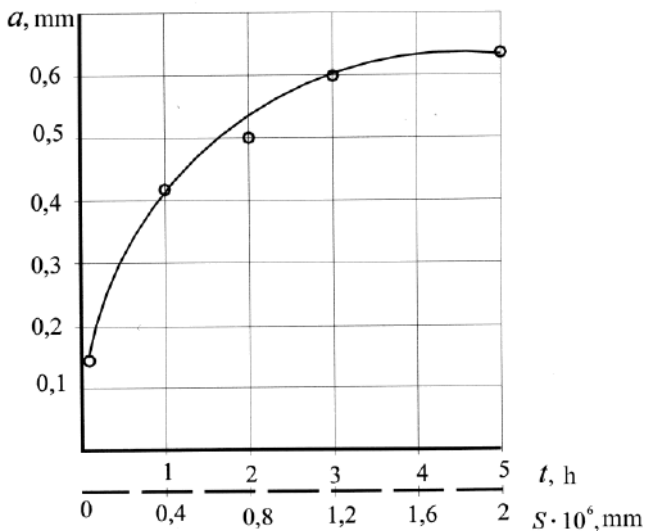


Fig. 2.4. Test results

As a result of the implementation of the further calculation algorithm using the MathCad program, the wear parameters were obtained: $m = 0,9028$; $K_w = 3,4986 \cdot 10^{-10}$ MPa^{-m}.

The contact parameters of two identical balls can be determined by the classical formulas following from the theory of Hertz.

Tests of lubricants on a four-ball machine without wear measurement, or with wear measurement, but without corresponding wear patterns, is qualitative in nature or gives an idea of the behavior of the tribosystem at extreme points. The theory of the test method for wear with lubrication according to the four-ball scheme with the determination of the parameters of steady-state wear models is proposed. The method is based on the solution of a contact problem for wearing balls. The approximate solution of the problem is based on the assumption of a uniform distribution of contact pressures at any moment of testing. When describing the process of ball wear, the contact problem with wear was reduced to an ordinary differential equation in total differentials, which was solved exactly. The calculation procedure for determining the parameters of wear models has been determined. A methodical example of the method implementation is given. The solution of direct and inverse contact problems taking into account wear makes it possible both to determine the parameters of the wear models based on the results of wear tests, and to carry out calculations of wear in this contact with the given parameters of the wear model.

2.2. Determination of wear resistance characteristics based on the results of laboratory wear tests

To solve the problem of quantifying the tribotechnical characteristics of lubricants and structural materials, an experimental setup using the prototype four-ball friction machine was used. The main part of the installation is a working unit, the construction of which is shown in Fig. 2.1. The upper ball 1 is based and centered in the spindle, which eliminates the beating of the ball during rotation and increases the rigidity of the drive unit. The lower three balls 2 with a diameter of 12.7 mm are mounted on the hardened and ground surface of the support 4. Fastening and self-centering of the lower balls is carried out by a nut 3 with a conical working surface. The top plane of the nut 3 is used as the measuring base. At the same time, the zone of the lower balls is maximally open to the study of the geometry of the wearing surfaces without disassembling the installation. Self-alignment of the upper and lower balls is provided by a radial spherical double-row ball bearing 5. To measure the friction torque is a ball thrust single-row bearing 6. Installation for testing is based and fixed on the base 7. A thermometer is used to control the temperature in the friction zone of the balls. The sensitive measuring element of the thermometer is placed through the central hole in the support under the lower balls. During testing, the lubricant temperature in the friction zone is continuously monitored.

Three test schemes were proposed: four balls, a ball-ring, a cone-ring (Fig. 2.5). This approach methodically provides the nomenclature of the most

common real friction pairs: rolling bearings, gears, cam mechanisms – the first scheme; bearings, articulated mechanisms, cylinder-piston group of engines – the second and third scheme. When testing in accordance with schemes 2 and 3, the working unit of the laboratory installation is used 1, where instead of three balls a ring is set, and in the spindle instead of a ball a cone is inserted.

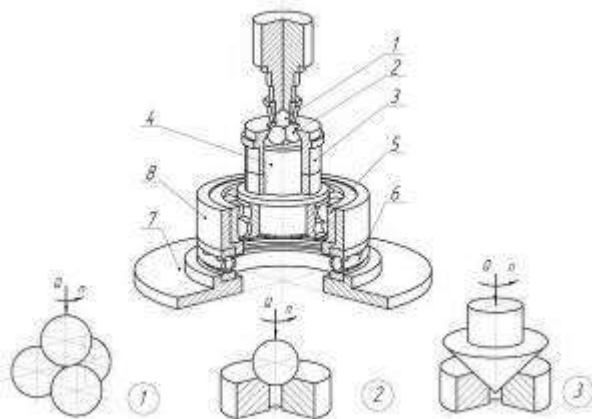


Fig. 2.5. The working unit of the laboratory installation and design test schemes

To measure the size of wear spots on the lower balls, an MPB-2 microscope with a scale division of 0.05 mm was used. The upper ball was rotated with the aid of the installation spindle and the microscope was mounted on the measuring plane of the nut 3 to measure the wear spot.

The wear spot diameter was determined as the geometric mean of the lengths of the ellipse axes of the ball wear spots.

During testing, the upper ball rotates and presses with force Q on three fixed lower balls (Fig. 2.6). After the tests, a circular radius wear area a is formed on the lower balls. The effect of elastic deformations of the balls on the formation of the contact area is neglected. The contact area of the upper and lower balls is filled with lubricant.

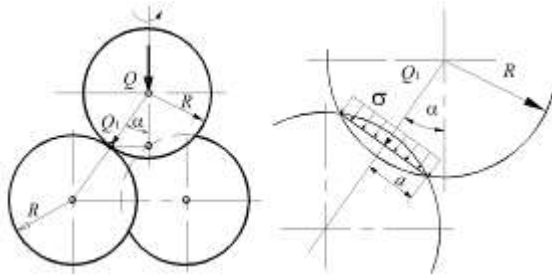


Fig. 2.6. Four ball test scheme

For a quantitative wear characteristic, the dependence of the wear rate on two dimensionless parameters is proposed: load and sliding speed in the form:

$$I = \frac{du_w}{dS} = k_w \left(\frac{\sigma}{E^*} \right)^m \left(\frac{VR^*}{v} \right)^n. \quad (2.44)$$

Dependence of linear deterioration u_w on radius of a platform of wear process a of the bottom spheres is defined from geometry of crossing of spherical surfaces (Fig. 2.6):

$$u_w(S) = \frac{a(S)^2}{2R}. \quad (2.45)$$

According to the results of tests for wear, the dependence of the radius of the circular wear area on the friction path is represented as a power approximation:

$$a(S) = cS^\beta. \quad (2.46)$$

Taking into account (2.46), expression (2.45) can be given the form:

$$u_w = \frac{c^2 S^{2\beta}}{2R}. \quad (2.47)$$

It is assumed that the contact pressures are evenly distributed over the contact area. Then the contact pressure is determined from the equilibrium condition at the contact of the balls:

$$\sigma = \frac{0,4082Q}{\pi a^2}. \quad (2.48)$$

In this case, the normal force is expressed from geometrical relations through the central force. Substituting the dependences (2.46–2.48) into the pattern of wear (2.44), after integrating along the friction path, we get:

$$\frac{c^2 S^{2\beta}}{2R} = K_w \left(\frac{0,4082Q}{c^2 \pi E^*} \right)^m \left(\frac{VR^*}{v} \right)^n \frac{S^{1-2\beta m}}{1-2\beta m}.$$

From the condition of satisfying the last equation for any S it follows:

$$m = \frac{1-2\beta}{2\beta}. \quad (2.49)$$

To find the parameter n tests are performed at two values of the sliding velocity and, whence two groups of data with parameters are obtained. After substitutions for two sliding speeds, we obtain a system of two equations:

$$\left. \begin{aligned} \frac{c_1^2 S^{2\beta}}{2R} &= K_w \left(\frac{0,4082Q}{c_1^2 \pi E^*} \right)^m \left(\frac{V_1 R^*}{v} \right)^n \frac{S^{1-2\beta m}}{1-2\beta m} \\ \frac{c_2^2 S^{2\beta}}{2R} &= K_w \left(\frac{0,4082Q}{c_2^2 \pi E^*} \right)^m \left(\frac{V_2 R^*}{v} \right)^n \frac{S^{1-2\beta m}}{1-2\beta m} \end{aligned} \right\}$$

From the resulting system we find the second parameter:

$$n = (2m + 2) \frac{\lg(c_1/c_2)}{\lg(V_1/V_2)}. \quad (2.50)$$

To find the coefficient K_w , we use one of the equations of the resulting system:

$$K_w = \frac{\beta c_1^{2m+2}}{R} \left(\frac{2\pi E^*}{0,4082Q} \right)^m \left(\frac{v}{V_1 R^*} \right)^n. \quad (2.51)$$

The obtained parameters (2.49–2.51) identify the wear law (2.44), which is used to quantify the wear of machine parts under specified operating conditions. Tests according to the pyramid scheme of four steel balls (Fig. 2.6) simulate the wear of non-conformal contact parts of steel and cast-iron materials (gears, cam mechanisms, rolling bearings, etc.) For testing bearing materials, including polymeric materials, for conformal contact (plain bearings, hinges, etc.) it is more rational to use the “ball - ring” scheme for testing.

In this case, the dependence (2.44) is also used as the law of wear. The design scheme for testing a ball in contact with a ring is shown in Fig. 2.7. The ball with a radius R rotates and presses with force Q on the internal chamfer of the ring hole with a radius r .

From the design scheme, ring wear u_w is characterized by moving the lowest point A of the sphere to a point A_1 . Then the dependence of the linear wear of the ring on the width of the contact area a will be determined:

$$u_w = A_1O - AO = \frac{(a+r)^2}{2R} - \frac{r^2}{2R} = \frac{a(S)r}{2R}. \quad (2.52)$$

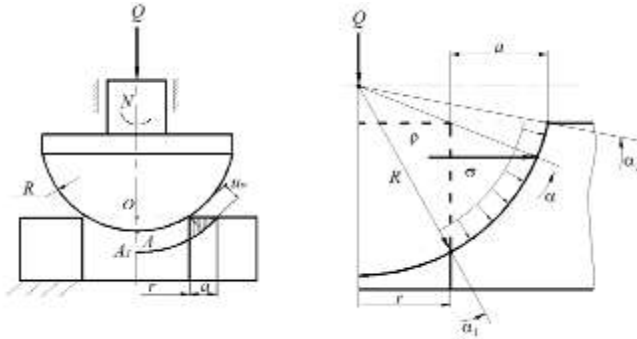


Fig. 2.7. Calculated contact model of a ball and a ring

The results of the ball ring wear test are also approximated by a power function of the form (2.46). The function of contact pressures with a uniform distribution is found from the equilibrium condition at the contact of the ball and the ring:

$$Q = \int_{\alpha_1}^{\alpha_2} \sigma \cos \alpha \cdot 2\pi R^2 \sin \alpha d\alpha. \quad (2.53)$$

After integrating the equilibrium equation and transformations, we obtain:

$$\sigma = \frac{Q}{2\pi a)sr}. \quad (2.54)$$

Substituting into the wear law (2.44) the expressions (2.53), (2.54) after integration we get:

$$\frac{cS^\beta r}{R} = K_w \left(\frac{Q}{c \cdot 2\pi r E^*} \right)^m \left(\frac{VR^*}{v} \right)^n \frac{S^{1-\beta m}}{1-\beta m}. \quad (2.55)$$

From the condition of satisfiability of equation (2.55) we find the parameter: $m = \frac{1-\beta}{\beta}$.

Other parameters of the law of wear are defined in the same way as for the four-ball scheme:

$$n = (m+1) \frac{\lg(c_1/c_2)}{\lg(V_1/V_2)};$$

$$K_w = \frac{\beta c_1^{m+1} r^{m+1}}{R} \left(\frac{2\pi E^*}{Q} \right)^m \left(\frac{v}{V_1 R^*} \right)^n.$$

In the proposed test schemes restriction is the material of the ball and the technological complexity of its manufacture. To expand the range of tested materials, a third “cone-ring” test scheme is proposed (Fig. 2.8). Making a conical sample is technologically simpler compared to making a ball. Thus, a “cone-ring” scheme is recommended for testing conformal contacts of parts from different construction materials.

Consider the contact interaction of the cone with the angle 2γ and the hole of the ring with a radius r . In this case, the ring is stationary, and the cone rotates and presses the ring with force Q (Fig. 2.8).

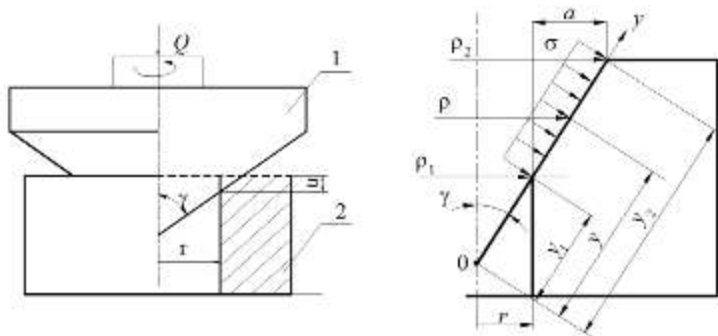


Fig. 2.8. Calculated contact model “cone-ring”

Wear area a and linear wear u_w are related by a geometric ratio:

$$u_w = a(S) \cos \gamma. \quad (2.58)$$

The function of contact pressures with a uniform distribution is found from the equilibrium condition at the contact of the cone and ring (Fig. 2.8):

$$Q = \int_{y_1}^{y_2} \sigma \sin \gamma 2\pi y \sin \gamma dy .$$

After integrating the equilibrium equation and transformations, we obtain:

$$\sigma = \frac{Q}{2\pi a(S)r} . \quad (2.56)$$

Substituting the obtained expressions (2.56, 2.57) after integration into the pattern of wear of the type, we get:

$$cS^\beta \cos \gamma = K_w \left(\frac{Q}{c2\pi r E^*} \right)^m \left(\frac{Vr}{v} \right)^n \frac{S^{1-\beta m}}{1-\beta m} . \quad (2.57)$$

By analogy with the previous test schemes, the parameters of wear are determined by the formulas:

$$m = \frac{1-\beta}{\beta} ; n = (m+1) \frac{\lg(c_1/c_2)}{\lg(V_1/V_2)} ;$$

$$K_w = \beta c_1^{m+1} \cos \gamma \left(\frac{2\pi r E^*}{Q} \right)^m \left(\frac{v}{V_1 R^*} \right)^n .$$

Test results for lubricants and construction materials

Initial data:

The scheme 1. Four balls.

$R = 6,35$ mm; $Q = 65$ N; 3. $N_1 = 200$ rev/min ($V_1 = 0,077$ m/s), $N_2 = 600$ rev/min ($V_2 = 0,19$ m/s); 52100 steel balls; motor oil API- SJ/CD, SAE - 15W/40 ($v = 12$ mm²/s).

The scheme 2. Ball-ring.

$R = 6,35$ mm, $r = 3$ mm; $Q = 65$ N; $V_1 = 0,063$ m/s, $V_2 = 0,19$ m/s); 52100 steel balls; rings – aluminium; motor oil API- SJ/CD, SAE – 15W/40 ($v = 12$ mm²/s).

The scheme 3. Cone-ring.

$\gamma = 30^0$, $r = 3$ mm; $Q = 65$ N; $V_1 = 0,063$ m/s, $V_2 = 0,19$ m/s; material of a cone – steel 45; rings – bronze CuSn10P; motor oil API-SJ/CD, SAE – 15W/40 ($v = 12$ mm²/s).

The test results are presented in Table 2.3.

Table 2.3

Dependence of wear processes a (mm) from duration of tests (200/600 of rev⁻¹)

Scheme	35 min	65 min	95 min	125 min	155 min
1	0,35	0,4	0,43	0,48	0,5
	0,48	0,54	0,63	0,65	0,67
2	0,125	0,2	0,25	0,275	0,35
	0,25	0,35	0,4	0,475	0,5
3	0,125	0,2	0,225	0,25	0,275
	0,225	0,325	0,375	0,4	0,425

As a result, the parameters of wear models of type (2.44) were determined, which are presented in Table 2.4.

Table 2.4

The laws of wear materials

Four balls	$I = 0,025 \left(\frac{\sigma}{E^*} \right)^{1,62} \left(\frac{VR^*}{v} \right)^{0,135}$
Ball-ring	$I = 4,7 \cdot 10^7 \left(\frac{\sigma}{E^*} \right)^{4,19} \left(\frac{VR^*}{v} \right)^{0,441}$
Cone-ring	$I = 2,19 \cdot 10^8 \left(\frac{\sigma}{E^*} \right)^{4,37} \left(\frac{Vr}{v} \right)^{0,403}$

The obtained laws of wear allow one to quantify the intensity of wear depending on: load characteristics, properties of structural and lubricant materials, kinematic and design parameters. Quantitative values of the wear rate allow optimizing the design parameters of parameters and operating conditions by the criterion of maximum wear resistance. In Fig. 2.9 shows the graphic dependences of the wear rate on the basic factors: contact pressure and sliding speed, obtained on the basis of the wear laws given in Table 2.2.

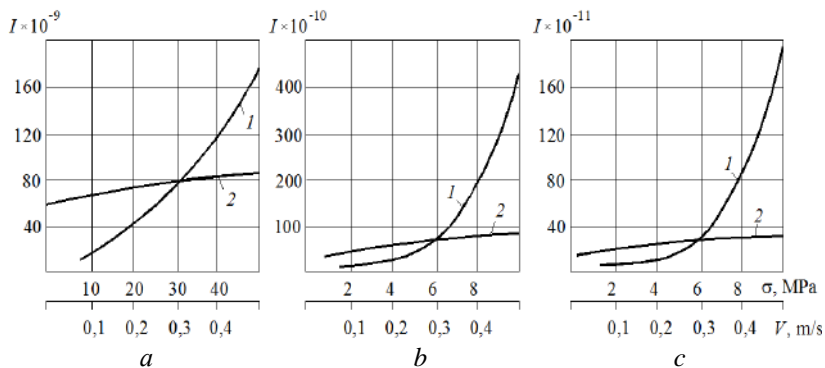


Fig. 2.9. The dependence of wear rate on contact pressure and sliding speed:
a – four balls; *b* – a ball ring; *c* – cone - ring

The laws of wear and their graphical interpretation indicate the insignificant effect of changes in the sliding rate on the wear process for these test conditions. Analytical methods for calculating the wear resistance of lubricated tribosystems require consideration of the nonlinearity of wear patterns due to the complex interrelationships of mechanical, thermal, and friction properties. A two-factor model of wear (contact pressure, sliding speed) in a dimensionless form, taking into account the properties of structural and lubricants of a friction pair, is proposed. On the basis of solving inverse wear-contact problems, calculation formulas were obtained for identifying the parameters of the wear law. The proposed methodology for identifying wear laws based on laboratory tests is recommended for predicting wear and optimizing the design and performance characteristics of lubricated tribosystems.

2.3. Study of the viscosity properties of lubricants by the pendulum method

2.3.1. Damped vibration method in the study of friction processes

The material of machine parts possesses a property to absorb energy at deformation. This physical property of material, typically called internal friction, is closely connected with its operational performance properties: strength and wear resistance. Internal friction in the volume of material was studied well enough and its patterns are widely used in materials science when creating the materials.

The laws that govern the processes of absorbing the external energy by the surface of machine parts are explored considerably less. Processes in the surface layer are more complex than in the volume. Two forms of

friction are combined here: internal and external. In this case, the processes proceed in the very small volumes of material and their study requires the application of fairly complicated methods of contact mechanics.

The methods for determining the characteristics of internal friction are divided into direct (energy, thermal, hysteresis loop) and indirect (damping oscillations, resonance curve, phase).

The testing procedures and the devices that implement the methods indicated are based on different techniques:

- the longitudinal or torsional vibrations of tubular samples;
- torsional vibrations of solid samples;
- the high-frequency longitudinal vibrations of a solid rod.

The test procedures, based on the lateral oscillations of the samples, have been used most frequently:

- at the cantilever fastening of a sample;
- at the freely hung samples;
- in pure bending conditions.

All the known procedures are implemented on rather sophisticated installations, equipped with devices for the automatic measurement of oscillation amplitudes.

Among many methods of determining the absorption coefficient, a damped oscillation method is the easiest one. As far as the study of surface energy properties is concerned, the damped oscillation method is most effectively realized with the help of swinging pendulums.

The pendulum damped oscillation method was first employed by Newton for investigating the resisting forces to motion of a solid body in fluids and gases. The obtained results laid the foundation for hydrodynamics of laminar flow and contemporary viscosimetry.

A wide application of a pendulum method for examining the processes of friction is explained by the fact that the damping is fully predetermined by external friction under different operating conditions: materials, surface condition, temperature, composition of lubricants, layer thickness. It is important that it is possible by a change in the shape of attenuation curves to draw conclusions about the influence of these conditions on the processes of friction.

A lack of reliable procedures for determining the characteristics of viscous friction considerably complicates the task of developing the designs of friction units of contemporary machines and the optimization of energy losses during friction in order to decrease them.

A number of papers address theoretical and experimental studies into the methods for determining the energy, absorbed by a surface, including the processes of friction at damped oscillations.

By using the pendulum method, described in monograph [13], it was established that under conditions of viscous friction, oscillation attenuation

curve on the elastic layer of molecules has a linear law. However, the oscillation attenuation curve on an unordered layer of lubricant is characterized by the logarithmic law of damping. These data were obtained experimentally and the study lacks a theoretical description of the mechanisms of viscous friction, which explain the results received.

Article [14] examined experimentally and theoretically free fluctuations of a physical pendulum, which rests with two balls on a flat surface. The theory of damping fluctuations proposed in the study for evaluating the energy losses is of a phenomenological nature and is not based on a strict mathematical description of the mechanisms of fluctuation process, which makes it difficult to give the quantitative assessment of losses caused by friction.

In paper [15], a differential equation for the swinging pendulum is obtained, taking into account the deformation of a surface and a deformation component of the friction force. However, the authors examined only a particular case of small deformations, commensurate with the dimensions of contact area of the ball support of a pendulum. This solution is not applicable for describing the macro-displacements in the support of a pendulum, characteristic for the actual friction units of sliding in machines.

Authors of article [16] conducted a nonlinear regression analysis based on the results of experimental studies into the damped oscillations of a physical pendulum, which made it possible to formulate the criteria for choosing a theoretical model of the dissipation of viscous friction. However, the experiments were performed for the conditions of balls rolling on the support, that is, for the small areas of contact in comparison with dimensions of the balls, which also does not make it possible to adequately utilize the obtained results for evaluating the characteristics of viscous friction in cylindrical sliding supports (bearings).

Paper [17] describes an experimental study of losses to friction in the friction pairs made of metal-polymer materials. In this case, dry friction without the use of a lubricant is examined, which is not characteristic for the cylindrical sliding supports that work under boundary or even liquid friction mode.

Article [18] explores approaches in the development of procedures for determining the characteristics of friction convenient for the practical application under operating conditions of machines. Simple formulas for calculating the coefficient of friction at reciprocating rocking movements on a pendulum device are proposed. The formulas received are not based on the differential equations, which describe the process of viscous friction, and yield only rough estimates of the indices of friction.

Paper [19] deals with the estimated-experimental procedures for determining the characteristics of friction based on a variation approach. This approach implies the use of approximating dependences of experimental data,

which renders the solution approximate, depending on the subjective factors.

The experimental method for measuring the characteristics of friction was applied in article [20] for examining special features of high-speed friction under conditions of thermal loading and at limited lubrication. The criterion of damping the friction fluctuations proposed in this case is not applicable to the case of viscous friction, where such fluctuations are practically absent as a result of the damping action of a layer of lubricant.

Paper [21] employed a pendulum method in order to solve a problem on determining the contact rigidity of steel spherical models at dynamic loading using the system of differential equations. However, the tangential component of contact stresses from the frictional forces in this case was not considered.

Articles [22, 23] proposed and implemented design concepts of devices for the accelerated tests on friction and adhesive properties of the actual friction units of the "wheel – rail" type. The design of a pendulum device, applied in the work, for studying the adhesive properties according to the scheme "cylinder – plane" does not allow using it for evaluating the viscous friction of cylindrical sliding supports.

2.3.2. Theoretical model of pendulum in the sliding supports with a lubricant for examining the viscous friction

Viscosity or internal friction is the most important physical property of oils, which ensures the separation of hard surfaces and their normal operation at minimal wear.

The tangential force T_{Fr} that occurs at relative sliding of the adjacent layers of a fluid (by force of viscous friction), is determined by the Newton law:

$$T_{Fr} = \mu \frac{dV_x}{dy} F,$$

where μ is the dynamic viscosity; F is the displacement area; V_x is the speed in direction of the x axis; dy is the direction perpendicular to the x axis.

By dividing the force of viscous friction T_{Fr} to the displacement area F , we shall obtain the stress of viscous shear:

$$\tau = \frac{T_{Fr}}{F} = \mu \frac{dV_x}{dy},$$

In the case of small thickness h of the layer, it is possible to accept:

$$\frac{dV_x}{dy} = \text{const} = \frac{V}{h}.$$

Thus we obtain: $\tau = \mu \frac{V}{h}$.

Let us examine the schematic of pendulum oscillations (Fig. 2.10) with a support in the form of sliding bearing 1. When the gap in a sliding bearing is fully filled with a lubricant, the working area of shaft friction along the lubricant is equal to:

$$F_{Fr} = \pi RB,$$

where B is the size of bearing on the generatrix; R is the radius of bearing.

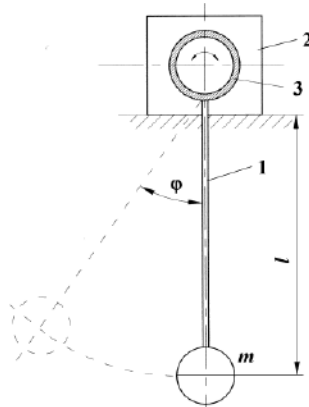


Fig. 2.10. Schematic of pendulum with a support in the form of a sliding bearing with a lubricant: 1 – pendulum; 2 – sliding support; 3 – oil
Shearing force over the entire circle in the bearing (Fig. 2.10):

$$T_{Fr} = \tau F_{Fr} = \mu \frac{V}{h} 2\pi RB.$$

If one considers that the linear sliding speed:

$$V = R\dot{\varphi} = R \frac{d\varphi}{dt},$$

we receive

$$T_{Fr} = \frac{\mu}{h} 2\pi R^2 B \dot{\varphi}, \quad (2.58)$$

where φ is the angle of rotation of the shaft.

The moment of resistance to the rotation of shaft from the viscous lubricant:

$$M_{\mu} = \mu^* R^2 \dot{\varphi}, \quad (2.59)$$

where

$$\mu^* = \frac{\mu}{h} 2\pi RB. \quad (2.60)$$

In addition to the viscous resistance to the rotation, the shaft is exposed to two more moments:

the inertial force moment:

$$M_j = J\ddot{\varphi} = ml^2\ddot{\varphi}, \quad (2.61)$$

and the pendulum weight moment:

$$M_Q = Ql \sin \varphi = mgl \sin \varphi. \quad (2.62)$$

The equation of equilibrium includes the sum of all moments:

$$M_\mu + M_j + M_Q = 0 \quad (2.63)$$

or

$$ml^2\ddot{\varphi} + \mu^* R^2 \dot{\varphi} + mgl \sin \varphi = 0. \quad (2.64)$$

At small oscillations $\varphi \approx \sin \varphi$, we have a classical oscillation equation with viscous resistance:

$$\ddot{\varphi} + 2n\dot{\varphi} + p^2\varphi = 0, \quad (2.65)$$

where $2n = \frac{\mu^* R^2}{ml^2}$.

Considering (2.60):

$$n = \frac{\pi\mu R^3 B}{hml^2},$$

$$p^2 = \frac{g}{l}. \quad (2.66)$$

Characteristic equation of the differential oscillation equation (2.65):

$$s^2 + 2ns + p^2 = 0,$$

has two imaginary roots:

$$s = -n \pm i\sqrt{p^2 - n^2} = -n \pm ip_1; \quad p_1 = (p^2 - n^2)^{\frac{1}{2}}.$$

In the presence of linear roots, equations (2.65) take the form:

$$\varphi = e^{-nt} (c_1 \cos p_1 t + c_2 \sin p_1 t) \quad (2.67)$$

or, by denoting:

$$c_1 = A \cos \varphi;$$

$$c_2 = A \sin \varphi,$$

we obtain another form of the solution:

$$\varphi = Ae^{-nt} \cos(p_1 t + \varphi), \quad (2.68)$$

where

$$A = (c_1 + c_2)^{\frac{1}{2}}; \quad \operatorname{tg} \varphi = -\frac{c_2}{c_1}. \quad (2.69)$$

Constants c_1 and c_2 are determined from the initial conditions (in the initial period of time the pendulum is deflected by angle φ_0):

$$\varphi(t=0) = \varphi_0; \quad \dot{\varphi}(t=0) = 0. \quad (2.70)$$

Considering the solution (2.69), we receive:

$$c_1 = \varphi_0,$$

$$\dot{\varphi}_0 = c_1 n + c_2 p_1 = 0,$$

$$c_2 = -\varphi_0 \frac{n}{p_1}. \quad (2.71)$$

By substituting constants c_1 and c_2 in (2.69), we obtain:

$$A = \varphi_0 \left(1 + \frac{n^2}{p_1^2} \right)^{\frac{1}{2}}. \quad (2.72)$$

It follows from the solution that in the presence of viscous friction the motion of load is described by the periodic damping oscillations with a period:

$$T = \frac{2\pi}{p_1} = \frac{2\pi}{\sqrt{p^2 - n^2}}, \quad (2.73)$$

where p_1 is the angular frequency of damping oscillations.

From the relation of two sequential maximum deflections of pendulum φ_k and φ_{k+1} from the position of equilibrium, we obtain:

$$\varphi_k = \varphi_{k+1} e^{nT}, \quad (2.74)$$

which corresponds to a geometric progression.

More frequently used in practice is the logarithm from the magnitude of ratio of the adjacent amplitudes, which are called the logarithmic damping decrement:

$$\delta = \ln \frac{\varphi_k}{\varphi_{k+1}} = nT. \quad (2.75)$$

If the oscillations are damped slowly and ratio $\frac{\varphi_k}{\varphi_{k+1}} \approx 1$ is close to unity, then:

$$\delta = \ln \frac{\varphi_k}{\varphi_{k+1}} = \ln \frac{\varphi + \Delta \frac{\varphi}{2}}{\varphi - \Delta \frac{\varphi}{2}} \approx \frac{\Delta \varphi}{\varphi}, \quad (2.76)$$

where

$$\Delta \varphi = \varphi_k - \varphi_{k+1};$$

$$\varphi = \frac{(\varphi_k + \varphi_{k+1})}{2}.$$

Thus, at slow damping, the logarithmic decrement is approximately equal to the ratio of amplitude change during period T to the mean amplitude φ . We should note that viscous friction does not practically affect the oscillation frequency.

2.3.3. Results of determining the characteristics of viscous friction by the method of pendulum in the sliding supports

The procedures for determining the characteristics of friction are proposed based on the given theory of pendulum oscillation in the sliding support with a lubricant: coefficient of energy absorption at friction and coefficient of fluid friction – viscosity.

Pendulum is an ideal instrument for determining the energy absorbed by a surface at contact interaction. The decrease in amplitude over a cycle is connected to a decrease in the potential energy of the load that causes oscillations. The less the losses the longer the pendulum oscillates and the longer the oscillations last the more accurate the measurement of energy losses is.

The basic pattern in the oscillations of a pendulum with viscous friction takes the form of the type (2.74).

By definition, absorption coefficient ψ is the magnitude, equal to the ratio of energy ΔP , lost over a cycle, to the total energy P over the cycle. Considering (2.76), we obtain:

$$\psi = \frac{\Delta P}{P} = \frac{2\Delta\varphi}{\varphi}. \quad (2.77)$$

Therefore:

$$\psi = 2 \frac{\varphi_k - \varphi_{k+1}}{\varphi_k} = \frac{2\Delta\varphi}{\varphi} = 2 \ln \frac{\varphi_k}{\varphi_{k+1}} \quad (2.78)$$

or

$$\psi = 2 \left(1 - \frac{\varphi_{k+1}}{\varphi_k} \right) = 2 \left(1 - e^{-nT} \right). \quad (2.79)$$

When calculating the absorption coefficient based on the results of tests at viscous friction, it is possible to examine several limits and to approximately determine the averaged value of coefficient ψ by formula:

$$\psi = \frac{2}{N} \frac{\varphi_k - \varphi_{k+N}}{\varphi_k}. \quad (2.80)$$

The procedure for determining the absorption coefficient by the damped oscillations of a pendulum:

- 1) the envelope curve $\varphi(t)$ is constructed;
- 2) absorption coefficient for two adjacent amplitudes is determined by formula (2.79);
- 3) or, for the section on the envelope curve from φ_k to φ_{k+N} , the absorption coefficient is computed by formula (2.80).

Example of determining the coefficient of energy absorption at friction.

It is required to determine the coefficient of energy absorption in the contact between a sliding bearing and a lubricant at the following initial conditions on the pendulum:

$$l = 350 \text{ mm}; Q = 2 \text{ H}; R = 15 \text{ mm}; B = 20 \text{ mm}; h = 0.05 \text{ mm}.$$

It is found from the experiment on the envelope curve:

$$T = 1 \text{ s}; \frac{\varphi_k}{\varphi_{k+1}} = 1,19.$$

Find by formula (2.75):

$$n = \frac{1}{T} \ln \frac{\varphi_k}{\varphi_{k+1}} = \ln 1,19 = 0,1739 c^{-1}.$$

The absorption coefficient is determined according to formula:

$$\psi = 2 \ln \frac{\Phi_k}{\Phi_{k+1}} = 0,3479.$$

Based on the obtained results, we shall also examine the procedure for determining the coefficient of fluid friction (viscosity).

If, in the course of experiment, the validity of dependence of the type (2.74) is established, and the oscillatory period T is found, then we receive from (2.75):

$$n = \frac{1}{T} \ln \frac{\Phi_k}{\Phi_{k+1}}. \quad (2.81)$$

We obtain from dependence (2.68):

$$n = \frac{\pi \mu R^3 B}{h m l^2} = \frac{\pi \mu R^3 B g}{h Q l^2}, \quad (2.82)$$

where $g = 9810 \text{ mm/s}^2$.

The magnitude of dynamic viscosity is determined from (2.82):

$$\mu = \frac{nhQl^2}{\pi R^3 Bg}. \quad (2.83)$$

At a small load, the thickness of oil film can be accepted equal to the gap:

$$\mu = \Delta = R_2 - R_1,$$

where R_2 is the radius of bushing; R_1 is the radius of shaft.

Example of determining the dynamic viscosity of lubricants.

The tests were conducted on the pendulum device whose design is shown in Fig. 2.11.

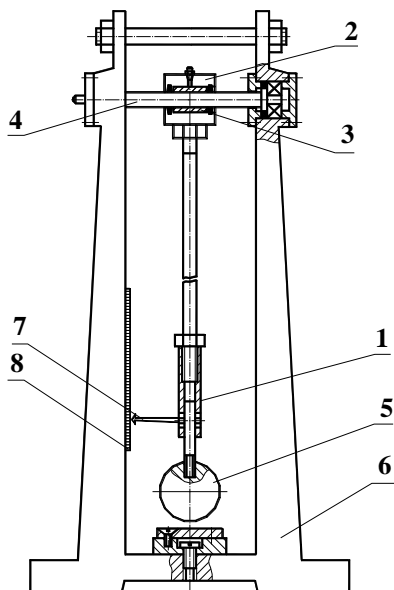


Fig. 2.11. Design of the pendulum device: 1 – suspension; 2 – sliding support; 3 – insert; 4 – shaft; 5 – load; 6 – housing; 7 – indicator; 8 – dial

The suspension of pendulum 1 in the upper part was fixed to cylindrical sliding bearing 2 with disposable inserts 3 made of the examined materials. The lubricant under pressure was fed through the lubricator in the bearing housing into the gap between the insert and shaft 4. Load 5 was attached to the lower part of the suspension. Indicator 7 on graduated dial 8 controlled the angle of pendulum deflection. Scale value of the dial is 1° .

Parameters of the pendulum device are as follows:

- length of pendulum $l = 350$ mm;
- weight of pendulum $G_1 = 2$ H; $G_2 = 4$ H; $G_3 = 2$ H;
- radius of bearing $R = 15$ mm;
- width of bearing $B = 20$ mm;
- thickness of the layer of the lubricant (it is accepted equal to the gap)

$h = 0.05$ mm.

During testing, we employed four types of materials of the inserts and three types of lubricants (Table 2.3).

Table 2.3

Results of determining the characteristics of viscosity of the lubricants

Bearing	Viscosity characteristics at loading
---------	--------------------------------------

material		Motor oil SAE 15W-5 (Agrinol, Ukraine)			Motor oil Formula Q8 (Q8Oils, Kuwait)			Solidol-S (Agrinol, Ukraine)		
		2H	4H	6H	2H	4H	6H	2H	4H	6H
Organic glass	<i>N</i>	22	26	28	18	22	26	7	11	16
	<i>n</i>	0.24	0.19	0.18	0.29	0.24	0.19	0.82	0.49	0.33
	μ	2.83	4.48	6.47	3.43	5.65	6.71	9.66	11.6	11.6
Copper	<i>N</i>	13	15	18	10	13	16	5	9	14
	<i>n</i>	0.41	0.35	0.29	0.55	0.41	0.33	1.22	0.61	0.38
	μ	4.85	8.32	10.3	6.47	9.71	11.6	14.4	14.4	13.4
Brass	<i>N</i>	18	24	28	14	19	22	6	12	16
	<i>n</i>	0.29	0.21	0.18	0.38	0.27	0.24	0.99	0.45	0.33
	μ	3.43	5.06	6.47	4.48	6.48	8.48	11.7	10.6	11.6
Bronze	<i>N</i>	14	17	19	12	14	17	5	9	13
	<i>n</i>	0.38	0.31	0.27	0.45	0.38	0.31	1.22	0.61	0.41
	μ	4.47	7.28	9.72	5.29	8.95	10.9	14.4	14.4	14.6

Note: *N* – number of oscillations to the full stop of a pendulum; *n* – coefficient of viscous resistance of a lubricant; μ – dynamic viscosity of a lubricant, Pa·s.

Initially, the pendulum deflected from the horizontal axis by 90°. Next, the dial (Fig. 2.11) registered a decrease in the deflection angle of the pendulum until its full stop. The accuracy of angle measurement reached 1° by the scale of the dial. Thus we obtained the experimental sample of values of the adjacent deflection angles of the pendulum φ_k and φ_{k+1} consisting of *N* values (number of oscillations until a full stop). Then we found their ratios φ_k/φ_{k+1} . The mean value of the obtained sample of values of the adjacent deflection angles was calculated by formula:

$$\frac{\sum_1^N \left(\frac{\varphi_k}{\varphi_{k+1}} \right)}{N}$$

The coefficient of variation in ratio φ_k/φ_{k+1} for the entire array of tests was within the limits $v = 0.15...0.25$. The coefficient of liquid resistance of lubricant *n* was calculated by formula (2.81) and next we calculated the value of dynamic viscosity μ by (2.83). Results of the calculation of these characteristics are given in Table 2.3.

An analysis of the obtained results (Table 2.3) reveals that all tested types of design materials, when lubricated with liquid oils, demonstrated an increase in the values of the indicator of dynamic viscosity μ at increasing load (Table 2.3). When lubricated with a grease lubricant, the indicator of dynamic viscosity changed insignificantly (not exceeding 10 %), which

indicates a better load-bearing capacity of grease lubricants.

The obtained values of viscous characteristics of the liquid lubricants depend on the type of material, which an insert of the sliding support was made of. Viscosity varies from the lowest to the largest value for the tested oils in the following order: organic glass – brass – bronze – copper. This is related to a different adhesive degree of the lubricants and surfaces of the examined materials. The degree of adhesion can be indirectly assessed by a contact-wetting angle of the surface of materials. The adhesion is stronger with better wettability.

The contact-wetting angle Θ was measured in the following way (Fig. 2.12). The drop of examined fluid 5 was applied by a pipette to the surface, then it was illuminated by strong luminous source 1 (we recommend using a point source) and projected onto screen 4. A hard surface was put up in parallel to the illuminating cone of rays so that the projection of the hard surface was projected onto the screen in the form of a thin line. The image of the drop on the screen was outlined or photographed 4.

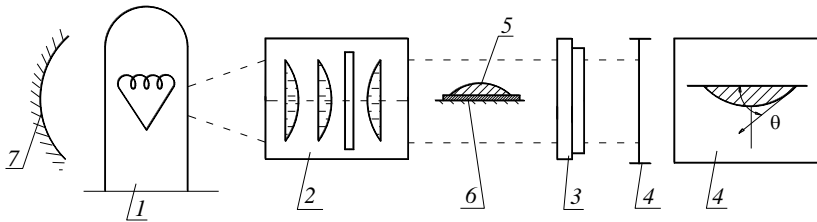


Fig. 2.12. Schematic of wetting angle measurement:

- 1 – source; 2 – condenser (illuminating lens); 3 – projection lens;
4 – screen; 5 – drop of oil; 6 – surface of material; 7 – reflecting mirror**

In the point of intersection of the drop's projection and the surface we built a tangent and determined the magnitude of contact angle.

As an example, we measured the angle of wetting the surface of samples made of organic glass, brass, bronze and copper with the motor oil SAE 15W-5 (Agrinol, Ukraine).

For statistical representativeness, each experiment on applying the drop of oil at the appropriate surface of the sample was repeated 5 times. Table 2.4 gives the averaged values, obtained when measuring the angle of wetting. The value of variation coefficient that characterizes the spread of obtained measurement results was within the limits $\nu = 0.15...0.2$, which indicates sufficient uniformity of the experimental sample.

Table 2.4

Results of determining the angle of wetting

Material	Organic glass	Brass	Bronze	Copper
----------	---------------	-------	--------	--------

Contact wetting angle Θ , degrees	41	29	23	19
$\cos \Theta$	0.755	0.875	0.921	0.945

Based on the analysis of measurement results of the contact-wetting angle (Table 2.4), it is possible to draw a conclusion that the contact oil – copper demonstrates the best wettability and the largest adhesion. The wetting angle decreases in the following order: bronze, brass, organic glass. Adhesive properties depend on the forces of intermolecular interaction between a lubricant and a hard surface. In this case, the stronger adhesion of the molecules of oil with the surface leads to an increase in the forces of viscous resistance to the displacement of boundary layers of the lubricant (viscosity).

The obtained results allow us to define certain problems in the tribology of oil layers in contact.

In accordance with the Newton concept, a complete cohesion of surfaces occurs in the contact of solid body and fluid. In this case, the speed of points at the surface of fluid and the points at the solid body surface coincide. In this case, a solid body, when moving over the surface of a fluid, must drag along all the points of the surface with which it comes into contact.

In reality, contact points of the surface of a fluid come into contact with a solid body only in a certain limited section, and then they go out of the contact and slide down from the surface. Thus, the surface of fluid slides over the solid body surface and so the external friction occurs between the solid body and surface of the fluid. This is not accounted for by classical hydrodynamics.

Let us denote the tangential forces between the layers of fluid through τ_f ; those between a solid body and a fluid – τ_s .

Then two cases are possible:

1) $\tau_f < \tau_s$ – sliding occurs between the layers of fluid – this is the internal friction in a fluid;

2) $\tau_f > \tau_s$ – sliding occurs between a solid body and the surface of a fluid – this is the external friction.

It is obvious that these are the different types of resistance to the motion of a body on the fluid. In a general case of the motion of a solid body on a fluid, these two types of resistance are combined, and it is not easy to separate them.

At the same time, such separation is possible when conducting the specialized experiments.

In some methods of determining the viscosity, the volumetric deformation of a lubricant occurs. When determining the kinematic viscosity, the viscosimeters of variable section are used. When a lubricant passes through such a viscosimeter, the lubricant undergoes volumetric deformations in the transition to a narrow cross section and shearing strains while passing a narrow section. In this case, the number of viscosity consists of two components: volumetric deformations and shearing strains. Solving the problem on the

separation of these components looks promising for the theory of lubricant.

Thus, it is possible to assume that the phenomenon of viscosity is composed of the three components: 1) internal friction from the shift between the layers of a lubricant; 2) external friction between a solid body and a lubricant; 3) internal friction and resistance from the volumetric deformation of a lubricant.

A lubricant possesses simultaneously the properties of a solid deformed body (frame) and a fluid (oil).

In the existing examination of mechanical properties of a lubricant, especially in thin layers, the characteristics of rigidity are not actually considered. This limits solving the problems on the contact interaction of bodies, separated by a layer of lubricant. Studying the normal and tangential rigid properties of thin films in a contact between solid bodies being deformed is one of the basic problems in the tribology of oil films.

As a result of the research carried out, the following conclusions can be formulated.

1. It is theoretically obtained that for a pendulum in the lubricated sliding supports, the process of oscillations is described by a second order differential equation with viscous resistance, proportional to the deflection velocity of a pendulum. An analysis of the exact solution of this problem reveals that the ratio of adjacent amplitudes of damped oscillations is a constant magnitude. Hence, it follows that the absorption coefficient is constant over the entire process of oscillations.

2. The methods of determining the basic characteristics of viscous friction are proposed based on the model of pendulum oscillations: coefficient of energy absorption and dynamic viscosity. It is established that for the case of viscous friction, the absorption coefficient is precisely equal to the doubled logarithmic damping decrement and is determined either by one or a cycle of oscillations. The obtained method for calculating the indicator of dynamic viscosity of a lubricant according to the decrement of pendulum oscillation damping is important for the practical application.

3. Research into the influence of different types of lubricating and design materials on the characteristics of viscous friction allowed us to define certain problems in the issues of contact interaction between the lubricated materials. It is in particular established that the actual viscosity of lubricants is composed of the three components:

- internal friction from the shift between the layers;
- external friction between a solid body and a lubricant;
- internal friction and resistance from the volumetric deformation of a lubricant.

2.4. Research of the contact and deformation properties of lubricated surfaces

Most of the machines' friction units operate in the conditions of boundary lubrication of contacting surfaces. While designing and improving these units, it is necessary to determine the force conditions of contact interaction and, first of all, normal pressures and shear stresses.

In the condition of lubricant's presence, pressure calculation is possible only if there is data on the normal deformation properties of surfaces coated with a layer of a lubricating film.

The research on the influence of the lubricating medium on the deformation during static indentation of the indenter in the material surface is well known and presented in [24]. The analysis of the received results shows that in all cases, the indenter penetration (deformation) into a lubricated surface is larger than into a dry one.

The study of the influence of loading conditions in contact in the presence of lubricants has been considered in a number of scientific papers. By using the pendulum method, described in monograph [24], it was established that under conditions of viscous friction, oscillation attenuation curve on the elastic layer of molecules has a linear law. However, the oscillation attenuation curve on an unordered layer of lubricant is characterized by the logarithmic law of damping. These data were obtained experimentally and the study lacks a theoretical description of the mechanisms of viscous friction, which explain the results received. Article [25] examined experimentally and theoretically free fluctuations of a physical pendulum, which rests with two balls on a flat surface. The theory of damping fluctuations proposed in the study for evaluating the energy losses is of a phenomenological nature and is not based on a strict mathematical description of the mechanisms of fluctuation process, which makes it difficult to give the quantitative assessment of losses caused by friction. In paper [26], a differential equation for the swinging pendulum is obtained, taking into account the deformation of a surface and a deformation component of the friction force. However, the authors examined only a particular case of small deformations, commensurate with the dimensions of contact area of the ball support of a pendulum. This solution is not applicable for describing the macro-displacements in the support of a pendulum, characteristic for the actual friction units of sliding in machines. Authors of article [27] conducted a nonlinear regression analysis based on the results of experimental studies into the damped oscillations of a physical pendulum, which made it possible to formulate the criteria for choosing a theoretical model of the dissipation of viscous friction. However, the experiments were performed for the conditions of balls rolling on the support, that is, for the small areas of contact in comparison with dimensions of the balls, which also does not make it possible to adequately utilize the obtained results for evaluating the characteristics of viscous friction in

cylindrical sliding supports (bearings). A calculation-experimental method for determining tangential contact frictional stresses using a variational principle was proposed in work [28]. In this case, a quadratic functional of deviation of the experimental function of tangential stresses from the equilibrium condition was constructed. The authors of [29] proposed theoretical dependences for a wear testing method using a standard four-ball scheme with determination of wear resistance parameters. The approximating function of the wear spot diameter on the friction path obtained by the results of wear tests was taken as the base of the method. The general methodology of this study can be used to develop a theory of test methods for other geometric schemes. In paper [30] to identify parameters of wear resistance in the wear model, a calculation-experimental method for determining calculated dependences of wear resistance parameters was developed on the basis of the wear test by the «cone – three balls» scheme. The results of wear tests of bronze conical specimens with a variable wear spot and two values of sliding velocity were taken as a base. The experimental method for measuring the characteristics of friction was applied in article [31] for examining special features of high-speed friction under conditions of thermal loading and at limited lubrication. The criterion of damping the friction fluctuations proposed in this case is not applicable to the case of viscous friction, where such fluctuations are practically absent as a result of the damping action of a layer of lubricant. Paper [32] employed a pendulum method in order to solve a problem on determining the contact rigidity of steel spherical models at dynamic loading using the system of differential equations. However, the tangential component of contact stresses from the frictional forces in this case was not considered. Articles [33, 34] proposed and implemented design concepts of devices for the accelerated tests on friction and adhesive properties of the actual friction units of the "wheel – rail" type. The design of a pendulum device, applied in the work, for studying the adhesive properties according to the scheme "cylinder – plane" does not allow using it for evaluating the viscous friction of cylindrical sliding supports. Experimental studies of the deformations of lubricated and dry contact were carried out by means Brinell's test. The indentation was carried out on a hardness tester with a force of 105 N with a steel ball from ShKh15 $d = 10$ mm. Simultaneously, prints were made in conditions of dry and lubricated contact. To analyze the magnitude of the strains, the grid method was used. The strain grid lines were made photos of and enlarged by means a digital camera (Fig. 2.13).



Fig. 2.13. The grid lines deformation

The grid lines through the lower points along the axis of the deformation of the lubricated surface show a larger degree of deformation compared to deformation of a dry surface. Based on the measurements of the grid lines, we obtained diagrams of the relative deformation of the material in depth along the axis of the holes. Relative deformation diagrams for lubricated and dry contact are shown in Fig. 2.14.

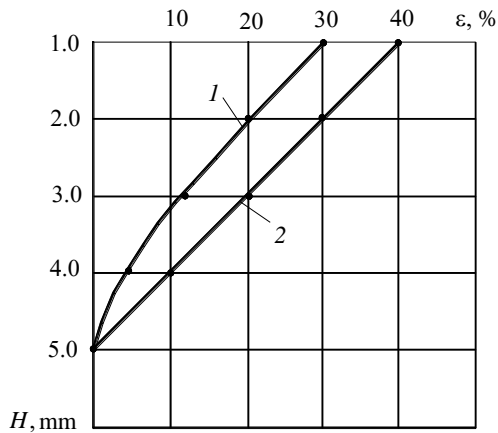


Fig. 2.14. Relative deformation diagram: 1 – dry surface; 2 – lubricated surface

Deformation diagrams' analysis shows that the degree of relative deformation of the material in depth is larger for a lubricated contact. In the case, the dependence of deformation on depth for a lubricated contact is linear in comparison with nonlinear deformation for dry contact.

To analyze the structure of the material in the result of deformations in a lubricated and dry contact, micrometric studies were carried out. Pictures of the material structure in the zone of the deformation holes for lubricated and dry contact are shown in Fig. 2.15.

Dry contact

Lubricated contact

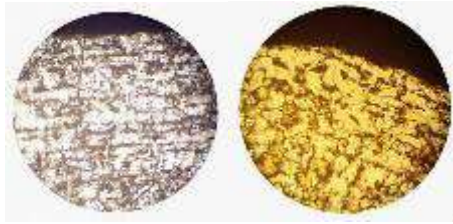
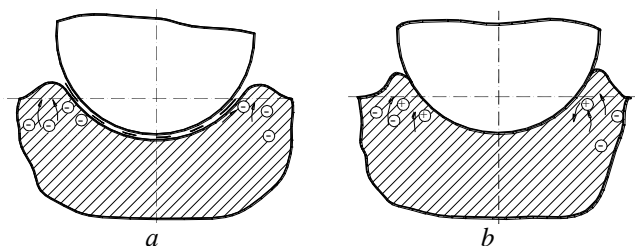


Fig. 2.15. Material microstructure in the zone of deformation hole for dry and lubricated contact

In both cases of steel sample surface deformation, grain elongation is observed near the surface. However, the depth of the layer of deformed grains and the distribution of the deformation depth over the surface of the hole are different. The depth of the grain deformation layer for dry contact is maximum in the center of the hole and decreases to its edges. For lubricated contact, the depth of the grain deformation layer is steady over the entire surface of the deformation hole. Such a difference in the surface layer material deformation determines its stressed state in the case of dry and lubricated contact.

Let us analyze the stress state of the surface layer during the contact interaction of the ball and the plane. During the contact interaction of the ball with the surface through a lubricating film, the metal is evenly deformed in the radial direction, while the surface layer is elongated. After removing the load, the elastically deformed subsurface layer tends to return the surface layer to its initial position, creating in it evenly distributed compression stresses (Fig. 2.16, *a*).



**Fig. 2.16. The scheme of internal stresses' formation:
a – lubricated contact; b – dry contact**

In case of dry contact (Fig. 2.16, *b*), the surfaces in the contact adhere due to high contact friction. Deformation of the material occurs normally deep into the surface. In this case, the subsurface layer in which compression stresses arise, is more intensively deformed, and in the surface - tensile stress.

Thus, the elastic-plastic non-lubricated contact contributes to a more intense accumulation of defects (dislocations, vacancies) in the surface layer and the concentration of internal stresses in comparison with the lubricated contact.

The destruction of surface layers in the process of wear is known to begin in places of stress concentration. Thus, to reduce wear, the contact conditions of the surfaces should ensure the deconcentration of internal stresses and their uniform redistribution in the volume to reduce crystalline defects.

The analysis of the deformation conditions for lubricated and dry contact during the static introduction of a spherical indenter showed the following:

1) indenter penetration depth into the lubricated surface is larger than into dry one on average by 8–10 %;

2) relative deformation deep into the surface of the material along the axis of the deformation hole is described by a linear regularity and non-linear for dry contact, which indicates an even decrease in stresses deep into the lubricated surface;

3) uniform distribution of the layer of deformed grains over the deformation zone for a lubricated contact indicates the uniform distribution of stresses over the deformation zone;

4) uniform distribution of stresses in the contact of lubricated surfaces reduces the appearance of imperfections in the crystal structure (vacancies, dislocations) in the surface layer. This contributes to increased wear resistance compared to contacting surfaces without lubrication.

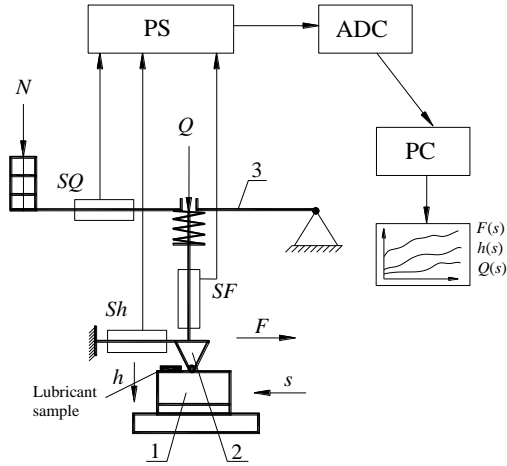
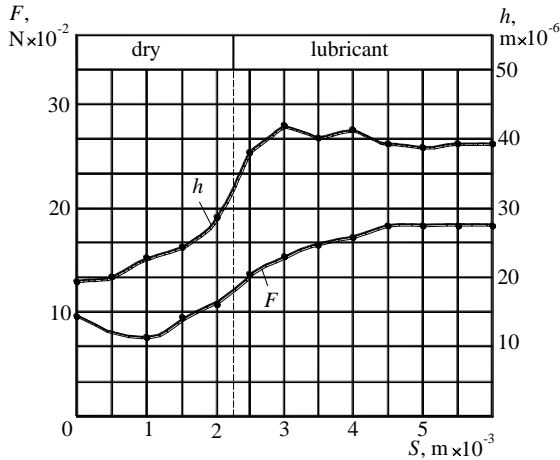


Fig. 2.17. Test scheme

Further studies of dry and lubricated surfaces' deformation properties were carried out for a moving indenter. Indenter 2 (Fig. 2.17) was loaded with axial load through a system of levers 3. Sample 1 with a lubricant sample moved in the longitudinal direction. The indenter penetrated into a dry surface and moved to the entrance to the lubricated zone. Herewith, the penetration depth and the movements resistance measurements were made.

Shell Helix 15W-40



Q8 Formula 15W-40

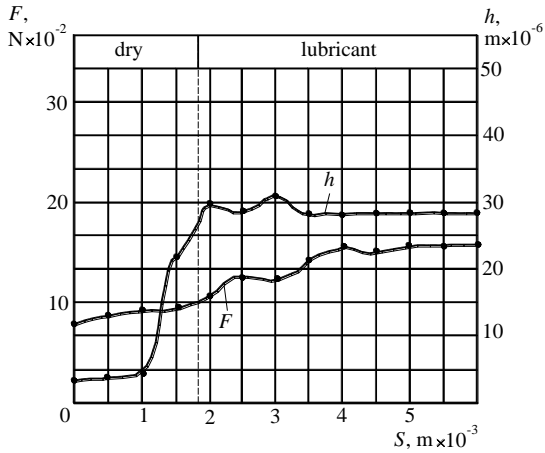


Fig. 2.18. Diagrams of changes of penetration depth h and resistance force F of the indenter on the size of moving S on dry and lubricated sample surface

A standard ball with a diameter of 2.5 mm made of ball-bearing steel was used as an indenter. The limits of the load, acting on the indenter made up 0.5...3 N. The accuracy of measuring the load acting on the indenter was 0.02 N. The samples were made of brass LC 59-1 as a standard microsection. The system for measuring the resistance to displacement consisted of a strain gauge with a sensor (measurement accuracy 0.02 N). The penetration depth measurement system included a strain gauge with a sensor with a measurement accuracy of 1 mkm. The signals from the strain gauges through the strain gauge were transmitted to an analog-and-digital converter and a computer. The voltage from the strain gauges in the time coordinate with a division value of 0.5 s was reproduced on the display screen. This corresponded to the indenter moving by a linear value of 28 mkm. The indenter was introduced into the dry surface of the sample with a constant force of 2.5 N. The sensor readings were taken for 100 s, which corresponded to a 5.6 mm displacement of the sample relative to the indenter. Fig. 2.18 shows diagrams of parameter changes for two lubricants types.

Consequently, it was found out that the penetration depth of the indenter increases when passing through the lubricated area, which indicates its easier deformation compared to penetration into a dry surface. The resistance force during the passage of the indenter along the lubricated area also increases, which is explained by the indenter deepening. This leads to an increase in the volume of the deformable material and the resistance force.

Conclusions

1. For studying the normal deformation properties of lubricated surfaces, a comparative analysis of lubricated and dry surface deformation conditions was carried out during tests by means of a Brinell test.

2. The analysis of the deformation conditions for the lubricated contact showed that the deformation deep into the surface of the material along the axis of the deformation hole is described by a linear regularity and a non-linear one for dry contact. A uniform distribution of deformed grains for a lubricated contact indicates a uniform distribution of stresses and a decrease in the concentration of structural defects. This accordingly contributes to increased wear resistance;

3. It is found out that the resistance force increases when the indenter moves along the lubricated area, which is explained by the indenter deepening. The results of observations showed an increase in the width of the grooves of the tracks in all cases after entering the blurred area by 20–35 percent.

4. The results obtained show that more intense deformation of irregularities in a lubricated contact helps to accelerate the running-in process and reduce contact pressures of contact areas.

5. Together with the traditional mechanism for reducing wear as a result of the formation of adsorbed layers on lubricated friction surfaces, the contact-deformation mechanism for reducing the wear of lubricated surfaces is justified.

2.5. The biological aspect of contact of lubricated surfaces

If a solid interacts with the other solid, a liquid, a gas these changes show themselves in a wear, friction, folding, and other deformations. In most cases it causes bodies' surface damage and is undesirable. The structure of surface layer of contacting bodies is of decisive importance. In particular, it applies to the state of machines details surface in the technique. Most traditional methods of details finish treatment result in the formation of chaotic type of surface underfeature with heterogeneous according to the form and size inequalities that is in its turn the result of the process of heterogeneity of material particles separation from general mass. The heterogeneous geometrical structure of the surface results in heterogeneous distribution of external surface stress. Contact interaction, wear and friction, on the different areas of the actual contact takes place with different intensity that puts obstacles in the way to balancing the system and its free energy minimization according to one of fundamental laws of nature. Thus, it's obvious that to provide a minimum system's free energy, its stability against external environment

influence it is necessary to aspire to optimization and regularization of bodies surface structure in the process of contact interaction. Complication of this task consists in the variety of technical contacts and contact phenomena, complicated contacts connection with microgeometry of contacting surfaces. The creation of machines details on the working surfaces with the purpose of optimization their microgeometry of different deepenings, that carry out the functions of oilwaies, has been in practice for a long time and played a certain role in the connections' longevity and reliability increase. A famous French patent is known to suggest without any scientific ground the decrease of all without exception surfaces that grind down to 30 % by formation of different sort of deepenings [35]. But simple diminishing of contact surface is not enough, as in this case contact stress on the contact surface unit will considerably increase and the wear speed will rise.

Surface parameters must be already optimal at the beginning of machines details exploitation, while for surfaces, treated by traditional methods, this process begins with a contact and few apexes' of inequalities intensive wear. One of effective methods of regularizing the form and sizes of the real contact areas of technical surfaces is superficially-plastic treatment (SPT): rolling-off, vibro roll forming, burnishing and others [35]. Due to such treatment the apexes of rough surface are folding plastically and are forming a relief that is more friendly to bodies contact interaction. At the beginning of the contacting practically all waves of inequalities enter in the interaction at once and in the process of wear the area of the contact will change incidentally. Managing the parameters of treatment, it is possible to get the most optimal for these conditions relief of surface. In the same way it is possible to create by means of superficially-plastic treatment (SPT) the guided contours of surface in a plan. In the conditions of setting certain kinematics of treatment, different contours (systems of channels and lugs) are created on the surface: transversal, lengthwise and angularly; straight-line and corrugated; crossing and noncrossing.

Besides handling the size of contact area the task of greasing conjugating surfaces during their comparative move is almost always set. The more reliable a lubricating material is held between contacting details, the less they are subjected to the wear. The type of surface plays not the last role here. The channels created during the processing on a surface perform the function of a tank for lubricant maintenance and distribution. By means of theoretical researches, alpha and operating tests it is determined what type, form and depth of contour is the most acceptable.

Among the parameters of regular contours the most important, from the point of forming operating characteristics of a surface, are: the direction of contour lines in relation to the direction of the relative sliding, relative surface area (relation of area, occupied by channels to the general area), depth and

form of oilwaies. Summarizing the researches results in the field of surfaces' with regular relief wear resistance [35, 36], it is possible to define such recommendations in relation to the above-mentioned parameters. The best results are performed by the transversal in relation to the direction of channel moving, as in this case more favourable conditions for lubricating are provided and in general a surface has greater bearing strength in comparison with lengthwise channels. What concerns relative area of the surface, the cases are considered to be optimal, when the area of oilwaies makes up 40–50 % of the general area of surface. For reliable lubricant maintenance, providing its crossflow from a channel to the area of surfaces contact, moving away contaminations the best results are performed by the channels of a circular form.

In this research the attempt to draw an analogy between results, obtained in the process of tracing wear resistance of technical surfaces with a regular relief and the way similar tasks get solution in nature, is made. As the object of comparison the skin on human extremities was examined. Among all body areas of a human being the skin of a palm is subjected to the largest contact stress and friction from the side of other articles during physical activity. Therefore for thousands of years of evolution the skin canopy of palms must have been adapted to prevent its damage and wear. We'll consider shortly the physiology [39] and geometrical structure of a skin surface.

The human-being skin consists of two layers (Fig. 2.19). An external layer is called epidermis 1, and the second, that is more deep, -derma 3. On the surface of derma, that is adjacent to the epidermis papillary layer 3 is located, which forms conical papillae which submerge in an epidermis.

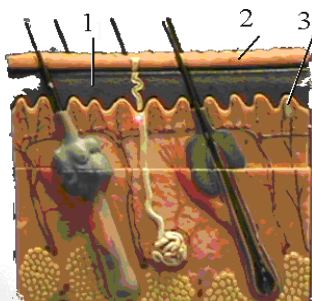


**Fig. 2.19. The structure of the finger skin of a human being:
1 – epidermis; 2 – papillary layer; 3 – comb**

On the greater part of the body dermal papillae are located chaotically, and on the palms, and on fingers in particular, they are folded in rows. That's why epidermis which replicates the structure of external derma layer,

forms small folds on these areas of body which represent and repeat the dermal papillae rows. These folds, visible on a skin surface with a naked eye, are called papilliferous lines (from lat. papillae - papillae) and are separated from each other by shallow furrows. Thus, the epidermis of palms' skin has not only a larger thickness (up to 3 mm) in comparison with other parts of the body but is also covered with a special relief in the form of papillary combs and furrows (especially on dactylar phalanxes). There are numerous pores - external openings of excretory channels of skin sweat-glands on the apexes of folds (combs of papilliferous lines). Except for sweat-glands the channels of fatty glands and glands of external secretion are also present at the skin surface. The types of skin glands excretions are represented below in a Table 2.5.

Table 2.5

Types of skin glands excretions

Skin glands	Inorganic	Organic
external secretion	chlorides, metal ions, ammonium hydrate, sulphates and phosphates	amino acids, carbamide, lactic and hydrochloric acid
fatty	–	fatty acids and glycerine, other alcohols and carbohydrates
sweat	sodium, potassium and iron ions	proteins, cholesterol, and carbohydrates

One of functions of the indicated excretions is lubricating the skin surface for its wear prevention during a contact with an environment. A lubricating substance is in the skin furrows; it greases the skin area that contacts with other objects, reducing the skin canopy wear.

Papilliferous lines, especially on the hands surfaces, form different patterns that are called papilliferous patterns. The outline of a papilliferous pattern is individual; it is finally formed in the process of antenatal development and is not subjected to any changes during the whole life. After epidermis damages the papilliferous pattern in regenerative process is restored. All variety of papilliferous patterns kinds, that may be found in natural environment, can be conditionally divided into three types: arc (simple and hip), loopback (left and right) and frizz (circle, a right and a left spiral) [37]. Surface appearance of the indicated relief types of skin surface is shown at the Fig. 2.20.



Loopback

Frizz

Fig. 2.20. Relief types of the finger skin surface of a human being

Scientists paid attention on the outline of the dactylar pattern a long time ago. In 1911 for the first time an English scientist Francis Galton offered the method of person authentication by means of finger-prints. Since then this method, known as dactylography, became widely spread in criminalistics for criminals search. Recently such powerful vehicle computer based complexes for finger-prints research appeared [38]. They are: AFIS (the USA), FAT01 (Belgium), Finger Verifer (Taiwan), ADIS (Russia). Except criminals' authentication these complexes are being used for access to the computer systems differentiation and as dactyloscopic locks for apartments. But in our case we are interested not in differences of finger skin patterns, but vice versa – in common things that were created by nature both for wear and damage prevention of skin extremities of a human being.

Analysing the skin furrows direction (Fig. 2.20), we can evidently see that they are situated mainly perpendicularly to possible direction of moving at a friction. That is in any direction, regardless the pattern type, on the way of moving transversal furrows and combs of skin of fingers are the first to be subjected to contact interaction. This coincides with conclusions, made for regular relief, inflicted on technical surfaces.

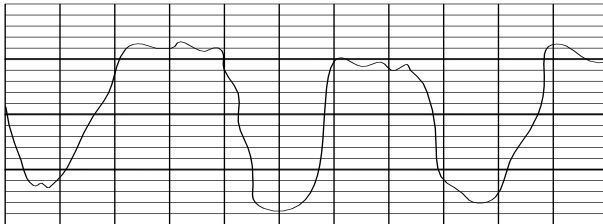


Fig. 2.21 The profilogram of the finger skin surface of a human being

For the analysis of the form of skin relief contour profilogram (Fig. 2.21) of the finger skin surface area was taken off. For this purpose the negative imprint of skin canopy was created by means of solidifiable layer of PVA glue, inflicted on a glass surface. The mean values of such contour parameters were defined: contour height (depth) – 300...400 mkm, step of furrows – 500 mkm. Besides, the analysis of the profilogram shows, that the areas of cavities and lugs are approximately equal and, thus, the area of channels occupies roughly 50 % of the whole skin surface. The combs of skin are located on one height and that is why enter the contact interaction almost simultaneously. Going back to regular reliefs on technical surfaces, we see

that the determined optimal values of parameters of these reliefs in majority coincide with the parameters of fingers skin relief of a human being.

The conducted comparative analysis of superficial structure of technical surfaces and human skin allows to draw certain analogies, extend a vision of engineering problems connected with microreliefs regularization, to have another look at the assignment of papilliferous lines of human being extremities.

References for chapter 2

1. Soldatenkov I. A., Mezrin A. M., Sachek B. Ya. Implementation of asymptotics of the wear contact problem solution for identifying the wear law based on the results of tribological tests, *Journal of Friction and Wear*, 2017, 38(3), pp. 173–177.

2. Soldatenkov I. A., Mezrin A. M., Sachek B. Ya. Implementation of a wear model of rigid bodies for identifying the wear law based on the results of tribological tests, *Journal of Friction and Wear*, 2015, 36(6), pp. 528–533.

3. Dykha A., Marchenko D. Prediction the wear of sliding bearings. *International Journal of Engineering & Technology*, 2018, 7 (2.23), pp. 4–8. doi: 10.14419/ijet.v7i2.23.11872

4. Bulgarevich, S.B., Boiko, M.V., Lebedinskii, K.S., and Marchenko D.Yu. 2014. Kinetics of sample wear on four-ball friction-testing machine using lubricants of different consistencies. *Journal of Friction and Wear*, 35(6), pp. 531–537. doi:10.3103/S106836661406004X

5. Leśniewski T., Krawiec S. The effect of ball hardness on four-ball wear test results, *Wear*, 2008 (264), Issues 7–8, pp. 882 -670.

6. Kaplun P.V., Dykha O.V., GoncharV.A. Contact durability of 40Kh steel in different media after ion nitriding and nitroquenching. *Materials Science*, 2018, 53 (4), pp. 468–474. DOI:<https://doi.org/10.1007/s11003-018-0096-0>

7. Dykha, A. Marchenko, D., Artiukh, V., Zubiekhina-Khaiat, O., Kurepin, V. Study and development of the technology for hardening rope blocks by reeling, *Eastern-European Journal of Enterprise Technologies*, 2018, № 2/1(92), pp. 22–32.

8. Dykha, A., Sorokatyi, R., Makovkin, O., Babak, O. Calculation-experimental modeling of wear of cylindrical sliding bearings. *Eastern-European Journal of Enterprise Technologies*, 2017, 5/1 (89), 51–59. doi: 10.15587/1729-4061.2017.109638

9. Dykha, A.V., Kuzmenko, A.G. Solution to the problem of contact wear for four-ball wear-testing scheme. *Journal of Friction and Wear*, 2015, 36(2), pp. 138–143. doi: 10.3103/S1068366615020051

10. Aulin, V., Hrynkiv, A., Dykha, A., Chernovol, M., Lyashuk, O., Lysenko, S. Substantiation of diagnostic parameters for determining the technical condition of transmission assemblies in trucks. *Eastern-European Journal of Enterprise Technologies*, 2018, 2 (1(92)), 4–13. doi: 10.15587/1729-4061.2018.125349
11. Dykha, A.V., Kuzmenko, A.G. Distribution of friction tangential stresses in the Courtney-Pratt experiment under Bowden's theory. *Journal of Friction and Wear*, 2016, 37 (4), 315–319. DOI: 10.3103/S1068366616040061
12. Kryshchtopa, S., Kryshchtopa, L., Melnyk, V., Dolishnii, B., Prunko, I., Experimental Research on Diesel Engine Working on a Mixture of Diesel Fuel and Fusel Oils. *Transport Problems*, 2017, 12 (2), 53–63
13. Bhushan, B. (2013). *Introduction to Tribology*. Second edition. New York: John Wiley & Sons, 721 p.
14. Dzhilavdari, I., Riznookaya, N. (2008). An experimental assessment of the components of rolling friction of balls at small cyclic displacements. *Journal of Friction and Wear*, 29(5), 330–338.
15. Dzhilavdari, I., Riznookaya, N. (2007). Specific features of the dynamics of small-amplitude pendulum swings in the presence of hysteresis friction. *Friction and Wear*, 28(2), 143–150.
16. Dzhilavdari, I., Riznookaya, N. (2008). Studies of the dynamics of free micro oscillations of a pendulum supported by two balls. *Journal of Friction and Wear*, 29(1), 1–8.
17. Kryshchtopa, S., Kryshchtopa, L., Bogatchuk, I., Prunko, I., Melnyk, V. (2017). Examining the effect of triboelectric phenomena on wear-friction properties of metal-polymeric frictional couples. *Eastern-European Journal of Enterprise Technologies*, 1/5 (85), 40–45.
18. Dykha, A., Kuzmenko, A. (2003). Method of determining the coefficient of friction of lubricated surfaces. *Problems of Tribology*, 1, 136–139.
19. Dykha, A., Kuzmenko, A., Babak, J. (2011). Contact mechanics and wear of lubricated tribosystem. *Khmelnitsky: KhNU*, 250 p.
20. Sorokaty, R., Dykha, A. (2015). Analysis of processes of tribo-damages under the conditions of high-speed friction. *Journal of Friction and Wear*, 36 (5), 422–428.
21. Sherif, H.A., Almufadi, F.A. (2016). Identification of contact parameters from elastic-plastic impact of hard sphere and elastic half space. *Wear*, 368-369 (3), 358–367.
22. Lewis, S.R., Lewis, R., Olofsson, U. (2011). An alternative method for the assessment of railhead traction. *Wear*, 271 (1–2), 62–70.
23. Lewis, S.R., Lewis, R., Richards, P., Buckley-Johnstone, L.E. (2014). Investigation of the isolation and frictional properties of hydrophobic

products on the rail head, when used to combat low adhesion. *Wear*, 314 (1–2), 213–219.

24. Bhushan, B. (2013). *Introduction to Tribology*. Second edition. New York: John Wiley & Sons, 721 p.

25. Dzhilavdari, I., Riznookaya, N. (2008). An experimental assessment of the components of rolling friction of balls at small cyclic displacements. *Journal of Friction and Wear*, 29(5), 330–338.

26. Dzhilavdari, I., Riznookaya, N. (2007). Specific features of the dynamics of small-amplitude pendulum swings in the presence of hysteresis friction. *Friction and Wear*, 28(2), 143–150.

27. Dzhilavdari, I., Riznookaya, N. (2008). Studies of the dynamics of free micro oscillations of a pendulum supported by two balls. *Journal of Friction and Wear*, 29(1), 1–8.

28. Dykha, A.V., Kuzmenko, A.G. (2016). Distribution of friction tangential stresses in the Courtney-Pratt experiment under Bowden's theory. *Journal of Friction and Wear*, 37 (4), 315–319. doi: 10.3103/s1068366616040061

29. Dykha, A.V., Kuzmenko, A.G. Solution to the problem of contact wear for four-ball wear-testing scheme. *Journal of Friction and Wear*, 2015, 36(2), 138–143. doi: 10.3103/S1068366615020051

30. Dykha, A., Sorokatyi, R., Makovkin, O., Babak, O. (2017). Calculation-experimental modeling of wear of cylindrical sliding bearings. *Eastern-European Journal of Enterprise Technologies*, 5 (1 (89)), 51–59. doi: 10.15587/1729-4061.2017.109638.

31. Sorokatyi, R., Dykha A. (2015). Analysis of processes of tribo-damages under the conditions of high-speed friction. *Journal of Friction and Wear*, 36 (5), 422–428.

32. Sherif, H.A., Almufadi, F.A. (2016). Identification of contact parameters from elastic-plastic impact of hard sphere and elastic half space. *Wear*, 368–369 (3), 358–367.

33. Lewis, S.R., Lewis, R., Olofsson, U. (2011). An alternative method for the assessment of railhead traction. *Wear*, 271 (1–2), 62–70.

34. Lewis, S.R., Lewis, R., Richards, P., Buckley-Johnstone, L.E. (2014). Investigation of the isolation and frictional properties of hydrophobic products on the rail head, when used to combat low adhesion. *Wear*, 314 (1–2), 213–219.

35. Shneider Yu. Exploitation characteristics of the details with regular microrelief: Machine building, Leningrad board, 1982. – 248 p.

36. Kragelskiy I. Friction and wear. – Moscow: Machine building, 1968.

37. Criminalistics. Under Prof. I. Krylov edition. – Leningrag University Publishing house, 1976, p. 143–144.

38. Biometric person authentication / Yevstigneev V., Chernomordik O. // Bank technologies. – 1997. – № 1.

39. Sapin M., Bilits G. Human anatomy. In 2 books: Manual for students of biological and medical majors. Book 2 – Moscow: ONIKS Publishing house: 1999. – 432p.

CHAPTER 3

Diagnostic Approaches to Assessing the State of Sliding Friction Tribosystems

3.1. Tribo-acoustic analysis of the processes of dynamic friction

Acoustic methods for analysis and control of friction processes is widely used in tribology [1–9]. The most widely methods acoustic emission ultrasonic frequency range with the use of special sensors of the contact type [1, 3, 4, 8]. Contactless acoustic control of sound and near infrasonic frequency bands based on the standard (or special) computer software is much easier in technical implementation, however, requires a separate analysis to separate the useful signal against the background noise. Before tribo-acoustics methods were used primarily to movable functional structures [2, 5, 6]. The fretting processes in nominally-fixed joints, at first glance, it's hard to hear in the General operating noise of the system, mechanism, or machine. However, because of the interrelatedness of dynamic processes in complex technical system, violation of integrity of any such connection will impact on the amplitude level and the spectral composition of the working noise. Due to the relatively low speeds slippage in modes of fretting characteristic frequency of acoustic emission fall exactly in the middle of the sound and infrasonic spectrum, which allows the use of normal sound recording equipment and standard computer software.

For research was used the installation [10] for testing the fretting, containing rotating elements, creating high level of contact noise Fig. 3.1, 3.2.

Fretting was carried out according to the scheme plane-the ball is in contact with unhardened steel 30 HGSA (lead top sample 1 in the diagram Fig. 3.1) and ball bearing steel LH-15 with a diameter of 12 mm (the lower led of the control body 14 in the diagram Fig. 3.1). The surface of the sample is pre-processed by grinding and subsequent polishing on the 9-th class of roughness ($Ra = 0,2 \dots 0,3 \mu\text{m}$).

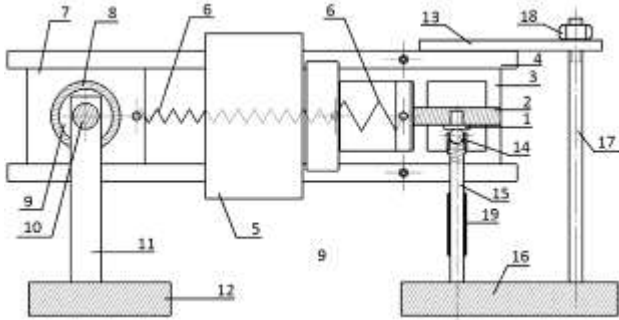


Fig. 3.1. The scheme of experimental installation:

- 1 – the leading pair of friction sample; 2 – sample holder; 3 – carriage;**
- 4 – guidance; 5 – electromagnet; 6 – springs; 7 – plate; 8 – hub;**
- 9 – angular contact ball bearing; 10 – shaft; 11 – tree stand; 12 – base;**
- 13 – strap; 14 – slave control body (ball); 15 – strain gauge beam; 16 – base;**
- 17 – pin; 18 – nut; 19 – the strain gages**

Reciprocating motion of the lead sample was provided by an electromagnet and a spring system. The amplitude of vibration was $20\ \mu\text{m}$. The slave control body (the ball) is clamped in the rim strain of the beam (Fig. 3.2). The normal contact load in the coupling ($\approx 50\ \text{N}$) was provided to two-thirds the weight of the drive and a third – Dimdim wrench force (Fig. 3.1), gradually attenuated in the process of fretting. The basic operating frequency of vibration was 100 Hz.

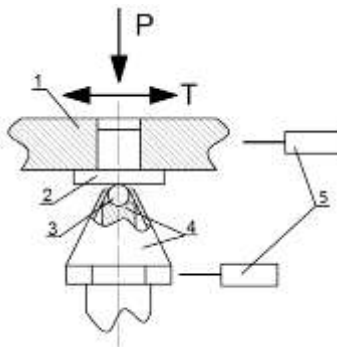


Fig. 3.2. Contact scheme: 1 – sample holder; 2 – sample;
3 – control e body (ball); 4 – the fixation system of the control body;
5 –the inductive sensors of micromovements; P – force; T – tangential force

For recording the acoustic signal used remote microphone brand Media-tech SFX microfone MT 383 installed at a distance of several

decimeters from the node friction. Computer processing of data was carried out by the program Audacity 2.0.4. As an additional informative channel was used for automated computer-based construction loop contact hysteresis in coordinates: the displacement of the slave control of the body – tangential force. The latter was measured respectively by means of an inductive sensor micrometric movements and the bridge of strain gages on the beam.

Acoustography pre-recorded in the idle operation mode – with an almost vertical position of the guides of the actuator. Then, in their horizontal position are installed starting clamp connections and made the test in the mode of fretting: from initial running-in process prior to the violation of the integrity of the connection, expressed in the qualitative change of the amplitude level and the spectral composition of the acoustic signal.

In Fig. 3.3 shows acoustography recorded for one minute each in the development of the testing process. They give a general idea about the process of fretting. Low-frequency instability characteristic of the initial stage of ageing (Fig. 3.3, *a*) is significantly reduced to approximately $1 \cdot 10^5$ cycles of the oscillations (Fig. 3.3, *b*), to be replaced by a longer period of optimal operation of the connection ($\approx 5 \cdot 10^5$ cycles Fig. 3.3, *b*).

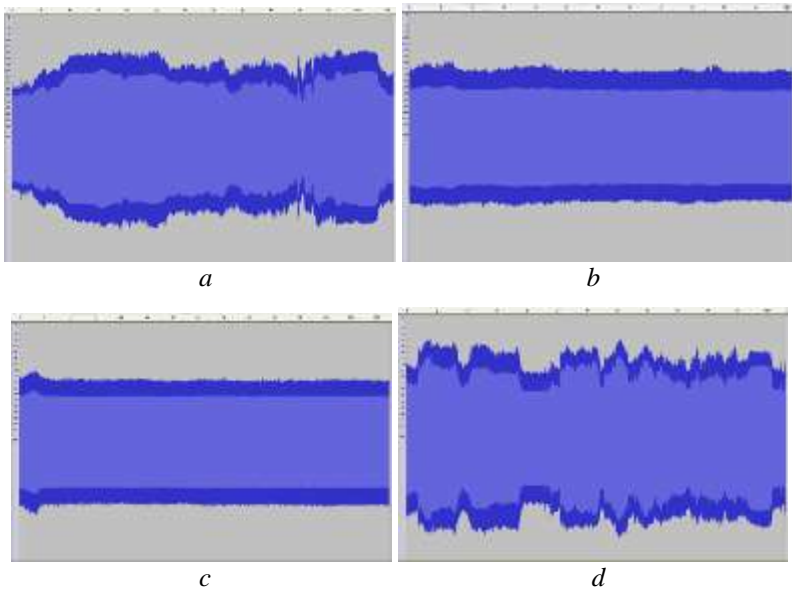


Fig. 3.3. Acoustography operating noise recorded on 1-th (*a*), 15 (*b*), 55 (*c*) and 88 minutes (*d*) minutes of testing. The horizontal axis shows time in minutes and seconds, vertical axis is the signal level in decibels

Severe violation of the integrity of the connection kicks in around the 88th minute of the test ($\approx 5,3 \cdot 10^5$ cycles – Fig. 3.3, c). The corresponding hysteresis loop (Fig. 3.4) more similar and less informative. However, at the final stage (Fig. 3.4, c) considerably strengthen high frequency components of the signals, followed by reduction of the tangential effort on the control body, and controlling a decrease in the amplitude of its oscillations, indicating the slippage in the contact.

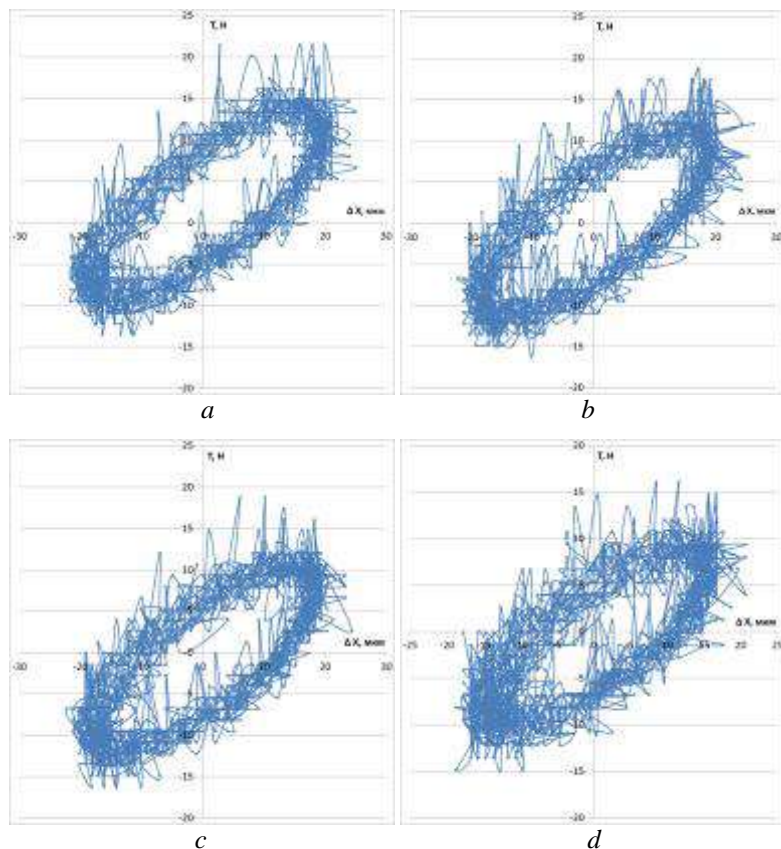
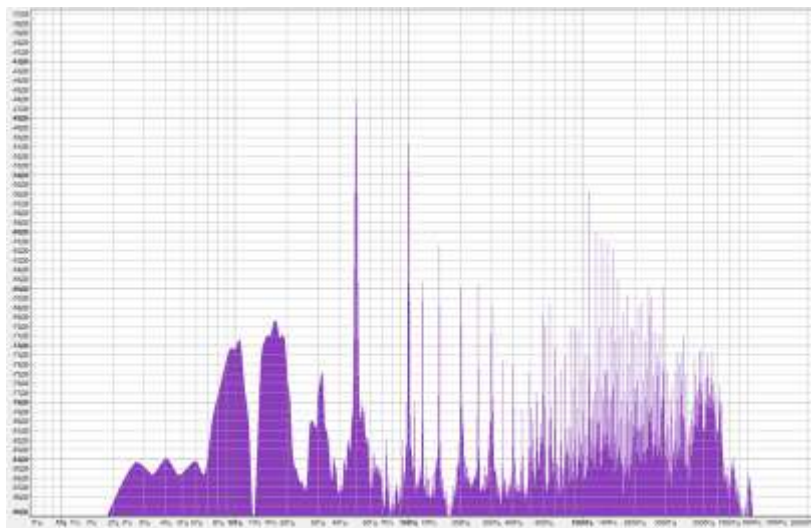


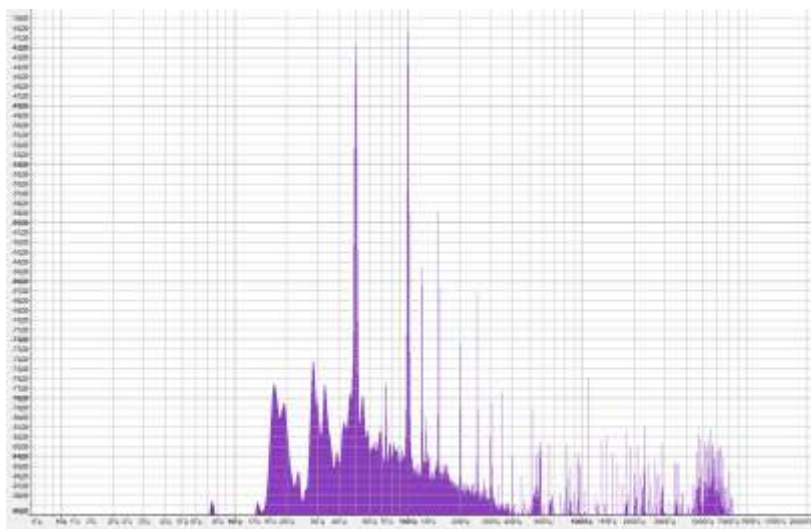
Fig. 3.4. The contact hysteresis loop, built for the 1st (a), 15 (b), 55 (c) and 88 minutes (d) minutes of testing

Of greatest interest in this case, the Fourier spectra of the above eco-storm – Fig. 3.5. They are dominated by two main pump frequency disturbances, 50 Hz and 100 Hz and their harmonics arising from the nonlinearity in a

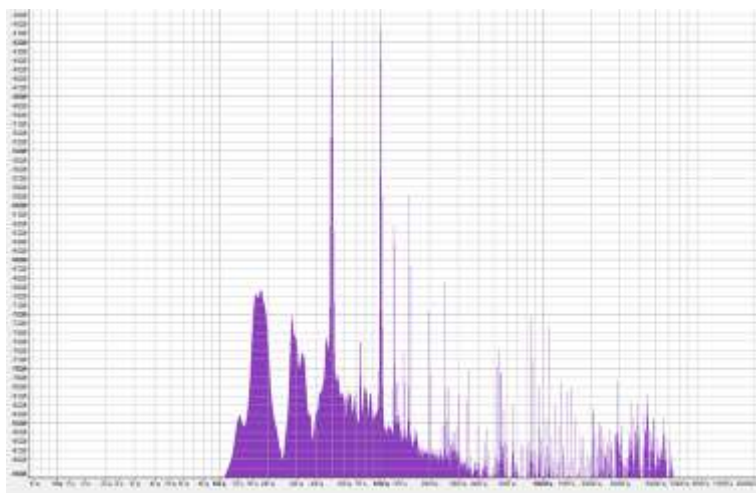
dynamic system and a corresponding disharmony of vibrations. These harmonics at the initial stage of running-in (Fig. 3.5, *a*) form a well-defined direct energy cascade towards high frequencies with the maximum at frequencies of 1–5 kHz.



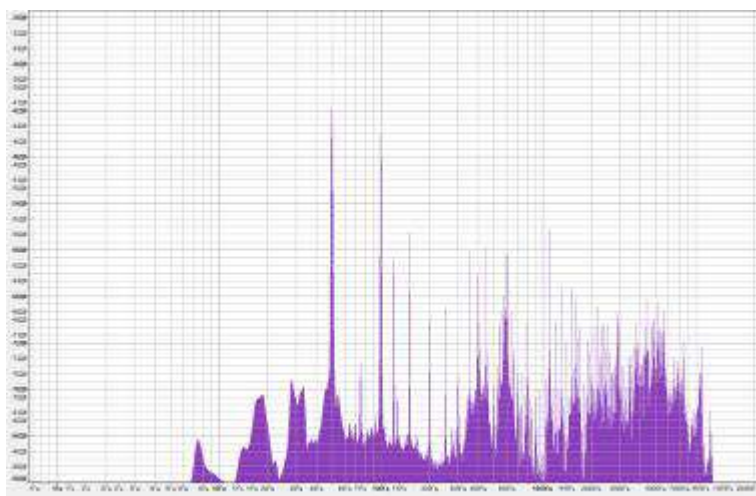
a



b



c



d

Fig. 3.5. Fourier spectra of acoustic emission signals recorded on the 1st (*a*), 15 (*b*), 55 (*c*) and 88 minutes (*d*) minutes of testing

The occurrence of this maximum is due to quasi-normal contact vibrations induced by the processes of microplastic deformations at the stage of running-in. The other – the reverse energy cascade is directed from the pumping modes in the low frequency near-infrasound region of the

spectrum (Fig. 3.5, *a*). Its origin is connected with guided slow angular movements of the guides of the actuator, which has a direct impact on the rapid vibration of the sample leading to friction and, consequently, on the processes of contact interaction in the zone of fretting.

This kind of low-frequency self-modulation of the friction process often is at the expense of cyclical damage accumulation and separation of wear particles [6]. In this case, such cyclicity is a consequence, not the cause of automodulation arising from the activation of the available degrees of freedom and feedback in the overall dynamic system of friction. Thus, the friction acts as a global (system-wide) and not just local (mesophysical) process.

In the run mode of the connection (Fig. 3.5 *b, c*) is characterized by a substantial weakening of the high frequency and midrange components of the acoustic spectrum, show a decrease in the initial rate of microplastic deformation. General view of the spectra in this case is close to the mean spectra of the idle mode of operation.

A qualitative change in the spectral composition of the acoustic emission of friction associated with the violation of the integrity of the connection is clearly seen in the spectrum of Fig. 3.5, *d*. Here again amplified high frequency components, and in addition to this there are two strong mid-frequency components of the ≈ 400 Hz and about 600 Hz. The latter is necessary to characterize the modes of the contact gap, because their appearance is directly related to the wear of units, with a corresponding decrease in the contact stiffness and slippage in the contact.

Thus, use a public domain sound recording equipment and standard computer software allows, at least with respect to low-noise experimental installations, to carry out contactless acoustic control of the integrity of nominally stationary friction joints under conditions of fretting. Violation of the integrity of such joints is recorded as a change in the overall shape of ecostorm operating noise, and (more reliably) – characteristic changes in the spectrum of sound with a strong mid-frequency components of the spectrum arising from the contact gaps.

Low frequency self-modulation of the friction process, which is manifested in the spectrum of the acoustic emission is a consequence of the dynamic targeting slow angular motion in the system friction. A-modulation is a mistake to ascribe directly of cyclical damage accumulation and separation of wear particles.

3.2. Quantum-acoustic analysis of tribosystem behavior

Classical tribology considers external friction as a dissipative, locally-determined form of interaction of rubbing bodies during the accidental realization of the actual contact areas. Methods from physical mechanics

have recently been widely used to study friction processes and adhere to the same concept, even though experimental results indicate the presence of wave processes in a tribosystem. The wave movement forms are not considered in the theory of dissipative self-organization of friction processes based on the so-called unbalanced thermodynamics. Entropy as a function of the system state is almost insensitive to the directional movement of the system or any wave movement of its elements. A thermodynamic flow considers only a form of chaotic movement that fully corresponds to the general provisions on dissipative friction. Wave vibrational processes are based on the interaction between the elasticity of contact and material inertia and are common to the wave and vibrational motion. A well-known concept of external friction is based on the slip of the indenter over an elastic-plastic deformable half-plane, it is limited to only one degree of freedom and eliminates all wave elastic bonds. Modern friction models are multifactorial, and triboacoustics has a wide range of research tools for the wave movements that accompany friction.

Thus, it is a relevant scientific task to study the physical and mechanical features of the tribotechnical contact from the positions of quantum-mechanical processes.

The study of the physics of friction processes from the positions of quantum-wave aspects has been receiving increased attention in recent times.

Based on the theory of macroscopic quantum electrodynamics for unstable systems, paper [11] calculated statistical parameters of the friction force at zero temperature. The quantum force of friction was determined at a time point corresponding to the generation of the first excitation for each pair of unstable oscillators. At the same time, the estimated ratios obtained did not address the actual friction processes of the technical systems.

It is shown in [12] that in a dissipative dynamic system driven by an oscillating force, the force of friction can create a quasi-stationary resistance that is always directed in the opposite way to the force caused by the spatial heterogeneity of vibrations. At the same time, the physical nature of the forces was not taken into consideration. The friction of the slip between a rigid hemispheric indenter and the deformable textured surface, which represents irregularities that change their shapes, was investigated in [13]. Friction fluctuations were observed when sliding in the direction perpendicular to the motion using optical images and friction profiles. Works [14, 15] report the experimental results of a triboacoustic control over the integrity of the nominally-immobile frictional connection under the conditions of fretting. Two opposite-directed wave energy cascades were observed under fretting modes. However, there is no theoretical analysis of the study results. The non-stable processes in the operation of friction nodes in automotive equipment in the presence of motor lubricants were considered in papers [16–19]. The experimental studies have established the effect of

various additives to oils on the stabilization of friction forces and reducing the wear of rubbing surfaces. Modern tribodiagnosing methods for assessing the technical condition of friction pairs are given, including based on the criterion of vibrational resistance. A problem of the vibrational frictional contact under conditions of adhesion wear is analyzed in [20]. It is shown that if the tangential amplitude is preserved in the wear range, energy dissipation can be controlled by the amplitude of normal vibrations. At the same time, the hypothesis put forward requires experimental confirmation. A model of the effect exerted by the system dynamics on the sliding friction is reported in [21]. The model shows that micro-vibrations play an important role in the dynamic effect on the system friction resistance. Determining the range of critical parameters makes it possible to systematically control friction resistance by adjusting the geometry and rigidity of the system. The estimation-experimental models of predicting the durability of cylindrical sliding tribo-systems, taking into consideration the dissipation of friction characteristics, are proposed in works [22, 23]. At the same time, the physical prerequisites of the dissipative processes are not fully disclosed. The studies of friction surfaces with regular geometric microelements [24–26] investigated the processes of exciting internal magnetic fields at the edges of discrete regions. It is shown that the combination of studies of friction and wear processes in areas such as mathematical statistics, contact mechanics, surface physics, provides a deeper explanation of non-stationary processes on discrete surfaces of contact elements. A model of the body wear at high friction speeds in a probabilistic statement is proposed in [27, 28]. The model is based on the thermokinetic theory of material destruction. The wear model patterns were identified considering the random nature of the factors involved. The model is represented in a discrete form and is not sufficiently adapted for numerical modeling. The physical basis of the frictional contact interaction of surfaces is analyzed in works [29, 30]. A physical pendulum was adopted as a tool for researching energy losses in tribosystems. The results of our analysis of the scientific literature reveal the need for deeper systemic research of quantum-mechanical processes in the contact interaction of technical tribosystems. Such studies could discover new features in the mechanics of a tribological contact and are promising for analyzing the durability of machine friction nodes.

3.2.1. The pseudo-equilibrium and collapse models of contact disturbance generation in tribosystems

The physical model under consideration is based on the interaction of thermal radiation with the vortex-wave forms of substance movement. It is known that the equilibrium thermal radiation is compatible with only two simple forms of macroscopic movements of matter – moving as a whole at a

constant speed and a solid-body rotation at a constant angular velocity. The tribocontact interaction of deformable solids significantly expands the types of mesoscopic and macroscopic movements of matter by various vortex-wave forms. It is natural to assume a certain transformation of thermal radiation in the interaction with such forms. To describe this transformation, a method of quasi-particles as elementary thermal excitations, adequate to the vortex-wave movements of matter, is used in this paper. These quasi-particles are the excited forms of the thermal radiation itself in comparison with its main form – the equilibrium thermal radiation.

An important feature of the model is the consideration of the dimensional factor. Characteristic gradients of contact stresses, velocities, and temperatures have a micron and submicron scale. At the same scale, there are the wavelengths corresponding to an extremum in the spectrum of equilibrium thermal radiation at room and elevated temperatures. This spatial resonance distinguishes the systems of dynamic contact interaction as the generators of the combined corpuscular-vortex-wave complexes of disturbances of the velocity field of the material environment and the field of thermal radiation.

Consider an ensemble of quasi-particles disturbances with the following characteristics:

$$E = \pm \vec{p}\vec{v}; \vec{p} = \hbar\vec{k}, \quad (3.1)$$

where E , \vec{p} , \vec{v} , \vec{k} are, respectively, the energy, pulse, speed, and wave vector of disturbances; \hbar is the Planck constant. After mutual substitutions, we obtain:

$$E = \pm \hbar k \vec{v} = \hbar \omega, \quad \omega = \pm k \vec{v}, \quad (3.2)$$

where ω is the cyclical frequency of disturbances. In this case, the group speed of the latter is determined in the following way:

$$\vec{v}_{gr} = \frac{\partial E}{\partial \vec{p}} = \frac{\partial \omega}{\partial \vec{k}} = \pm \vec{v}. \quad (3.3)$$

Introduce the corpuscular-wave mass m of disturbance quants in a regular way:

$$\vec{p} = m\vec{v} = \hbar\vec{k}. \quad (3.4)$$

As a result, the equivalent energy ratios follow from (3.1) to (3.4):

$$E = \hbar \omega = \pm m (\vec{v})^2 = \pm \frac{\hbar^2}{m} (\vec{k})^2. \quad (3.5)$$

The \pm signs in expressions (3.1) to (3.5) correspond to two possible directions of time. Between these two possibilities, the first one (a plus sign) is usually selected, corresponding to the positiveness of the absolute temperature T and the non-negative increase in entropy ΔS :

$$T > 0; \Delta S \geq 0. \quad (3.6)$$

Here, take into consideration a second possibility (a minus sign in (1) to (3.5)):

$$T < 0; \Delta S \leq 0. \quad (3.7)$$

In this context, introduce a pair of disturbances with the total energy ΔE (considering the signs in (3.1)):

$$\Delta E = \bar{p}\bar{v} - \bar{p}'\bar{v}', \quad (3.8)$$

where strokes indicate disturbances that develop over time opposite to those without strokes. The total pairs' energy module is limited from below by the basic principle of quantum mechanics – the principle of uncertainty:

$$|\Delta E| \geq \hbar/|\Delta t|, \quad (3.9)$$

where Δt is the finite lifecycle of disturbances that form a pair. On the other hand, by virtue of the same principle of uncertainty, the energy ΔE can be regarded as the energy of self-disturbance, ratio (3.8) – as the condition of the energy balance in the triad of disturbances. It should be supplemented with the momentum conservation law in the following form:

$$\Delta \vec{p} = \vec{p} - \vec{p}'; \quad \Delta \vec{k} = \vec{k} - \vec{k}'. \quad (3.10)$$

It is necessary to note the widespread use of expressions in the form (3.10) in the calculations of non-linear transmission of energy and pulse by the triads of wave disturbances in the theories of quasi-two-dimensional turbulence [31], as well as spiral three-dimensional turbulence. The most well-known result of these calculations is the reverse energy cascade (in the direction of large spatial scales), opposite to the direct cascade of conventional three-dimensional turbulence [31]. Turbulence in the system of quasi-particles under consideration is represented by continual clusters on the spectra of disturbances. Here, the focus is on the narrow-band highlighted peaks on these spectra, due to the exchange interaction of quasi-particles. Unlike the vast turbulent clusters, which are quantum fluid, such highlighted components of spectra can be considered within the concept of the quasi-ideal quantum gas. The statistics of such gas are determined by the spin of quasi-particles, equal, in this case, to $s = 1/2$ (in the units of the Planck constant). The possibility of coherent amplification of disturbances is predetermined by the pairing of quasi-particles with opposite spins. The

effect of attraction, required for such pairing, is provided by the exchange of phonons. Depending on the sign of the spirals of disturbances in pairs, it is possible to form thermal complexes both on running waves and on standing waves. By considering these pairs of disturbances to be bosons, we use the statistics by Bose-Einstein, taking into consideration the possibility of exchange interaction in the ensemble of disturbances:

$$\langle n_E \rangle = \frac{1}{e^{\frac{E}{kT}} - 1}, \quad (3.11)$$

where $\langle n_E \rangle$ is the average number of quasi-particles in a quantum state with the energy E ; k is the Boltzmann's constant.

Given the variable number of disturbances, the chemical potential in (3.11) is accepted to equal zero. In the case of tribodynamics, we note that the disturbance energy E lies in the acoustic range while the average thermal energy kT is many orders of magnitude higher. By decomposing exponent (3.11) into a series and discarding small terms, we obtain a simpler ratio for the average filling numbers:

$$\langle n_E \rangle \approx \frac{kT}{E}; \quad \langle E \rangle = E \cdot \langle n_E \rangle \approx kT. \quad (3.12)$$

Here $\langle E \rangle$ is the average energy of the entire ensemble of identical quasi-particles in a certain quantum state. The approximate equality of this energy to the average thermal energy determines the possibility of effective energy exchange between the ensemble of disturbances and the thermostat. This exchange is carried out with the help of photons of forced thermal radiation. Given the aforementioned observation, the conditions $E \ll kT, \langle n_E \rangle \ll 1$ are met. This determines the high effectiveness of exchange interaction in a given system of disturbances. For bosons, it has the character of attraction, which, as will be shown using real examples, can significantly exceed the repulsive contact forces of electromagnetic origin.

The potential for exchange interaction can only be revealed in a coherence environment. The functioning of tribosystems under the mode of a coherent acoustic radiation generator was generally considered in work [22]. Significant clarifications should be made to the physical mechanisms of these types of disturbance processes. First of all, regarding the unbalanced environment itself, as well as the structure of the composite resonator.

Statistics (3.11) describe the equilibrium states of the ensemble of quantum objects. The peculiarity, in this case, is that the forced disintegration of unstable quasi-particles with the radiation of acoustic and electromagnetic

waves at the high efficiency of heat pumping is possible in the case of the equilibrium distribution of these quasi-particles by energies. Unlike stable particles, whose system requires the inversion of the populations of energy levels.

The simultaneous stabilization both for wavelength and frequency predetermines the multi-level structure of the resonator of the contact generator of disturbances. The main role here is given to the mesoscopic spherical resonator, formed as part of the corpuscular-vortex-wave thermal complexes. The radius r of such a resonator is determined from the following ratio:

$$\lambda = 2\pi r = \frac{2\pi}{\tilde{k}} = \frac{h}{mv} = \frac{b}{T} = \frac{ch}{4,965kT}. \quad (3.13)$$

Here, λ , \tilde{k} , v are, respectively, the wavelength, wavenumber, and the module of quasi-particles velocity, b is the Win's constant; c is the speed of light in a vacuum; $h = 2\pi\hbar$ is the Planck constant; 4.965 is the root of the transcendent equation for finding a Win's constant.

Ratio (3.13) reflects the stabilization of the wavelength of the thermal complex (the radius of the resonator r) based on an extremum in the spectrum of equilibrium thermal radiation corresponding to the temperature T . Combining the above expressions, we obtain additional ratios for the cyclical frequency and velocity of the corpuscular-vortex-wave thermal complexes:

$$\omega = \pm \frac{(4,965kT)^2}{\hbar mc^2}, \quad (3.14)$$

$$\frac{v}{c} = \frac{4,965kT}{mc^2}. \quad (3.15)$$

Expressions (3.14), (3.15) describe the right-hand (high-frequency) side of the threesomes of disturbances (3.8). The low-frequency part of these threesomes with the energy ΔE competes with two high-frequency components in view of the sharp increase in the role of forced thermal radiation relative to the spontaneous one with an increase in the wavelength. This causes the formation of low-frequency clusters of the contact-induced disturbances in the infrasound part of the acoustic spectrum. The macroscopic resonator of the disturbance contact generator is formed by the whole set of feedbacks in a tribosystem [32]. Here, there is the possibility of both the high-frequency stabilization at their natural shapes of oscillations of the elements of a tribosystem and the low-frequency one – at the angular shapes of rotating parts and the slacked shapes of the drive's oscillations.

In addition to the pseudo-equilibrium scheme of disturbance generation, another scheme is also possible – with a collapsed energy pumping. It is at

the heart of emergency and catastrophic regimes. Spreading in the material of contact and sub-contact layers, the corpuscular-vortex-wave thermal complexes can attach to themselves the material mass M , enclosed in the volume of the spherical resonator and determined from the following ratio:

$$\frac{Mv^2}{2} = kT. \quad (3.16)$$

In this case, the above expressions yield a limit on the density of the attached substance (for the high-frequency component of disturbances):

$$\rho = \frac{59,58}{ch^3} (\pi mkT)^2. \quad (3.17)$$

Due to the contact break, the effective density of the attached substance can dynamically vary and auto-adjust to condition (3.17). It also follows from (3.17):

$$\frac{Mc^2}{mc^2} = \frac{2}{(4,965)^2} \frac{mc^2}{kT} = \frac{2}{4,965} \frac{c}{v}. \quad (3.18)$$

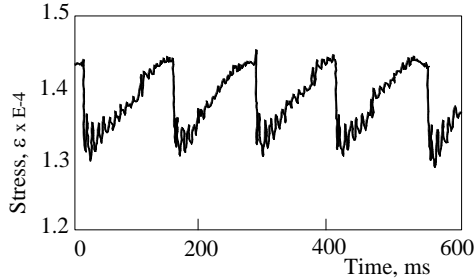
If the entire energy $Mc^2 \gg E$ (or its large part εMc^2) is added to (3.11), the average filling numbers are zeroed and a thermal complex collapses. The correlated destruction of many thermal complexes leads to a colossal release of energy in tribological standards. For example, a single micron-scale spherical resonator with an attached condensed substance of conventional densities contains the energy of $Mc^2 > 10^2$ J, while, as it is estimated in [33], the plastic deformation of the volume of matter with a side of 0.1 mm requires $\sim 10^4$ J only. Even the small magnitude of the attachment ratio $\varepsilon \ll 1$ can provide the effects of negative friction (at local time stages) at the most common functioning of tribosystems, which has no explanation in conventional approaches [32].

Consider specific experimental confirmations of the considered mechanism of contact disturbance generation in tribosystems.

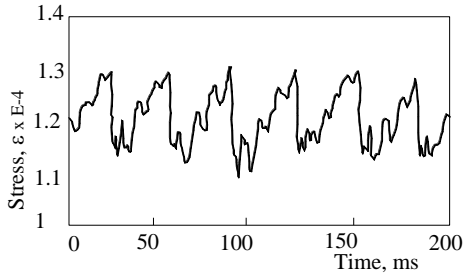
3.2.2. Generating disturbances under the modes of fretting, sliding and rolling friction

The destructive nature of the fretting process at low speeds of reverse slip (slippage) is caused by the generation and collapse of the corpuscular-vortex-wave thermal complexes. The characteristic speeds of fretting of the order of $10^{-5} \dots 10^{-3}$ m/s at normal temperatures and the values of m , equal to the masses of atoms and molecules of matter, correspond to expression (3.15). As an example, Fig. 3.6 shows the contact stress oscillograms in the polymeric substrate of the tribopair steel–plate made from polymethylmethacrylate

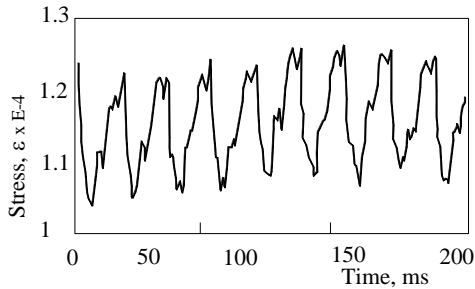
(PMMA) depending on the average speeds of reverse friction. The acoustic range of the tribopair sound is shown in Fig. 3.7. The dominant frequency here is $\nu \approx 4.3$ kHz; it corresponds to expression (14) at $T \approx 300$ K, $m = 1$ u (hydrogen). The long-wave packet of disturbances in Fig. 1 is stabilized at a frequency of 43 Hz, corresponding to (3.14) at $T \approx 300$ K, $m = 100$ u (the $C_5O_2H_8$ PMMA molecule). The optimal sliding speed, $V = 400$ micrometer/s (Fig. 3.6, *c*) is exactly the same as expression (3.13) at these parameters.



a



b



c

Fig. 3.6. Oscillograms of sub-contact stresses in the polymeric substrate of the steel–PMMA tribopair at the following average reverse friction speeds [24]:
a – 40 $\mu\text{m/s}$; *b* – 200 $\mu\text{m/s}$; *c* – 400 $\mu\text{m/s}$

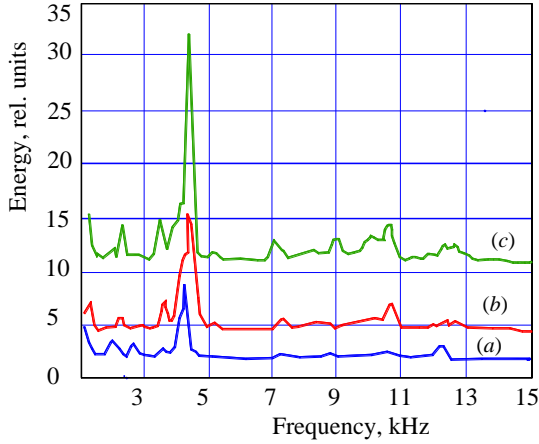
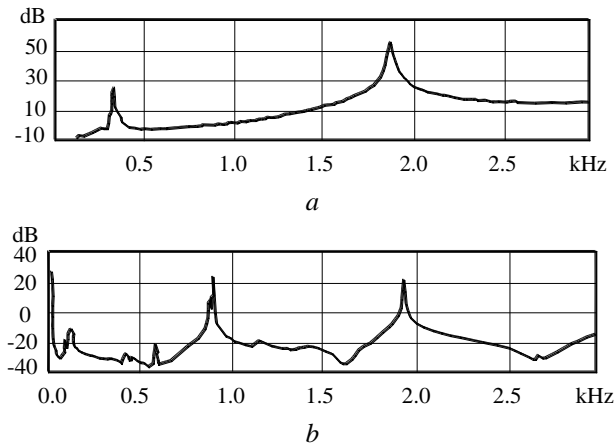
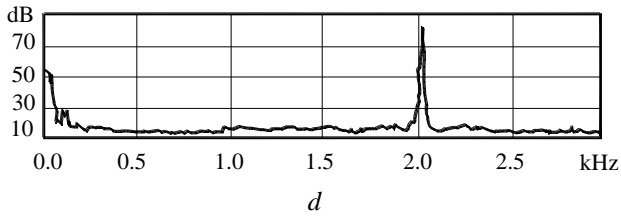
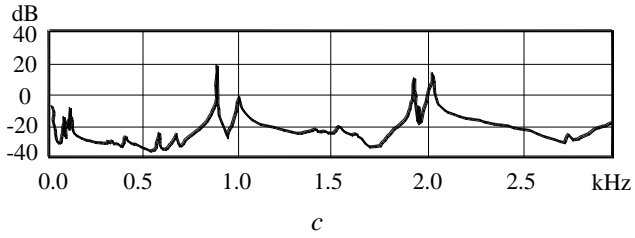


Fig. 3.7. The spectra of acoustic emission of the steel-PMMA tribopair at the following reverse friction speeds [34]:
a – 40 $\mu\text{m/s}$; *b* – 200 $\mu\text{m/s}$; *c* – 400 $\mu\text{m/s}$

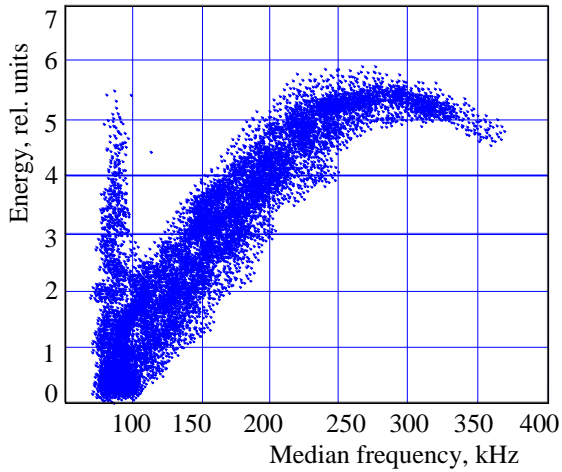
Fig. 3.8 shows the transfer functions of the rod-disk tribopair and the spectrum of the acoustic emission of this tribopair [35]. The characteristic frequency $\nu \approx 2.2$ kHz on this spectrum corresponds to expression (3.14) at $T \approx 300$ K, $m = 2$ u. It is necessary to pay attention to the low-frequency cluster of an acoustic emission signal (Fig. 3.8, *d*), due to the generation of long-wave packets of disturbances. The specified characteristic frequency of $\nu \approx 2.1...2.2$ kHz is also present in the spectra of acoustic friction emission reported in works [36, 37].





**Fig. 3.8. Transfer functions: *a* – disk; *b* – rod;
c – the disk-rod system under static contact conditions;
d – the spectrum of sound generated at the friction of a tribopair**

An example of the acoustic friction emission in the ultrasonic region of the spectrum is shown in Fig. 3.9 [37].



a

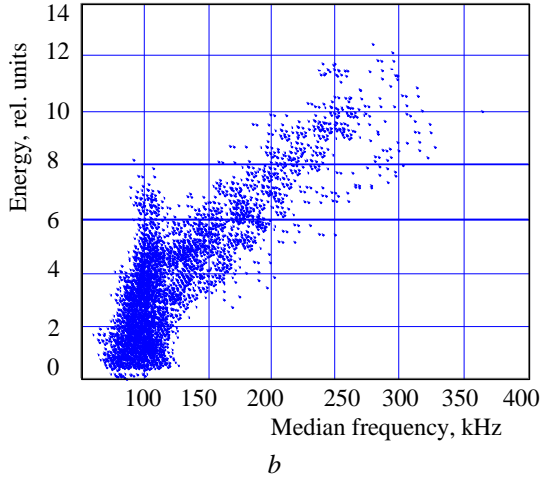


Fig. 3.9. Dependence of the energy of an acoustic signal on the median frequency at friction in the system ball-disk with a load on the ball: $a - 2\text{N}$; $b - 3\text{N}$ [37]

That clearly reflects the quantum nature of the disturbances generated by friction. There is also a division of the acoustic emission signal into two clusters: a narrow-band low-frequency and high-frequency broadband. In this interpretation, this division corresponds to the equilibrium (in each of the two thermostats separately) and the unbalanced composition of the disturbances. In the latter case, jet forms of a vortex field of velocities are generated, thereby forming the wear particles. Suppressing such forms by increasing a contact load (Fig. 3.9, b) reduces wear [37]. The role of adhesion in the formation of wear particles is also well-emphasized. In this regard, we note that the exchange interaction considered here is the same as the adhesion. Therefore, the cumulative effect can significantly exceed the controversial action of the forces of elasticity in the sub-contact layers, which leads to jamming.

The frequency of an acoustic friction emission $\nu \approx 100$ kHz is very typical for triboprocesses in the ultrasonic region of the spectrum of disturbances generated [37, 38]. From our point of view, this frequency corresponds to the generation of disturbances near the melting point of steel: $T \approx 1,500$ K, $m = 1 u$ (hydrogen), according to (3.14). For an unbalanced high-frequency cluster in Fig. 3.9, a with a maximum at $\nu \approx 270$ kHz, an effective hydrogen temperature can be introduced:

$$T_H = \frac{(h\nu \cdot m_H c^2)^{1/2}}{4,965k}. \quad (3.19)$$

This expression follows from (3.14) when taking into consideration the ratio $\omega = 2\pi\nu$, assuming $m = m_H = 1$ u. In this case, the temperature $T_H \approx 2,400$ K significantly exceeds the melting point of steel, which determines the local imbalance of the friction process under the modes corresponding to the high-frequency cluster in Fig. 3.9. The division of the spectrum of acoustic friction emission into narrowband and broadband clusters is noted in the literature on tribospectroscopy [38].

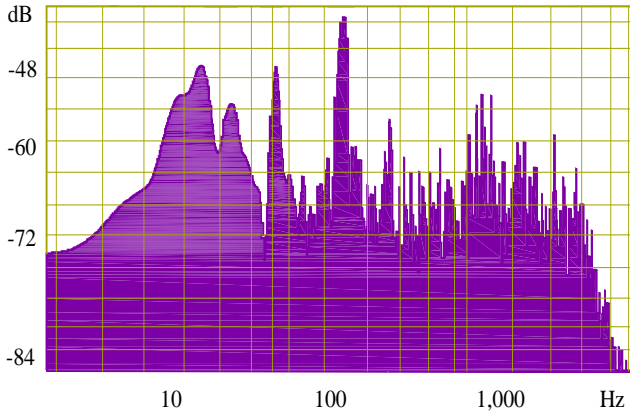


Fig. 3.10. Spectrum of acoustic emission when rolling a ball in the bearing with a diameter of 6 mm over the glass sloping plane of a mirror

Exchange interaction is manifested under the normal modes of tribosystem operation. As an example, Fig. 3.10 shows the spectrum of the acoustic emission, accompanying the rolling of a ball in the bearing with a diameter of 6 mm over the polished glass plane of a mirror.

The dominant peak at the frequency $\nu \approx 250$ Hz corresponds to the formation of thermal complexes on water molecules ($m = 18$ u at room temperature according to expression (3.14)). Fig. 3.11 shows the results of a statistical analysis of the process of such rolling. The total time of the ball's movement on the plane was compared with the standard rolling time calculated using the standard ratios of solid mechanics. A dotted line in Fig. 3.11 corresponds to a zero-friction movement. The formal positivity of the tangential contact reaction (negative friction) below this line is explained by the quantum generation of longwave disturbances considered here. Similar dynamic characteristics with negative friction were obtained in the tests of roll bearings (Fig. 3.12) and have a similar explanation.

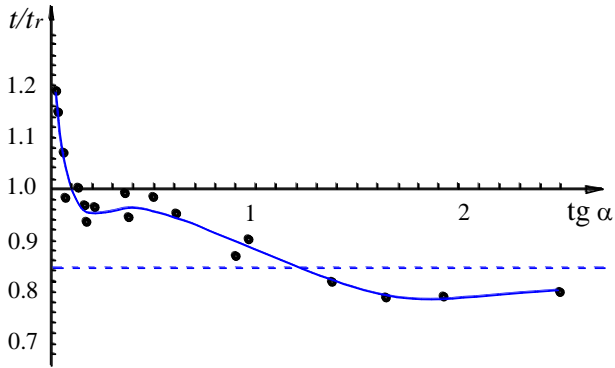


Fig. 3.11. Dependence of the ratio of the time of the ball's movement on a sloping plane to the calculated rolling time according to the standard scheme of solid mechanics on the tangent of the angle of the plane tilt

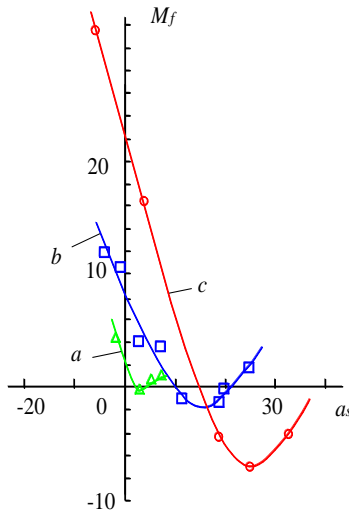


Fig. 3.12. Dependences of the average reduced friction force moment in a roll bearing on the average reduced load accelerations in the Atwood's experimental machine at the average values of angular velocities of block rotation: $a - 5.0 \pm 0.5$ rad/s; $b - 9 \pm 1$ rad/s; $c - 16 \pm 1$ rad/s

Therefore, external friction should be considered as a self-coordinated process of dynamic interaction, based on the transmission of a wave pulse with the generation of disturbances.

3.2.3. Contact-induced flutter and buffeting under the cutting modes of materials

The collapse component of the disturbance generation is significantly amplified under the modes of the destruction of materials, including when cutting. Fig. 3.13 shows the examples of the spectra of acoustic emission, accompanying the cutting of steel rods on a turning machine under the non-regular modes of flutter-buffeting. There is clearly a reverse energy cascade in the ensemble of quasi-two-dimensional spherical disturbances generators, carried out at the mesoscopic level. The macroscopic stabilization of these disturbances at the drive's natural frequencies ($\nu_1 \approx 13$ Hz, $\nu_2 \approx 40$ Hz) predetermines the dominant narrowband maxima in the central part of the spectrum. At the same time, the pronounced flutter peaks in the high-frequency region correspond to (3.14) at the following parameter values: $m = 2$ u, $T \approx 340$ K (frequency $\nu \approx 2.7$ kHz in Fig. 3.13, *a*), $m = 1$ u, $T \approx 350$ K (frequency $\nu \approx 5.6$ kHz in Fig. 3.13, *b*).

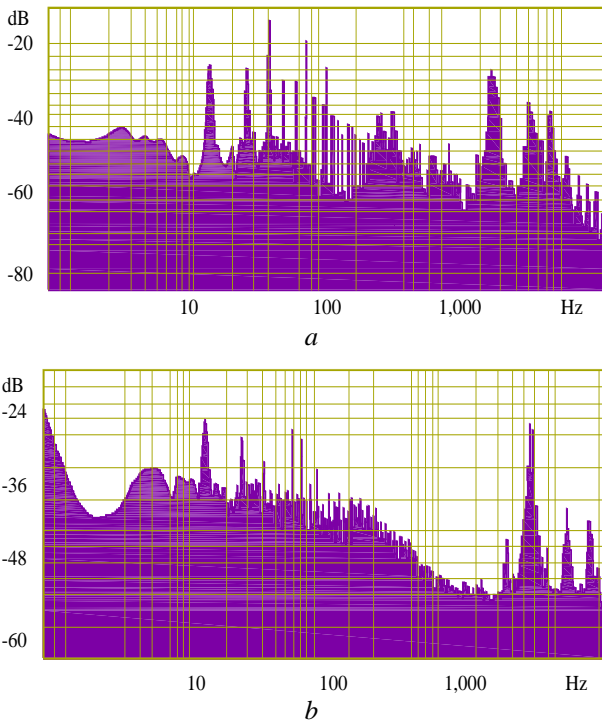


Fig. 3.13. Spectra of acoustic cutting emission under the dynamically loaded flutter-buffeting modes: *a* – non-hardened steel 40 Kh13; *b* – hardened steel

Dividing an acoustic emission signal at cutting into two clusters associated with the short-wave and long-wave packets of disturbances forms in a series of cases a characteristic drop in the central part of the spectrum (Fig. 3.14, *a*). The absence of dominant discrete lines here indicates the imbalance of the process of generating disturbances. In this case, the effective temperature (by hydrogen) is $T_H \approx 430$ K. A similar drop in the spectrum of disturbances also occurs during the impact interaction between the teeth of transmission gears in electromechanical machines (Fig. 3.14, *b*). The effective temperature here is $T_H \approx 380$ K. It should be noted that the introduction of such temperatures is quite conditional because in the friction zone there is a hierarchy of disturbances with different temperature values. Its high-temperature components produce the ultrasonic signals of acoustic emission (Fig. 3.9).

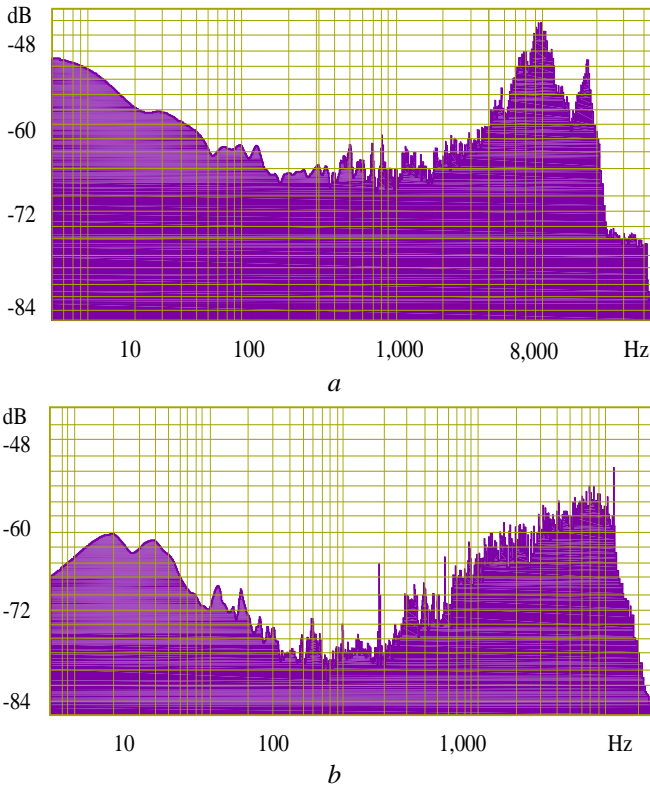


Fig. 3.14. Acoustic emission spectra: *a* – when sharpening a steel strip with an abrasive circle; *b* – when the electromechanical surface grinder is idle

At the same time, the ultrasonic signals under the cutting modes at frequencies $\nu \approx 3...30$ MHz, observed in [28], correspond, according to expression (3.16), to the thermal complexes on electrons ($m = m_e$) at very moderate temperature values.

3.2.4. Corpuscular-vortex-wave mechanism of selective transfer and hydrogen wear

Processes as different in their tribological significance as the selective transfer (a wearless effect) and hydrogen wear have similar mechanisms of their origin. The known criticality of the selective transfer of copper atoms (and other metals) to the temperature regime and the composition of a lubricant (3.29, 3.30) is explained by condition (3.25), which imposes certain restrictions on the parameters of the formation of corpuscular-vortex-wave thermal complexes in the friction zone. Specifically, at $m \approx 63$ u (copper) and $T \approx 300$ K, it follows from (19) that the value of $\rho \approx 1.26$ g/cm³ is almost equal to the density of glycerin, or the density of the oil freon mixture in the compressor systems of refrigeration installations.

On the contrary, replacing glycerin, for example, with Vaseline oil ($\rho \approx 0.8...0.9$ g/cm³) does not meet condition (3.19), which explains the known lack of the selective copper transfer in this case [29, 30]. The special properties of the servovite film under a selective transfer mode (porosity, defectiveness, low shear resistance) are directly provided by the collapsed processes in the disturbance system considered here. The same processes in the vortex-wave transfer of hydrogen atoms into metals produce the exact opposite result – gradual (wear dispersion) or instant destruction of the surface layer of friction.

The difference here lies in the ratio ε of the substance attachment inside the mesoscopic perturbators. The vortex-wave transfer of these disturbances deep into the contact zone also explains the expressed plastic deformations in the depths of the friction zone in the absence of strong plastic deformations directly on the surface of friction, observed in [26, 27].

Thus, the practical examples considered have confirmed the proposed physical mechanism of the contact generation of disturbances in tribosystems.

3.2.5. Results of studying the quantum-mechanical processes in the contact interaction of tribosystems

The dynamic contact of deformable solids is a source of disturbances in a broad range, often leading to devastating consequences. The presence of contact gaps in the dry and boundary friction modes, the temporal and spatial discreteness of contact limit the possibilities of the continuum mechanics and classical field theory methods when describing such modes. In this

case, we propose the ideas and methods developed in quantum field theory, as well as in the theory of turbulence. One of the most effective methods of this kind is the description of disturbances in the form of a quantum ensemble of quasi-particles involved in a specific exchange interaction, which is absent in classical mechanics. To analyze tribotechnical processes based on the quantum-mechanical approach, we have derived estimation ratios (3.14), (3.15) for the frequency and speed of wave tribodisturbances. Our analysis of experimental characteristics of friction processes at fretting, sliding and rolling friction has shown conformity to theoretical dependences. It has been established that the destructive nature of the fretting process at the low values of reverse sliding speeds is predetermined by the generation and collapse of the corpuscular-vortex-wave thermal complexes. The example of acoustic friction emission in the ultrasonic region of the spectrum has confirmed the quantum nature of the disturbances generated by friction (Fig. 3.9). The high-frequency spectrum of acoustic emission corresponds to the unbalanced composition of the disturbances and leads to the formation of wear particles. The exchange interaction in the tribosystem with rolling on the plane has been considered. The results of a statistical analysis of such rolling showed the presence of the effect of negative friction (Fig. 3.11, 3.12), caused by the quantum generation of longwave disturbances. The results obtained indicate that external friction should be considered as a self-agreed process of dynamic interaction, based on the transmission of a wave pulse with the generation of disturbances.

The exchange interaction arising against the background of ordinary electromagnetic processes determines, in particular, the catastrophic modes of contact-induced flutter and buffeting, which are also characteristic of hydro (aero) dynamic systems under conditions of discontinuity of the flow. An analysis of the results (Fig. 3.13, 3.14) shows that the collapse component of the generation of disturbances is significantly enhanced under the modes of the destruction of materials during cutting.

A rare beneficial effect associated with the exchange interaction in tribo-equipment is a known wearless effect (selective transfer), whose theory needs to be significantly clarified. The controversial mode here is hydrogen wear, described so far without taking into consideration the exchange interaction and a vortex-wave transport in the tribosystems. Studies have shown that the special properties of the servovite film under a selective transfer mode are directly provided by the collapse processes in the disturbance system. Similar processes in the vortex-wave transfer of hydrogen atoms into metals produce the opposite result – the destruction of the surface layer of friction.

The specificity of contact friction is also evident in sharp temperature gradients, which causes the formation of corpuscular-vortex-wave thermal

complexes involved in the exchange interaction. Co-operative processes in the system of such thermal complexes are, in fact, the main source of contact-induced disturbances.

The obtained results and their analysis allow us, based on methods of diagnosing the quantum-wave signals during the operation and study of friction nodes, to reasonably analyze and predict the progress of friction and wear processes, to prevent the occurrence of emergency operation of machines and mechanisms.

At the same time, it should be pointed out that the limitation of this study is to consider the approximated problem of quasi-ideal quantum gas. Additional consideration of the interaction of disturbances requires consideration not only of the discrete components of the spectra but also of the turbulent spectral clusters reflecting the processes of cascading energy transport in the system under consideration.

In the future, it is expedient to devise specific technical procedures and methods for suppressing contact-induced disturbances associated with emergency modes of operation of tribosystems. It is also advisable to generalize the results obtained for similar hydro(aero)dynamics problems associated with critical modes of operation.

Conclusions

1. It is analytically presented a method to describe disturbances in a tribosystem in the form of a quantum ensemble of quasi-particles involved in a specific exchange interaction. A physical model of the contact generation of disturbances in tribosystems has been constructed, which takes into consideration the exchange interaction and collapse of the corpuscular-vortex-wave thermal complexes.

2. It has been established that the destructive nature of the process of fretting at the low values of reverse sliding speeds is caused by the generation and collapse of the corpuscular-vortex thermal complexes. An example of acoustic friction emission in the ultrasonic region of the spectrum was used to show that the high-frequency component of the spectrum corresponds to the unbalanced composition of the disturbances and leads to the formation of wear particles. The results of a statistical analysis of the exchange interaction in the tribological system with rolling showed the presence of the effect of negative friction caused by the quantum generation of longwave disturbances.

3. It has been established that the collapse component of the disturbance generation is significantly enhanced under the modes of the destruction of materials, including the cutting of materials.

4. Based on the corpuscular-vortex-wave mechanism, it is shown that the properties of the servovite film under a selective transfer mode are

provided by the collapse processes in the disturbance system. Similar processes in the vortex-wave transfer of hydrogen atoms in metals lead to the wear and destruction of the surface layer.

3.3. Diagnostics-experimental analysis of friction pairs at stick-slip sliding

With small movements in speed (10...100 mm/min), movement with jumps is observed in translational friction pairs (stick-slip movement). This is typical for sliding friction in machine tools and instruments, sliders, presses and other machines. On the type of movement in this case, the magnitude of the friction force and its changes have a decisive influence. At low speeds, there is a transition from the forces of friction of a fixed body to the forces of friction of motion and vice versa. This is due to the instability of the process of formation and destruction of adhesive contact between the surfaces. As a result, the positioning accuracy of the machine components decreases, additional dynamic loads are created, failures occur and the wear rate of the machine parts increases. In this regard, the study of the processes of uniformity of movement and accuracy of the installation movements is given great importance. In this paper, we studied the characteristics of the frictional interaction of translational friction pairs with various types of lubrication of the contacting surfaces.

The influence of friction mode on the nature of the motion of mechanical objects is studied in a number of articles. The paper [41] presents a demonstration of an oscillator with sliding friction that exhibits very good agreement with a linear fall off in amplitude. The demonstration also confirms that sliding friction is proportional to the magnitude of the normal force. The paper [42] introduces a more detailed friction model, one that explicitly considers deformation of and adhesion between surface asperities. Using probabilistic surface models for two nominally flat surfaces, the stick-slip model sums adhesive and deforming forces over all asperities. However, these studies do not take into account the damping properties of the lubricant. The lubricant has a decisive influence on the processes of friction and oscillations. In studies [43–44], methods for determining the parameters of sliding friction under damped oscillations are considered. Mathematical models and methods for identifying their parameters on the basis of experiments are proposed. The method of laboratory testing for friction has a great influence on the accuracy of the results of studying vibrations under friction. Works [45–46] propose various hardware (acoustic, electrical) to control the characteristics of sliding friction. These studies have a positive contribution to the study of the processes of friction, but they do not always determine the sufficient accuracy of the friction parameters. The result of friction on the law of

motion is the accuracy of moving and positioning machine parts. In [47] the numerical simulations, the displacement of the moving part and the driving force of the controller are considered in cases of no friction, friction without stiction effect (sliding friction), and stick-slip friction. From these conditions, the influence of the friction on the sliding stability of the controller and the motion accuracy of the machine tool are analyzed and predicted. The study [48] gives an analysis of the basic friction models with tests and compares friction models in the literature: Coulomb friction model, Stribeck friction model, Dahl model, LuGre model, and the elastoplastic friction model on the same testbed. The experiments and models were done and the reasons for the difference in the basic of these models were investigated. Friction cannot be considered separately from modern surface engineering methods. The processes of friction depend on the properties of materials and coatings of the contacting bodies. In work [49] the influence of ionic nitriding on the processes of friction and wear under conditions of translational and swinging movement is considered. Resistance to wear of materials is also largely determined by friction processes. In work [50], the parameters of the friction process in the complex are presented in the model of wear proposed by the authors. The importance of laboratory and theoretical studies of friction parameters for practical applications follows from the literature review. For modern machines, friction is a necessary element that determines the accuracy of their operation. Thus, the study of friction processes requires more careful and detailed study.

For an experimental study of the friction force during the movement of a loaded plate on a lubricated and dry surface, the "LRX-E" model "Lloyd instruments" universal machine was used. The main characteristics of the testing machine are as follows:

1. Maximum force: 2.5 kN.
2. Error measuring force: 0.005 % of maximum value.
3. The limits of change of the speed of movement: 0.1...1020 mm/min.
4. The amount of movement: 1...1500 mm.
5. Error of measurement of movement <5.

The testing machine (Fig. 3.25). Is a laboratory computerized complex allowing to carry out various tests in the "force-displacement" format. In our case, it was configured to test for sliding friction in accordance with the international standard ASTM D1894. When testing, a steel, ground ($Ra = 1 \mu\text{m}$) plate 1 (Fig. 3.15.) measuring $63.5 \times 63.5 \text{ mm}^2$ and weighing 2N slid along the burnished surface of the Table 3.1. The horizontal position of the table was controlled by level 6. The plate movement was carried out by means of tensile flexible filament 3 through block 4. The upper end of the thread was fixed in the grip 5. The grip 5 was fastened in the traverse and with the help of a screw was moved along the guide column. To measure the forces and displacements, a special strain gauge type LASERSCAN LR 01/2932 was

used. The control of the testing process was carried out using the control panel 7 on the basis of a liquid crystal display. The software “Nexygen V4.5” and “Ondio V 4.5” was used to automate the test process with the specified parameters, automatically display the test results and statistical data processing. To study the friction force during the movement of a loaded plate on a flat surface, the following conditions were taken:

1. The speed of movement of the movable plate, mm/min.
2. Distance of movement, mm.
3. Types of lubrication: 1-dry; 2- motor oil Formula Q8 (API- SJ/CD, SAE - 15W/40); 3- consistent oil Agip F1 CR MU3 (Castrol).
4. Loading mode: 1 – 2N; 2 – 7.5 N; 3 – 13.5 N.

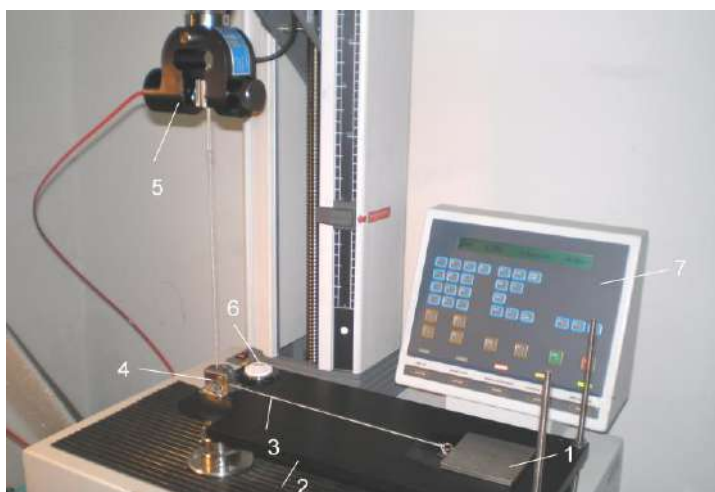
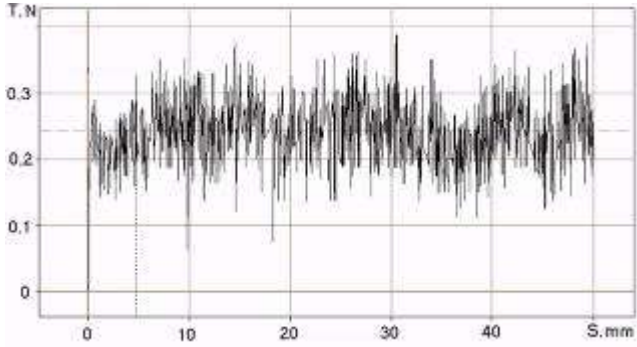
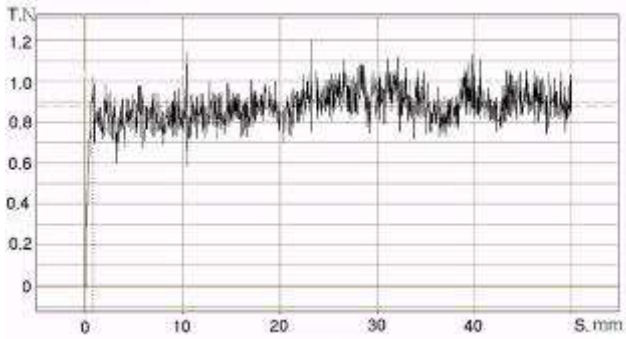


Fig. 3.15. Testing machine LRX-E

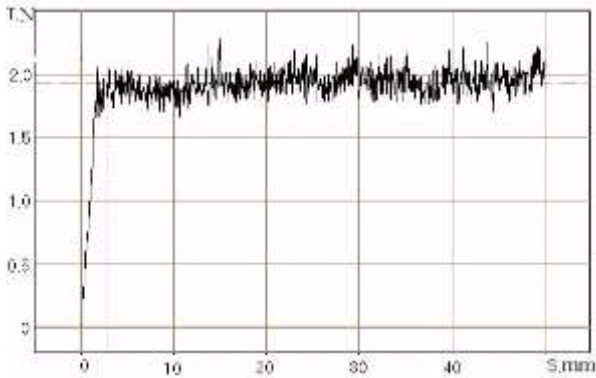
The test results are presented in the graphs on Fig. 3.16–3.18. Depending on the type of disturbing forces, the fluctuations of the friction force can be either deterministic (often periodic) or random. In our case, the reasons for the fluctuation of the friction force are the following: the random type of interaction of the roughness of the contacting surfaces (as a result, there is a random process of formation and destruction of frictional bonds between the surfaces); time dependence and different intensity of molecular adhesion forces (adhesion) between dry and lubricated surfaces; adhesive properties of lubricants; non-uniform distribution of the lubricant layer over the sample surface thickness. As a result, there is a stick–slip movement of a moving specimen (at relatively low sliding speeds) with random transitions from static friction to movement friction.



$$Q = 2N \quad (\bar{f} = 0,12; \bar{T} = 0,24N)$$

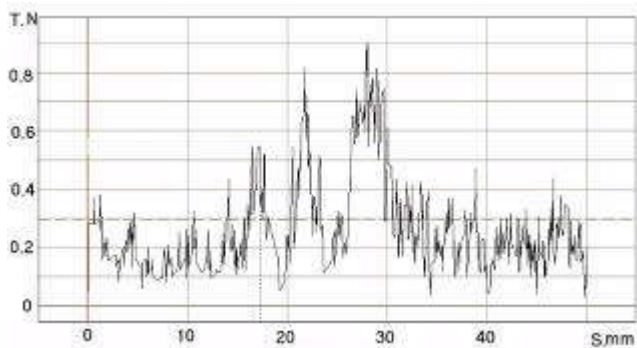


$$Q = 7,5N \quad (\bar{f} = 0,117; \bar{T} = 0,88N)$$

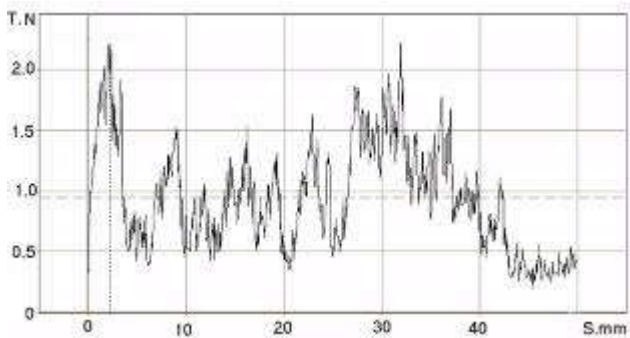


$$Q = 13,5N \quad (\bar{f} = 0,14; \bar{T} = 1,9N)$$

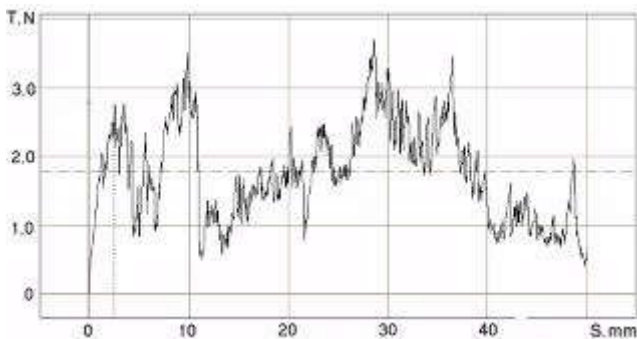
Fig. 3.16. Dependence of the friction force T on the displacement S during dry contact



$$Q = 2N \quad (\bar{f} = 0,147; \bar{T} = 0,295N)$$

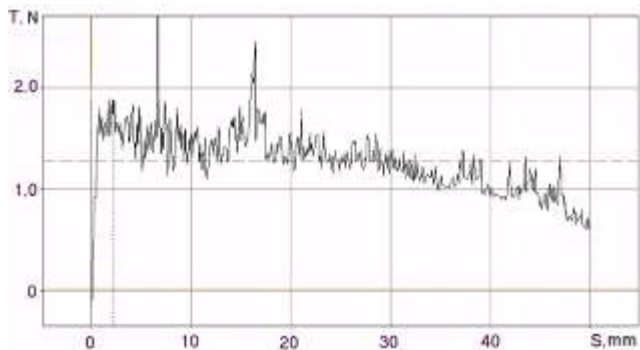


$$Q = 7,5N \quad (\bar{f} = 0,12; \bar{T} = 0,9N)$$

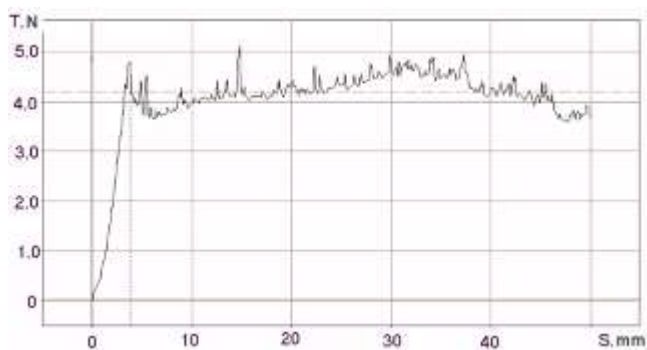


$$Q = 13,5N \quad (\bar{f} = 0,14; \bar{T} = 1,9N)$$

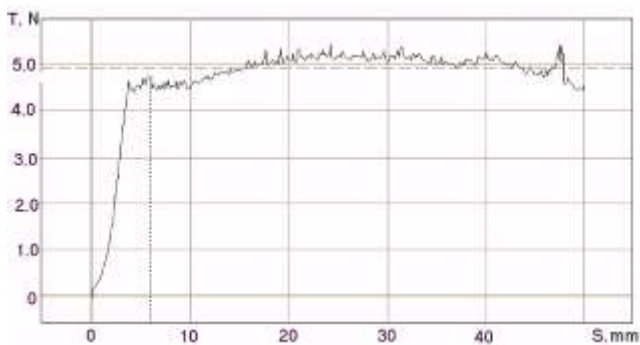
Fig. 3.17. Dependence of the friction force T on the displacement S with motor oil Formula Q8



$$Q = 2N \quad (\bar{f} = 0,64 ; \bar{T} = 1,28N)$$



$$Q = 7,5N \quad (\bar{f} = 0,56 ; \bar{T} = 4,22N)$$



$$Q = 13,5N \quad (\bar{f} = 0,36 ; \bar{T} = 4,92N)$$

Fig. 3.18. Dependence of the friction force T on the displacement S with grease

The friction force can take any value in a certain range. Therefore, the random process of friction force change should be characterized not by amplitude, frequency and phase, but by the mean value \bar{T} , standard deviation σ_T , coefficient of variation ν_T , minimum T_{\min} and maximum values T_{\max} and the range of change of the friction force ΔT .

To determine these characteristics, a statistical processing of the test results obtained on a testing machine was carried out. The results of statistical processing are shown in table 3.1.

An analysis of the results obtained by studying the friction force indicates the following.

With a dry contact of the ground plate with the surface of the table, relatively low friction forces take place compared to even the lubricated contact. This can be explained by the low adhesion of the surface of the steel plate to the surface of the table, covered with a layer of protective oxide film.

When the plate moves along the motor oil layer, the friction force in comparison with the dry contact should decrease, but the results suggest that it is approximately at the same level as in the case of dry friction. Obviously, this is due to the additional resistance to movement due to the high adhesion of the lubricant to the surfaces at low sliding speeds. This effect is even more pronounced with the grease.

Table 3.1

Statistical parameters of friction force changes

Lubricant	Q, N	T_{\min}, N	T_{\max}, N	$\Delta T, N$	\bar{T}, N	σ_T, N	ν_T
Dry	2	0,08	0,4	0,32	0,24	0,078	0,325
	7,5	0,59	1,3	0,71	0,88	0,117	0,132
	13,5	1,63	2,27	0,64	1,9	0,14	0,073
Motor oil Formula Q8 (API- SJ/CD, SAE - 15W/40)	2	0,04	0,89	0,85	0,295	0,179	0,607
	7,5	0,26	2,25	1,98	0,9	0,508	0,564
	13,5	0,41	3,81	3,4	1,9	0,72	0,378
Agip F1 CR MU3 (Castrol)	2	0,6	2,4	1,8	1,28	0,293	0,229
	7,5	3,64	5,13	1,49	4,22	0,297	0,070
	13,5	4,42	5,49	1,07	4,92	0,27	0,055

The dispersion of the friction force relative to the average value decreases with increasing load and with dry and lubricated contact. This is due to the increase hardness in contact with increasing load.

Stick-slip change in friction force is associated with the transition from friction of non-mobility to friction of motion. On the basis of the obtained experimental results, it is possible to establish some quantitative

characteristics of such a movement: the number of oscillations (jumps) per unit of time v_c ; the average movement in a contact before a shift in a contact s_c ; the average resistance force in a contact before a shift T_c . As a result of the graph analysis of Fig. 3.16–3.18, the following numerical values of these characteristics are established (Table 3.2).

The analysis of the obtained results shows that the greatest frequency of friction force oscillations occurs during dry contact. In this case, weak adhesion forces act and changes in the friction force are repeated more often than for contact with a lubricant. When using a lubricant, a large force is required to shift the contact layer and a correspondingly longer time for shear is required. Plastic lubricants at the same time have the best damping properties, since jumps of friction during their use are performed with the least frequency. However, the coefficient of friction is quite large (up to 0.5) due to the high adhesive properties of greases.

The obtained results of the quantitative analysis of the stick-slip movement with various lubricants are recommended for practical use in industry. The correct selection of lubricant and loads ensures minimum values of vibrations of the friction units of machines. This consequently improves the positioning accuracy of the machines.

Table 3.2

Characteristics of the hardness of the contact layer for moving loaded plate

Lubricant	Q, N	v_c, sec^{-1}	$S_c, \mu m$	T_c, N
Dry	2	5,3	156	0,15
	7,5	7,7	109	0,26
	13,5	7,4	114	0,29
Motor oil Formula Q8 (API- SJ/CD, SAE - 15W/40)	2	2,9	286	0,28
	7,5	4,1	204	0,84
	13,5	4	208	0,97
Agip F1 CR MU3 (Castrol)	2	2,9	285	0,36
	7,5	2	417	0,57
	13,5	2,1	400	0,45

On the basis of the laboratory diagnostic complex “LRX-E”, studies of the characteristics of friction during movement with a low speed of the loaded plate on the working surface in the presence of lubrication were carried out. As a result of processing the experimental data, statistical characteristics of the friction parameters were obtained, which characterize the effect on them of the load and lubrication mode. The quantitative characteristics of the plate motion, which characterize the deformation properties of the contact layer, are established.

References for chapter 3

1. Sviridenok, A.I., Myshkin, N.K., Kalmykova, T.F., and Kholodilov, O.V., *Akusticheskie i elektricheskie metody v tribotekhnike (Acoustic and Electrical Methods in Tribotechnology)*, Belyi, V.A., Ed., Minsk: Nauka i Tekhnika, 1987.
2. Akay, A., Acoustics of friction, *J. Acoust. Soc. Am.*, 2002, vol. 111, no. 4, pp. 1525–1548.
3. Vlasov, V.M., Mel'nichenko, N.V., and Reizer, E.S., Acoustic emission diagnostics of destruction of the seizure bridge in friction of steels without lubrication, *Trenie Iznos*, 1989, vol. 10, no. 2, pp. 257–261.
4. Fadin, Yu.A., Leksovskii, A.M., Ginzburg, B.M., and Bulatov, V.P., Periodicity of acoustic emission in dry friction of a steel-brass pair, *Pis'ma Zh. Tekh. Fiz.*, 1993, vol. 19, no. 5, pp. 10–13.
5. Gritsenko, B.P., Role of the acoustic oscillations generated by friction in fracture of tribological systems, *Trenie Iznos*, 2005, vol. 26, no. 5, pp. 481–488.
6. Kolubaev, A.V., Kolubaev, E.A., Vagin, I.N., and Sizova, O.V., Sound generation in sliding friction, *Tech. Phys. Lett.*, 2005, vol. 31, no. 10, pp. 813–816.
7. Rubtsov, V.E., Kolubaev, E.A., Kolubaev, A.V., and Popov, V.L., Using acoustic emission for the analysis of wear processes during sliding friction, *Tech. Phys. Lett.*, 2013, vol. 39, no. 2, pp. 223–225.
8. Zaporozhets, V.V. and Stadnichenko, V.N., Automated systems for tribodiagnostics of contact interactions, *J. Frict. Wear*, 2015, vol. 36, no. 3, pp. 241–248.
9. Dykha, A.V. and Kuz'menko, A.G., Distribution of friction tangential stresses in the Courtney-Pratt experiment under Bowden's theory, *J. Frict. Wear*, 2016, vol. 37, no. 4, pp. 315–319.
10. Kurskoi, V.S., Slashchuk, V.A., and Slashchuk, A.A., UA Patent 94006, *Byull. Izobret.*, 2014, no. 20.
11. Silveirinha, M. G. (2014) Theory of Quantum Friction, *New J. Phys.* 16, 063011 <https://iopscience.iop.org/article/10.1088/1367-2630/16/6/063011/pdf>
12. Esirkepov, T. Zh., Bulanov, S.V. (2017) Paradoxical stabilization of forced oscillations by strong nonlinear friction. *Physics Letters A*, Volume 381, Issue 32, <https://doi.org/10.1016/j.physleta.2017.06.007>
13. Suzuki, K., Hirai, Y., & Ohzono, T. (2014). Oscillating friction on shape-tunable wrinkles. *ACS applied materials & interfaces*, 6(13), 10121–10131. <https://doi.org/10.1021/am5010738>
14. Dykha, A. V., Zaspas, Y. P., & Slashchuk, V. O. (2018). Triboacoustic Control of Fretting. *Journal of Friction and Wear*, 39(2), 169–172. <https://doi.org/10.3103/S1068366618020046>

15. Dykha, A., & Matyukh, S. (2018). Triboacoustic diagnostic fixed joints of machines. In MATEC Web of Conferences (Vol. 182). EDP Sciences. <https://doi.org/10.1051/mateconf/201818202017>
16. Aulin, V., Hrynkiv, A., Lysenko, S., Rohovskii, I., Chernovol, M., Lyashuk, O., Zamota, T. (2019). Studying truck transmission oils using the method of thermal-oxidative stability during vehicle operation. *Eastern-European Journal of Enterprise Technologies*, 1 (6 (97)), 6–12.
17. Aulin, V., Hrynkiv, A., Lysenko, S., Zamota, T., Pankov, A., Tykhyi, A. (2019). Determining the rational composition of tribologically active additive to oil to improve characteristics of tribosystems. *Eastern-European Journal of Enterprise Technologies*, 6 (12 (102)), 52–64.
18. Aulin, V., Hrynkiv, A., Lysenko, S., Lyashuk, O., Zamota, T., Holub, D. (2019). Studying the tribological properties of mated materials C61900 - A48-25BC1.25BNo. 25 in composite oils containing geomodifiers. *Eastern-European Journal of Enterprise Technologies*, 5 (12 (101)), 38–47. doi: <https://doi.org/10.15587/1729-4061.2019.179900>
19. Aulin, V., Hrynkiv, A., Lysenko, S., Dykha, A., Zamota, T., Dzyura, V. (2019). Exploring a possibility to control the stressedstrained state of cylinder liners in diesel engines by the tribotechnology of alignment. *Eastern-European Journal of Enterprise Technologies*, 3 (12 (99)), 6–16. doi: <https://doi.org/10.15587/1729-4061.2019.171619>
20. Li, Q., & Popov, V. L. (2018). On the possibility of frictional damping with reduced wear: A note on the applicability of archard's law of adhesive wear under conditions of fretting. *Physical Mesomechanics*, 21(1), 94–98. <https://doi.org/10.1134/S1029959918010137>
21. Wetter, R., & Popov, V. L. (2016). The Influence of System Dynamics on the Frictional Resistance: Insights from a Discrete Model. *Tribology Letters*, 61(2). <https://doi.org/10.1007/s11249-015-0635-x>
22. Aleksandr, D., Dmitry, M. (2018). Prediction the wear of sliding bearings. *International Journal of Engineering & Technology*, 7 (2.23), 4–8.
23. Dykha, A., Sorokaty, R., Makovkin, O., Babak, O. (2017). Calculation-experimental modeling of wear of cylindrical sliding bearings. *Eastern-European Journal of Enterprise Technologies*, 5 (1 (89)), 51–59.
24. Marchuk, V. Y., Kindrachuk, M. V., Mirnenko, V. I., Mnatsakanov, R. G., Kornienko, A. O., Bashta, O. V., & Fedorchuk, S. V. (2019). Physical interpretations of internal magnetic field influence on processes in tribocontact of textured dimple surfaces. *Journal of Nano- and Electronic Physics*, 11(5). [https://doi.org/10.21272/jnep.11\(5\).05013](https://doi.org/10.21272/jnep.11(5).05013)
25. Marchuk, V., Kindrachuk, M., & Kryzhanovskyi, A. (2014). System analysis of the properties of discrete and oriented structure surfaces. *Aviation*, 18(4), 161–165. <https://doi.org/10.3846/16487788.2014.985474>

26. Kindrachuk, M. V., Vol'chenko, I., Vol'chenko, D., Skrypnyk, V. S., & Voznyi, V. (2019). Energy Levels of Different Types of Contacts of Microirregularities of Friction Couples. *Materials Science*, 54(6), 843–854.
27. Sorokaty, R., Chernets, M., Dykha, A., Mikosyanchyk, O. (2019). Phenomenological Model of Accumulation of Fatigue Tribological Damage in the Surface Layer of Materials. *Mechanisms and Machine Science*, 73, 3761–3769. doi: https://doi.org/10.1007/978-3-030-20131-9_371
28. Dykha, A., Sorokaty, R., & Dytyniuk, V. (2019). Model of accumulation of tribo damage in high-speed friction. In *Proceedings of 10th International Scientific Conference BALTRIB 2019* (pp. 180–186). Vytautas Magnus University. <https://doi.org/10.15544/baltrib.2019.29>
29. Dykha, A., & Makovkin, O. (2019). Physical basis of contact mechanics of surfaces. In *Journal of Physics: Conference Series* (Vol. 1172). Institute of Physics Publishing. <https://doi.org/10.1088/1742-6596/1172/1/012003>
30. Dykha, A., Aulin, V., Makovkin, O., & Posonskiy, S. (2017). Determining the characteristics of viscous friction in the sliding supports using the method of pendulum. *Eastern-European Journal of Enterprise Technologies*, 3(7–87), 4–10. <https://doi.org/10.15587/1729-4061.2017.99823>
31. Danilov, S.D., Gurarie, D. (2000). Quasi-two-dimensional turbulence. *Physics-Uspexhi*, 43(9):863. <http://dx.doi.org/10.1070/PU2000v043n09ABEH000782>
32. Zasp, Y. (2012, December). Coherent tribodynamics. *Journal of Friction and Wear*. <https://doi.org/10.3103/S1068366612060128>
33. Myshkin, N., & Markova, L. (2018). Trends in on-line tribo-diagnostics. In *Applied Condition Monitoring* (Vol. 8, pp. 203–223). Springer. https://doi.org/10.1007/978-3-319-61134-1_6
34. Briscoe, B. J., Chateauminois, A., Chiu, J., & Vickery, S. (2001). Acoustic noise emission in a model PMMA/steel fretting contact. In *Tribology Series* (Vol. 39, pp. 673–681). Elsevier. [https://doi.org/10.1016/s0167-8922\(01\)80149-8](https://doi.org/10.1016/s0167-8922(01)80149-8)
35. Akay, A. (2002). Acoustics of friction. *The Journal of the Acoustical Society of America*, 111(4), 1525–1548. <https://doi.org/10.1121/1.1456514>
36. Kolubaev, A. V., Kolubaev, E. A., Vagin, I. N., & Sizova, O. V. (2005). Sound generation in sliding friction. *Technical Physics Letters*, 31(10), 813–816. <https://doi.org/10.1134/1.2121824>
37. Rubtsov, V. E., Kolubaev, E. A., Kolubaev, A. V., & Popov, V. L. (2013). Using acoustic emission for the analysis of wear processes during sliding friction. *Technical Physics Letters*, 39(2), 223–225.
38. Myshkin, N. K., & Markova, L. V. (2018). Trends in on-line tribo-diagnostics. In *Applied Condition Monitoring* (Vol. 8, pp. 203–223). Springer. https://doi.org/10.1007/978-3-319-61134-1_6

39. Zinin, M. A., Gavrilov, S. A., Shchedrin, A. V., & Garkunov, D. N. (2011). Influence of metal-cladding additive valena on combined machining. *Russian Engineering Research*, 31(9), 880–884. <https://doi.org/10.3103>
40. Shchedrin, A. V., Bekaev, A. A., Garkunov, D. N., Mel'nikov, E. A., & Gavriluk, V. S. (2011). Improvement in hybrid drawing by a tool with regular microgeometry on the basis of metal-coating additives. *Russian Engineering Research*, 31(4), 365–368.
41. M. Kamela, *The Physics Teacher*, V. 45, 110 (2007); <https://doi.org/10.1119/1.2432089>
42. M. Bengisu, A. Akay, *J. Acoust. Soc. Am.* 105 (1), (1999)
43. A. Dykha, V. Aulin, O. Makovkin, S. Posonskiy, *Eastern-European Journal of Enterprise Technologies*, V. 3, 7 (87), (2017), doi: 10.15587/1729-4061.2017.99823
44. A. Dykha, A. Kuz'menko, *J. Frict. Wear*, V. 37, 4, (2016)
45. V. Aulin, A. Hryniv, A. Dykha, M. Chernovol, O. Lyashuk, S. Lysenko, *Eastern-European Journal of Enterprise Technologies*, V. 2, 1(92), (2018), doi: 10.15587/1729-4061.2018.125349
46. A. Dykha, S. Matyukh, *Triboacoustic diagnostic fixed joints of machines*, MATEC Web Conf., 182, (2018), <https://doi.org/10.1051/mateconf/201818202017>
47. Thi-Na Ta, Yunn-Lin Hwang, Jeng-Haur Horng, *Jurnal Tribologi* 19 (2018) 107-120.
48. Y. F. Liu et al.: Experimental comparison of five friction models on the same test-bed, *Mech. Sci.*, 6, 15–28, (2015)
49. P. Kaplun, O. Dykha, V. Gonchar, *Materials Science*, V. 53, 4 (2018), doi: 10.1007/s11003-018-0096-0
50. A. Dykha, R. Sorokatyi, O. Makovkin, O. Babak, *Eastern-European Journal of Enterprise Technologies*, V. 5, 1 (89), (2017), doi: 10.15587/1729-4061.2017.109638
51. Dykha A., Matyukh S. *Triboacoustic diagnostic fixed joints of machines // MATEC Web Conf.*, 182 (2018) 02017. 17th International Conference Diagnostics of Machines and Vehicles. DOI: <https://doi.org/10.1051/mateconf/201818202017>. https://www.matec-conferences.org/articles/mateconf/pdf/2018/41/mateconf_diagnostyka2018_02017.pdf

CHAPTER 4

Technological Support of Wear Resistance of Cylindrical Tribosystems

4.1. Hardening of cylindrical friction surfaces with a roller tool

The problem of increasing wear resistance, contact strength and resistance to contact spalling is becoming increasingly relevant as intensity of handling equipment operation is constantly increasing. The most economical extension of the rope block service life is possible by improving properties of the surface layer. Surface properties can be controlled by changing the surface layer structure and physical and mechanical properties.

When operating equipment for general technical purposes, large-sized steel parts that perceive contact loads, such as cable blocks, tackle blocks, pulleys, etc. often fail. Significant work forces in the presence of misalignment of interconnected parts often bring about spalling and wear of the working friction surfaces, shape distortion, alteration of clearances between the parts. As a result, service life of handling equipment and machinery units in general is reduced. Numerous studies [1] have shown that up to 85 % of machine failures occur in operation not because of an insufficient structural strength of the parts and units but because of contact damage and wear of conjugated friction surfaces.

Application of thermal or thermochemical strengthening methods in the manufacture of large size rope blocks is limited by their dimension and weight. The most simple, available, and often solely possible, method for strengthening such blocks is surface processing by cold plastic working, namely reeling or hammering. To improve appearance and increase wear resistance of the surface layer, finishing surface plastic deformation (SPW) is applied and in order to increase fatigue strength and contact strength of parts, work hardening is used. Therefore, the study of the effect of the reeled surface layer properties on tribotechnical characteristics is an urgent scientific and technical problem. During operation of rope blocks, rope interacts with the surface of the block groove. Because of elastic deformation

and torsion of the rope under load, it slips and rotates round its axis. This brings about various types of damage: the groove wear, appearance of cracks, collar spalling, general deformations, and other flaws. A fundamental contribution to the theory, calculation, and design of a "rope block – rope" friction couple is made in [2, 3]. The proposed theoretical calculations in the design of the "rope block – rope" friction couple have low accuracy because of numerous simplifications and assumptions in the calculation method.

The issues of wear, study of surfaces subjected to contact loading as well as improvement of physical properties of surface layers are considered in [4–6]. These studies do not take into account the phenomenon of slippage of contact friction surfaces which in turn affects the mechanism of wear of the tribological couple. Blocks are made of cast iron or steel by casting, pressing, or welding [7]. The use of cast iron for casting the blocks increases wear resistance of the block by 10–12 % compared to the steel blocks. Worn cast-iron (SCh 15-32) rope blocks are replaced by blocks of steel (25L) [8]. However, the proposed methods of hardening and restoring rope blocks, namely, restoration of the blocks with the help of automatic surfacing, welding, electromechanical processing, electroplating, etc. are very costly and of a low material-output ratio. Therefore, it is more advisable to take measures to harden the rope blocks and increase their longevity, especially with the help of SFW. Consequently, many methods are effective for certain operation conditions (uniform loading, absence of abrasive wear, etc.) and ineffective [3] in other conditions (impact loads, large specific loads, abrasion, etc.). However, for a large number of enterprises, the equipment requiring quenching and cementation is economically unjustified and therefore the issue of techno-economic feasibility of its acquisition appears often.

When deciding on the expediency of hardening and restoration of parts, one should proceed from the technical feasibility of the enterprise in question. It is necessary to ensure performance of the part after its hardening and restoration for the entire inter-recouple service life of the unit encompassing this part and economic feasibility of hardening and restoration.

Solution of the tribo-contact problem for a friction couple was made on the basis of the wear model in [9]. The proposed solution is quite complex for practical implementation since it requires division of the wear area into discrete sections. It does not take into consideration technological features and the form of the contact friction couple.

Analysis of the change in contact pressure was made in [10] during wear of coating in a friction couple for a nonlinear form of the wearing law. As a wearing law, a dependence of the wear rate on speed and contact pressures was taken. A nonlinear Winkler model was adopted to describe deformation properties of contacting materials. The proposed algorithm for solution of the wear-contact problem of the friction couple will face

significant difficulties in the case of loading the friction couple. This is determined by the problems of mathematical nature when using non-linear equations describing geometry of the contact couple in arbitrary equations.

Solution of an inverse wear contact problem for identifying parameters of the dependence of wear intensity on pressure and speed of sliding taking into account their distribution over the contact spot has been made in [11]. Based on the wear experiment by the "finger-disk" scheme, expressions for determining these parameters were obtained. However, assumption of stability of the wear spot accepted in the work in accordance with the test scheme does not make it possible to use the obtained solution for the test schemes with a variable contact (wear) spot.

A study of wear of a working "rope block – rope" friction couple caused by difference in diameters is presented in [12]. It was established on the basis of this study that the difference between the radii of the rope and the rope block profile leads to a change in distribution of contact pressures, and a phenomenon of axial slippage of the rope occurs which in turn leads to wear of the contact friction surfaces. However, the article does not present the dependence on quality of processing the friction surfaces of the "rope block – rope" couple. The mechanism of wear of the "rope block – rope" friction couple and distribution of residual stresses in the substrate surface were studied in [13]. The results of this study indicate that the rate of wear of the alloyed steel depends on diameter of the rope wires. The mechanism of wear of annealed low-alloy steel is characterized by fatigue and abrasive wear but the wire demonstrates partial adhesion because of microabrasive wear when a fatigue crack appears. Distribution of the residual stress contacts does not depend on the motion speed. Therefore, there are constant values in the contact surface. Analysis of the nature of failure of the parts that wear from the contact load of the friction surfaces showed that failure of rope blocks begins mostly in the surface layer and the resistance to this failure is determined by quality of the surface layer. Therefore, it is possible to influence quality of the surface layer by changing methods of surface treatment to provide predefined tribological characteristics to the friction surfaces.

To solve these problems, there is a need for a comprehensive study of new technological processes and the use of advanced methods of SFW. The study of wear processes and development of a strengthening technology require the use of laws and methods of continuous medium mechanics, mathematical and applied theory of plasticity, as well as the phenomenological theory of deformability. Thus, further theoretical and experimental studies of physical and mechanical properties of the surface layer and microstructural studies of steel specimens after reeling them with rollers are needed. It is necessary to investigate diffusion of chemical elements in the surface layer during surface deformation by means of microchemical analysis

and carry out tribological studies of wear of contact friction surfaces during reeling with allowance for slippage. All these measures will make it possible to create a method, a process, and a device for strengthening the rope blocks by reeling and solve production problems during its implementation.

4.1.1. Materials and methods used in the tribological study of the effect of reeling parts on the contact strength

Electron microscopy studies were carried out using a UEMV-100K microscope on thin foils prepared from the specimens taken at various distances from the surface and then thinned to a thickness transparent for electrons. Depth and degree of work hardening during plastic deformation of the surface layer were estimated using the regression analysis method. To this end, rupture tests were conducted on 0.2...0.4 mm thick flat specimens cut from a part at various distances from the part surface with the help of Shovenar machine with film recording of specimen deformation versus load diagrams. The study of the degree of hardening with analysis of the change of microhardness and diffusion of chemical elements in the surface layer in the process of SFW was carried out as follows. Microhardness after reeling the specimens in various conditions was determined using the PMT-3 microhardness meter. Determination of microstructure was carried out with the help of the KMT-1 device. Investigation of chemical distribution of strengthening elements by means of microchemical analysis was carried out on a raster electron microscope with the Superprobe-733 micro-X-ray micro-chemical analyzer from Jeol Company (Japan).

The study of pressure on the surface of plastic contact of the roller with the part during work hardening was carried out on 6.4 mm thick models prepared of an optically sensitive material ED6-M with the PPU-4 polarization installation (Russia). The TRB-S-DE tribometer (Switzerland) was used in the study of wear of the contact friction surfaces during reeling taking into consideration slippage to determine tribotechnical characteristics of the "disk-sphere" friction couple and the MI wear machine was used for modeling slippage with its upper shaft rotatable to ensure transverse slip. The VLR-200 (Russia) laboratory scale was used to measure weight loss in specimens. Experimental studies of the technological process of hardening the rope block surface by reeling were carried out on a universal 1K65 screw-cutting machine. The technological process was recorded on Panasonic SDR-S26 video camera with a subsequent frame-by-frame examination. Force on the roller varied within $\pm 5\%$ since the friction force of the rolling bearings was not more than 0.008. This provided a uniform deformation of the surface layer in the rope block groove. The degree of work hardening was measured and determined after reeling with the help of TIME Hardness Tester TH130 (India) universal integral dynamic hardness meter. Roughness

of the rope block working surface before reeling was measured using reference roughness comparison specimens OSh (GOST 9378-93 made in accordance with requirements of GOST 2789-73). After reeling, roughness was measured with the help of replicas prepared from self-curing Protacril-M plastic using the profilographer-profilometer of A1 type (GOST 19299-73 and GOST 19300-73), model 252 manufactured by Caliber Enterprise (Russia).

The reeled rope blocks were tested for spalling with ropes in production conditions on KRUPP ship reloaders (Germany) with a hoisting capacity of 40 tons, MGZ OJSC, and KS-3575 autocranes with a hoisting capacity of 10 tons, Mykolayivbudmekhanizatsiya JSC (Ukraine).

4.1.2. Results of tribological tests and process parameters of reeling steel parts with rollers

Vickers hardness under force of 0.10 kN and mechanical characteristics σ_B , $\sigma_{0.2}$ and δ were determined on specimens taken from a shaft made of 40 grade steel and reeled under a reeling force of 50.0 kN (Fig. 4.1).

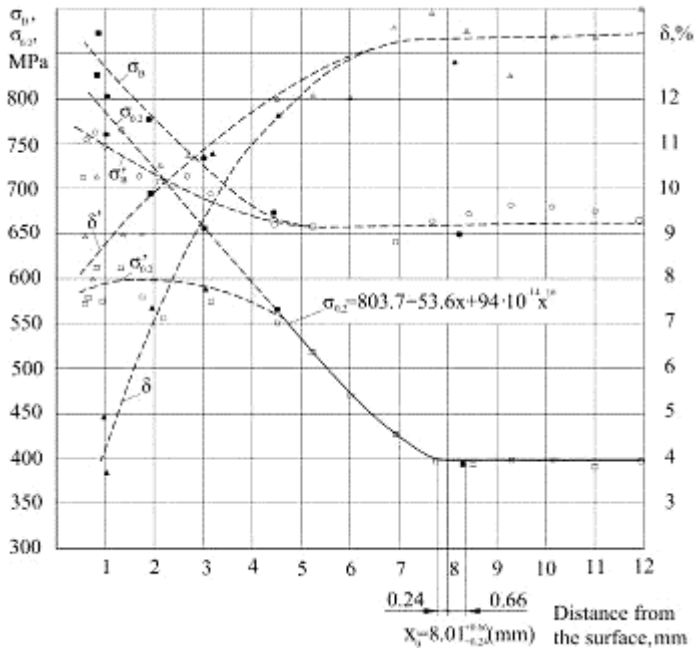


Fig. 4.1. Mechanical properties of the surface layer of the shafts reeled with toroidal rollers with diameter $D_p = 105$ mm, profile radius $r_p = 10$ mm:

σ_B , $\sigma_{0.2}$ and δ are properties in a circular direction; σ'_B , $\sigma'_{0.2}$, δ' are properties in the axial direction

Statistical estimation of accuracy in determining the depth of work hardening was made proceeding from the changes in hardness $HV10$ and the yield strength of the work hardened metal layer. A hypothesis of normality of distribution of measurements of initial hardness and yield strength was verified by the Kolmogorov criterion. After that, the results of hardness tests were statistically analyzed by the small specimen technique.

Nonlinear regression analysis was used to determine the depth of work hardening (estimated by the start of change in mechanical properties $HV10$ and $\sigma_{0.2}$ of the deformed layer) and estimate accuracy of determining the depth of work hardening.

To describe the regression lines, the functions were taken [1]:

$$y = a_1 + b_1x + b_2x^m \quad (4.1)$$

and

$$y = a_1 + b_1x + b_2 \lg x, \quad (4.2)$$

where y is hardness or yield strength; x is the distance of the measuring point from the reeled surface.

Statistical processing of the results obtained in determining the coefficients a_1 , b_1 , b_2 in the regression equations was performed according to the least squares method. Dispersion coefficients, work hardening depth and its confidence intervals and the standard deviation were estimated as well.

In the process of the regression analysis, the values of coefficients of the regression equations (4.1), (4.2) and the abscissa of the extremum point were initially calculated taking into account the values of mechanical properties which differed significantly from the initial ones. After the points of measuring initial mechanical properties were shifted in the direction of the x -axis, up to coincidence of their abscissas with the abscissa of the extremum point of the regression line, solution was performed again, but with taking into consideration measurements of the initial mechanical properties altered in this way. The solution was repeated until the difference between abscissas of the points of extremum of two last regression lines did not exceed a specified number equal to 0.01 mm. Calculations were carried out on a PC. Coefficient m of the parabolic regression line acquired values from 2 to 25. The line having smallest residual dispersion S^2 was selected from various regression lines. The best regression line has appeared to be a parabolic dependence. For all tested specimens, the hypothesis of equality of mean values of work hardening depth determined by the results of measuring hardness and yield strength checked by the Student's criterion was not confirmed.

The study results have shown that yield strength of the work hardened layer increased to a greater extent than hardness (100–130 % versus 20–60 %). Due to this, the boundary of the work hardened layer was more clearly defined by the change in the yield strength. Use of cylindrical needle rollers of a small diameter leads to a sharp increase in the deformation ratio in a thin surface layer which was indicated by grain elongation in the direction of reeling seen in the optical microphotographs. Accuracy of determining boundary of the work hardened layer by regression analysis according to the results of measurement of yield strength is twice as high in comparison with those obtained in Vickers hardness tests. The 95 % confidence intervals for the work hardening depth calculated from the results of measurement of yield strength make up 11–36 % of the work hardening depth and 32–75 % for the hardness tests. The depth of work hardening which is determined by variations in the yield strength was 25–50 % more than the depth determined by Vickers hardness tests. This difference increases with a decrease in the degree of work hardening. The depth of work hardening determined according to the values of yield strength for circular and close to them imprints ($b/a \leq 2$) corresponded to that calculated by Heifets method even with a rather small reduced curvature of the contact between the roller and the part ($k = 0.0835 \text{ mm}^{-1}$). It has been established that the yield strength was a more sensitive mechanical characteristic for determining the depth of plastic deformation than hardness. The depth of penetration of compressive stresses was close to the depth of work hardening determined by the yield strength. Influence of conditions of reeling with rollers on the change of microstructure of the worked metal was studied in reeling with cylindrical and toroidal rollers of small diameter. Microstructure of the specimens prior to surface work hardening consists of pearlite grains surrounded by hypo-eutectoid ferrite (Fig. 4.2, *a*).

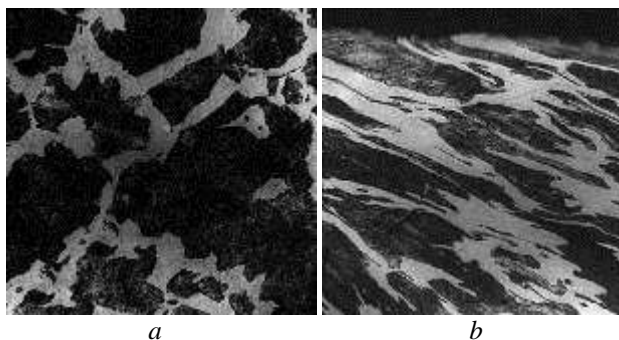


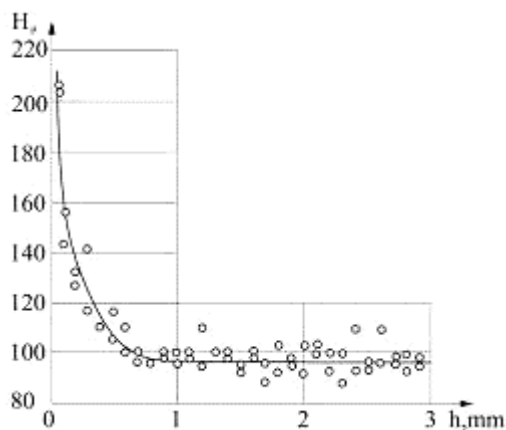
Fig. 4.2. Microstructure of normalized 40 grade steel specimens surface layer: before reeling (*a*); after reeling (*b*) ($\times 300$)

After reeling, changes in the microstructure observed on optical-digital microphotographs could only be found in the surface layers of the shaft reeled with a roller (Fig. 4.2, *b*). The changes were seen as a considerable elongation of both ferrite and perlite grains in a circular direction of reeling. It was established that at the distance from the surface (16.42 mm), the ferrite plates of perlite did not contain dislocations. In some locations, there were isolated dislocations in the ferrite-cementite interface. Ferrite grains in the specimens were constrained by flat straight boundaries. Inside the grains, there was a three-dimensional net of low density dislocations.

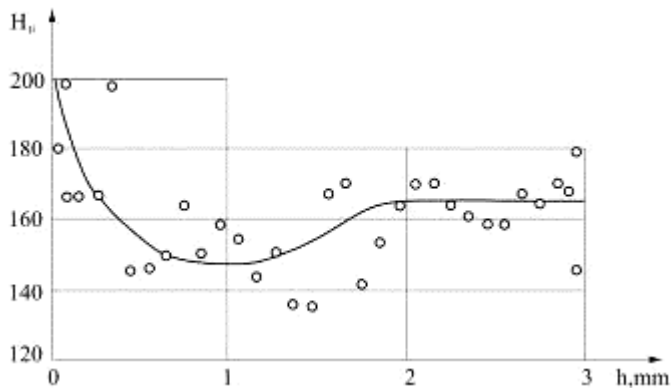
As the electron-diffraction examination has shown, strengthening of the surface layers during reeling shafts with a roller was mainly due to emergence of dislocation cells in the structure of the excessive ferrite grains. Higher degree of work hardening when reeling with a needle roller manifested itself by a higher density of dislocations and a reduced size of cells in the substructure of ferrite grains and a thicker grid of dislocations in the ferrite plates of perlite. In some locations, bend and fracture of cementite plates was observed which indicated the limit degree of plastic deformation of the surface layer. This was confirmed by the beginning of peeling of the surface reeled with a five-millimeter roller.

Distribution of microhardness H_{μ} in the depth of three specimens is shown in Fig. 4.3.

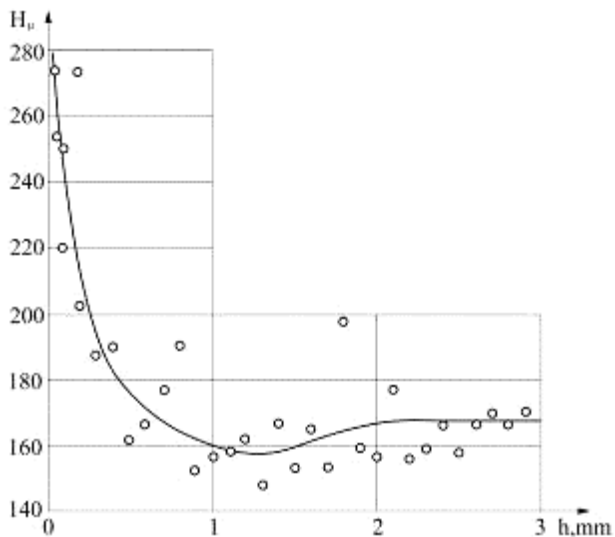
In the graphs of Fig. 4.3, *b*, *c* for the specimens of 45 grade and 40X grade steel, a decrease in microhardness $H_{\mu(t,z)}$ in the transition zone between the hardened layer and the initial metal with microhardness $H_{\mu(i)}$ was found. The average values of $H_{\mu(t,z)}$ and $H_{\mu(i)}$ of normally distributed values were compared with the help of t , the Student criterion.



a



b



c

Fig. 4.3. Distribution of microhardness in the depth of the hardened layer: Armco iron, $r_p = 2.5$ mm, $P = 1.5$ kN (a); 45 grade steel, $r_p = 5$ mm, $P = 5$ kN (b); 40X grade steel, $r_p = 2.5$ mm, $P = 5.5$ kN (c)

For this purpose, the reduced variance was determined:

$$S^2 = \frac{(n_1 - 1)S_1^2 + (n_2 - 1)S_2^2}{n_1 + n_2 - 2} \quad (4.3)$$

and

$$t = \frac{\bar{x}_1 - \bar{x}_2}{S \sqrt{\frac{1}{n_1} + \frac{1}{n_2}}}, \quad (4.4)$$

where n_1, n_2 is the number of measurements of H_{μ} in the transition zone and in the initial metal, respectively; S_1^2, S_2^2 is dispersion of $H_{\mu(t,z)}$ and $H_{\mu(i)}$ values, respectively; \bar{x}_1, \bar{x}_2 is the mean value of $H_{\mu(t,z)}$ and $H_{\mu(i)}$, respectively.

If $|t| \geq t_{\alpha}, K$, then difference between mean values is significant. The value of the confidence probability was taken equal to 0.95, ($\alpha = 0,05$), the number of degrees of freedom was determined from the expression $K = n_1 + n_2 - 2$.

It was established that the content of Cr and C in the transition zone decreased by 20–30 % and increased to 10–15 % in the hardened layer. In reeling 40X grade steel and 45 grade steel, a significant reduction of microhardness was observed in the transition zone between the hardened layer and the initial metal. When Armco iron was reeled, such decrease was not detected (Fig. 4.4, *a*). Based on these studies, a hypothesis of diffusion of strengthening chemical elements (Cr, C) from the intermediate layer to the part surface was advanced. The main mechanism of diffusion during SFW was the gradient of dislocation density. The method of photoelasticity has shown that during elastoplastic deformations, stresses in the surface of contact of the roller with the part were distributed along a curve close to elliptic, the difference was not more than 7 %.

It was established that when slippage was up to 2 %, a sharp change in the coefficient of friction could be observed after which it remained practically constant due to the spread of slippage over the entire contact area: an obvious dependence of the value of the maximum friction coefficient on the state of the friction surface. For example, in the process of abrupt change of the coefficient of friction for hardened and not hardened specimens, with lubrication and without it, the zone (crosshatched area) was detected when running-in was achieved faster for the specimens reeled with rollers (Fig. 4.4, *a*). It can be stated that the surface roughness only affects at small slips (up to 3 %) while reeling with rollers creates specified tribotechnical properties with reduced wear indicators in the surface layer.

Fig. 4.4, *b* shows dependence of the coefficient of friction on the surface roughness for the specimens before reeling and after reeling with a roller and Torsiol-55 lubricant applied. It was established that with a decrease in surface roughness after reeling with rollers, lubricated specimens had a

decreased coefficient of friction. When reeling with slippage, the main mechanisms of wear were oxidizing and fatigue (spalling) wear [14, 15]. Spalling deformation increased with an increase in slippage if tangential stresses were sufficiently large.

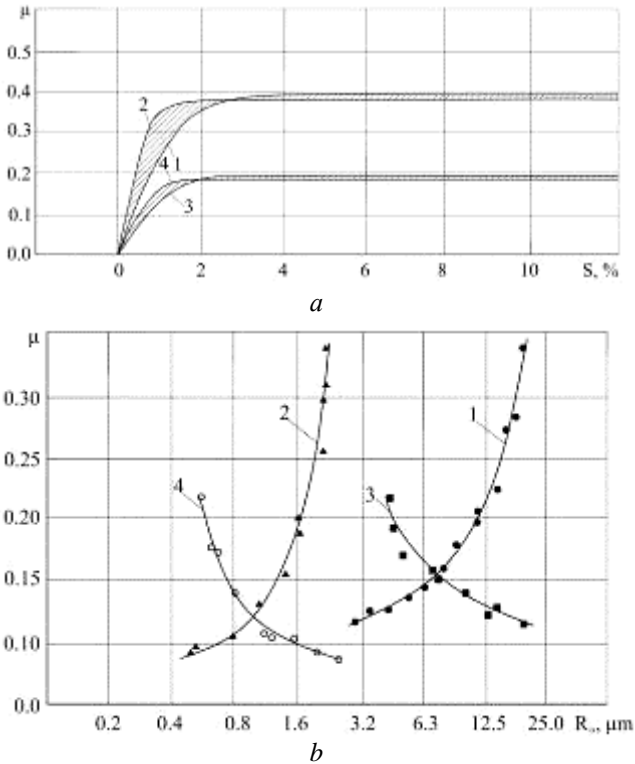


Fig. 4.4. Dependence of the coefficient of friction: on the magnitude of slip (a); on the surface roughness (b): non-reeled nonlubricated specimen (1); the nonlubricated specimen reeled with a roller (2); the non-reeled lubricated specimen (3); the lubricated specimen reeled with a roller (4)

A procedure for determining the force of reeling with a wedge roller was developed. In order to prevent excessive work hardening and peeling of the reeled metal, a limitation for the reeling force at an average angle of indentation not more than 5° was introduced. With the help of nomogram, rolling force was determined as dependent on the size of the part and the round roller and the reduced profile radius of the roller were chosen to determine the design parameters. The method of reeling steel parts [16] was

developed and a theoretical analysis of geometrical parameters was made for reeling the rope blocks with a wedge roller. For this case, beating, eccentricity and diameter of the roller, its curvature, curvature of the reeled part and normal strengthening between the roller and the part in the deformation zone at all points of the profile were calculated.

Calculations have shown that in order to prevent formation of waviness on the reeled surface, the profile radius r_p is made of a variable value which ensures constancy of the angle $\varphi = 5^\circ$ of the roller indentation in all sections of the part profile. The design of the device for reeling the rope blocks is shown in Fig. 4.5. It was patented and invention patents were granted [16].

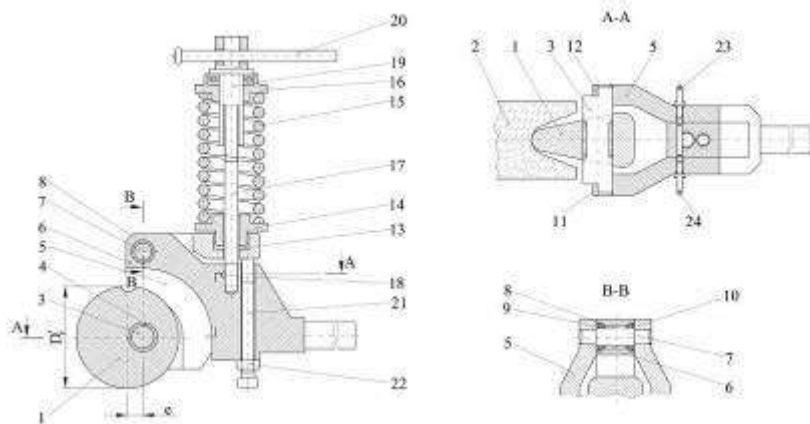


Fig. 4.5. The device for reeling rope blocks with a wedge roller:
roller (1); reeled part (2); shaft (3, 7); bearings (4, 8, 9, 10); lever (5); bracket (6);
plates (11, 12); spherical washer (13); sleeve (14); spring (15); sleeve (16);
pulling rod (17); pin (18); nuts (19, 22); handle (20); screw (21); eye bolts (23, 24)

The developed device and technology of reeling the rope blocks by a wedge roller provide low roughness and a high degree of surface work hardening. This effect is achieved by maintaining constant the average angle φ of the roller indentation into the surface to be worked and mounting of the roller unit on the rolling bearings. This contributes to a uniform deformation of the surface layer in absence of waviness and leads to an increase in durability of the workpiece.

In the course of the experimental study, estimation of dependence of performance of the reeling process on the angle of indentation of the roller, profile radius of the roller, reeling speed and the number of revolutions of the rope block was made.

When plotting the diagram, factors were applied on the abscissa axis in an order of decreasing their rank and the sum of the ranks for the corresponding factor was applied on the ordinate axis. With the help of the obtained diagram, an assessment of significance of the factors was made. To determine the factors that do not influence the technological process, the Student criterion (t criterion) was used.

After analysis and rejection of the mentioned minor factors, a classical diagram of the ranks with a decrease in their magnitude depending on the influence of the factor on the quality of realization of the technological process was constructed. The check of significance of the expert opinions consisted in election of 10 experts, with the number of factors in the matrix being 12 and the number of degrees of freedom $f = 11$.

Analysis of expert opinions ("psychological experiment") and statistical processing have allowed us to conclude on the impact on the course and quality of implementation of the technological process. The four factors had the most affect: roller profile radius X_1 , mm; speed of reeling X_2 , m/min; angle of the roller indentation X_3 , degrees; number of the rope block revolutions X_4 , rev. The three-level, four-factor Box plan of the second order was used.

After statistical processing of the experimental data on a PC with the help of Statistica and Excel programs, mathematical models were obtained. These models were obtained for surface roughness (SR) and hardening degree (HD) which describe the technological process of reeling the rope blocks using a wedge roller device.

The regression equations take the form:

$$\begin{aligned}
 SR = & 1,9224 - 0,2789 \cdot X_1 + 0,2520 \cdot X_2 - \\
 & - 0,5837 \cdot X_3 - 0,4970 \cdot X_4 - 0,014 \cdot X_1 \cdot X_2 + \\
 & + 0,280 \cdot X_1 \cdot X_3 - 0,002 \cdot X_1 \cdot X_4 - 0,154 \cdot X_2 \cdot X_3 + \\
 & + 0,257 \cdot X_2 \cdot X_4 + 0,359 \cdot X_3 \cdot X_4 - 0,094 \cdot X_1^2 - \\
 & - 0,522 \cdot X_2^2 + 1,405 \cdot X_3^2 - 1,280 \cdot X_4^2;
 \end{aligned} \quad (4.5)$$

$$\begin{aligned}
 HD = & 47,5008 - 0,2578 \cdot X_1 - 0,7167 \cdot X_2 + \\
 & + 0,135 \cdot X_3 + 0,1157 \cdot X_4 - 0,127 \cdot X_1 \cdot X_2 + \\
 & + 0,236 \cdot X_1 \cdot X_3 - 0,535 \cdot X_1 \cdot X_4 - 0,124 \cdot X_2 \cdot X_3 + \\
 & + 0,115 \cdot X_2 \cdot X_4 - 1,062 \cdot X_3 \cdot X_4 - 0,483 \cdot X_1^2 - \\
 & - 0,106 \cdot X_2^2 - 0,925 \cdot X_3^2 + 0,931 \cdot X_4^2.
 \end{aligned} \quad (4.6)$$

After statistical processing, analysis of the obtained regression equations was made with encoded values of factors (Table 4.1). Study of optimization criteria depending on the change of independent factors was carried out using the method of two-dimensional sections.

Table 4.11

Data of encoding the test results

Indicator	-1	0	1
X_1 – The roller profile radius, mm	10	15	20
X_2 – Speed of reeling, m/min	20	50	80
X_3 – Angle of roller indentation, deg.	2.5	5	7.5
X_4 – Number of the rope block revolutions, rev.	100	200	300

The mathematical models were checked for the rope blocks made of steel. When analyzing the values of coefficients at factors in the regression equation (4.5), a conclusion can be drawn that the process quality is most influenced by the angle of roller indentation (X_3) and the number of revolutions of the rope block (X_4). Similarly, it can be seen from equation (4.6) that the most important are the roller profile radius (X_1) and the speed of reeling (X_2). For a more thorough study of the process, an analysis of possible combinations of pairwise combination of factors was made. Two factors were equalized in turn to zero leaving the other two unequal to the target value. Regression equation for surface roughness and the degree of hardening at possible combinations of factors was obtained. Equating to zero the value of the angle of roller indentation (X_3) and the number of revolutions of the rope block (X_4), regression equations were obtained in the form:

$$SR = 1,9224 - 0,2789 \cdot X_1 + 0,2520 \cdot X_2 - 0,014 \cdot X_1 \cdot X_2 - 0,094 \cdot X_1^2 - 0,522 \cdot X_2^2; \quad (4.7)$$

$$HD = 47,5008 - 0,2578 \cdot X_1 - 0,7167 \cdot X_2 - 0,127 \cdot X_1 \cdot X_2 - 0,483 \cdot X_1^2 - 0,106 \cdot X_2^2. \quad (4.8)$$

Let us take partial X_1 and X_2 derivatives and obtain a system of equations for each of the optimization criteria:

$$\begin{cases} \frac{\partial SR}{\partial X_1} = -0,0144 \cdot X_2 - 0,1886 \cdot X_1 - 0,2789 = 0; \\ \frac{\partial SR}{\partial X_2} = -1,0452 \cdot X_2 - 0,01440 \cdot X_1 + 0,25204 = 0. \end{cases} \quad (4.9)$$

$$\begin{cases} \frac{\partial HD}{\partial X_1} = -0,12771 \cdot X_2 - 0,96658 \cdot X_1 - 0,25778 = 0; \\ \frac{\partial HD}{\partial X_2} = -0,21326 \cdot X_2 - 0,12771 \cdot X_1 - 0,71667 = 0. \end{cases} \quad (4.10)$$

After solving the system of equations by each of the mathematical models, coordinates of the centers of surface response were determined for each of the optimization criteria and the value of the target function in the found Y_S center. The angle of rotation of the axes in the origin of coordinates of the mathematical model was determined in a canonical form by formula:

$$\arctg 2\alpha = \frac{B_{12}}{B_{11} - B_{22}}. \quad (4.11)$$

Coordinates of response of the surface centers were calculated: for the surface roughness: $X_1 = -1.49$; $X_2 = 0.26$; $\alpha = -0.96^\circ$; $Y_S = 2.16$; for the degree of hardening: $X_1 = 0.19$; $X_2 = -3.47$; $\alpha = 9.36^\circ$; $Y_S = 48.72$.

Coefficients of the regression equations of the characteristic equations for each of the optimization criteria were determined in a canonical form:

$$f(\lambda) = \begin{vmatrix} B_{11} - \lambda & B_{12} / 2 \\ B_{21} / 2 & B_{22} - \lambda \end{vmatrix} = 0, \quad (4.12)$$

to that end, the equations were reduced to the form:

$$\lambda^2 - I \cdot \lambda + D = 0. \quad (4.13)$$

Roots of this equation are the coefficients of a mathematical model in a canonical form. After the calculations, the regression equations were obtained in a canonical form:

for the surface roughness:

$$SR - 2,164 = -0,094 \cdot X_1^2 - 0,522 \cdot X_2^2, \quad (4.14)$$

for the degree of hardening:

$$HD - 48,7 = -0,096 \cdot X_1^2 - 0,493 \cdot X_2^2. \quad (4.15)$$

The results obtained by combining the X_1 and X_2 factors are shown in Fig. 4.6.

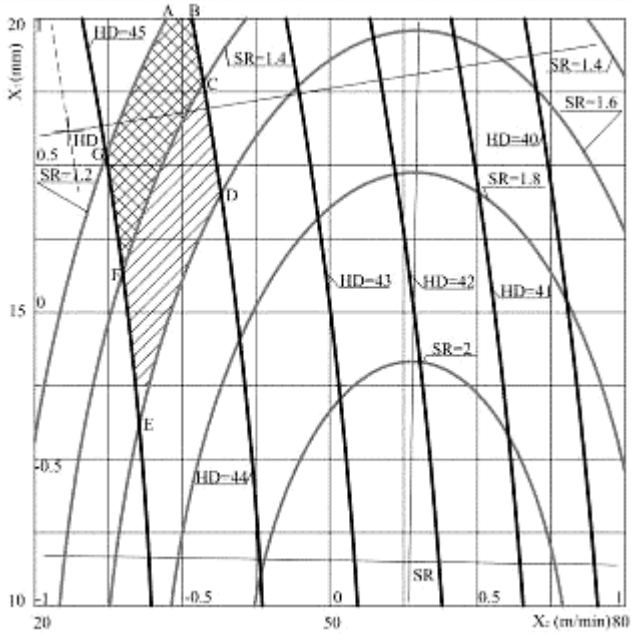


Fig. 4.6. Two-dimensional cross sections of the response surface after combination of the X_1 and X_2 factors at $X_3 = 0$ and $X_4 = 0$

Consideration of the constructed diagrams makes it possible to draw a conclusion that the zone of optimal combination of factors is constrained by SR and HD curves at A, B, C, F, G points. In this case, the surface roughness will lie within $1.2 \mu\text{m} < \text{SR} < 1.4 \mu\text{m}$, and the degree of hardening $44\% < \text{HD} < 45\%$.

With such indicators of the optimization criteria, the value of the roller profile radius should be 16...20 mm and the speed of reeling 27...36 m/min.

Consecutively changing the combination of factors, two-dimensional sections of the response surfaces were obtained for all possible combinations of factors.

For example, by combining the values of the angle of indentation (X_3) and the number of revolutions of the rope block (X_4) at $X_1 = 0$ (the roller profile radius) and $X_2 = 0$ (speed of reeling), the following regression equations were obtained:

$$\begin{aligned}
 \text{SR} = & 1,9224 - 0,5837 \cdot X_3 - 0,4970 \cdot X_4 + \\
 & + 0,359 \cdot X_3 \cdot X_4 + 1,405 \cdot X_3^2 - 1,280 \cdot X_4^2;
 \end{aligned}
 \tag{4.16}$$

$$HD = 47,5008 + 0,135X_3 + 0,1157X_4 - 1,062X_3X_4 - 0,925X_3^2 + 0,931X_4^2. \quad (4.17)$$

Solution to the system of equations has produced coordinates of the centers of the response surfaces: – for the surface roughness: $X_3 = 0.22$; $X_4 = -0.16$; $\alpha = 3.81^\circ$; $Y_S = 1.89$; – for the degree of hardening: $X_3 = 0.08$; $X_4 = -0.01$; $\alpha = 14.8^\circ$; $Y_S = 47.50$.

Fig. 4.7 shows results obtained for equations (4.16) and (4.17) from which it is evident that the zones of the optimal combination of factors are constrained by the SR and HD curves in A, B, C and C, D, E points. In this case, surface roughness in both zones is about 1 μm , the degree of hardening is 47 % at the roll indentation angle of $4^\circ \dots 7^\circ$ and the number of the rope block revolutions of 265...300 rev.

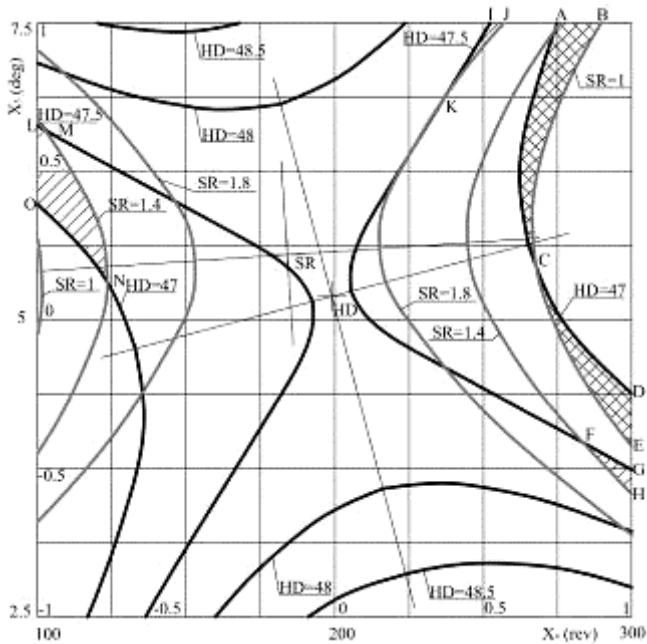


Fig. 4.7. Two-dimensional cross sections of the response surfaces for combining X_3 and X_4 factors at $X_1 = 0$; $X_2 = 0$

Significance of the obtained estimates of coefficients and the adequacy of the model was checked using the Cochran's G-criterion and the Fisher's F-criterion.

When optimizing the technological process of reeling the rope block with a wedge roller, optimum working conditions were obtained by planning the experiment. They have appeared to be the following: the roll profile radius (X_1) 15 mm, the reeling speed (X_2) 40–50 m/min, the roll indentation angle (X_3) 5 degrees, the number of the rope block revolutions (X_4) 160–180 rev. (Fig. 4.6, 4.7).

Their optimal combination forms quality of the technological process of steel part surface hardening by reeling with rollers at indicators of surface roughness (SR) of 1...1.9 μm and the hardening degree (HD) of 46.5...56 %.

Data on wear are given in Table 4.2.

Table 4.22

**Spalling the rope block working surface (800/120)
of the KRUPP ship reloader**

Wearing part	Wear, mm	Operation period, mos.	Average wear <mm/mo
Non-reeled block	4.3	4	1.0
	3.8	3	1.26
Reeled block	3.9	16	0.24
	3.2	12	0.26

It has been shown that reeling of the rope block working profile with rollers increases the contact strength and therefore imparts a 3 to 4 times higher durability. Accordingly, durability of ropes also improves as bending of the rope wires on irregularities of the worn rope block is eliminated.

The procedure of the rope block reeling to increase wear resistance and contact strength has been implemented on Krupp ship reloaders (Germany) in the cargo port of Mykolayiv Alumina Plant OJSC (Ukraine) and the auto cranes KS-3575 built by Mykolayivbudmechaniizatsiya JSC (Ukraine).

**4.1.3. Results of tribological studies and process conditions
of reeling steel parts with rolls**

Yield strength of the work hardened layer increases to a greater extent than hardness (100–130 % versus 20–60 %). Due to this, boundary of the deformed layer is more clearly found by the change of the yield strength. Use of cylindrical needle rollers of small diameter in the reeling process results in a sharp increase in the degree of deformation in a thin surface layer which is recorded on optical microphotographs as grain elongation in the direction of reeling.

Accuracy of determining boundary of the work hardened layer by the method of regression analysis using the results of measuring the yield strength is two times higher than in the case of using the results of Vickers

hardness tests. The 95-% confidence intervals for the depth of work hardening with toroidal and cylindrical rollers calculated on the basis of the results of measuring the yield strength make up 11–36 % of the depth of work hardening and the corresponding figures for hardness tests are 32–75 %.

Strengthening of the surface layers by reeling the shafts with a roller is mainly due to the emergence of dislocation cells in the structure of grains of excess ferrite. Ferrite plates of perlite show smaller deformation. Deformations of cementite plates during reeling with toroidal rollers were not detected.

An increase in the degree of work hardening by reeling with a needle roller manifests itself in a higher density of dislocations and the reduced cell size in the substructure of ferrite grains, as well as in a thicker grid of dislocations in ferrite plates of perlite. In some locations, bending and fracture of cementite plates occur indicating the extreme degree of plastic deformation of the surface layer. This is confirmed by the onset of peeling on the surface reeled with a 5 mm roller.

Diffusion of chemical elements of the surface layer in the process of surface deformation was studied. It was established that the content of Cr and C in the transition zone was 20–30 % lower and 10–15 % higher in the hardened layer. Based on these studies, a hypothesis of diffusion of strengthening chemical elements (Cr, C) from the intermediate layer to the surface of the part was put forward. The main mechanism of diffusion during SFW is the dislocation density gradient.

When friction surfaces are contacting each other with a slip less than 5 %, wear does not depend on the surfaces hardness but when hardness of one of the surfaces increases, then an increased wear of the other surface should be taken into account. Roughness of the friction surfaces affects the coefficient of friction and the speed of the tribo-contact wear when reeling proceeds with a slippage, e.g. with the decrease in roughness of the surface after its reeling with rollers, the coefficient of friction decreases in presence of lubrication.

When slippage measures up to 2 %, a sharp change of the coefficient of friction can be observed after which it remains virtually unchanged due to the spread of slippage over the entire contact area [16].

When reeling proceeds with slippage, the main mechanisms of wear are oxidizing and fatigue (spalling) wear. Spalling deformation increases with the growth of slippage if tangential stresses are sufficiently high.

A procedure for determining conditions of reeling the rope blocks with a wedge roller was developed. In order to prevent excessive hardening and scaling of the reeled metal, a limitation to the reeling force with an average angle of indentation not more than 5° was introduced.

The method of reeling the rope blocks and other steel parts of rotation having a complex profile was developed to improve wear resistance and contact strength [14]. Advantage of the wedge roller consists in

equilibrium of the axial component of the reeling force and reeling of the working profile of the rope block is possible on horizontal and vertical lathes in a single positioning.

The device and technology of the rope block reeling with a wedge roller have been developed to provide low roughness and high degree of work hardening of the surface [15]. This effect is achieved by maintaining constant the average angle ϕ of roller indentation into the surface to be worked and mounting the roller unit in rolling bearings. This contributes to the uniform deformation of the surface layer in absence of waviness and leads to higher wear resistance and contact strength and hence durability of the rope blocks.

A set of laboratory devices was developed to determine roughness of the reeled surface by means of replicas and the degree of work hardening of the working surface. This will assist in studying physical and mechanical properties of steel parts of a complex shape working under a contact loading, including the rope blocks. This ensures obtaining of correct indicators of the technological process of work hardening using the designed device with a wedge roller.

Tribotechnical characteristics of the reeled rope blocks were defined with the help of a device with a wedge roller: the angle of indentation and the profile radius of the wedge roller, the number of revolutions of the steel rope block and speed of reeling. This has made it possible to ascertain possible limits of variation of main design and technological conditions of strengthening with the proposed device and elucidate shape of the wedge roller.

As a result of experimental study with the use of the method of steep convergence, optimal design and kinematic parameters of the reeling process were determined. Optimum working conditions were obtained by planning the experiment with optimization of the technological process of reeling the rope block with a wedge roller. They are the roller indentation angle: 5° , the roller profile radius: 15 mm, the number of the rope block revolutions: 160–180 rev., the speed of reeling: 40–50 m/min.

The optimum combination forms quality of the technological process of surface hardening of the rope blocks by reeling with rollers with the following indicators: surface roughness of 1...1.9 μm and hardening degree of 46.5...56 %.

The conducted experimental studies have proved adequacy of the results obtained in physical and mathematical modeling of the tribotechnical processes occurring during reeling the working friction surface of the rope block with a wedge roller. This allows us to recommend the developed mathematical models for their application in hardening steel parts working in conditions of wear and action of contact forces in the mechanical engineering and other industry sectors.

The proposed hardening technology can be used for other large-sized steel parts working in wear conditions in various industries. Tribological studies of the "rope block – rope" friction couple during reeling taking into account slippage do not provide absolute correspondence with the actual course of the wear process but is a necessary step in the development of computational engineering methods for predicting wear resistance of friction units which will facilitate development of techniques to improve their service life. Further studies in this direction should be conducted by dissemination of the proposed technology to other machinery friction units and their corresponding laboratory wear test patterns.

Conclusions

1. With application of the regression analysis methods, the actual accuracy of determining the depth of hardening has been estimated using the data on changes in mechanical properties of the surface layer metal. It was established that accuracy of determining the boundary of the work hardened layer according to the yield strength change is twice as high as that according to the hardness change. It was shown that the depth of work hardening which is determined according to the changes in the yield strength is 25–50 % greater than the depth determined according to the Vickers hardness change. This difference grows with the decrease in the work hardening degree.

2. Diffusion of strengthening chemical elements taking place in the surface layer during the process of surface deformation was studied. It was established that the content of Cr and C decreased by 20–30 % in the transition zone and increased to 10–15 % in the hardened layer. When reeling steel of 40X and 45 grades with rollers, a significant reduction of microhardness in the transition zone between the hardened layer and the initial metal was observed. When reeling Armco iron, this reduction cession was not detected. Based on these studies, a hypothesis of diffusion of the strengthening chemical elements Cr and C from the intermediate layer to the surface of the part due to the dislocation density gradient has been advanced. When contacting of friction surfaces occurs with a slip of less than 5 %, wear does not depend on hardness of these surfaces. However, when hardness of one of the surfaces increases, the increased wear of the other surface should be taken into consideration. Roughness of the friction surfaces affects the coefficient of friction and wear rate when reeling with slippage. For example, when surface roughness decreases after reeling with rollers, coefficient of friction decreases in lubricated surfaces. Therefore, contact fatigue strongly depends on evenness of rotation and deformation which determines dependence on slippage, the tribosystem rigidity and shape deviation from ideal bodies of rotation.

3. A procedure for calculating the depth of work hardening for the case of reeling the part friction surface with a wedge roller was proposed and the limits of its rational application were set. An original technique of reeling steel parts was developed in order to increase their contact strength and wear resistance. This technique makes it possible to intensify the process and optimize conditions of plastic deformation, increase productivity of the reeling process, and achieve specified tribotechnical properties of the friction surfaces in large-sized steel parts.

4.2. Discrete electromechanical hardening of steel shafts

One of the main reasons for the high wear of machine parts and mechanisms is the insufficient use of modern methods of surface engineering (methods of applying protective coatings and hardening). The methods of surface engineering reduce the consumption of expensive materials, increase the reliability of machines and mechanisms, and increase the life of their machines. Strengthening technologies can differ in energy costs, equipment costs and environmental damage caused. The technology of hardening by the creation of coatings of a discontinuous discrete structure occupies a special place among the known technologies for hardening surfaces. Discrete coatings harden individual areas located on working surfaces in a certain order. Discrete surfaces increase wear resistance due to the effective use of the phenomenon of structural and energy adaptability of materials by means of a special friction surface architecture. Discrete sections in the surface layer of increased hardness, optimal geometry and depth of penetration into the surface eliminate the concentration of stresses from contact loads. Such structures interrupt the processes of formation of cracks, plastic deformation, reduce the propensity to contact bonding of parts, which significantly increase the strength and operational reliability of friction pairs. The main advantage of discrete surfaces is the possibility of mobile changes in the size of discrete sections on the surface of the substrate and the selection of materials on the physical and mechanical characteristics. This allows you to create conditions for regulating the temperature regime, achieving the lowest coefficient of friction and wear, managing and minimizing the stress-strain state of the surface.

In modern researches progressive methods of hardening and increase of wear resistance of cylindrical tribosystems are considered. Such methods of hardening include methods of discrete hardening of friction surfaces. The work [17] was devoted to technological methods of ensuring wear resistance of sliding bearing parts. A regular profile of lubrication grooves was proposed for the boundary lubrication mode. A surface layer with improved antifriction properties is formed in the process of discrete hardening. The work did not place emphasis on the effect of regular lubrication profiles on the wear

resistance of the bearing parts. In the work [18] the study of the efficiency of hardening the parts working in spalling conditions through reeling with rollers were performed with the help of physical simulation and showed the high effect of hardening cast steels. In the work [19] the influence of the stress-strain state on the parameters of discrete hardening is investigated. In [20] the characteristics of the stress-strain state in work-pieces are investigated by the experimental method to coordinate grid during new intensive modes of a stretch-forging in combined dies. The dependence of the surface layer stresses resulting from the shaft-sleeve contact interaction in the sliding bearing on its wear resistance was considered. Instead of contact pressures, surface stressed state which was numerically estimated by the finite element method was taken as the determining factor of the wear rate. It is difficult to use this approach in the engineering practice of calculating bearing wear at the design phase. In work [21] it is shown that the combination of scientific research on friction and wear processes in different scientific and engineering areas, such as mathematical statistics, mechanics of contact, physics of surfaces and magnetism and hydrodynamics, provides a deeper explanation of the processes that take place on discrete surfaces of contact elements. A calculation-experimental method for determining tangential contact frictional stresses using a variational principle was proposed in work [22]. In the article [23] authors substantiate the possibility of application of the method of electric-spark alloying of the surface layers of 40Kh steel by electrodes made of T15K6 and VK8 hard alloys for the purposes of hardening of the working surfaces of elements of the drilling equipment. The following works consider the problems of calculations and tests on friction and wear of cylindrical sliding pairs. The authors of [24] proposed theoretical dependences for a wear testing method using a standard four-ball scheme with determination of wear resistance parameters. The approximating function of the wear spot diameter on the friction path obtained by the results of wear tests was taken as the base of the method. The general methodology of this study can be used to develop a theory of test methods for other geometric schemes. The work [25] was devoted to experimental study of friction losses in friction pairs made of materials. The experimental method for measuring the characteristics of friction was applied in article [26] for examining special features of high-speed friction under conditions of thermal loading and at limited lubrication. The criterion of damping the friction fluctuations proposed in this case is not applicable to the case of viscous friction, where such fluctuations are practically absent as a result of the damping action of a layer of lubricant. Therefore, the purpose of the work is to develop an effective method for increasing the wear resistance of cylindrical parts of the "shaft" type by discrete electromechanical treatment on the basis of modeling the stressed surface state and wear tests.

4.2.1. Fundamentals of the method of discrete hardening of cylindrical parts

The principle of the electromechanical processing (Fig. 4.8) is to surface hardening with concentrated energy flows. In this case there is a thermo-deformation action in the transmission of electric current of high density ($100\text{--}110\text{ A/m}^2$) and low voltage ($2\text{--}7\text{ V}$). The electric current passes through the contact area 3 of the component and the deforming electrode tool 5 with roller 4 or plate. Current strength and secondary voltage are regulated by 1 depending on the contact area and the quality requirements of the surface layer.

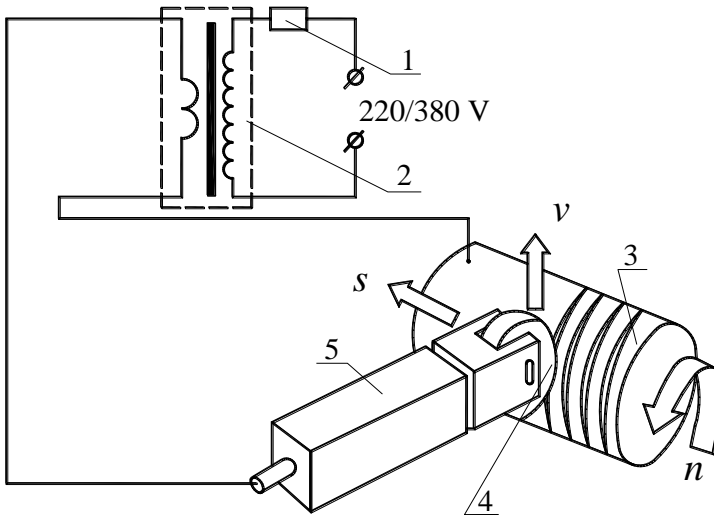


Fig. 4.8. Scheme of discrete electromechanical hardening:
1 – regulator; 2 – transformer; 3 – detail; 4 – roller; 5 – tool

When a large amount of Joule's heat is emitted, there is a high-speed heating (1000 C/s) of micro-volume surface with its plastic deformation. Then there is an intense cooling due to the dissipation of heat inside the material. As a result, a fine-dispersed and solid martensitic structure "white layer" with high durability and wear resistance is formed in the surface layer. For electromechanical hardening, the tool design is proposed (Fig. 4.9). The tool includes a body 1 with a rod 2 and a working head 3 with a carbide roll 4. Electric current is fed to the roller 4 through current collectors 5,6. In the adaptation, the tool is fixed through the beam 7.

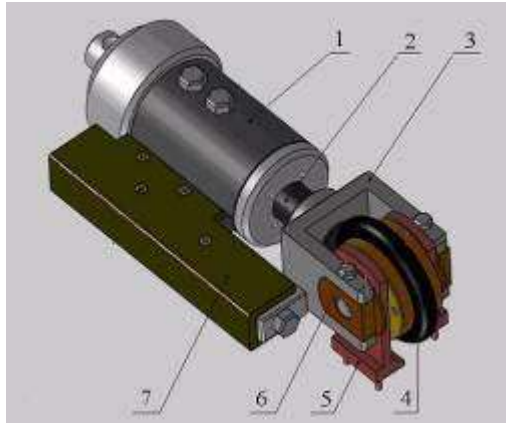
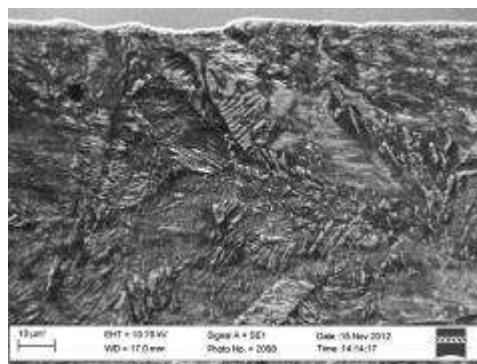
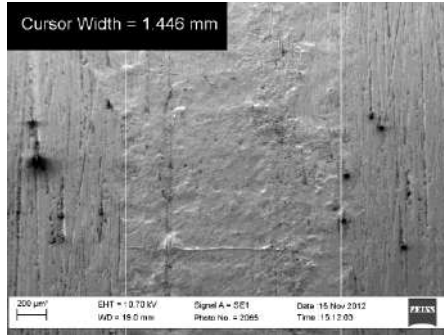


Fig. 4.9. Tool for electromechanical hardening

Discrete hardening when using this tool is carried out due to the pitch of the screw tracks on the cylindrical surface. In addition, the surface of the workpiece is strengthened and is smoothed out of mechanical grinding by a carbide grinding roller. The hardening technology makes it possible to form both unidirectional and cross reinforcement paths with a given pitch. To study the efficiency of discrete trip using linear tracks, metallographic studies were carried out using the ZEISS EVO 40XVP microscope. On the surface a thin reinforced layer of martencite is formed (Fig. 4.10, *a*) with a hardness of 500...600 MPa for Vickers and a sublayer of considerable depth $h = 0.6...0.8$ mm. The structural structure of the sublayer is complex: martensitic quenching, sorbitol quenching, release trooscite as a result of the decomposition of austenite in different temperature zones.





b

Fig. 4.10. The topography and microstructure of a hardened surface layer

Fig. 4.10, *b* shows the topography of the strengthening track obtained at a load of 500 N. On topography significant smoothing of the lines after grinding is possible due to surface-plastic deformation processes.

4.2.2. The calculation model of the contact tool-detail

The choice of technological modes of discrete strengthening of steel parts of the "shaft" type requires the need to assess the depth of the wear-resistant "white layer". This value is close to the contact depth of the tool with the sample. To determine the contact parameters of the roller-tool and the cylindrical part, computer simulation was carried out using the ANSYS software. To evaluate the contact interaction of the tool with the detail, a computer simulation of the ANSYS software system was performed. The calculated finite element model (Fig. 4.11) consisted of 380 thousand elements.

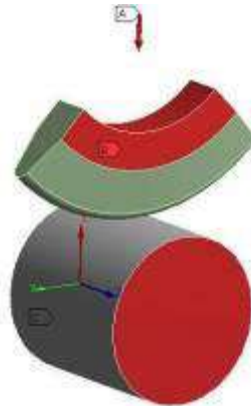


Fig. 4.11. Tool-detail contact model for computer simulation

As a result of the numerical solution of the problem, the dimensions of the contact area were obtained and the stress-strain state was estimated (Fig. 4.12). At a maximum load of 500 N, the length and width of the elliptical contact area are, respectively, 1.7 by 0.6 mm (Fig. 4.12). The analysis showed that maximum stresses and deformations arise at a certain distance from the surface and reach values of 300 MPa. Relative plastic deformations make up about 5 %.



Fig. 4.12. Estimated area contact when loading on a roller 500 N

To the contact area was applied an external thermal flow with a given equivalent temperature and the temperature distribution along the depth of the material was investigated. The analysis of the isotherms in depth (Fig. 4.13) showed that the minimum temperature (700...800 °C), at which the "white layer" is formed, is located at a distance from the surface of about 200...250 microns.

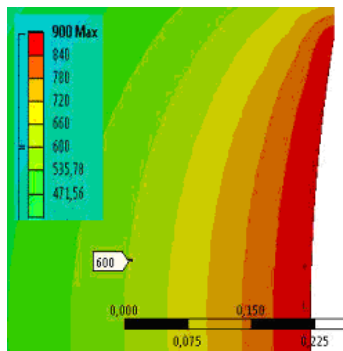


Fig. 4.13. Distribution of temperature fields along the depth of the part

It should be noted that the maximum stresses and deformations are at the same distance from the surface, which contributes to the formation of a strengthened zone. Relative deformations from the temperature action reach values of 1 %, with relative total deformations of 0.7 %.

4.2.3. Stress-deformed state and geometrical parameters with the electromechanical strengthening

Electromechanics treatment forms on-the-spot a structure with the set distributing of properties of durability on the local volumes of surface. The fixed surface shows by itself a regular discrete structure which consists of elements of “white layer”. Researches show on the study of mechanisms of formation of elements of ‘white layer’ that it is possible to form discrete structures with the necessary location of the surface fragments with changing the technological parameters of electromechanics treatment (EMT). It is necessary for effective work of surface EMT, that the mutual location of the fixed fragments and area of coverage of surface took into account the features to construct details. Optimum from point of operating descriptions EMT of surface will be fixed with the formed specific structures and fragments of white layer. Further, an analysis of the behavior of a heterogeneous material whose surface is modified by elements of a white layer with a higher strength is compared with the matrix material under friction conditions. For the simulation, a finite-element model of a bar measuring $15 \times 15 \times 6$ mm, each of which was presented in the form of 30 elements, consisting of 27,000 elements (Fig. 4.14), was used.

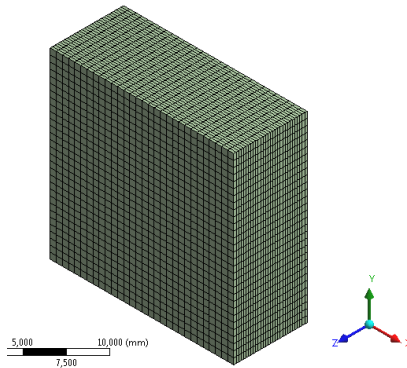


Fig. 4.14. Finished element model of hardened body

Friction conditions were modeled by applying to the hardened surface normal and tangent stresses, respectively, 1 and 0.1 MPa. Samples after electromechanical treatment are bodies with a non-uniform surface, which is reinforced by locally strengthened zones. The formation of a discrete structure in the surface layer leads to a change in the stress-strain state. The stress - deformed state of the body will depend on the nature of the applied loads and on the relative position of the strengthened areas. When simulating a surface that is reinforced by non-intersecting tracks, the equivalent stresses on the Mises are about 400 MPa (Fig. 4.15).

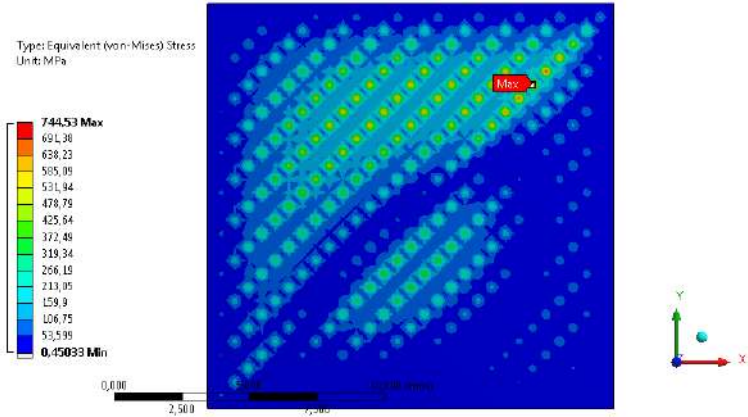


Fig. 4.15. Distribution of Mises stresses for non-intersecting tracks

When choosing the parameters of electromechanical strengthening, one must strive to minimize the stress-strain state of the surface layer. The analysis of various geometric variants of surface treatment showed that the scheme with cross strength tracks would be most optimal. The analysis of the obtained results showed that due to the optimum mutual arrangement of the strengthening of the sites, it is possible to achieve a minimum influence of stress concentration. A comparative analysis of equivalent stresses (by Mises), strengthened according to the optimal pattern of the sample, shows that the maximum stresses are 3.77 MPa (Fig. 4.16).

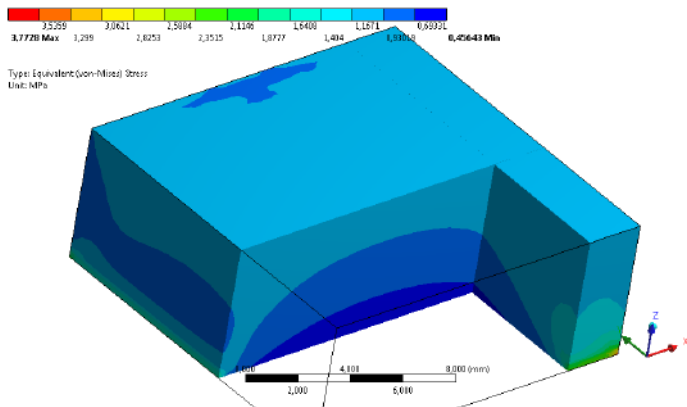


Fig. 4.16. Equivalent (Mises) stresses of an optimally strengthened body

An analysis of the distribution of tangential stresses has shown that there are stretching and compression tangential stresses of absolute magnitude on the surface. The maximum values are 0,02 MPa, which is equal to the maximum value of stresses of the unstable body 0,019 MPa (Fig. 4.17).

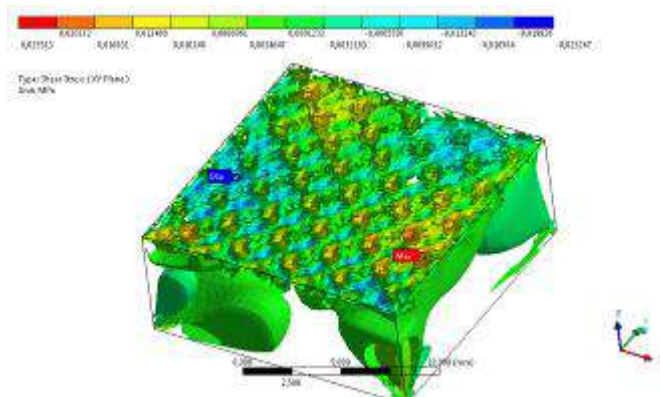


Fig. 4.17. Iso-surface of the distribution of tangential stresses in the plane XY of an optimally strengthened body

Thus, by the right choice of the treatment scheme, the mutual arrangement of wear-resistant elements, a minimum stress concentration in the surface layer can be achieved. In the course of operation, the wear resistance of the surface will significantly increase. An analysis of various geometric variants of surface treatment showed that for the chosen scheme, the optimum area of surface hardening was 0.54. Increasing or decreasing the coverage area resulted in an increase in all components of the stress-strain state.

4.2.4. Calculation-experimental investigation of wear resistance at discrete hardening

For a comparative evaluation of wear of cylindrical parts after a discrete electromechanical strengthening, the theoretical model of wear is proposed in the form of a dependence of the wear intensity on the dimensionless parameters of contact pressure and speed in the form:

$$\frac{du_w}{dS} = K_w \left(\frac{\sigma}{HB} \right)^m \left(\frac{V}{V^*} \right)^n, \quad (4.18)$$

where σ is pressure in contact, MPa; HB is the Brinell hardness, MPa; u_w is linear wear of cylindrical surface, m; S is the friction path for the cylinder, m; K_w , m , n are the parameters of wear; V , V^* is the test speed and the base speed, m/s.

In the wear model (4.18) the parameters K_w , m , n characterize the influence of determining factors of contact pressure and slip speed on wear. These parameters characterize the conditions of wear of the tribosystem and are determined as a result of solving the inverse of wear-contact task based on the results of experimental tests according to the "cylinder-ball" scheme (Fig. 4.17).

The main stages of the solution are as follows. Distribution of contact pressure: $\sigma = \frac{Q}{\pi \bar{a}^2}$. Geometric condition in contact: $u_w(S) = \frac{a(S)^2}{2R^*}$ as the dependence of wear on the path of friction.

Experimental dependence of the radius of the cylinder's wear track on the friction path in the form of power approximation $\bar{a}(S) = cS^\beta$, where c, β are the parameters of approximation, which are determined by the results of the tests. As a result of the substitution of the relations in the model (4.18) we obtain the equation of solving the problem:

$$\frac{\bar{a}^2(S)}{2R^*} = K_w \int_0^S \left[\left(\frac{Q_1}{\pi \bar{a}^2(S)} \right) \frac{1}{HB} \right]^m \left(\frac{V}{V^*} \right)^n dS. \quad (4.19)$$

After integration (4.18) for the tests with two slip rates, the expressions for calculating wear parameters are obtained:

$$m = \frac{1-2\beta}{2\beta}; \quad n = (2m+2) \frac{\lg(c_1/c_2)}{\lg(V_1/V_2)}; \quad K_w = \frac{\beta c_1^{2m+2}}{R^*} \left(\frac{HB}{Q} \right)^m \left(\frac{V^*}{V} \right)^n. \quad (4.20)$$

To test samples that were strengthened by electromechanical treatment, a multifunctional laboratory installation was modified (Fig. 4.19).

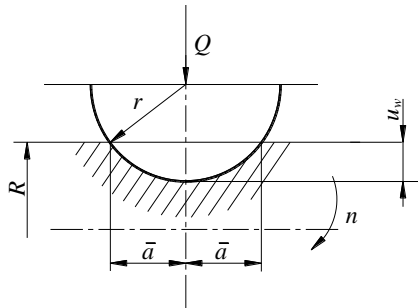


Fig. 4.18. Scheme of contact "cylinder - ball": Q is load; n is the speed of rotation; \bar{a} is the half-width of the contact; R, r are the radius of the cylinder and balls

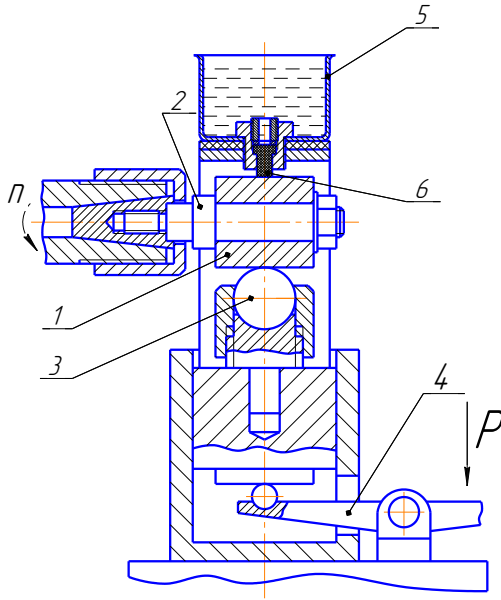


Fig. 4.19. Modernized test setup: 1-shaft; 2-control sample

The samples from 40Kh steel in a normalized state and after processing with non-cross and cross paths were tested. The force of pressing the ball was 50 N, the lubrication of the surface of the sample was carried out with Castrol 10W-40 oil.

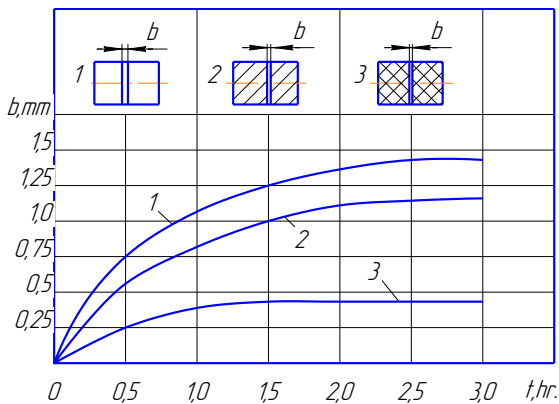


Fig. 4.20. Dependence of wear on the duration of tests

The test results showed that the wear resistance of the samples after electromechanical treatment is 1.26...3.62 times higher than the wear resistance of the non-hardened sample. The increase in wear resistance is due both to the formation of discrete zones of higher hardness, and to the magnitude and distribution of stresses in the surface layer.

When processing according to scheme 2, there are significant tangential tension stresses, which are practically absent in the processing under scheme 3. The tensile stresses reduce wear resistance. The reduction of wear on sample 2 compared to the sample without processing is due to the positive effect of discrete strengthening. The results of determination of wear parameters are presented in Table 4.3.

Table 4.3

Parameters of wear resistance			
sample	m	n	K_w
1	1,058	0,685	$2,571 \cdot 10^{-11}$
2	1,079	0,5184	$1,939 \cdot 10^{-11}$
3	1,1896	0,130	$5,522 \cdot 10^{-12}$

The obtained results indicate that the wear of unstable samples significantly depends on the slip speed. Examined electromechanical treatment samples have a high wear resistance at high slip speeds. Dependence (4.18) calculated the intensity of wear of samples depending on the contact pressure (Fig. 4.21).

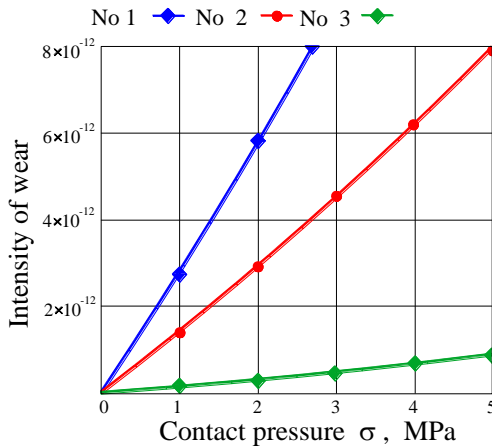


Fig. 4.21. Dependence of the intensity of wear on the contact pressure

As a result, they increased the wear resistance by 3 times during cross-turning compared to unidirectional discrete rolling. This can be justified by the fact that the cross-sectional formation of discrete zones results in a greater strengthening effect due to a more favorable stressed surface condition.

Conclusions

It has been established that continuous strengthening of surfaces does not allow to provide the necessary durability in tough operating conditions.

A new method of increasing the wear resistance of steel parts by discrete electromechanical processing has been developed by forming linear reinforcement areas with controlled geometry. A computer simulation of the conditions of the contact between the tool roller and the machined shaft has been carried out. The contact areas, contact stresses, depths of deformation and temperature distribution in depth are calculated. It has been established that the main factor controlling the wear resistance of discrete surfaces is their surface tension under friction conditions. Computer simulation of the stress state of the surface showed that the scheme would be optimal in the form of cross-sectional areas of processing.

The results of the calculation of the intensity of wear showed that for a cross-section discrete profile wear resistance of samples from steel 40Kh was 3 times higher.

References for chapter 4

1. Babei, Y. I., Butakov, B. I., Sysoev, V. G. (1995). Surface hardening of metals. K.: Scientific Opinion, 256 Analysis of piezomotor driver for laser beam deflection. *Journal of Vibroengineering*, Vol. 11, Issue 1, 2009, p. 17-26.
2. Kindrachuk, M. V., Kornienko, A. O., Fedorchuk, S. V., Tisov, O. V. (2006). Stress-deformed state of composite material loaded with friction and temperature. *Problems of tribology. Khmelnytsky*, 1, 153–157.
3. Aulin, V., Arifa, W., Lysenko, S., Kuzyk, A. (2016). Improving of the wear resistance of working parts agricultural machinery by the implementation of the effect of self-sharpening. *International Journal of Engineering and Technology (UAE)*, 5 (4), 126–130. doi: 10.14419/ijet.v5i4.6386.
4. Kuzmenko, A. G., Dykha, A. V. (2007). Contact, friction and wear of oiled surfaces: monograph. Khmelnytsky: KhNU, 344.
5. Braude, B. I., Gohberg, M. M., Zvyagin I. E. (1988) Handbook for cranes: in 2 t. M.: Mechanical Engineering, 1: Characteristics of materials and loads. Basics of calculation of cranes, their drives and metal constructions, 536.
6. Chernets, M. V. (2015). Prediction of the life of a sliding bearing based on a cumulative wear model taking into account the lobing of the

shaft contour. *Journal of Friction and Wear*, 36(2), 163-169. doi:10.3103/S1068366615020038.

7. Soldatenkov, I.A. (2010). Evolution of contact pressure during wear of the coating in a thrust sliding bearing. *Journal of Friction and Wear*, 31(2), 102–106. doi:10.3103/S1068366610020029.

8. Togawa, K., Arai, S., Uwatoko, M. (2012). Influence of Traction Sheave P.C.D. Difference on Sheave and Rope. *Journal of the Proceedings of the Elevator, Escalator and Amusement Rides Conference*, 2011, 31–34. doi: 10.1299/jsmearc.2011.31.

9. Ryu, J. B., Chae, Y. H., Kim, S. S. (2005). A Fundamental Study of the Tribological Characteristics of Sheave Steel against a Wire Rope. *Journal of the Key Engineering Materials*, 297–300, 1382–1387. doi: 10.4028/0-87849-978-4.1382.

10. Dykha, A.V., Kuzmenko, A.G. (2015). Solution to the problem of contact wear for four-ball wear-testing scheme. *Journal of Friction and Wear*, 36(2), 138–143. doi: 10.3103/S1068366615020051.

11. Dykha, A., Aulin V., Makovkin, O., Posonskiy S. (2017). Determining the characteristics of viscous friction in the sliding supports using the method of pendulum. *Eastern-European Journal of Enterprise Technologies*, 7 (87), 4–10. doi: 10.15587/1729-4061.2017.99823.

12. Butakov, B. I., Shebanin, V. S., Butakova, G. S., Marchenko, D. D. (2010). Pat. 93252 Ukraine, IPC 24 V 39/04. A method of finishing and strengthening the processing of surfaces of the bodies of rotation of a complex profile and a device for its implementation. 2010, Bul. No. 13.

13. Butakov, B. I., Shebanin, V. S., Butakova, G. S., Marchenko, D. D. (2013). Pat. 2493954 Russian Federation, IPC At 24 V 39/04, B 21 N 1/22. A device for finishing and strengthening the surfaces of bodies of rotation of a complex profile. 2010, Bul. No. 27.

14. Marchenko, D.D., Butakov B. I. (2013). Promoting Contact Strength of Steel by Rolling. *Journal of Friction and Wear*, 34(4), 308–316. doi: 10.3103/S106836661304003X.

15. Study and development of the technology for hardening rope blocks by reeling / [Text] / A. Dykha, D. Marchenko, V. Artiukh, O. Zubiexhina-Khaiat, V. Kurepin // *Eastern-European Journal of Enterprise Technologies*. – 2018. – Vol. 2, Issue 1 (92). – P. 22–32. DOI: 10.15587/1729-4061.2018.126196

16. Dykha A., Marchenko D. Increase of reliability and wear resistance of cylindrical blocks with surface plastic deformation. // *JVE Book Series on Vibroengineering. Quality and reliability of technical systems: Theory and practice* – Vol. 2. Vilnius: JVE International Ltd, 2018. pp. 104–118. <https://1drv.ms/b/s!Am41DJRc50G-maESLLEMCqUA6ZI2mQ>

17. Kindrachuk, M., Radionenko, O., Kryzhanovskiy, A., Marchuk, V. The friction mechanism between surfaces with regular micro grooves under boundary lubrication. *Aviation*, 2014, 8 (2), 64–71. <http://dx.doi.org/10.3846/16487788.2014.926642>
18. Marchenko, D.D., Dykha, A.V., Artyukh, V.A., Matvyeyeva, K. S. Studying the Tribological Properties of Parts Hardened by Rollers during Stabilization of the Operating Rolling Force. *J. Frict. Wear* 41, 58–64 (2020). <https://doi.org/10.3103/S1068366620010122>
19. Vynar, V.A., Dykha, M.O. (2013). Influence of the stress-strain state on the wear resistance of the surface of 40Kh Steel after discrete electromechanical treatment. *Materials Science*, 2013, 49 (3), 375-381. <https://doi.org/10.1007/s11003-013-9625-z>
20. Kukhar, V.V., Vasylevskiy, O.V. Experimental research of distribution of strains and stresses in work-piece at different modes of stretchforging with rotation in combined dies. *Metallurgical & Mining Industry*. 2014, Issue 3, 71–78.
21. Marchuk, V., Kindrachuk, M., Kryzhanovskiy, A. System analysis of the properties of discrete and oriented structure surfaces. (2014) *Aviation* 18 (4), pp. 161-165. <http://dx.doi.org/10.3846/16487788.2014.985474>
22. Dykha, A.V., Kuzmenko, A.G. Distribution of friction tangential stresses in the Courtney-Pratt experiment under Bowden's theory. *Journal of Friction and Wear*, 2016, 37 (4), 315–319. doi: 10.3103/s1068366616040061. <https://link.springer.com/article/10.3103/S1068366616040061>
23. Kryshchtopa S.I., Petryna D.Yu., Bogatchuk I.M., Prun'ko I.B., Mel'nyk V.M. Surface Hardening of 40KH Steel by Electric-Spark Alloying. *Materials Science*, 2017, 53 (3), 351–358.
24. Dykha, A.V., Kuzmenko, A.G. Solution to the problem of contact wear for four-ball wear-testing scheme. *Journal of Friction and Wear*, 2015, 36(2), 138–143. doi: 10.3103/S1068366615020051. <https://link.springer.com/article/10.3103/S1068366615020051>
25. Kryshchtopa, S., Kryshchtopa, L., Bogatchuk, I., Prunko, I., Melnyk, V. Examining the effect of triboelectric phenomena on wear-friction properties of metal-polymeric frictional couples. *Eastern-European Journal of Enterprise Technologies*, 2017, 1/5 (85), 40–45. doi: 10.15587/1729-4061.2017.91615
26. Sorokatyi R., Dykha A. (2015). Analysis of processes of tribo-damages under the conditions of high-speed friction. *Journal of Friction and Wear*, 2015, 36 (5), 422–428. DOI:10.3103/S106836661505013X. <https://link.springer.com/article/10.3103/S106836661505013X>

WEAR MODELS AND DIAGNOSTICS OF CYLINDRICAL SLIDING TRIBOSYSTEM

Authors:

Aleksandr Dykha

Dr. Sci. Eng., Khmelnytskyi National University,
Department of Tribology, Automobiles and Materials Science
Institutska str., 11, Khmelnytsky, Ukraine, 29016
E-mail: tribosenator@gmail.com
+038 097 55 469 25

Juozas Padgurskas

Dr. Sci. Eng., Institute of Power and Transport Machinery
Engineering, Vytautas Magnus University
V. Putvinskio g. 23, Kaunas, Lithuania
E-mail: juozas.padgurskas@vdu.lt
+370 37 222 739

Janusz Musial

Prof. dr hab. eng, Faculty of Mechanical Engineering,
UTP University of Science and Technology
Al. prof. S. Kaliskiego 7, 85-796 Bydgoszcz, Poland
E-mail: jamusual@utp.edu.pl
+48 52 3408132

Serhii Matiukh

Associate Professor, PhD, Khmelnytskyi National University
Institutska str., 11, Khmelnytsky, Ukraine, 29016
E-mail: matuh@meta.ua
+38 097 99 807 52